A new link between translation termination and NMD complexes

Etienne Raimondeau

Communauté
UNIVERSITÉ Grenoble Alpes

EMBL

THESIS / THÈSE

To obtain the title of / Pour obtenir le grade de

DOCTEUR DE LA COMMUNAUTE UNIVERSITÉ GRENOBLE ALPES

Discipline / Spécialité : **Biologie Structurale et Nanobiologie**

Arrêté ministériel : 7 août 2006

Presented by / Présentée par

Etienne Raimondeau

Thesis supervisor / Thèse dirigée par **Prof. Christiane Schaffitzel**

Thesis prepared at / Thèse préparée au sein du **European Molecular Biology Laboratory (EMBL), Grenoble Outstation** in / dans **l'École Doctorale de Chimie et Sciences du Vivant**

A new link between translation termination and NMD complexes

Un nouveau lien entre les complexes de terminaison de la traduction et de la NMD

Public defense on / Thèse soutenue publiquement le **03.11.2016**
Jury members / Devant le jury composé de :

Prof. Winfried Weissenhorn President/Président
Professor, University of Grenoble Alpes, France.

Dr. Niels Gehring Reviewer / Rapporteur
Group Leader, University of Cologne, Germany.

Prof. Sven Danckwardt Reviewer / Rapporteur
University Professor, University of Mainz, Germany.

Prof. Christiane Schaffitzel Thesis Supervisor / Directrice de Thèse
Team Leader, EMBL-Grenoble, France.

À mes parents

Contents

List of Figures

List of Tables

Nomenclature

3' UTR	3' untranslated region
40S	Eukaryotic small ribosomal subunit
60S	Eukaryotic large ribosomal subunit
80S	Eukaryotic ribosome
ATP	Adenosine-5'-triphosphate
ATPase	ATP hydrolase
CMV	Cytomegalovirus
Cryo-EM	Cryo-electron microscopy
DNA	Deoxyribonucleic acid
EBM	Exon junction complex-binding motif
EJC	Exon junction complex
GTP	Guanosine-5'-triphosphate
GTPase	GTP hydrolase
LB	Lysogeny broth
MIF4G	Middle domain of eukaryotic initiation factor 4G (eIF4G)
MVHC-STOP	Model mRNA used in Chapter 4
NGD	No-go decay
NMD	Nonsense mediated mRNA decay
NSD	No-stop decay
NTC	Normal termination codon

ORF	Open reading frame
PABPC	Human cytoplasmic poly(A)-binding protein
PABPN	Human nuclear poly(A)-binding protein
PTC	Premature termination codon
Pab1p	Yeast poly(A)-binding protein
PostTC	Post-terminating ribosome
PreTC	Pre-terminating ribosome
RNA	Ribonucleic acid
RNC	Ribosome-nascent chain complex
Toeprinting	Primer extension inhibition
UPF	Upstream frameshifting genes products
VCE	Vaccinia capping enzyme
eEF	Eukaryotic elongation factor
eIF	Eukaryotic initation factor
eRF	Release factor
mRNA	Messenger RNA
mRNP	Messenger ribonucleoprotein
rpm	Rotations per minute
sup35	Yeast eukaryotic release factor 3 (eRF3)
sup45	Yeast eukaryotic release factor 1 (eRF1)
tRNA	Transfer RNA
yNC	Yeast nascent chain

1. Preface

My doctorial work was focusing on termination of translation and nonsense mediated mRNA decay in yeast and human. The main work of my thesis has been performed with proteins of human origin and has led to the submission of a manuscript. This thesis is thus written in a cumulative style. The second chapter contains a general introduction on termination of translation and nonsense mediated mRNA decay. The third and fourth chapter detail the work undertaken, focusing on yeast and human respectively. Both chapters are formatted as independent manuscripts and contain the classical "Results" and "Material and methods" sections. The fifth and final chapter discuss the main conclusions of both manuscripts.

2. Introduction

Resumé en français

Depuis la formulation de la théorie fondamentale de la biologie moléculaire par Francis Crick, en 1958, notre compréhension de l'expression génétique a beaucoup progressé. L'expression des gènes est un processus hautement complexe, impliquant de nombreux complexes cellulaires travaillant de concert. Les cellules ont développé différents mécanismes de contrôle qualité pour chaque étape de l'expression génétique afin de maintenir l'intégrité de l'information. La dégradation des ARNm non-sens (Nonsense-mediated decay ou NMD) a été mise en évidence il y a plus de 30 ans. Au cours de la terminaison de la traduction, la NMD discrimine les codons stop prématurés (PTC) des codons stop physiologiques et déclenche la dégradation des ARNm aberrants. Cette voie représente un des principaux mécanismes de contrôle qualité de la cellule et est le gardien de l'expression génétique. La NMD est d'une importance éminente du point de vue médical bien qu'elle ait une activité à double tranchant. Des mécanismes de reconnaissance ainsi que des ARN substrats pour la NMD ont été mis à jour.

Les facteurs principaux de la NMD : UPF1, UPF2 et UPF3 sont conservés de la levure à l'homme (Upf1p, Upf2p et Upf3p chez la levure), ces protéines permettent la reconnaissance des PTCs. Ces dernières interagissent avec la machinerie de la traduction comportant les ribosomes, les facteurs de terminaison eRF1 et eRF3 et une variété de facteurs additionnels parmi lesquels le Exon Junction Complexe (EJC) et la protéine poly(A)-binding (PABPC1 ou Pab1p chez la levure) qui sont positionnés sur l'extrémité 3' non-traduite de l'ARNm (3'UTR). La reconnaissance d'un PTC déclenche la phosphorylation de UPF1 chez les mammifères et aboutit à la dégradation de l'ARNm défectueux.

Le but de notre étude est d'apporter de nouvelles connaissances sur les interactions entre facteurs de terminaison et facteurs NMD. Plus particulièrement, ce travail se concentre sur la terminaison de la traduction chez la levure en présence de Pab1p et de Upf1p ainsi que sur l'impact des facteurs NMD sur la terminaison de la traduction chez l'homme.

2.1 The mRNA life cycle

2.1.1 Transcription and mRNA processing in the nucleus

Transcription is the first step in gene expression and enables the conversion of a defined segment of DNA into RNA. RNA biogenesis takes place in a highly structured and dynamic nuclear environment in eukaryotes (Venkatesh & Workman, 2015). RNA polymerase II (Pol II) is responsible for the synthesis of mRNAs and a few non-coding RNAs (Sainsbury et al., 2015; Cramer et al., 2001). To promote efficient and accurate processing of pre-mRNAs into mature mRNAs, multiple processing factors, such as the capping enzymes, and splicing factors amongst others, interact with the carboxy-terminal domain (CTD) of the large subunit of the RNA Pol II in a phosphorylation-dependent manner (Moore & Proudfoot, 2009; Bentley, 2014; Venkatesh & Workman, 2015). During each step of the processing, factors remain associated with mRNAs and lead to the assembly of the messenger ribonucleoprotein (mRNP).

The first step in the maturation process requires the addition of a 7-methylguanosine cap (m7GpppN) to the pre-mRNA 5´ end. In mammals, capping is performed by two enzymes: the mRNA capping enzyme (a triphosphatase with guanylyltransferase activity), and a guanine-7-methyltransferase (Bentley, 2014). The 5' end cap is then recognized by the cap-binding complex (CBC), formed by CBP20 and CBP80 (Mazza et al., 2001), and remains bound to the mRNA until it is exported from the nucleus (Figure 2.1). Correct capping is crucial for the protection of mRNAs from degradation by 5'-3' exonucleases, which are present in the nucleus as well as the cytoplasm (Schoenberg & Maquat, 2012) and for translation initiation.

During the early stages of transcription, the genetic information on pre-mRNAs is discontinuous and subdivided into exons and introns. While exons harbor protein-encoding sequences, introns play a regulatory role (for example in alternative splicing (Chen & Manley, 2009) and in nonsense-mediated decay (NMD) (Alexandrov et al., 2012; Ottens & Gehring, 2016)). Recognition and excision of introns involves a vast variety of factors assembled into the spliceosome. The spliceosome complexes are formed stepwise, by the addition or removal of small nuclear ribonucleoproteins (snRNPs from U1 to U6) and a broad collection of additional proteins. Most notably, the spliceosome allows the deposition of Serine/Arginine-rich (SR) proteins and of the exon junction complex (EJC) which are critical for post-transcriptional processes (Figure 2.1)(Hocine et al., 2010; Huang & Steitz, 2005; Hir et al., 2015). Splicing is a major step in the regulation of gene expression and splicing-defective transcripts are subjected to degradation (Doma & Parker, 2007)(see section 2.2.1). As such, mis-regulation of splicing is associated with multiple diseases in humans such as leukemia (Cazzola et al., 2013).

The last step of the transcription is characterized by 3' end processing of mR-

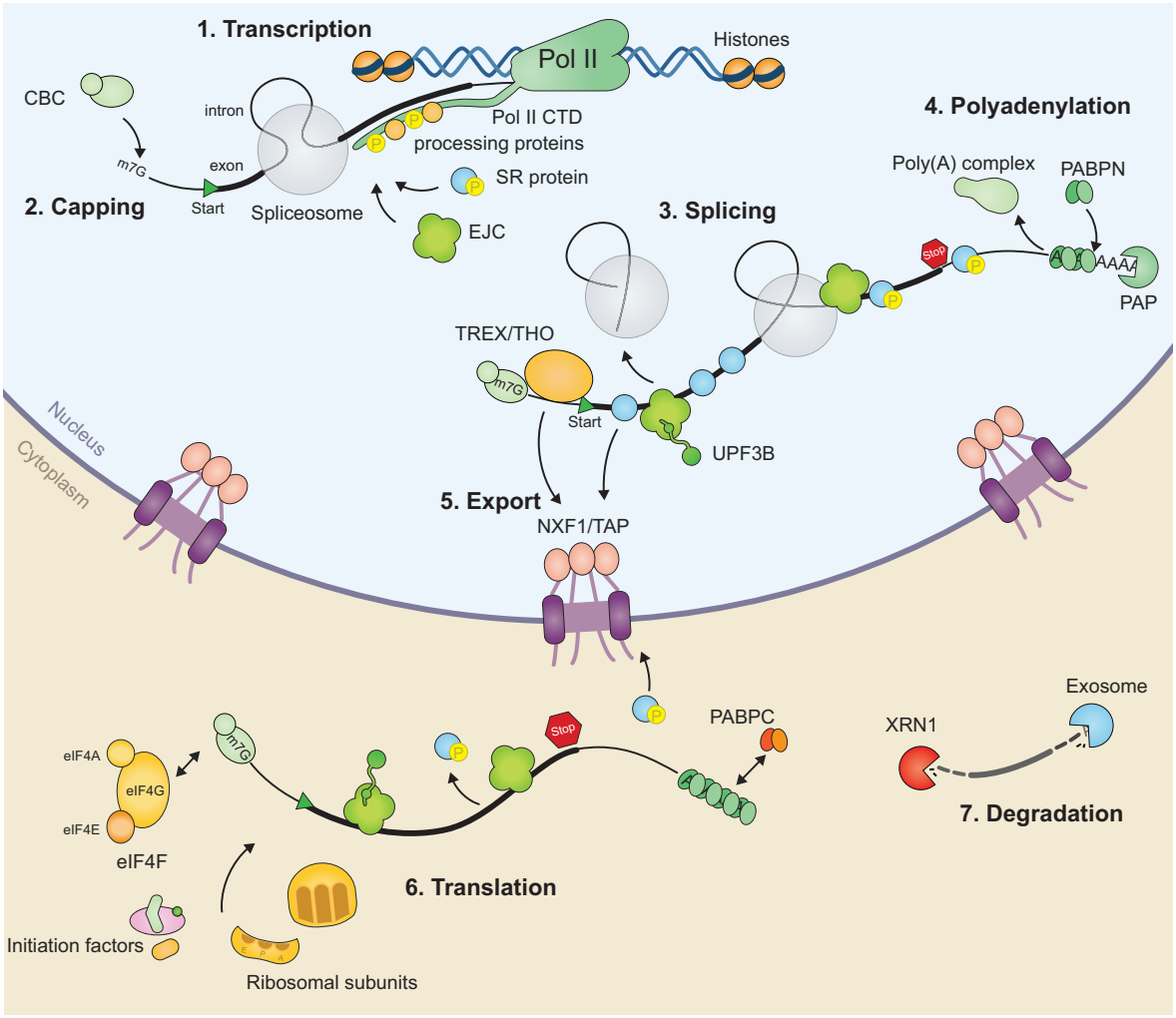

Figure 2.1: The life of mRNA. ***1.*** *Pre-mRNAs are synthetized by Pol II in the nucleus from the DNA sequence bound to histones. Phosphorylation of residues (yellow P) in the Pol II C-terminal domain allows the binding of various processing factors such as transcription, capping, splicing or polyadenylation factors.* ***2.*** *The 5'end cap (m7G) is recognized by the Cap Binding Complex (CBC) during the early stage of pre-mRNA processing.* ***3.*** *The assembly of the spliceosome (grey) occurs co-transcriptionally. mRNA exons are represented as a thick black line and the introns as a thin black line. The excision of introns by the spliceosome leads to the deposition of the EJC, UPF3B and phosphorylated Serine/Arginine-rich (SR) proteins on the spliced mRNA.* ***4.*** *3' end cleavage is performed by the poly(A) complex and the poly-adenosine sequence is added by poly(A) polymerase (PAP) and recognized by the poly(A) binding protein in the nucleus (PABPN).* ***5.*** *Mature mRNPs are bound by the TREX/THO complex and by hypophosphorylated SR proteins, which allow the binding to the nuclear pore proteins NXF1/TAP.* ***6.*** *In the cytoplasm, CBC is exchanged against the eIF4F cap-binding complex (formed by eIF4A, eIF4E and eIF4G) and PABPN is replaced by poly(A) binding protein in the cytoplasm (PABPC). Translation initiation factors and the ribosomal subunits assemble to translate the mRNA. Phosphorylated SR proteins can be reimported into the nucleus after dissociation from the mRNA.* ***7.*** *At a later stage, mRNAs are degraded by XRN1 and the exosome Adapted from (Moore & Proudfoot, 2009; Hir et al., 2015)*

NAs. The cleavage and polyadenylation of mammalian pre-mRNAs is carried out by a multisubunit complex (called poly(A) complex in Figure 2.1) (Porrua & Libri, 2015). Subsequently, the poly(A) tail is coated by nuclear poly(A)-binding proteins (PABPN). These are essential for mRNA protection from 3' end degradation, and for translation in addition to nuclear export (Gross et al., 2007; Xie et al., 2014). It has been reported that ~50% of human genes can be alternatively polyadenylated, generating isoforms with a different 3' UTR (Tian et al., 2005). Differently polyadenylated transcripts show different levels of mRNA stability or cellular localization which could also have implications for health and diseases (Subtelny et al., 2014; Danckwardt et al., 2008).

In metazoans, mature mRNPs are recognized by NXF1/TAP-p15 receptors for export through the nuclear pore complex (NPC) (Köhler & Hurt, 2007). The transcription export complex (TREX) and SR proteins are the main adaptors linking mRNAs to the export receptors. The phosphorylation levels of the SR proteins have been suggested to signal mRNAs ready for export (Reed & Cheng, 2005; Katahira, 2012). Export competent mRNP particles can then dock to the NPC for translocation through the pore.

2.1.2 Translation

In the cytoplasm, CBC is replaced by the eukaryotic initiation factor 4F complex (eIF4F) and PABPN is exchanged against a cytoplasmic PABP (PABPC1). The interaction between eIF4F subunit, eIF4G, and PABPC1 facilitates circularization of the mRNA and thereby initiates translation and efficient protein synthesis (Wells et al., 1998).

The general mechanism of translation has been recognized for 40 years, but recent advances in biochemistry and cryo-electron microscopy have enabled further research to gain a more detailed, molecular understanding of the process. More detailed initiation and elongation mechanisms have been reviewed in detail, for example in (Hinnebusch, 2014; Jackson et al., 2010; Dever & Green, 2012). The factors involved in translation termination are described more precisely in section 2.3.3.

2.1.2.1 Initiation

Translation initiation is the process of the assembly of the translation components to form a translation-ready 80S ribosome on the start codon of the mRNA. Firstly, the 40S small subunit of the ribosome associates with Met-tRNA^{Met} and initiation factors eIF1A, 1, 3 and 5 to form a 43S preinitiation complex. The attachment of the 43S complex to the mRNA is mediated by the capping complex eIF4F and initiation factor eIF3 (Jackson et al., 2010). At this stage, the 43S complex is found in an 'open' conformation, which allows translocation along the mRNA in the 5' to 3' direction for

the methionine initiation codon (des Georges et al., 2015). Start codon recognition leads to conformational changes, which switch the complex to a 'closed' conformation, so called the 48S initiation complex, locking it onto the mRNA (Hussain et al., 2014). GTP hydrolysis by initiation factor eIF2 results in the displacement of initiation factors eIF1, eIF3 and eIF5 and recruitment of the 60S large ribosomal subunit. The 80S ribosome initiation complex is then 'committed' to protein synthesis (Hinnebusch, 2014; Jackson et al., 2010).

2.1.2.2 Elongation

After initiation, elongation factor eEF1A directs aminoacylated tRNAs in a GTP-dependent manner to the A-Site. Codon recognition triggers tRNA stabilization in the A-site and GTP hydrolysis by eEF1A. This enables the release of eEF1A from the ribosome and the tRNA to reach the evolutionary conserved peptidyl transferase center in the 60S subunit, a process called accommodation. The 60S catalyzes peptide bond formation leading to deacetylation of the P-site tRNA and the transfer of the nascent peptide chain to the A-site tRNA. Translocation of the ribosome along the mRNA is supported by elongation factor eEF2 and requires GTP. After translocation, GTP hydrolysis and release of eEF2-GDP, the ribosome is ready for a new cycle of elongation. (Dever & Green, 2012).

2.1.2.3 Termination

Termination of translation occurs when a stop codon (UAA, UGA, and UAG) reaches the A-site of the translating ribosome (called the Pre-Terminating Ribosome, PreTC) (Figure 2.2). The recognition of the stop codon is achieved by the synergy of the two eukaryotic release factors: eRF1 (sup45 in yeast) and eRF3 (sup35 in yeast) (Figure 2.6). The structure of a human ribosomal termination complex was solved by single particle cryo-electron microscopy and allowed the generation of an atomic model of eRF1/eRF3a bound to the ribosome (Des Georges et al., 2014; Brown et al., 2015). eRF1 recognizes the stop codon sequence in the A-site of 40S (the decoding center) and triggers peptidyl-tRNA hydrolysis (Dever & Green, 2012; Jackson et al., 2012). eRF3 is a ribosome-dependent GTPase which stimulates eRF1-mediated peptide release and reciprocally, eRF1 stimulates the GTP binding to eRF3 (Pisareva et al., 2006). Upon binding to eRF3a-GTP, eRF1 adopts a shape mimicking the tRNA structure. This allows the N-domain of eRF1 to reach deep into the decoding center of the small ribosomal subunit. Stop codon recognition in the decoding center leads to a rearrangement of both ribosomal subunits and yields the formation of a post-termination complex (PostTC). This was initially shown by a forward toeprint shift (of approximately 2 nucleotides) in a reconstituted *in vitro* system (Alkalaeva et al., 2006) (Figure 2.2).

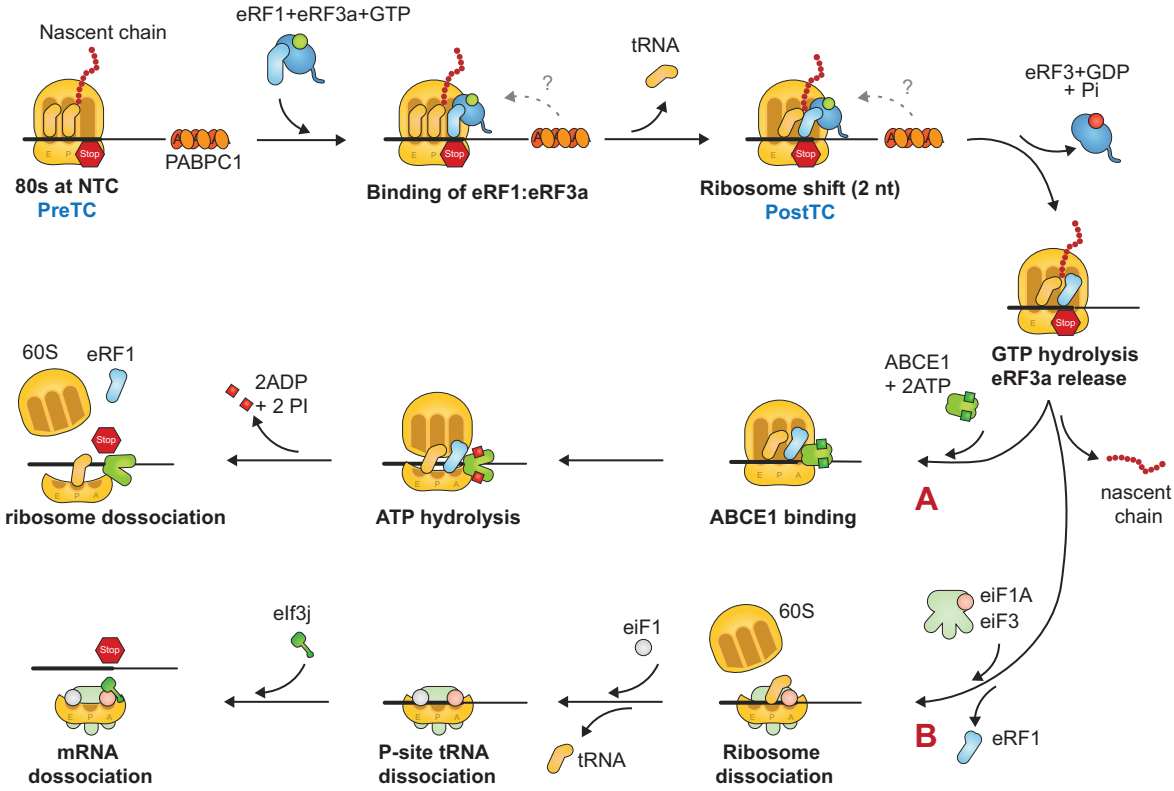

Figure 2.2: Overview of translation termination and recycling. *Translation is carried out by the 80S ribosome consisting of the small 40S subunit and the large 60S subunit. The stop codon in the A-site of pre-termination complex (PreTC) is recognized by eRF1 bound to eRF3a-GTP. Stop codon recognition and eRF1 accommodation in the ribosome result in a 2 nucleotide shit (forming post-termination complex - PostTC). Following GTP hydrolysis by eRF3a, eRF1 triggers the release of the nascent chain. These steps may be stimulated by the poly(A)-binding protein (PABPC1). Subunit dissociation and recycling are promoted by ABCE1 ATPase activity (A pathway). Alternatively eIF1A and eIF3 association with the postTC lead to ribosomal dissociation (B pathway). Subsequently, eIF1 and eIF3j allow the removal of the P-site tRNA and the mRNA from the 40S subunit. After recycling, the components are ready for a new round of translation. Adapted from (Alkalaeva et al., 2006; Pisarev et al., 2007, 2010; Schweingruber et al., 2013)*

Upon GTP hydrolysis, the eRF1 GGQ motif can be accommodated in the peptidyl transferase center of the large ribosomal subunit (60S) and triggers peptidyl-tRNA hydrolysis (Brown et al., 2015).

2.1.2.4 Recycling

Termination complexes need to be disassembled for the components to be reused for a new round of translation. In the current model of recycling of postTCs, eRF3a most likely dissociates from the ribosome following GTP hydrolysis while eRF1 remains bound. A highly conserved ATPase ABCE1 has been shown to mediate recycling of postTCs by interacting with ribosome-bound eRF1 (Figure 2.2A) (Pisarev et al., 2010; Franckenberg et al., 2012). Alternatively, using fully reconstituted *in vitro* translation, Pisarev and colleagues showed that eIF3, eIF1, eIF1A and eIF3j could mediate the recycling of postTCs under low Mg^{2+} conditions (Figure 2.2B). eIF3 promotes the splitting of ribosomal subunits. Subsequently, eIF1 and eIF3j can the release the tRNA from the P-site and mRNA from the 40S subunit, respectively (Pisarev et al., 2007).

2.1.3 mRNA degradation

mRNA decay affects not only aberrant mRNAs, but also normal mRNA transcripts which lead to fully functional proteins. Overall protein synthesis depends not only on the efficiency of transcription and translation but also on the rate of mRNA decay.

In eukaryotes, the main bulk of mRNAs in the cell are degraded via shortening of the poly(A) tail by a deadenylase protein complex such as CCR4-NOT or Poly(A)-specific nuclease (PARN)(Schoenberg & Maquat, 2012). Subsequently, either the 5' end cap is removed in a process called decapping, enabling decay from the 5' to the 3' direction by the exonuclease XRN1; or the unprotected 3' end can be degraded in the 3' to the 5' direction by a protein complex called the exosome. Alternatively to poly (A) tail shortening, mRNAs can be subjected to endonuclease cleavage followed by decay by XRN1 or the exosome. (Garneau et al., 2007). Components involved in 5' to 3' mRNA decay are localized in cytoplasmic loci called P-bodies. P bodies have been suggested to be important loci dedicated to mRNA storage and decay (Garneau et al., 2007). Interestingly, the main NMD factors UPF1, UPF2 and UPF3 have been found in these cellular sites (Eulalio et al., 2007) (section 2.3.2).

2.2 mRNA quality control

Every step of mRNA biogenesis is associated with mRNA quality control, which detects errors in the transcript. Mutations at the DNA or RNA level, or errors during

transcription or mRNA processing can cause aberrant mRNAs. Grossly mutated mRNAs are retained and degraded in the nucleus, whereas mRNAs containing more subtle errors are likely to be exported in the cytoplasm and engaged in translation. Such mRNAs encode potentially harmful proteins and thus need to be eliminated. RNA quality control pathways have been proposed to act along a unified principle (Doma & Parker, 2007). They can be viewed as a series of checkpoints where control and degradation proteins compete in a kinetic manner against the normal translation factors (Figure 2.3). Decades of research have highlighted the importance of mRNA surveillance as a mechanism not only to degrade aberrant mRNAs but also as an important means to fine-tune the expression of genes (Schoenberg & Maquat, 2012).

2.2.1 Nuclear RNA quality control

Grossly aberrant or improperly processed mRNAs are retained in the nucleus for degradation (Doma & Parker, 2007). Mechanisms have evolved to prevent the export of misprocessed transcripts: studies in yeast and mammals have revealed the existence of capping quality control mechanisms which allow for the specific removal of an unmethylated cap and which subsequently targets the pre-mRNA for degradation (Jiao et al., 2013; Doma & Parker, 2007).

The spliceosome cycle requires successive discrete conformation steps facilitated by ATPase/helicases (Villa et al., 2008; Bourgeois et al., 2016). Effective splicing is in direct competition with degradation, therefore mRNA features which slow down ATP hydrolysis by helicases, and thus spliceosome cycle, will subject these pre-mRNAs to quality control and degradation (Doma & Parker, 2007). Additional controls involve nuclear retention of unspliced transcripts (Hocine et al., 2010). 3' end processing of mRNAs is also rigorously controlled. In yeast, Rrp6p has been shown to be a critical factor for 3' end processing quality control. In deletion strains (rrp6Δ), hypoadenylated mRNAs, which would normally be targeted for nuclear degradation, were stabilized and exported. Similarly, mRNAs containing an aberrant cleavage or transcription termination site were stabilized (Allmang et al., 1999; Burkard & Butler, 2000).

Export into the cytoplasm is the last step of nuclear quality control, in which incorrectly processed mRNA can be detected and degraded. Misprocessed mRNAs cannot assemble into mRNP particles containing appropriate export factors, for example TREX or SR, and therefore are retained in the nucleus (Reed & Cheng, 2005; Katahira, 2012).

Aberrant mRNA retained in the nucleus can be degraded from 3' to 5' by the nuclear exosome, or from 5' to 3' by nuclear endonucleases. Dependent upon the defects present, mRNAs are degraded by either one of the mechanisms with differing efficiency. For example, defects in polyadenylation will be more efficiently degraded by

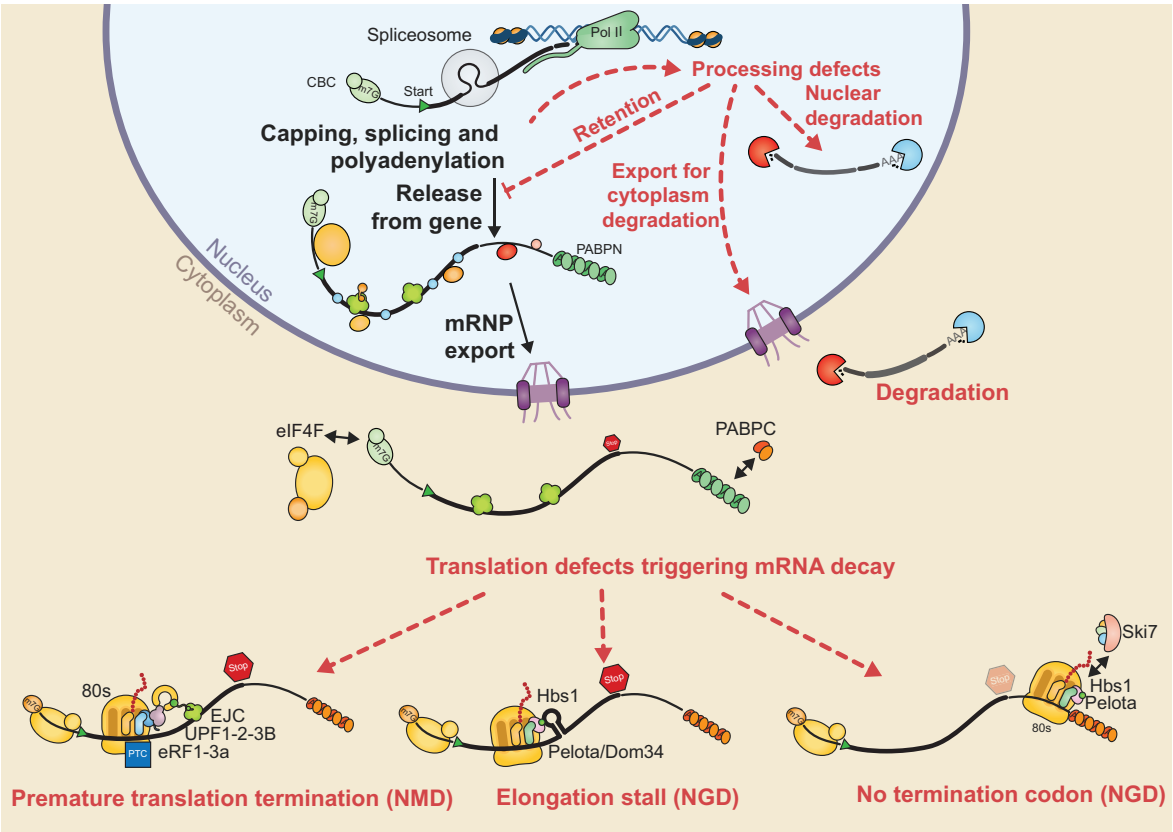

Figure 2.3: mRNA quality control pathways in the cell. *Defects can occur during pre-mRNA processing (capping, splicing and polyadenylation) in the nucleus. These can lead to retention of the pre-mRNA in the nucleus and nuclear degradation or export to the cytoplasm for degradation. During translation in the cytoplasm, errors in the mRNA can be detected by the mRNA surveillance pathways. A premature termination codon (PTC in blue box) is detected by the nonsense-mediated mRNA decay (NMD) pathway involving the eRF1, eRF3a and UPF1-UPF2-UPF3B proteins and triggered by the presence of an exon junction complex (EJC) in the 3'UTR. Stalled elongating ribosomes are recognized by the Pelota/Dom34-Hbs1 complex in no-go decay (NGD). The absence of a stop codon can be detected by the Ski7 complex or the Pelota/Dom34-Hbs1 complex in the non-stop decay (NSD). Adapted from (Doma & Parker, 2007; Schweingruber et al., 2013)*

the nuclear exosome (Garneau et al., 2007; Hocine et al., 2010).

2.2.2 Cytoplasmic mRNA quality control

Cytoplasmic mRNA surveillance pathways are classified by the type of mRNA targeted. Quality control depends on translation: nonsense mediated mRNA decay (NMD) targets mRNA with a premature termination codon (PTC); non-stop decay (NSD) specifically targets mRNA lacking a stop codon and no-go decay (NGD) targets mRNA with stalling secondary structures or sequences (Shoemaker & Green, 2012)(Figure 2.3).

Stalling of protein synthesis can result from secondary structures such as stem loops or certain sequences comprising rare codons or damaged RNA bases. In eukaryotes, the A-site of stalled ribosomes is recognized by NGD factors Pelota (Dom34 in yeast) and

Hbs1 (Shoemaker et al., 2010). Interestingly, Dom34 and Hsb1 share homology with release factors eRF1 and eRF3, suggesting that NGD involves a modified termination event (Shoemaker & Green, 2012). Following Hbs1 dissociation, ABCE1 associates with the Dom34 to promote recycling of the stalled ribosome (Pisareva et al., 2011; Shoemaker & Green, 2011; Young et al., 2015). The N-terminal domain of Hbs1 extends to the head of the 40S subunit and was proposed to act as an mRNA sensor and to stimulate the recycling of the NGD stalled ribosomes (Becker et al., 2011; Franckenberg et al., 2012).

NSD recognizes mRNAs which lack a proper termination context: for example, 3' end truncated mRNA which lacks a stop codon and a poly(A) tail or an mRNA missing only the stop codon. According to the current model in yeast, Ski7, another eRF3 paralogue, binds to the stalled ribosome and promotes mRNA degradation by interaction with the exosome (Shoemaker & Green, 2012). Moreover, it is postulated that the translation of the poly(A) tail into polylysine by the ribosome would lead to translation stalling due to the positively charged peptide in the exit tunnel. In such a context similar to NGD, Dom34 and Hsb1 are recruited to the stalled translation machinery (Ito-Harashima et al., 2007).

mRNAs containing PTCs are recognized and degraded via the NMD pathway which is discussed in the next section.

It is worth noting that the recognition of NGD targets and the subsequent recycling of stalled ribosomes is currently the best understood, compared to the other surveillance pathways.

2.3 Nonsense mediated mRNA decay

Nonsense mRNA decay was initially discovered in *Saccharomyces cerevisiae* and *Caenorhabditis elegans* over 30 years ago (Losson & Lacroute, 1979; Maquat et al., 1981). The core NMD machinery is conserved from yeast to human (Culbertson & Leeds, 2003). NMD specifically recognizes and degrades transcripts containing a premature termination codon (PTC). Mutations in the core NMD factor genes are linked to neurodevelopmental disorders, mental disorders and are associated with specific tumor types (Ottens & Gehring, 2016). Beyond its clinical significance, NMD serves as a posttranscriptional regulator of gene expression and plays a role in important cellular processes such as development and differentiation (Weischenfeldt et al., 2008; Avery et al., 2011; T. Li et al., 2015; Lou et al., 2014), cellular stress response (Gardner, 2010; Sakaki et al., 2012), neural activity (Giorgi et al., 2007; Colak et al., 2013) and immunity (Gloggnitzer et al., 2014) (reviewed by (S. Lykke-Andersen & Jensen, 2015; Ottens & Gehring, 2016)).

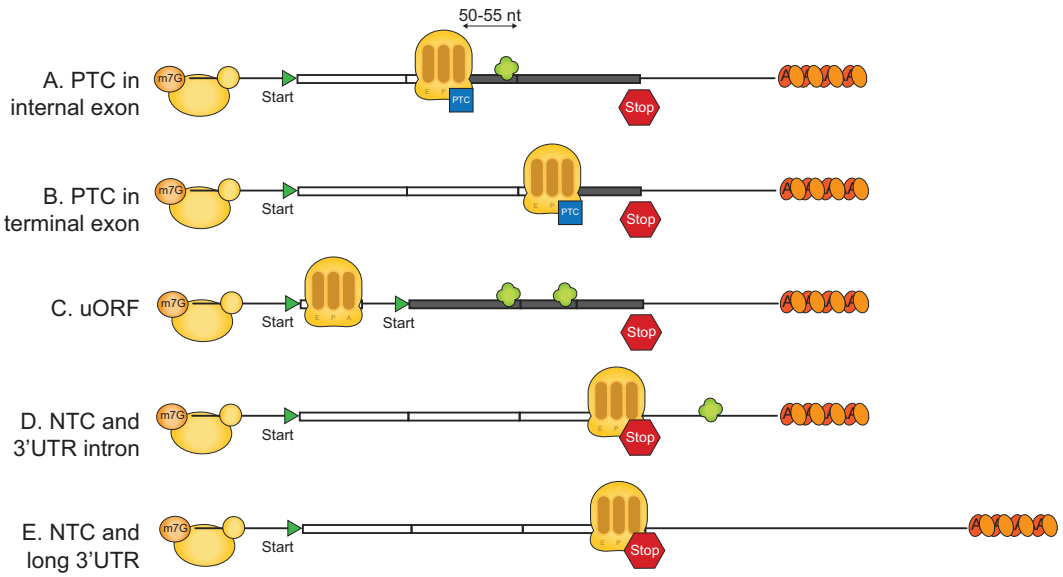

Figure 2.4: mRNAs triggering the NMD pathway. ***A.*** *PTCs in an internal exon are the classical example for an NMD substrate in mammals. Such PTC would elicit NMD if it is located ~50-55 nt upstream from an EJC which remain bound downstream of the PTC (see section 2.3.4).* ***B.*** *PTCs in the terminal exon are typically found in yeast, although it can also be found in higher eukaryotes.* ***C.*** *Upstream ORFs (uORFs) located 5' of the main ORF are known to trigger NMD. In this case, EJCs are bound to the downstream mRNA and there is an unusually long 3' UTR.* ***D.*** *3'UTR introns will result in the deposition of an EJC downstream of the normal termination codon (NTC) and trigger NMD.* ***E.*** *Long 3' UTRs are known to activate the NMD pathways in multiple organisms. mRNAs are represented by black lines: translated exons are shown as white boxes and untranslated exons as grey boxes. 5' and 3' UTRs are represented by black lines. The start codon is illustrated as a green arrow, the stop codon as a red sign and PTC as a blue square. The 5' cap (m7G) is bound to eIF4F complex (yellow) and the poly(A) tail is complexed with PABP (orange). The translating ribosomes are shown in yellow and the EJCs in green. Adapted from (Schweingruber et al., 2013)*

2.3.1 NMD Substrate

NMD was originally thought to trigger the degradation only of PTC-containing mRNAs. PTCs can arise at the DNA level by mutations or at the RNA level due to transcription or mRNA processing errors, which occur mainly during splicing. 75% of human pre-mRNAs are alternatively spliced (Johnson, 2003) and 45% of those can generate at least one isoform, which will be degraded by NMD (Lewis et al., 2003). Transcriptome-wide experiments have shown that NMD is also triggered by 5-15 % of normal transcripts, whereby the termination codon is interpreted by the cell as "premature" (Figure 2.4) (He et al., 2003; Guan et al., 2006; Mendell et al., 2004; Tani et al., 2012). This applies to the termination codons of some upstream open reading frames (uORFs), termination codons upstream of 3' UTR introns or unusually long 3' UTRs. This can also include termination codons introduced into a transcript by somatic rearrangements during early stages of T and B cell maturation, ribosomal frameshifting, or mRNA editing (Rehwinkel et al., 2006; Schweingruber et al., 2013; Fatscher et al., 2015).

Translation is indispensable for the recognition of a PTC, and NMD is triggered by an aberrant termination event (Shoemaker & Green, 2012; Kervestin & Jacobson, 2012). Decades of research have unveiled common features possessed by NMD substrates (Figure 2.4). During the translation of NMD targets, termination often occurs in an unusual position, either too far from the poly(A) tail and downstream RNPs, or with an EJC located in the 3'UTR downstream of the termination codon. NMD activation is discussed in section 2.3.6.

2.3.2 Core UPF proteins

Key factors for NMD were identified in early genetic screens in *Saccharomyces cerevisiae* as the Upstream frameshifting genes products: Upf1p, Upf2p and Upf3p (known in human as UPF1, UPF2 and UPF3 respectively)(Leeds et al., 1992). These NMD core proteins are conserved from yeast to human (Figure 2.5). UPF1 and UPF2 are cytoplasmic proteins although UPF2 appears to have a perinuclear localization. UPF3 shuttles between the nucleus and the cytoplasm (J. Lykke-Andersen et al., 2000). UPF proteins interact with each other and are associated with mRNAs, the translation machinery and numerous other factors (He et al., 1997; Atkin et al., 1997; Kashima et al., 2006; Melero et al., 2012).

2.3.2.1 UPF1

UPF1 is a superfamily I 5' to 3' RNA helicase and RNA-dependent ATPase (Bhattacharya et al., 2000). UPF1 is the most conserved NMD factor (48.5 % identity between yeast

and human) and appears to be the central effector in the pathway (Culbertson & Leeds, 2003). UPF1 contains a C-terminal domain, a helicase domain formed by an ATPase motif surrounded by two RecA-like domains and an N-terminal cysteine- and histidine- (CH) rich region (Figure 2.5). In the absence of UPF2, the CH domain interacts with the helicase domain thereby preventing untimely helicase and ATPase activities of UPF1 (Clerici et al., 2009; Chakrabarti et al., 2011; Chamieh et al., 2008). Furthermore, in yeast, the CH domain has been reported to bind to the ribosomal protein Rps26 (Min et al., 2013), to recruit the decapping enzyme Dcp2 (He & Jacobson, 2015a). Phosphorylation and dephosphorylation cycles of UPF1 at N- and C-terminal S/T-Q sites are essential for NMD and seem to be a prerequisite for the recruitment of the decay inducing enzymes SMG6 and SMG5/7 (see section 2.8)(Durand et al., 2016). The discrimination between early termination-related and late mRNP remodeling/degradation-related functions of UPF1 is supported by the timing of the phosphorylation by SMG1 kinase and the accessory factors SMG8 and SMG9 (see 2.3.6).

2.3.2.2 UPF2

UPF2 is described as a ring-like scaffold protein and acts by bridging UPF1 at the terminating ribosome and UPF3B, which is bound to a downstream EJC (Melero et al., 2012). 20.8 % of the UPF2 protein sequence is conserved between human and yeast protein (Culbertson & Leeds, 2003). It is composed of three 'conserved middle domain of eIF4G domains' (MIF4G) (Figure 2.5). MIF4G is a common domain found in mRNA-associated proteins such as CBC80 and eIF4G. While the function of the first two MIF4G domains in UPF2 remains enigmatic, the third MIF4G domain is known to interact with a region in the RNA-Recognition Motif-like (RRM-like) domain of UPF3B (Kadlec et al., 2004; Clerici et al., 2014). UPF2 C-terminal domain interacts with UPF1 CH domain and activates the helicase and ATPase function of UPF1 (Clerici et al., 2009; Chakrabarti et al., 2011).

Initially, UPF2 was thought to be a platform for the recruitment of SMG1-8-9 and to promote UPF1 phosphorylation (Melero et al., 2014). However, recent findings indicate that the presence of UPF2, rather than activating the kinase, destabilizes SMG-1–8–9-UPF1 leading to release of UPF1 from the complex (Deniaud et al., 2015). Recently, human UPF2 has been shown to directly interact with eRF3a (but not with eRF1) through a protein region known as the UPF3B interaction domain, which overlaps with MIF4G domain 3 (López-Perrote et al., 2015). UPF2 binds strongly to UPF3B and, consequently the addition of UPF3B could displace eRF3a from UPF2.

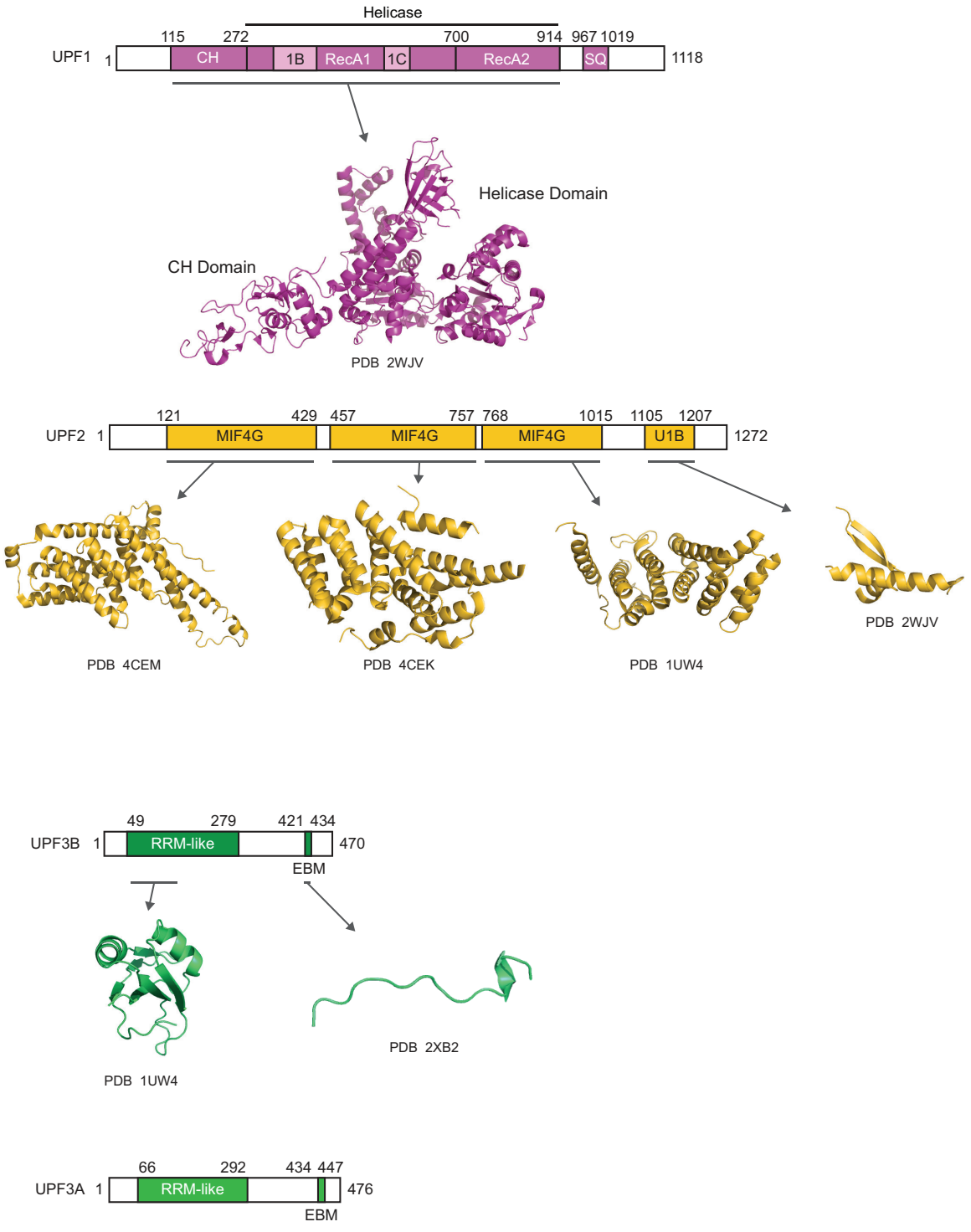

Figure 2.5: Schematic representation of human core NMD factors UPF1, UPF2, UPFB and UPF3A. *Known crystal structures are included with their respective PDB ID and mapping regions. SQ: Serine Glutamine rich domain; CH: Cysteine Histidine rich domain, Helicase domain : RecA1 and RecA2 translocate the mRNA, 1B and 1C are involved in RNA binding and ATP hydrolysis ; MIF4G: middle domain of eIF4G; U1B: UPF1-binding domain; RRM-like: RNA Recognition Motif like domain; EBM: Exon junction complex-binding motif. Numbers indicated the amino acid boundaries of the different domains. Adapted from (Clerici, 2009)*

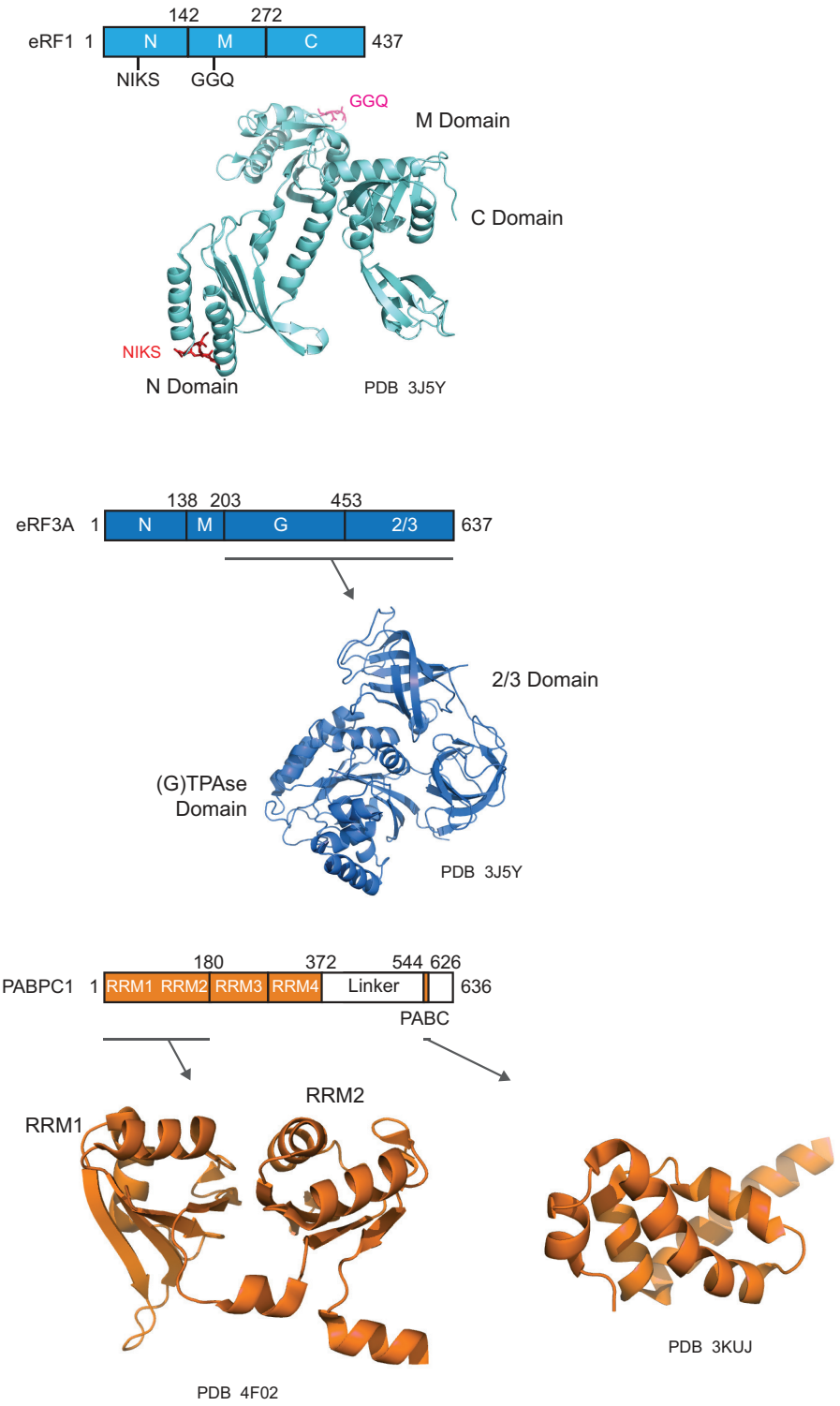

Figure 2.6: Schematic representation of human termination factors eRF1, eRF3a and PABPC1. *Known crystal structures are included with their respective PDB ID and mapping regions. N: N-terminal domain; M: Middle domain; C: C-terminal domain; 2/3: 2 and 3 domains; G: GTPase domain; RRM: RNA Recognition Motif; PABC: Poly(A) binding protein C-terminus. The NIKS motif in eRF1 is involved in stop codon recognition and the GGQ motif is required for peptide release. Numbers indicated the amino acid boundaries of the different domains. Adapted from (Clerici, 2009)*

2.3.2.3 UPF3

UPF3 is a basic protein and is found in two paralogues in higher eukaryotes: UPF3A and UPF3B (or UPF3X as it is expressed on the X chromosome) (J. Lykke-Andersen et al., 2000; Serin et al., 2001). In contrast, yeast and invertebrate express only one protein (16.8 % identity between yeast and human proteins) (Culbertson & Leeds, 2003). UPF3A has also two isoforms : UPF3AL and UPF3AS. The latter lacks exon4 and cannot interact with UPF2 (Serin et al., 2001). UPF3 is a shuttling nucleocytoplasmic protein which contains a N-terminal RRM-like domain involved in the interaction with UPF2 (Kadlec et al., 2004)(Figure 2.5). The C-terminal region of the protein is predicted to be largely disordered (see appendixB.3). A 13 amino acid motif in the C-terminal of the protein is conserved in higher eukaryotes and between UPF3A and UPF3B isoforms. This motif allows binding to a composite surface on the EJC formed by eIF4A3, MAGOH and EJC factor Y14 (Gehring et al., 2003; Buchwald et al., 2010). This domain is lacking in yeast, flies and worms. In higher eukaryotes, UPF3B is thought to associate with the EJCs during splicing and to be exported to the cytoplasm together with mRNAs (J. Lykke-Andersen et al., 2000; Kim, 2001).

UPF3B has been reported to stimulate translation during tethering experiments. This effect could not be observed with UPF3BΔ49-279 which was missing the RRM-like domain and was independent of UPF2 and Y14 binding (Kunz et al., 2006). The loss of UPF3B expression is correlated with an upregulation in UPF3A levels, leading to the hypothesis that UPF3A can compensate for UPF3B activity (Chan et al., 2009). This functional redundancy would allow a cell specific fine-tuning of the NMD activation. UPF3A is considered as a weak NMD activator but this hypothesis has recently been challenged by a study suggesting that UPF3A is inhibiting NMD by sequestering UPF2 away from the other NMD factors (Shum et al., 2016).

By binding to the EJC and UPF2, UPF3B has been proposed to bridge downstream RNPs to the translation termination complex at a PTC. However, the exact function of UPF3 remains enigmatic, especially its role in EJC-independent NMD (Bühler et al., 2006).

2.3.3 Normal vs aberrant termination of translation

Despite a decade of research, the mechanism of discrimination between NTCs (normal termination codon) and PTCs is still poorly understood. Evidence has accumulated that the recognition of a PTC by the eukaryotic release factors is kinetically different from the recognition of an NTC (Amrani et al., 2004; He & Jacobson, 2015b). NMD factors were shown to bind to terminating ribosomal complexes at a PTC (Kashima et al., 2006; López-Perrote et al., 2015). In yeast, eRF1 (sup45), Upf2p and Upf3p but not Upf1p compete for eRF3 (sup35) binding. Upf1p binds to eRF1 and eRF3, and

the interaction inhibits the ATPase activity of Upf1p (Wang et al., 2001).

Eukaryotic eRF1 mimics the L-shape of tRNA. It is composed of 3 domains: N-terminal (N), middle (M), and C-terminal (C) domain (Figure 2.6). The N domain is involved in the recognition of the stop codon through the highly conserved NIKS and YxCxxxF motifs (Kryuchkova et al., 2013). The M domain of eRF1 contains a universally conserved Gly-Gly-Gln (GGQ) motif that reaches into the ribosomal peptidyl transferase center to trigger the peptidyl-tRNA hydrolysis. The mutation of G183 (G180 in yeast) to an alanine residue in the GGQ motif (AGQ mutant) has been shown to stall termination. This mutant can still bind to the ribosomes and eRF3, but it cannot trigger the release of the nascent chain (Frolova et al., 1999). eRF1 and eRF3 interact through their respective C-terminal region (Cheng et al., 2009). Yeast expresses one eRF3 protein, but two isoforms exist in higher eukaryotes: eRF3a and eRF3b. eRF3a has been shown to be the main effector in termination (Chauvin et al., 2005), and consists of 3 domains: N-terminal (N) domain, GTPase (G) domain and beta barrels 2/3 domains (Figure 2.6). The GTPase activity of eRF3a is stimulated by eRF1 and the ribosome. The N domain was initially thought to be dispensable for termination, but has since been shown to be required for the interaction with the Poly(A)-Binding Protein (PABPC1 and Pab1p in human and yeast respectively) (Kozlov & Gehring, 2010).

PABPs consist of an N-terminal region comprising 4 RNA-Recognition motifs (RRMs) and a C-terminal region, called MLLE (or PABC) (Figure 2.6). The MMLE domain mediates the binding to the human eRF3a N-terminal, PABP-binding motif 2 (PAM2) (Kozlov & Gehring, 2010). In yeast, despite of the lack of a PAM2 motif, eRF3 has some ability to bind to Pab1p as well (Kervestin et al., 2012; Xie et al., 2014; Roque et al., 2014).

The normal termination process is suggested to be fast and efficient (as described in section 2.1.2.3 and Figure 2.2), in contrast to termination at a PTC. An abnormal pausing at a PTC, attributed to the absence of downstream termination-promoting factors such as PABPC1, would allow enough time for the core NMD factors to assemble on the terminating ribosome (Amrani et al., 2004; Singh et al., 2008). UPF1 and PABPC1 are proposed to compete for eRF3 binding on the terminating ribosome (Singh et al., 2008). This is suggested to be the basis for discrimination between a PTC and an NTC (Amrani et al., 2004; P. V. Ivanov et al., 2008). This model is supported by the fact that PABPC1 can bind to eRF3a and that tethering of PABPC1 downstream of PTCs as well as shortening the 3' UTR interferes with NMD and stabilizes the mRNA (Kozlov & Gehring, 2010; Joncourt et al., 2014; Fatscher et al., 2014). However, PABPC1 interaction with eRF3a N-terminal may be important for post-termination and reinitiation but not for mRNA decay (Joncourt et al., 2014; Durand & Lykke-Andersen, 2013; Roque et al., 2014). Moreover, UPF1 was reported to bind to eRF1

and eRF3 and to inhibit termination of translation(Wang et al., 2001; P. V. Ivanov et al., 2008).

More recently, PABPC1 has been proposed to modulate UPF1 ATPase activity to promote the release of UPF1 from non-target mRNA (S. R. Lee et al., 2015). However, this model cannot explain how mRNAs without poly(A) tails are subjected to NMD and how transcripts with a long 3'UTR evade NMD (Singh et al., 2008).

2.3.4 NMD links splicing and translation

The EJC core is composed of the proteins eIF4A3 (eukaryotic initiation factor 4A3), MAGOH, Y14 (also known as RNA-binding motif 8A) and MLN51 (metastatic lymph node 51). EJCs are deposited 24 nt upstream of an exon-exon junction during splicing (Le Hir et al., 2001). Multiple observations have led to propose the EJC as an NMD activator (Hir et al., 2015). Mammalian NMD is enhanced if a PTC is located at least 50-55 nt upstream of an exon junction (Nagy & Maquat, 1998; Thermann et al., 1998). NMD factors UPF3B, and possibly UPF2, are associated with the EJC core components (Kim, 2001; J. Lykke-Andersen et al., 2001; Buchwald et al., 2010). In addition, RNA degradation can be artificially enhanced by tethering EJC components downstream of an NTC (J. Lykke-Andersen et al., 2001; Gehring et al., 2003, 2005). Vice versa, PTC-containing mRNAs can be stabilized by the elimination of the EJC core components (Shibuya et al., 2004; Palacios et al., 2004). A model was thus proposed in which EJCs deposited at exon-exon junctions would be displaced from the mRNA by elongating ribosomes during the pioneer round of translation(Gehring et al., 2009). EJCs found downstream of a PTC cannot be removed from the mRNA, explaining the '50-55 nt boundary rule' for NMD activation(Nagy & Maquat, 1998). UPF1, in complex with the release factors at the termination site, is suggested to be subsequently activated by UPF2 and UPF3 bound to the EJC.

However, the EJC cannot be the only criterion for NMD activation: transcriptome-wide studies have shown that 50 % of the EJCs are distributed on non-canonical locations on the mRNA (Singh et al., 2012; Saulière et al., 2012), that the EJC promotes the translation of spliced transcripts (Nott et al., 2004; Chazal et al., 2013) and that the EJC is absent in lower organisms (such as yeast). In addition, this model fails to explain NMD of intron-less mRNAs (EJC-independent NMD) (Rajavel & Neufeld, 2001; Bühler et al., 2006). The EJC is therefore considered as a non-essential enhancer of NMD.

2.3.5 UPF1 phosphorylation triggers NMD

In addition to the core UPF proteins, in higher eukaryotes, a set of additional proteins is needed for the activation of the NMD pathway. SMG1 is a phosphatidylinositol 3

kinase-related kinase (PIKK) and phosphorylates four S/TQ sites on UPF1 (Yamashita et al., 2001). This is considered to be a key step in the activation of the NMD pathway and the point of no return for the degradation of the mRNAs by the NMD machinery. SMG8 and SMG9 are thought to stabilize SMG1, to modulate its kinase activity, and to assist in the selection of phosphorylation sites (Melero et al., 2014; Deniaud et al., 2015). SMG1 can be immunoprecipitated in a complex including UPF1, eRF1 and eRF3a forming the so-called SURF complex (Figure 2.7) (Kashima et al., 2006). UPF1 phosphorylation has been proposed to occur in the, still hypothetical, complex named DECID which forms when the SURF complex interacts with UPF2 and UPF3 bound to the downstream EJC (Kashima et al., 2006). Structural and biochemical studies have shown that the UPF1 helicase domain interacts with the SMG1 kinase domain and that the UPF2 MIF4G-3 domain binds to SMG1. Different binding sites in the MIF4G-3 domain of UPF2 interact with SMG1 and UPF3B, and thus there is the possibility of the formation of a DECID complex (Clerici et al., 2014; Melero et al., 2014). Interestingly, Upf1p and Upf2p phosphorylation were observed in yeast, however there is no direct evidence that phosphorylation cycles have a direct influence on the activity of yeast NMD factors (Wang et al., 2006).

Numerous additional factors have been linked to human NMD including DHX34, NBAS, RUVBL1, RUVBL2, MOV10, GNL2 and SEC13 (Longman et al., 2013; Izumi et al., 2010; Gregersen et al., 2014; Casadio et al., 2015). Recent evidence indicates that DHX34, an RNA helicase of the DEAH box family, could function as a scaffold protein to help in the recruitment of UPF1 to SMG1 (Hug & Cáceres, 2014; Melero et al., 2016).

2.3.6 Model for NMD activation

Slow translation termination at a PTC can be attributed either to the delay in recruitment of factors promoting fast termination (such as PABPC1) or to the presence of aberrant mRNPs in the 3'UTR which enhance NMD (specifically EJCs). All current models of NMD consider UPF1 as the main effector interacting with the release factors and the ribosome. However, these models propose different strategies for NMD activation. It is now understood that different branches of NMD exist, depending on context of the organism, cell and transcript. Different activation strategies for NMD have been unveiled. Some NMD events are independent of UPF2 (Gehring et al., 2003; Fanourgakis et al., 2016), of UPF3B (Chan et al., 2007) or of the EJC (Bühler et al., 2006). UPF3B has been proposed to elicit UPF2-dependent and -independent NMD depending on the EJC context (Gehring et al., 2005). Whilst the exact molecular mechanism behind the different branches of NMD remains enigmatic, there is a consensus model, described below, which can be applied to lower organisms, but also higher organisms

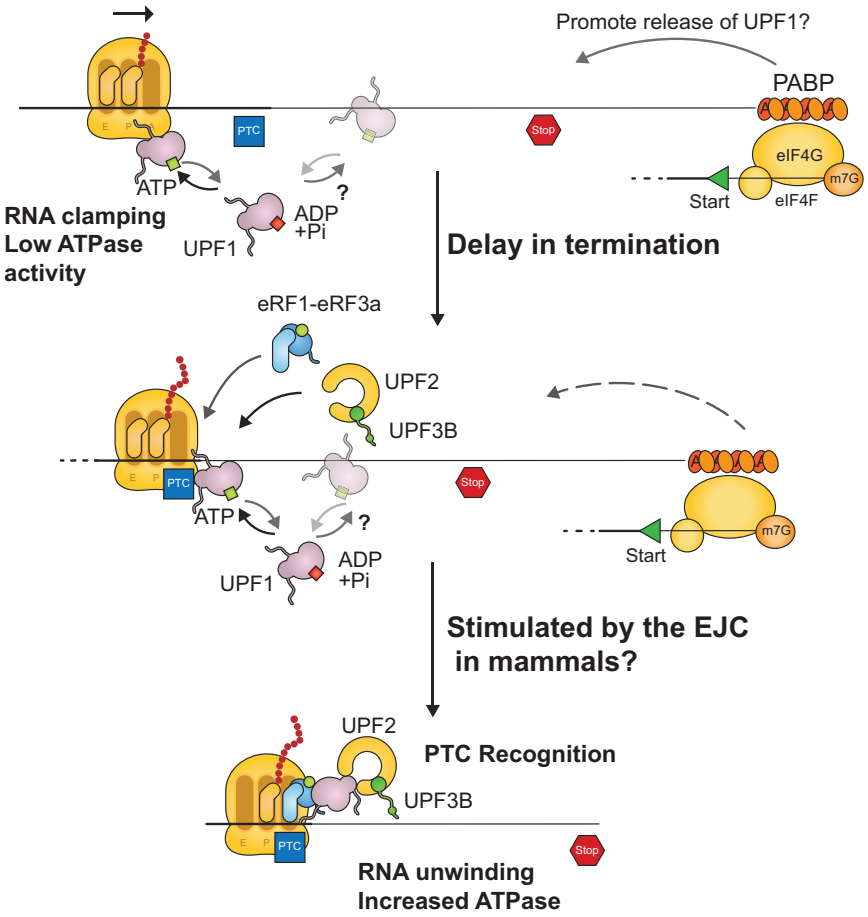

Figure 2.7: Current general model for NMD activation. *UPF1 associates transiently with the elongating ribosome and possibly with the mRNA. Release from the mRNA is modulated by the ATPase activity of UPF1 and possibly PABP bound to the poly(A) tail. Termination is slowed down at a premature termination codon (PTC) due to a delay in the recruitment of the release factors allowing UPF2 and UPF3 to bind to UPF1. This step may be promoted in mammalian by the presence of the exon junction complex (EJC) downstream of a PTC. PTC recognition stabilizes UPF1 on the targeted mRNA. UPF2- and UPF3-binding switches UPF1 to the RNA-unwinding mode and increases its ATPase activity. Adapted from (He & Jacobson, 2015b)*

with an additional layer of complexity.

2.3.6.1 PTC recognition in mammals

Transcriptome-wide studies have remodeled the understanding of UPF1 association with mRNA (Hogg & Goff, 2010; Zünd et al., 2013). It has been shown that UPF1 preferentially binds to transcripts containing NMD-inducing 3' UTRs. UPF1 localizes more abundantly to the 3' UTR of these transcripts, in a length, but not a sequence-dependent manner. This association is translation-independent, but it has been proposed that elongating ribosomes are able to displace UPF1 from the mRNA. This suggests that all mRNAs are primed for NMD, but only NMD-targets can activate UPF1 for NMD. In mammals, the EJC is likely to enhance the activation of UPF1 by acting as a platform for the recruitment of UPF3B and/or UPF2. The preferential binding of UPF1 to the NMD target has been attributed to the ATPase activity of UPF1 (Kurosaki et al., 2014; S. R. Lee et al., 2015). ATPase deficient mutants have been found to associate indifferently to NTC- or PTC-containing mRNAs compared to wild-type (WT) UPF1. In addition, the ability of UPF1 WT to bind PTC-containing transcripts can be modulated by artificial tethering of PABPC1 to the mRNA, but the ability of the ATPase mutant cannot be modulated (S. R. Lee et al., 2015). This concept was introduced only few years ago, and it is still debated whether UPF1 associates with mRNA regardless of translation or whether UPF1 associates transiently with elongating ribosomes (He & Jacobson, 2015b) and whether PABPC1 has a direct effect on NMD or if this effect is mediated by eIF4G (Durand & Lykke-Andersen, 2013; Joncourt et al., 2014).

2.3.6.2 PTC recognition in lower eukaryotes

The conservation of the core NMD factors UPF1, UPF2 and UPF3 from yeast to human points to a fundamental mechanism conserved through evolution. Deletion of the genes for these factors promotes read-through at PTCs (Maderazo et al., 2000; Wang et al., 2001). Interestingly, NMD factors partially regulate Mg^{2+} uptake by the cell, which in turn modulates read-through (Johansson & Jacobson, 2010). The regulation of Mg^{2+} uptake may reflect a function of the core NMD factors at an early stage of aberrant termination, possibly stimulating the recruitment of the release factors or their activity (He & Jacobson, 2015b). The deletion of the core NMD factors is also linked to defects in reinitiation and ribosome recycling (Ghosh et al., 2010) indicating a pivotal role in these processes at a later stage of translation termination at a PTC. This dual function has been attributed to different levels of ATPase activity of UPF1 and to the presence of UPF2 and UPF3 at a later stage. During elongation, UPF1 may transiently associate with the ribosome or the mRNA (Figure 2.7). Modulation of UPF1 ATPase,

in clamping conformation, would allow the discrimination between target and non-target mRNAs (S. R. Lee et al., 2015). Recruitment of UPF2 and UPF3 stabilizes UPF1 on the termination complex, because of a delay in termination (He & Jacobson, 2015b). In this complex, UPF1 ATPase activity would be increased and its helicase would switch from a clamping to an unwinding mode (Chakrabarti et al., 2011). In this conformation UPF1 is likely to promote subsequent steps in termination and recycling (Kervestin & Jacobson, 2012).

2.3.7 NMD degradation of mRNA

NMD-targeted transcripts can follow one out of several routes to degradation. In yeast, mRNAs are mainly degraded via deadenylation-independent decapping by Dcp1/2 and 5' to 3' digestion by Xrn1(Muhlrad & Parker, 1999; He & Jacobson, 2001). In humans, phosphorylated UPF1 recruits SMG6 and SMG5-7 which then recruit the mRNA degradation factors (Figure 2.8)(Durand et al., 2016). SMG5, SMG6 and SMG7 are conserved in metazoans (except SMG7 in *Drosophila melanogaster*) (Gatfield et al., 2003; Okada-Katsuhata et al., 2012; Chakrabarti et al., 2014). Depending on the presence of SMG6 or SMG5-7, mRNAs can be subjected either to deadenylation-dependent decapping or to endonucleolytic cleavage, followed by degradation by the exosome and Xrn1 (Lejeune et al., 2003; Huntzinger et al., 2008; Eberle et al., 2009).

In the first decay route, phosphorylated UPF1 recruits the SMG5-7 heterodimer to the mRNA (Fukuhara et al., 2005; Chakrabarti et al., 2014). SMG7 can promote deadenylation by interaction with the CCR4-NOT complex. Interestingly, the CCR4-NOT interaction with PABPC1 could be favored by the presence of a long 3' UTR as found in NMD substrates (Kozlov & Gehring, 2010). After deadenylation, decapping is performed by Dcp1/2, followed by 5' to 3' exonucleolytic digestion by Xrn1 (Unterholzner & Izaurralde, 2004; Loh et al., 2013). Moreover, UPF1 can interact directly with Dcp2 to promote decapping (He & Jacobson, 2001).

In the second decay pathway, UPF1 appears to initiate the decay by recruiting SMG6, via phosphorylated and un-phosphorylated protein regions of UPF1 (Okada-Katsuhata et al., 2012; Chakrabarti et al., 2014). UPF1 is able to recruit SMG6 while it is still associated or near the stalled ribosome (Eberle et al., 2009). SMG6 exhibits nuclease activity due to an N-terminal PIN (PilT N-terminus) domain (Glavan et al., 2006) and cleaves the target mRNA in the vicinity of the PTC, generating 5' and 3' fragments which are degraded by the exosome and Xrn1 respectively (Huntzinger et al., 2008; Eberle et al., 2009; Boehm et al., 2014). SMG6 and UPF3B contain an exon junction complex-binding motif (EBM), and both proteins compete for EJC binding. Due to the fact that UPF3B binds with stronger affinity than SMG6 to the EJC and that UPF3B is recruited during splicing, it has been proposed that UPF3B dissociates

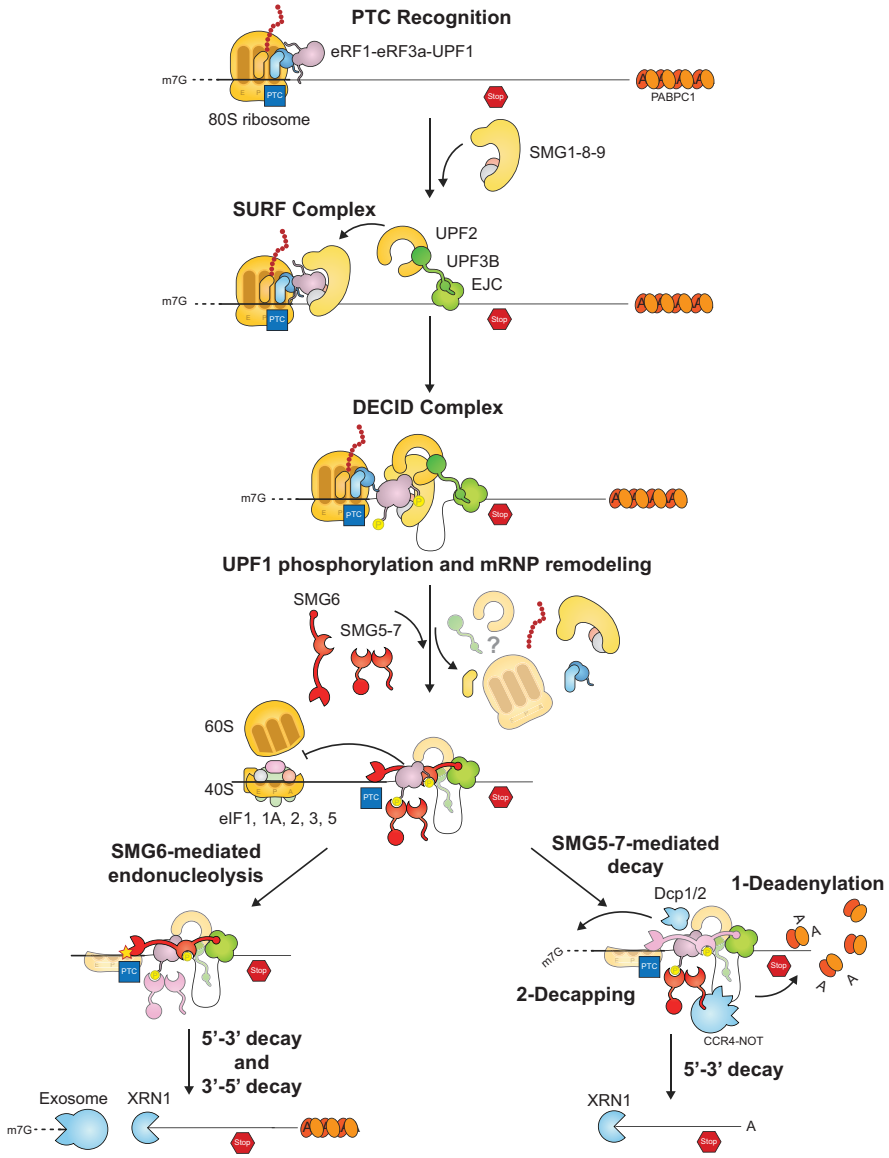

Figure 2.8: Model for mRNA decay by NMD in mammals. *Premature termination codon (PTC) recognition results in the recruitment of SMG1-8-9 to the terminating ribosome with the release factors and UPF1 bound, forming the SURF complex. Subsequently, UPF2-UPF3B bound to the exon junction complex (EJC) joins the SURF complex to form the DECID complex resulting in UPF1 phosphorylation (Yellow P) by SMG1-8-9. UPF1 phosphorylation triggers the dissociation of the DECID complex. Subsequently, SMG6 and SMG5-7 are recruited by UPF1 phosphorylation sites. It is unknown whether 40S ribosome, UPF2 and UPF3B are part of this complex. Phosphorylated UPF1 represses initiation of translation by inhibiting the formation of 80S ribosomes. Decay can be carried out by two routes. SMG6 endonucleolytic activity can cleave the mRNA in the vicinity of the PTC allowing the digestion of the mRNA from the 5' to 3' end by XRN1 and from the 3' to 5' end by the exosome. Alternatively, SMG7 can promote deadenylation by the CCR4-NOT complex. The decapping complex, Dcp1/2, cleaves the 5' cap allowing decay 5' to 3' end by XRN1. Adapted from (Isken et al., 2008; Schweingruber et al., 2013)*

from the EJC prior to the subsequent binding of SMG6 (Kashima et al., 2010).

Recent studies have identified an additional route for mRNA decay. Proline-rich nuclear receptor coregulatory protein 2 (PNRC2) can interact with UPF1 and DCP1 enabling a polyadenylation-independent decapping (Cho et al., 2009). The inactivation of SMG5, SMG6 and SMG7 leads to the accumulation of phosphorylated UPF1 indicating that these proteins are involved in the dephosphorylation of UPF1. SMG5-7 is thought to be responsible for the recruitment of the phosphatase (Ohnishi et al., 2003). Protein Phosphatase 2A (PP2A) allows UPF1 dephosphorylation which is critical for functional cycles of NMD. Consistently, cell treatment with a PP2A inhibitor suppresses NMD (P. V. Ivanov et al., 2008).

2.3.8 NMD and human diseases

2.3.8.1 Disorders associated with NMD factor mutations

Several mutations in UPF3B are linked to X-linked intellectual disability (XLID), autism and schizophrenia (Tarpey et al., 2007; Laumonnier et al., 2010; Addington et al., 2011; Lynch et al., 2012; Xu et al., 2013). Some mutations result in the introduction of a PTC in the UPF3B transcript, triggering degradation by NMD (Tarpey et al., 2007; Laumonnier et al., 2010). Missense mutations observed in patients with neurodevelopmental disorders are mostly located between amino acids 160 to 366, a UPF3B region with unknown function. For example, tyrosine 160 is conserved between vertebrates and flies in UPF3B, in human UPF3A and in the *C.elegans* ortholog of UPF3. The mutation of this residue in human UPF3B is linked to nonsyndromic XLID and autistic features (Tarpey et al., 2007). In addition, this residue is thought to be critical for UPF3B NMD function, especially in neural stem cells, as shown by tethering experiments (Alrahbeni et al., 2015).

It is thought that UPF3B is widely expressed in neurons and dendritic spines and thus NMD is critical for neural development (Laumonnier et al., 2010; Alrahbeni et al., 2015). This idea is also supported by the fact that *de novo* mutations in UPF2 have been identified in patients with schizophrenia (Gulsuner et al., 2013).

Somatic mutations in UPF1 have been identified in pancreatic adenosquamous carcinoma (ASC) tumors and could not be detected in normal pancreatic cells (Liu et al., 2014). The effect of UPF1 mutations in the cell remains unclear, but they are likely to disturb proper NMD functioning.

2.3.8.2 Clinical relevance of NMD

Mutations leading to a PTC account for approximately 30% of all known disease-associated mutations (reviewed by (Bhuvanagiri et al., 2010)). However, NMD can be

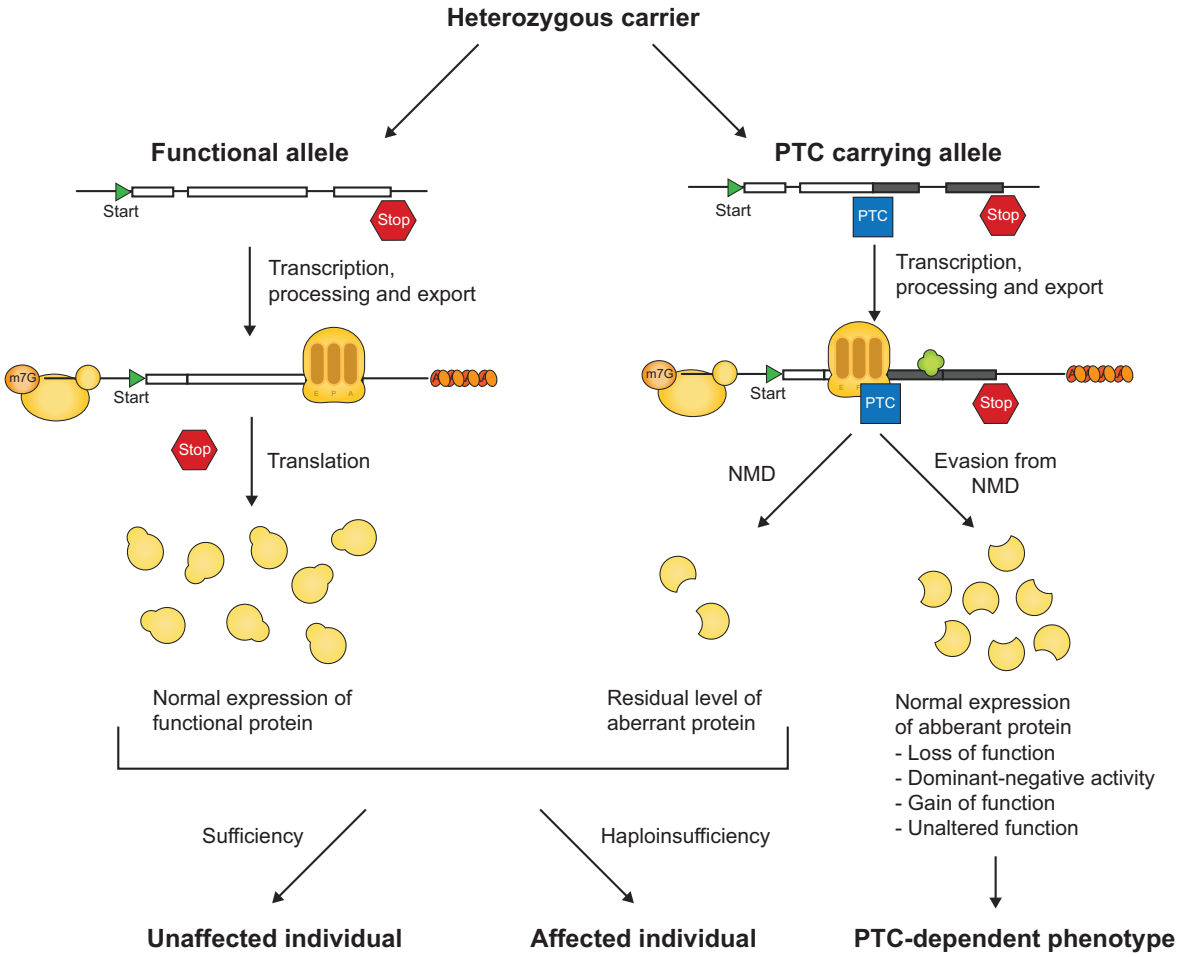

Figure 2.9: NMD can modulate the phenotypic outcome of nonsense mutations. *In heterozygous carriers, only one allele is affected by a premature termination codon (PTC) (right) while the other allele is fully functional (left). This results in aberrant mRNA and functional mRNA, respectively. After translation, the faulty mRNA can trigger NMD yielding only small amounts of truncated protein. The total amount of protein is thus reduced which may be either sufficient (left) or insufficient (middle) to retain a normal phenotype. If the faulty mRNA evades NMD (right panel), this will result in different phenotypes, dependent upon the associated mutation. Adapted from (S. Lykke-Andersen & Jensen, 2015)*

beneficial regarding many of these nonsense mutations, as it degrades the transcript produced by the aberrant allele, allowing the unaltered allele to produce sufficient protein to restore the normal phenotype. In absence of NMD, the mutated transcript could result in a C-terminally truncated protein, which has a dominant negative effect and thus is harmful to the cell (Figure 2.9). This is exemplified by β-thalassemia which is caused by nonsense mutations in the first or second exon of the β-globin gene. The mutant transcripts are targeted by NMD resulting in a very low copy number of aberrant β-globin in heterozygous red blood cells. The individual is thus asymptomatic since the production of normal β-globin can be compensated by the functional allele (Thein et al., 1990). In contrast, if a PTC is found in the last exon of the β-globin gene, the resulting transcript is able to evade NMD. The truncated β-globin chains precipitate and this over-activates the proteolytic mechanism of the red blood precursor cells. The resulting clinical phenotype is a form of inherited anemia called β-thalassemia intermedia (Hall & Thein, 1994).

However, NMD can also deteriorate the clinical phenotype and cause haplo-insufficiency. This occurs when the functional allele cannot express enough functional protein (Figure 2.9). For example, some nonsense mutations in the dystrophin gene trigger NMD and lead to the degradation of C-terminally truncated, functional proteins. The resulting clinical phenotype is a severe form of Duchenne muscular dystrophy (Kerr et al., 2001). However, if the PTC escapes NMD, it results in the production of a partially functional protein, which is associated with a much milder form of the disease called Becker muscular dystrophy. The germline mutations of the cadherin-1 (CDH1) gene are another example. 80 % of CDH1 mutations associated with hereditary diffuse gastric cancer are nonsense mutations. Some data indicate that transcripts with a PTC which trigger NMD and thus the degradation of C-terminally truncated CDH1 are linked to an unfavorable progression of the cancer (Karam et al., 2008). Similar associations have been established for other cancer-associated proteins such as BRCA1, TP53 and WT1 (Bhuvanagiri et al., 2010).

The central role that NMD plays in disease emphasizes the need for clinical treatment strategies to inhibit or enhance NMD efficiency depending on the missense mutations associated with the disease.

2.3.8.3 Clinical approach to NMD-associated diseases

In cases where NMD worsens the clinical phenotype or causes haplo-insufficiency, potential treatments should aim to inhibit NMD and/or translation termination at a PTC in order to maintain an appropriate quantity of functioning full length proteins. Currently, the most promising approach for these conditions is with drugs that increase stop codon read-through during translation. Current read-through therapies include aminoglycosides (which reduce the codon:anticodon pairing accuracy), Ataluren (a compound

also known as PTC124, promoting stop codon read-through by an unknown mechanism (Martin et al., 2014)) and suppressor tRNAs (which incorporate an amino acid into the transcript at the stop codon). However, these therapies have major drawbacks in terms of delivery and adverse side effects (Bhuvanagiri et al., 2010).

2.4 Scope of this work

Despite decades of research and major progress in our understanding of NMD, the molecular interplay between the translation termination apparatus and the NMD factors, which allows the discrimination between a normal and an aberrant stop codon, has remains unclear. Current models are usually based on *in vivo* data (pulldown and mutational analyses) and limited structural information from sub-complexes. The interaction network between purified factors is yet to be established, and the temporal aspect of the multiprotein complex assembly remains to be elucidated. Ultimately, a better understanding of the molecular mechanism of NMD will facilitate the development of therapeutic strategies for the treatment of PTC-associated diseases.

This thesis aims to elucidate the mechanism of recognition of a terminating ribosome stalled on a PTC. This is investigated by producing full length purified yeast and human NMD and translation factors and by studying the interactions between those individual factors and the terminating ribosome. The first section of this work focuses on solving high resolution structures of the ribosome in normal and aberrant termination contexts. The yeast poly(A) binding protein was proposed to stimulate efficient translation termination and to antagonize NMD by competing against Upf1p for eRF3 binding (Amrani et al., 2004; Singh et al., 2008). At the start of this project, only the binding of human PABPC1 to eRF3a was resolved and no structural information was available for the terminating ribosome bound to the release factors in absence or presence of Pab1p and Upf1p. Using a yeast cell-free *in vitro* translation system, ribosome nascent chain complexes were produced and purified in order to reconstitute different termination complexes for structural studies. The second part of this work aims to elucidate the influence of human NMD core factors on the terminating ribosome. Based on co-immunoprecipitation experiments, UPF1 was proposed to interact with the release factors but direct evidence was lacking. This work describes an approach that combines a fully reconstituted mammalian *in vitro* termination system (as described by (Alkalaeva et al., 2006)) with *in vitro* and *in vivo* interaction studies to decipher the UPF-eRF interactome during translation termination.

3. Structural studies of yeast termination complexes

Resumé en français

Le travail présenté dans ce chapitre se concentre sur la terminaison de la traduction chez la levure en présence de Pab1p et de Upf1p. L'objectif était d'obtenir des informations biochimiques et structurales sur la fixation des ribosomes et leurs reconnaissances par les facteurs NMD Upf1p et Pab1p permettant la discrimination entre un codon stop prématuré ou physiologique. Afin de répondre à ce problème, nous avons reconstitué *in vitro* la traduction chez la levure et généré des complexes de terminaison. Ces derniers comprennent des complexes ribosome-nascent chain (RNC) positionnés sur un codon stop, eRF1 mutant, eRF3 ainsi que l'addition de Upf1p ou de Pab1p. La première partie de ma thèse a été la mise en place d'un système de traduction *in vitro* en utilisant des extraits de levure. Ce système a permis de générer des RNCs que nous avons purifié par deux étapes : ultracentrifugation sur un coussin de sucrose et purification par affinité. Dans une seconde partie, les facteurs de terminaison et NMD ont été purifiés. Il s'est avéré impossible d'isoler un complexe entre les facteurs de terminaison et Upf1p ou Pab1p. Nous avons donc utilisé une approche liant de manière covalente eRF3 et Pab1p. Ceci a permis de purifier un complexe entre eRF1 : Pab1p lié à eRF3 qui a pu être ensuite ajouté aux RNCs afin de reconstituer un complexe de terminaison. Suite à une analyse par cryo-microscopie électronique, un volume 3D du complexe a été obtenu. Il se compose d'un ribosome en cours de traduction occupé par un ARNt sur le site P et une densité pour les facteurs de terminaison sur le site A. Malheureusement, aucune densité n'a pu être observée dans ce volume pour Pab1p.

Ce chapitre met en lumière la complexité de la discrimination des PTC par la NMD et établit une procédure pour la reconstitution de complexes de traduction chez la levure.

3.1 Introduction

Translation termination at PTCs is described as slow and inefficient (Amrani et al., 2004). The abnormal pausing, attributed to the absence of downstream termination-promoting factors, allows sufficient time for the core NMD factors to assemble on the ribosome (Amrani et al., 2004; Singh et al., 2008). In *S. cerevisiae*, NMD transcripts are often characterized by the increased distance of the aberrant stop codon from the poly(A) tail of the mRNA. It was thus proposed that the potential termination-stimulatory effect of Pab1p could be antagonized by Upf1p to activate NMD (Amrani et al., 2004; Singh et al., 2008). Moreover, it has been suggested that both Upf1p and Pab1p compete for eRF3 binding (Wang et al., 2001; Cosson et al., 2002a; Kobayashi et al., 2004). However, recent evidence has challenged this view as it was discovered that the deletion of the Pab1p interaction domain of eRF3 impacts termination of translation, but not nonsense-mediated mRNA decay (Roque et al., 2014). The molecular mechanism of PTC recognition remains unknown in yeast and higher eukaryotes, partially due to the lack of structural information for the relevant complexes.

The aim of the work presented in this chapter was to obtain structural and biochemical evidence to answer two main questions: How are stalled ribosomes recognized by NMD factors or Pab1p? How do the interactions between each NMD factor and with the translation machinery influence the discrimination between normal and aberrant termination codons? To address these questions, we focused on using *Saccharomyces cerevisiae* as a model organism. Yeast termination complexes were reconstituted by the addition of either Upf1p or Pab1p to ribosome-nascent chain complexes (RNC) stalled at a stop codon in presence of eRF1AGQ mutant and eRF3. With the use of a fusion protein to link eRF3 to Pab1p, eRF1AGQ:Pab1p-eRF3 complexes could thus be purified and added to the RNCs in order to reconstitute the termination complexes. Following single particle analysis by electron cryo-microscopy (Cryo-EM), a 3D volume was obtained which was composed of a translating ribosome with a P-site tRNA and density for the release factors in the A-site. Unfortunately, no density was observed for Pab1p.

3.2 Results

3.2.1 Yeast RNC preparation

Firstly, a yeast cell-free translation system was used to prepare RNCs (Waters & Blobel, 1986). Purified plasmids encoding for the yeast synthetic nascent chain (yNC) mRNAs were transcribed *in vitro* using T7 RNA polymerase and purified by lithium chloride followed by ethanol/sodium acetate precipitations. The *in vitro* translation of the yNC mRNA was carried out in a reaction mix containing yeast cell extract (RH2585 strain see section 3.4.2) for 45 minutes at 25°C. The reaction was stopped by addition of cycloheximide, a translocation inhibitor. Ribosomes were separated from the translation mixture by ultracentrifugation through a high salt sucrose cushion. Subsequently, non-translating ribosomes were removed by an affinity purification step using an N-terminal tag encoded by the yNC mRNA (Figure 3.1). Secondly, pure eRF1AGQ:eRF3-Pab1p complexes were added to the RNCs for reconstruction of the yeast translation termination complex. These complexes were then used for grid preparation and single particle cryo-EM analysis, as described in section 3.2.3.

The yNC plasmid construct (referred to as SBP-yNC) used to generate ribosome nascent chain complexes, was established for cryo-EM analyzes of translating yeast ribosomes.(Beckmann et al., 2001; Halic et al., 2004; Becker et al., 2011). In this construct, the open reading frame (ORF) is preceded by a T7 promoter for *in vitro* transcription. The ORF comprises an N-terminal streptavidin binding peptide tag (SBP) for affinity purification, followed by a coding sequence for the 120 N-terminal amino acids of the type II membrane protein dipeptidyl aminopeptidase B (DPAP-B). The nascent chain is sufficiently long to ensure that the tag exits the ribosomal tunnel and is able to bind to the streptavidin affinity column. In the yNC construct, the DPAP-B sequence is followed by phosphoglycerate kinase 1 (PGK1) 3' untranslated region (3' UTR), 3 BoxB tags (for affinity purification via the mRNA if needed) and a 73 nt poly(A) tail. The presence of the poly(A) tail enabled the reconstruction of termination complexes with Pab1p and the presence of a long 3' UTR mimicked an NMD substrate which would allow the reconstruction of complexes with Upf1p.

3.2.1.1 Optimization of the yeast cell-free translation reaction

Capping optimization

The addition of a 5' cap to the synthetic mRNA is critical for efficient *in vitro* translation. Caps were added using the ScriptCap m7G Capping System (CellScript) or using purified vaccinia capping enzyme (VCE) (Figure 3.2A). Our purified VCE was tested free of RNAse contaminants after incubation of the enzyme with an mRNA reporter and subsequent electrophoresis resulted in intact mRNA with no signs of degradation.

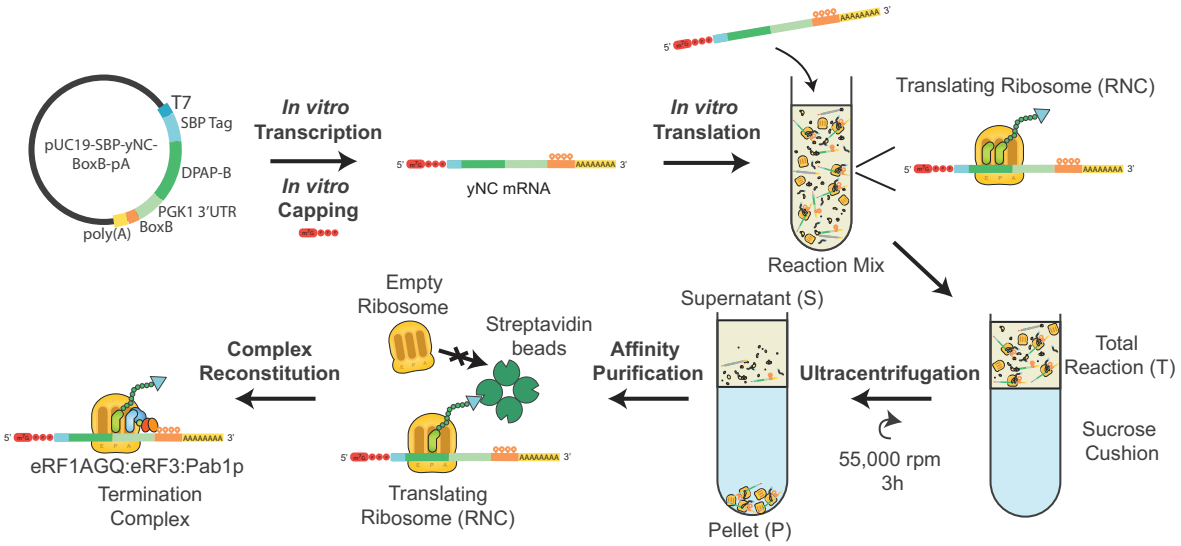

Figure 3.1: In vitro ribosome-nascent chain complex preparation scheme. *RNCs are produced by in vitro transcription using T7 polymerase followed by in vitro translation using yeast extract. The DNA constructs used are described in section 3.4.1.1. Following in vitro translation, ribosomes are separated from the translation mix by ultracentrifugation through a sucrose cushion. RNCs are further purified by affinity chromatography via the N-terminal Streptavidin binding peptide of the nascent chain construct which binds to streptavidin beads. Termination complexes are reconstituted by addition of purified release factors eRF1, eRF3 and Pab1p.*

Using a defined amount of luciferase mRNA reporter, different amounts of VCE were tested and the respective translation activity was monitored. 1 µg of VCE for 5 µg of mRNA reporter was found to maximize the translation efficiency in the assay, as indicated by the relative light unit intensity in the luciferase assay (Figure 3.2B). Since uncapped mRNA cannot be translated efficiently by the yeast *in vitro* translation system, an excess of VCE was used to ensure capping. 2.5 µg of VCE was used throughout this study to cap 5 µg of mRNA. The capping efficiency was also tested with the yNC mRNA to ensure that a 2:1 ratio of mRNA and VCE allows efficient translation of the yNC mRNA. The translation efficiency was assessed by SDS-PAGE gel and Western blot against the SBP tag. Following western blotting using streptavidin coupled to HRP (horseradish peroxidase), a band at 20kDa indicating yNC translation could be detected in the total reaction lane, only if the mRNA was capped before the *in vitro* translation (Figure 3.2C). This band was also present in the pellet fraction, indicating that the yNC was still attached to ribosomes and thus could be pelleted by ultracentrifugation.

Optimization of the *in vitro* translation protocol

The protocol used for *in vitro* translation in this work is based on previously published protocols (Beckmann et al., 2001). The mRNA concentration in the *in vitro* translation system was optimized. We reasoned that optimal translational activity of our system

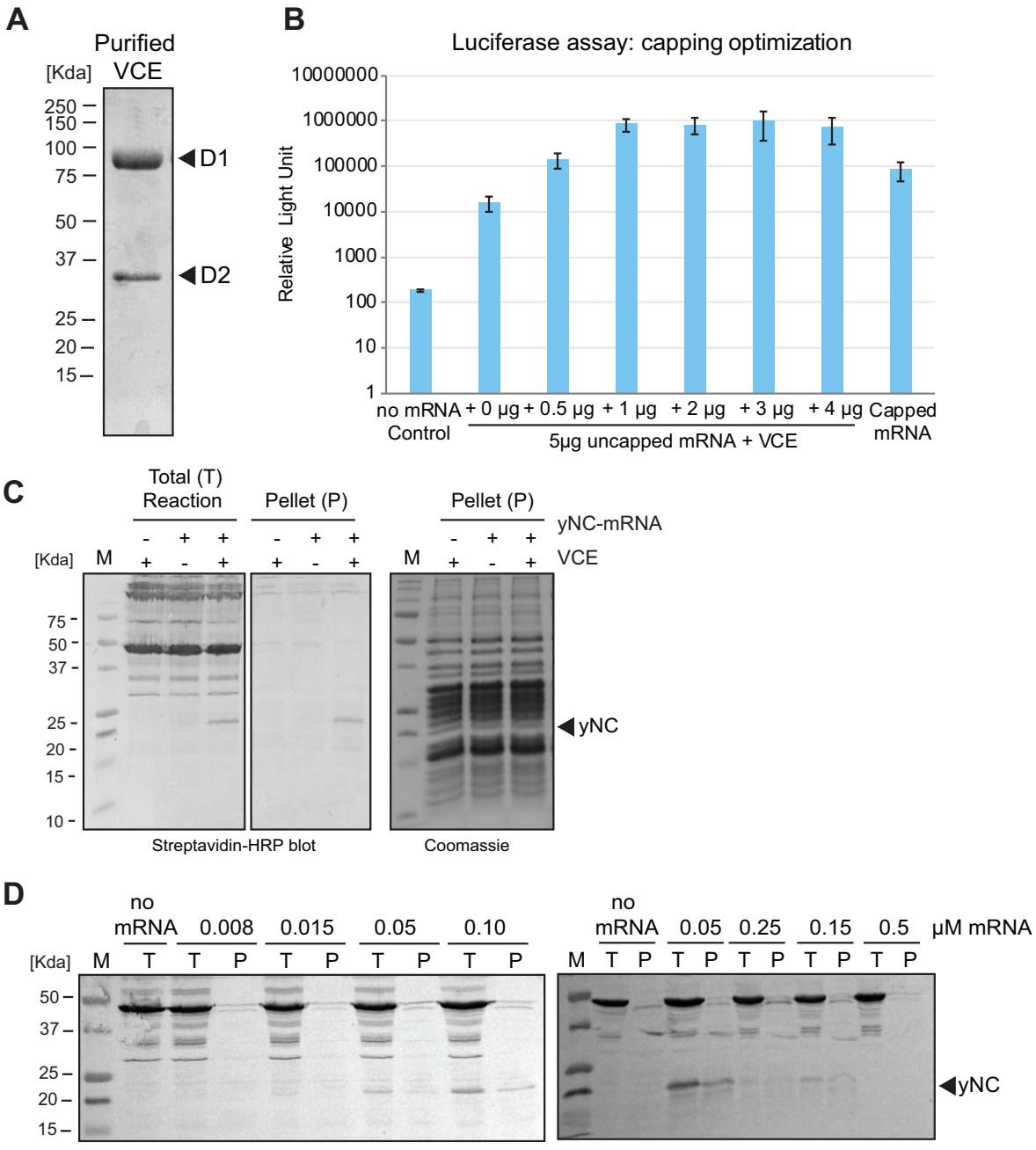

Figure 3.2: Optimization of the in vitro translation reaction. ***A.*** *SDS-PAGE analysis of purified vaccinia capping enzyme (VCE) enzyme showing pure subunits (D1 and D2 respectively) after size exclusion chromatography (coomassie stain).* ***B.*** *Luciferase assay using the yeast in vitro translation system and varying amounts of VCE to 5 µg reporter mRNA. The luciferase activity was measured without mRNA as a negative control. A capped mRNA provided by Ottilie von Loeffelholz served as a positive control.* ***C.*** *Coomassie stained SDS-PAGE and Western blot analysis of the in vitro translation reaction starting from capped (+VCE) or uncapped (-VCE) yNC-mRNA. Western blotting was performed after sucrose cushion ultracentrifugation (Pellet - P) with streptavidin-HRP (1/4,000 dilution).* ***D.*** *Different concentrations of SBP-yNC mRNA were used in 100 µL of yeast cell-free translation reaction. Western blot analysis was performed using streptavidin-HRP for the total reaction (T) and after sucrose cushion ultracentrifugation (Pellet - P). M: protein molecular weight standards (kDa) (1/4,000 dilution).*

would result in a maximal detection of yNC protein after ultracentrifugation in the ribosomal pellet (TLA-55 Rotor (Beckmann Coulter), 55,000 rpm for 3 h at 4°C). Tests were carried out with increasing concentration of mRNA (ranging from 8 nM to 0.5 μM) (Figure 3.2D). We found that the yNC presence in the ribosomal pellet was increasing until 100 nM of mRNA; and decreasing if larger mRNA concentrations were used, possibly indicating too much competition between mRNAs for ribosomes and for translation factors. 100 nM (30 μg/mL) of SBP-tagged yNC mRNA was thus determined to be the optimal concentration and used for the rest of this study except indicated otherwise.

Additional optimization tests

It was hypothesized that limiting the competition between exogenous and endogenous material in the *in vitro* translation would improve the RNC yield. In an effort to prove this, endogenous mRNAs were removed by incubating the cell extract with oligo(dT) resin prior to the *in vitro* translation reaction (Supplemental Figure 3.11A). Using luciferase assays, we compared oligo(dT) purified with unpurified yeast extracts and it was found that they were minimal difference in yNC synthesis between the two extracts (Supplemental Figure 3.11B). It was concluded that the amount of yNC mRNA, optimized in the previous section, outcompeted the remaining endogenous mRNA efficiently during *in vitro* translation. Therefore, it was decided not to deplete endogenous mRNAs from the extracts and to supply 100 nM of yNC mRNA to the *in vitro* translation reaction instead.

Following the same principle, a yeast strain (TB50) was engineered in collaboration with the Robbie Loewith laboratory in order to substitute endogenous eRF1 by a mutant which could be removed from the extract by TAP purification (IgG coupled beads followed by TeV cleavage). Following eRF1 depletion (Supplemental Figure 3.11C), the translation efficiency of the different yeast extracts was estimated by a luciferase assay. As shown in Supplemental Figure 3.11D, translation with TB50 was less efficient compared to RH2585 and thus we decided not to use TB50. Additional tests were performed in order to optimize the *in vitro* translation system and thus the yield of RNC preparation. Since the capping step appeared to be the limiting step in the system, a capping independent initiation of translation approach was tested by adding a cricket paralysis virus internal ribosome entry site (CrPV-IRES) sequence in the yNC mRNA (Supplemental Figure 3.12A). This approach was unsuccessful as no translation activity could be observed.

3.2.1.2 RNC purification and stalling optimization

RNCs were purified in a two-step process (Figure 3.1). In the first step, ribosomes and ribosome-associated proteins were removed from the translation reaction mixture by ultracentrifugation through a high salt sucrose cushion. In the second step, an affinity purification step was performed to specifically purify ribosomes translating the yNC mRNA. Two different tags were tested in order to purify the RNC by affinity, strepavidin binding peptide (SBP) and Strep-tagIII (3Strep). We decided to use a yNC with an SBP tag for the yNC purification as it yielded higher protein concentration (Supplemental Figure 3.12B to E).

Since eRF1AGQ cannot release the nascent chain from the ribosome, the addition of exogenous release factors to the *in vitro* translation system should efficiently stall, and possibly stabilize, the ribosomes. Thus, the addition of eRF1AGQ could increase the fraction of terminating ribosomes in the reaction. Different concentrations of the release factor complex eRF1AGQ:eRF3 were added at a 1:1 ratio to the *in vitro* translation system up to a concentration of 8 µM. It was found that 4 µM of the release factor complex greatly enhanced the yNC yield after ultracentrifugation through a high salt sucrose cushion (Figure 3.3A). Different concentrations of Pab1p were added to the *in vitro* translation reactions, but no major changes in RNC yields were observed (Figure 3.3B). Thus, 4 µM RF complex, but no Pab1p was added to the translation mixture.

In previous cryo-EM studies of termination complexes "CMV-stalled" ribosomes were used (Bhushan et al., 2010; Preis et al., 2014; Matheisl et al., 2015). During the early stage of the cytomegalovirus (CMV) infection, glycoprotein 48 (gp48) expression is blocked by an upstream open reading frame (uORF2). Ribosomes are stalled on the uORF2 due to interactions between the encoded nascent chain and the ribosomal exit tunnel (Bhushan et al., 2010). Based on this knowledge, this stalling motif was added to the yNC mRNA sequence for two reasons: firstly, the CMV motif is thought to efficiently stall pre-terminating ribosomes. Secondly, contacts between CMV and the ribosome could stabilize the ribosome-nascent chain complex with the SBP tag at the exit of the ribosomal tunnel. The last 30 amino acids of the DPAP-B coding sequence were thus replaced by the CMV uORF2 (referred to as SBP-yNC-CMV). The stalling activity of the CMV peptide was determined using the yeast cell-free translation system (Figure 3.3C, D). Compared to SBP-yNC, the translation of SBP-yNC-CMV led to the appearance of a higher molecular weight band in the Western blot, indicating that a large fraction of yNC remained bound to the P-site tRNA (tRNA-yNC). The CMV stalling motif thus allowed the stabilization of both P-site tRNAs and translating ribosomes. This also resulted in the reduction of co-purification of free yNC peptides together with the RNCs. The elution fraction of the RNCs translating SBP-yNC-CMV was analyzed by 2 % uranyl acetate negative stain electron microscopy (Figure 3.3E).

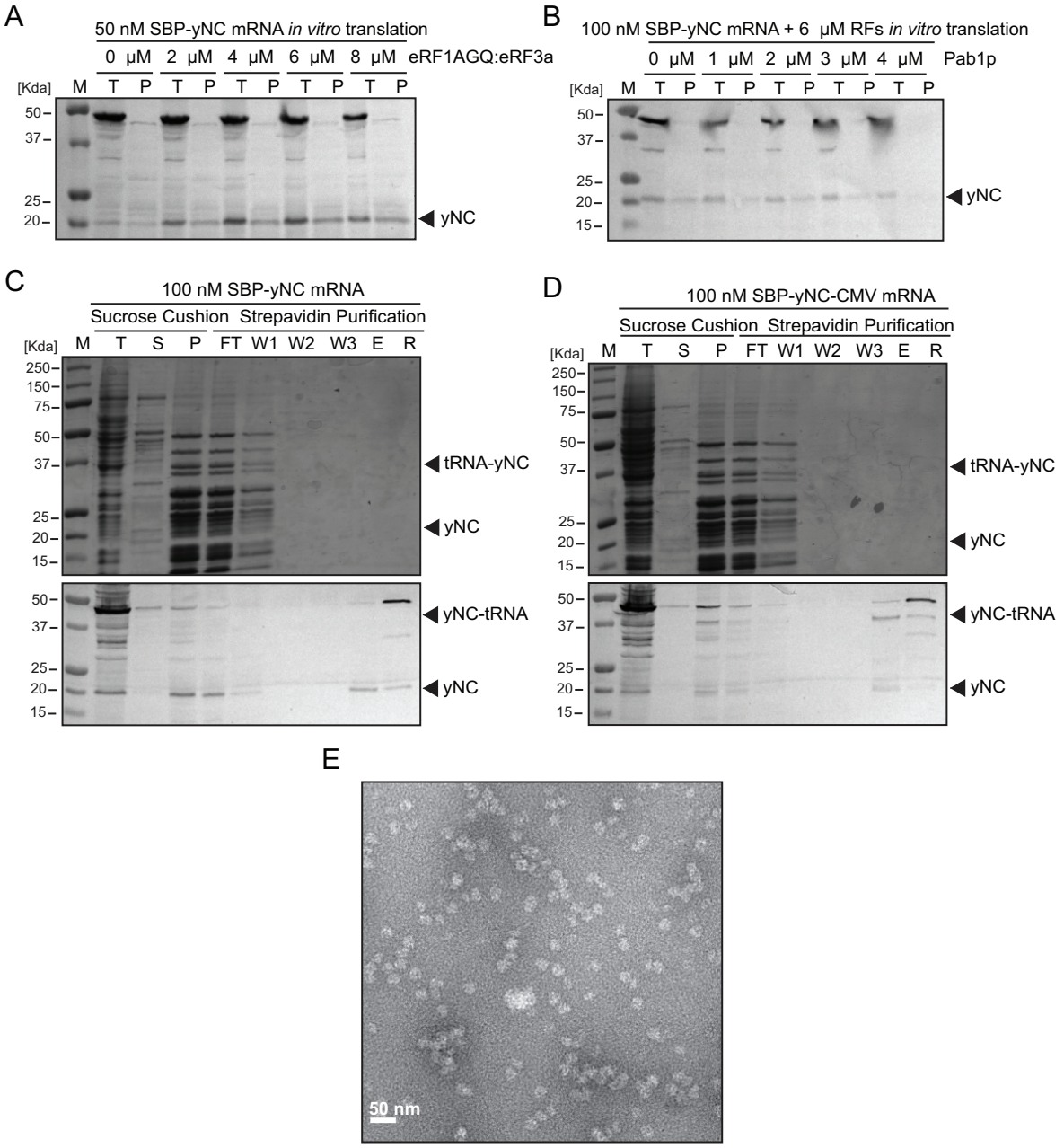

Figure 3.3: Optimization of the RNC purification. A. B. *Western blotting was performed using streptavidin-HRP (1/4,000 dilution) for the total reaction (T) and after sucrose cushion ultracentrifugation (Pellet - P) with the addition of release factors or Pab1p as indicated. 100 µL translation reaction.* ***C, D.*** *SDS-PAGE followed by coomassie staining (above) or Western blot analysis (below) of in vitro translation reactions using SBP-yNC (C) or CMV stalling motif-containing SBP-yNC (D). After ultracentrifugation, the pellet fraction was resuspended and subjected to affinity purification using streptavidin beads. Western blots were performed using streptavidin-HRP. Total reaction (T), supernatant (S), pellet (P), flow-through (FT), washes (W1-3), elution (E) fractions and resin (R) are indicated. Two bands can be detected for the SBP tagged yNC: a lower band at 20kDa indicating free protein (yNC) and a higher one at 40kDa indicating that the yNC is still bound to the P-site tRNA (tRNA-yNC).* ***E.*** *2% uranyl acetate negative stain EM analysis (50,000 x) of the Elution fraction of the purified SBP-yNC-CMV RNCs from (D). M: protein molecular weight standards (kDa).*

The micrographs showed a large amount of intact ribosomes and only few polysomes, indicating a good quality sample. Overall, the purification yield was doubled with mRNAs containing the CMV motif. The final RNC concentration was on average 3 pmol/mL compared to 1.5 pmol/mL RNCs without the CMV motif.

3.2.2 Purification of termination complexes

3.2.2.1 Protein purification

eRF1AGQ, eRF3 and Pab1p full length proteins were C-terminally tagged with a hexahistidine tag and were purified from BL21 (DE3*). Upf1p was produced with an N-terminal 6xHis tag using the MultiBac insect cell expression system (Fitzgerald et al., 2006). Proteins were purified by Ni-NTA (Qiagen) affinity chromatography, followed by an anion exchange chromatography (MonoQ, GE Healthcare). Subsequently, they were further purified by size-exclusion chromatography (SEC) via a Superdex 200 column (GE Healthcare). The purity of the proteins was assessed by SDS-PAGE (Figure 3.4), and the activity of the release factors was tested by a luciferase assay. Despite our efforts, Upf2p could not be expressed in *E.coli* or insect cells (Supplemental Figure 3.13A). Upf3p could be purified from *E.coli* (Supplemental Figure 3.13B and C).

3.2.2.2 Protein complex purification

In order to reconstitute the yeast termination complexes, release factor complexes had to be purified before addition to the RNCs. Incubation of equimolar ratios of eRF1AGQ and eRF3 resulted in a complex which eluted earlier than the individual proteins, indicating a higher molecular weight (Figure 3.4E). SDS-PAGE analysis showed that eRF1AGQ and eRF3 co-eluted from the gel filtration column in the same fractions, thus confirming complex formation (Figure 3.4E). When Pab1p or Upf1 were added to the release factors, no high molecular peak was observed by chromatography. Gel analysis confirmed that Pab1p or Upf1 eluted in later fractions compared to the eRF1AGQ:eRF3 complex (Figure 3.4F, G). This indicated that Pab1p and Upf1p bound with low affinity to the eRF and the complex possibly dissociates during SEC.

In order to increase the local concentrations of Pab1p and Upf1p and thus promote complex formation, fusion protein constructs between eRF3 and Pab1p or Upf1p were generated. A similar strategy was previously used in the laboratory to generate a stable complex of a signal recognition particle and its receptor in the presence of translating ribosomes (Estrozi et al., 2011). The proteins were linked by a 58 amino acid glycine/serine linker and both possible orientations were tested (eRF3-Pab1p and Pab1p-eRF3 or eRF3-Upf1p or Upf1p-eRF3). Recombinant proteins with an N-terminal hexaHis tag and a C-terminal StrepTagII were expressed in *Sf21* insect

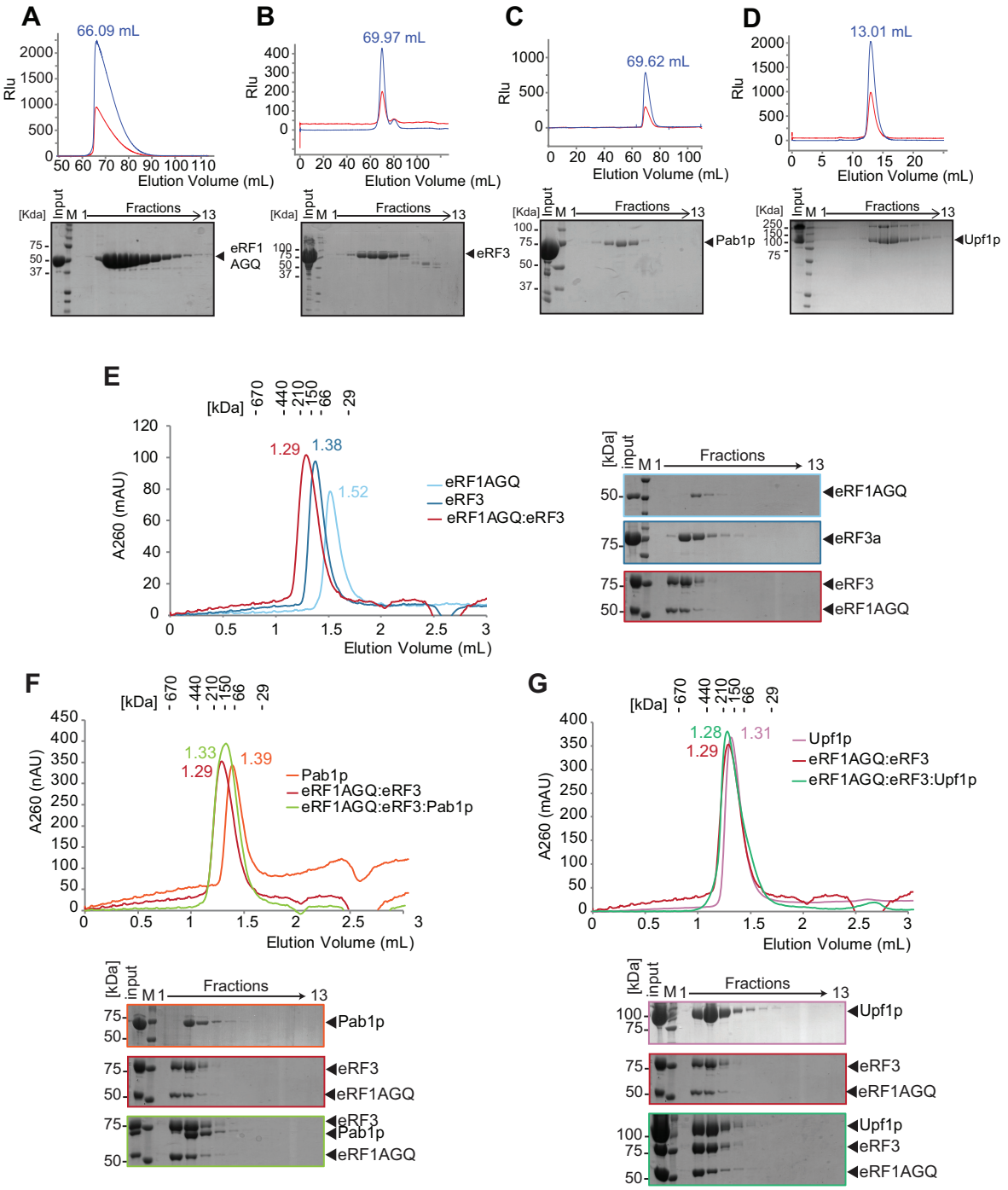

Figure 3.4: eRF1AGQ, eRF3, Upf1p and Pab1p purification. ***A. B. C.*** *Size exclusion chromatography (SEC) via Superdex 200 16/60 (GE Healthcare) with eRF1AGQ, eRF3 or Pab1p.* ***D.*** *Same as (A) with Upf1p and Superdex 200 10/300 (GE Healthcare). SDS-PAGE analysis of the elution fractions is shown under each chromatogram (coomassie stain) . Absorbance at 280 nm and 245 nm (relative light unit - rlu) is displayed in blue and red, respectively* ***E.*** *SEC elution profile of eRF1AGQ (red), eRF3 (dark blue) or both (red) (left). 7 µM of each protein was loaded onto a Superdex 200 column. Calibration of the column was performed with globular proteins (shown above). Elution fractions were analyzed by SDS-PAGE (right).* ***F.*** *SEC elution profile as in (E) of eRF1AGQ:eRF3 (red), Pab1p (orange) or all proteins (green).* ***G.*** *SEC elution profile as in (E) of eRF1AGQ:eRF3 (red), Upf1p (purple) or all proteins (dark green). The elution volume (in mL) is indicated for each experiment; M: protein molecular weight standards (kDa).*

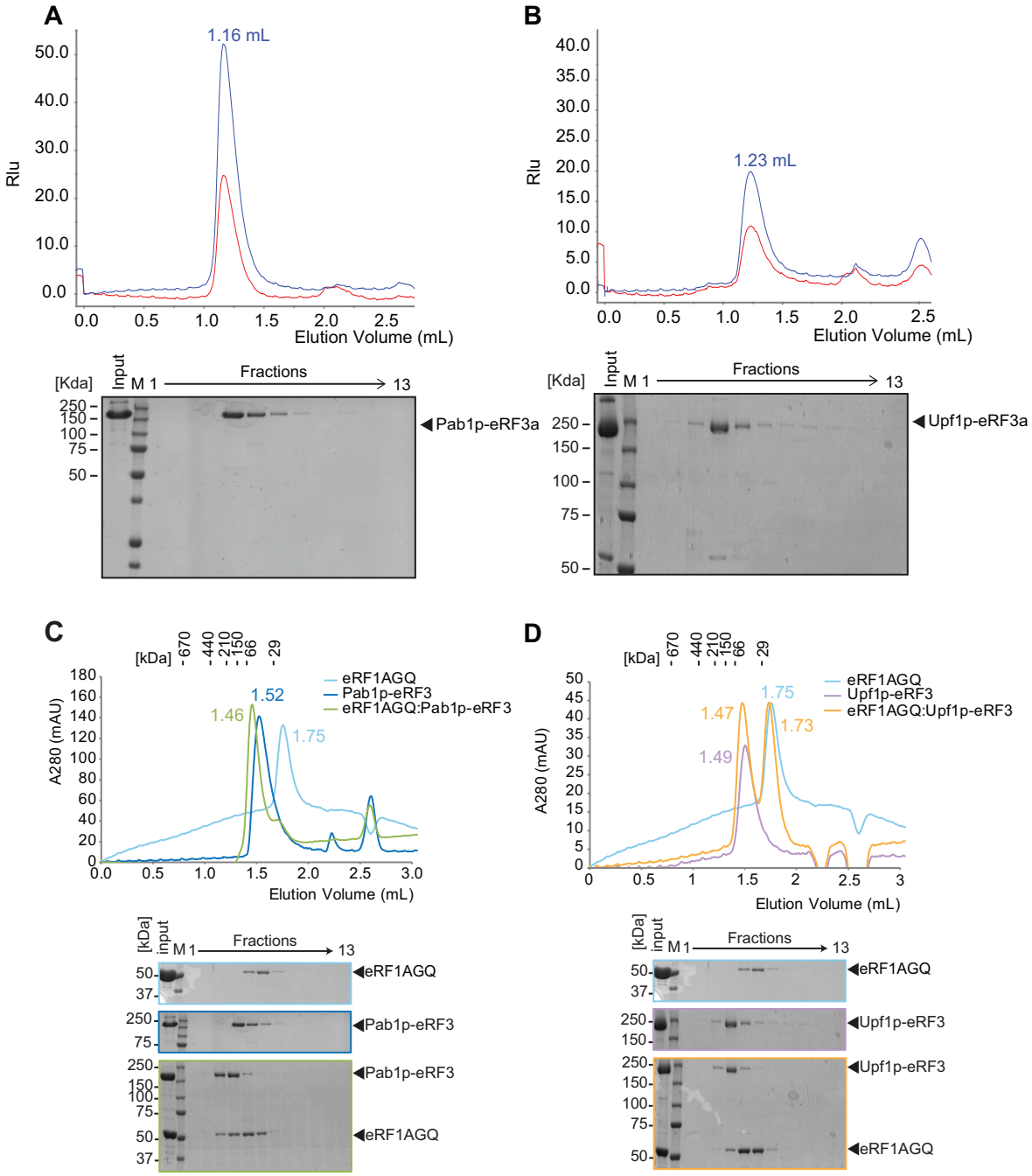

Figure 3.5: Upf1p-eRF3 and Pab1p-eRF3 purification and complex formation with eRF1AGQ. A. B. *Size exclusion chromatography (SEC) using a Superdex 200 PC 3.2 column (GE healthcare) of Pab1p-eRF3 (A) or Upf1p-eRF3 (B). SDS-PAGE analysis of the elution fractions is shown under each chromatograph (coomassie stain). Absorbance at 280 nm and 245 nm (relative light unit - rlu) is displayed in blue and red, respectively.* ***C.*** *SEC elution profile of eRF1AGQ (red), Pab1p-eRF3 (blue) or both (green) (left). 7 µM of each protein was loaded onto a Superdex 200 column. Calibration of the column was performed with globular proteins (shown above). Eluation fractions were analyzed by SDS-PAGE (below).* ***D.*** *SEC elution profile as in A. of eRF1AGQ (red), Upf1p-eRF3 (purple) or both (orange). Elution in mL is indicated for each elution peak. M: protein molecular weight standards (kDa).*

cells. The expression of the fusion proteins with a C-terminal eRF3 showed higher expression levels than the N-terminal eRF3 constructs. Therefore, we chose to focus on the purifications of Upf1p-eRF3 and Pab1p-eRF3. The fusion proteins were purified employing the same procedure as the single proteins, but a Strep-Tactin affinity purification step was added after the Ni-NTA (Qiagen) affinity purification step for Upf1p-eRF3a in order to remove protein degradation products (Figure 3.5A, B).

Incubation of equimolar ratios of eRF1AGQ and Pab1p-eRF3 resulted in a complex eluting at a higher apparent molecular weight than the individual proteins (1.46 mL vs 1.52 and 1.75 mL) (Figure 3.5A). SDS-PAGE analysis showed that eRF1AGQ and Pab1p-eRF3 co-eluted from the SE column in earlier fractions, confirming complex formation (Figure 3.5A). When eRF1AGQ was mixed with Upf1p-eRF3, two individual elution peaks were observed. The first peak corresponded to the Upf1-eRF3 fusion protein and the second peak corresponded to eRF1AGQ (Figure 3.5C). Gel analysis indicated that eRF1AGQ eluted 100 µL (two fractions) earlier in the presence of Upf1p-eRF3 (Figure 3.5D). It was concluded that the complex could not be purified under the conditions tested, however it is possible that the complex forms at higher concentrations. We thus chose to focus our efforts on termination complexes using Pab1p-eRF3 rather than Upf1p-eRF3.

3.2.3 Single particle cryo-electron microscopy

3.2.3.1 Reconstitution of ribosomal termination complexes

Co-sedimentation experiments were performed to determine whether the purified eRF1AGQ:Pab1p-eRF3 complex could bind specifically to ribosomes. 80S ribosomes were isolated from yeast extract by sucrose gradient centrifugation and incubated with eRF1AGQ:Pab1p-eRF3 complexes. Incubation was performed at 25°C using different ratios of ribosomes and eRF1AGQ:Pab1p-eRF3 complexes and different salt concentrations in the sucrose cushion; in addition GMPPNP was added to block the GTPase activity of eRF3 and to stabilize the interaction. Subsequently, the mixture was loaded onto a 1 M sucrose cushion and subjected to ultracentrifugation. Centrifugations without ribosomes served as controls (Figure 3.6A). eRF1AGQ:Pab1p-eRF3 co-migrated with the ribosomes through a sucrose cushion (Figure 3.6A, lane 6), indicating that both proteins could bind to ribosomes, but not at high salt concentrations (Figure 3.6, lane 12). The band intensity for eRF1 was weaker than Pab1p-eRF3 (Figure 3.6A, lane 6) indicating that in this assay eRF1 binding was not optimal. We found that a ten-fold molar excess of eRF-Pab1 complexes with 100 mM KCl and 200 µM GMPPNP were the optimal conditions for ribosomal binding.

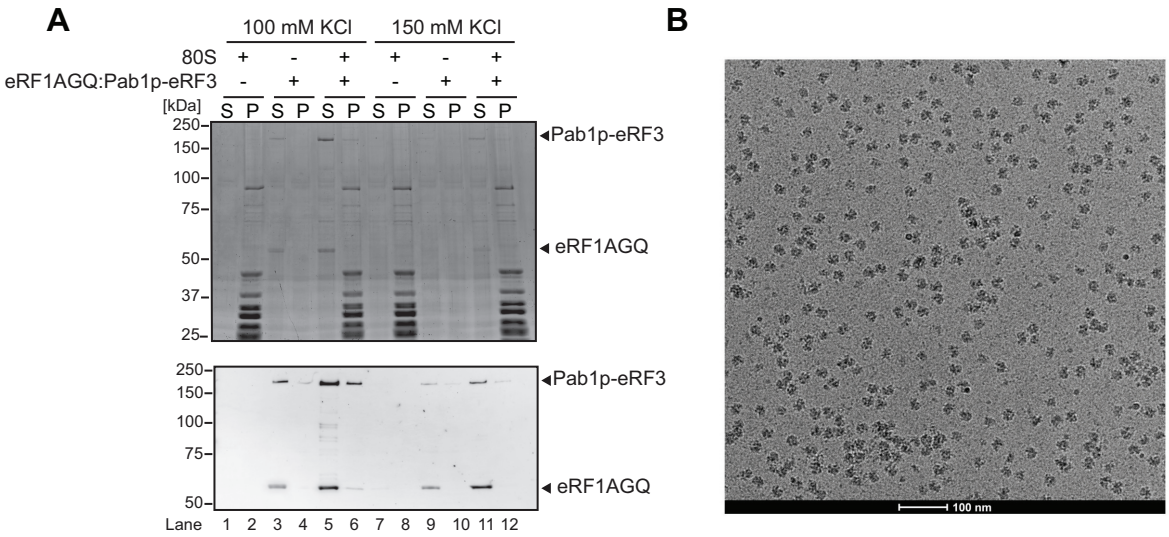

Figure 3.6: Reconstitution of yeast termination complexes. A. *Reactions containing 2 pmols of 80S ribosomes and 10 time excess of eRF1AGQ:Pab1p-eRF3 complex were centrifuged through a sucrose cushion with two different KCl concentrations. Supernatant (S) and pellet (P) fractions were analyzed by SDS-PAGE and stained with SYPRO Ruby stain or Western blot using a mouse Anti-6xHis tag antibody (1/5,000 dilution) and a secondary Alexa 532-labeled anti-mouse antibody (1/10,000 dilution).* ***B.*** *Cryo-EM micrographs of frozen, reconstituted RNC-CMV with 10 fold molar excess of eRF1AGQ:eRF3-Pab1p complexes collected on the F20 microscope (IBS) at a 50,000x magnification.*

3.2.3.2 Single particle analysis of RNC-eRF1AGQ:Pab1p-eRF3

Grids were frozen in the EM facility of the Institut de Biologie Structurale (IBS) using the Vitrobot (FEI) and 2 pmol of RNCs mixed with 20 pmol eRF1AGQ:Pab1p-eRF3. Micrographs were collected on the Polara F30 (FEI) equipped with a 4k x 4k Gatan CCD camera (Figure 3.6B) at 50,000 x magnification using low dose conditions. A test dataset was composed of 42,239 ribosomal particles, manually picked using EMAN boxer (Tang et al., 2007). For unsupervised 3D classification a reconstruction of the *S. cerevisiae* empty 80S ribosome (EMDB 2275, low-pass filtered at 30 Å) was used as a template. Broken particles, ribosomes without P-site tRNA (non-translating ribosomes) or ribosomes with missing A-site density (non-terminating ribosomes) were sorted out (Figure 3.7A). 2,480 particles (corresponding to ~5% of the data) formed a new class where densities could be observed in the P-site and A-site of the ribosome. The P-site density was well defined and indicated the presence of peptidyl-tRNA in the RNC. The A-site density was not well defined, but it was sufficient to confirm the presence of eRF1 and eRF3 in our reconstruction (Figure 3.7B-E). Despite efforts to further sort the data computationally, density for Pab1p could not be observed in any of the reconstructions. Sorting was hampered by the small size of the particle pool representing translation termination complexes. Thus, we could not visualize Pab1 in the termination complexes despite being physically linked to eRF3.

This initial cryo-EM reconstruction helped to formulate hypotheses and draw con-

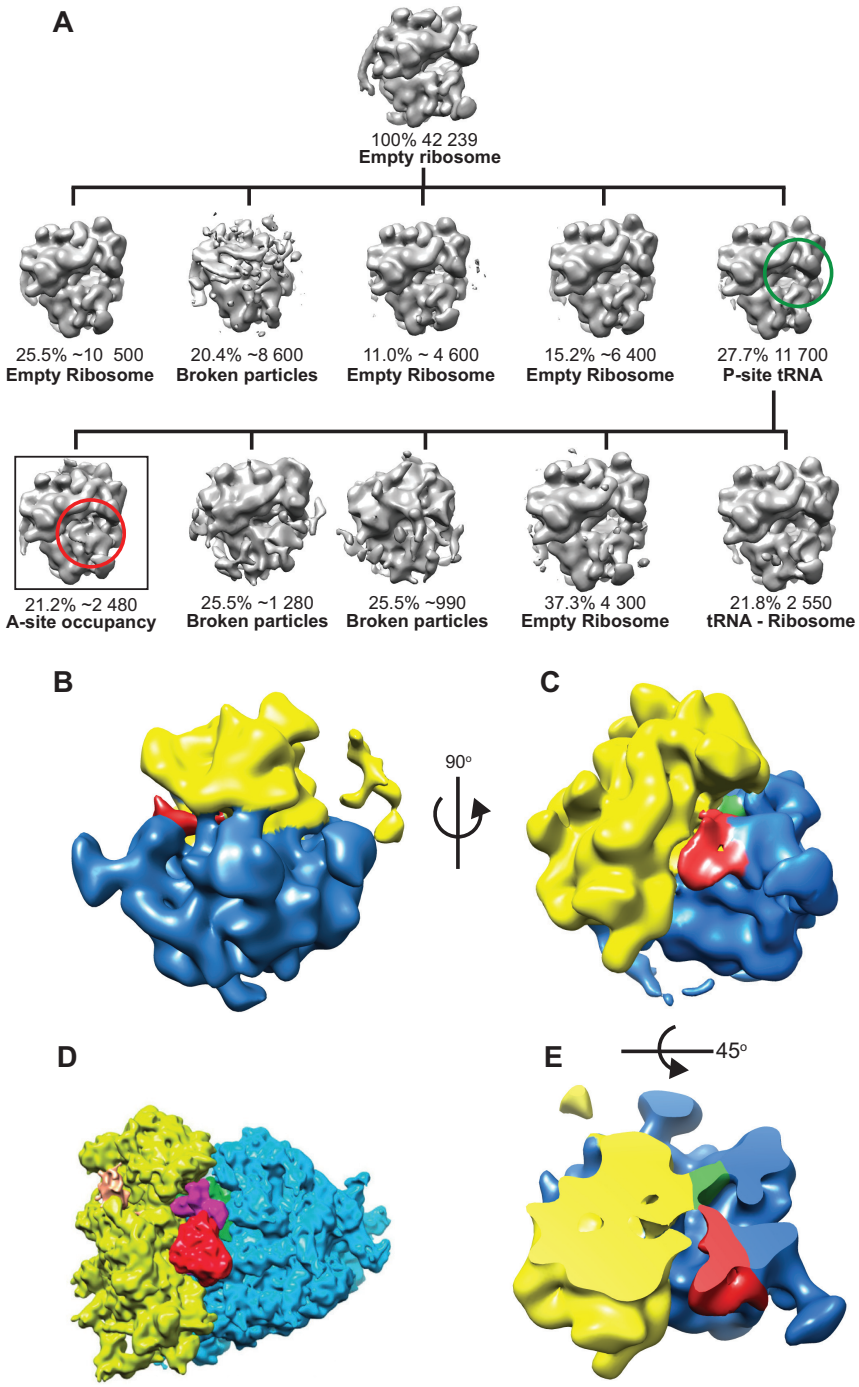

Figure 3.7: Single particle analysis of RNC:eRF1AGQ:eRF3-Pab1p. A. *Using a reconstruction of an S. cerevisiae 80S empty ribosome (EMDB 2275) as an initial model for the 3D reconstruction, the entire data set was sorted into 5 classes. 11,700 particles showed P-site tRNA (indicated in a green circle). Subsequently, this class was used for a second round of 3D classification to sort for density in the A-site (indicated in a red circle). The final volume further refined is shown in a black square. The occupancy of each particle pool is indicated. Images show structures derived from sub-data sets after computational sorting.* ***B.*** *The 40S subunit is colored in yellow, 60S in blue, the release factors in red and the P-site tRNA in green. The map is shown in a top (B), side (C) and sliced (E) view. For comparison, the map of a human termination complex is shown in panel D (Franks et al., 2010).*

clusions about the sample preparation: only 25% of the particles contained P-site tRNA indicative of translating ribosomes. Strikingly, only 5% of the dataset showed density for the release factors (but not for Pab1p). Thus, the sample quality needed be improved in order to increase ribosome occupancy. Moreover, the binding affinity between Pab1p and the release factors should be investigated more thoroughly to ensure that a ternary complex can indeed be formed in the presence of the ribosome.

3.2.4 Concluding experiments

3.2.4.1 RNC purification steps optimization

In order to increase the occupancy of P-site tRNA, we tried to reduce unspecific binding of non-translating ribosomes to the resin. The streptavidin beads were thus preincubated with Bovine serum albumin (BSA) and total yeast RNA overnight. This incubation helped to minimize the co-purificaton of ribosomes and yNC peptide versus yNC-tRNA bound to RNCs (Figure 3.8), indicating that the fraction of translating versus non-translating ribosomes was efficiently increased.

3.2.4.2 eRF3 complex with Upf1p and Pab1p characterization

In order to investigate the complex formation of the release factors with Upf1p or Pab1p, we decided to study the interaction between eRF3 and Upf1p or Pab1p first. Co-incubation of equimolar ratios of eRF3 and Pab1p (20 μM as an alternative to 7 μM in Figure 3.5) did not result in a complex as demonstrated by the lack of an apparent higher molecular weight peak compared to the individual proteins (Figure 3.9A). SDS-PAGE analysis revealed that a mixture of eRF3 and Pab1p eluted from the gel filtration column in the same fractions as the single proteins (Figure 3.9A). However, if eRF3 was mixed with Upf1p, the complex eluted slightly ahead of the single proteins (1.29 mL compared to 1.31 mL and 1.38 mL) (Figure 3.9B). SDS-PAGE analysis suggested that the proteins were coeluting in earlier fractions than the proteins alone, indicating that a complex can be formed at higher concentrations. An attempt was then made to mix the three proteins together in order to verify if Upf1p and Pab1p could bind cooperatively to eRF3 (Figure 3.9C). The resulting elution volume was not significantly different from the elution volume of eRF3 mixed with Upf1. However, the SDS-PAGE analysis showed that Pab1p co-eluted together with eRF3 and Upf1 (Figure 3.9C) suggesting a weak interaction between Pab1p and these proteins.

In order to further investigate whether a complex is formed between Upf1p and release factors *in vitro*, pulldown assays were performed. Briefly, reaction mixtures containing oligohistidine (His)-tagged eRF3 with eRF1AGQ or Upf1p or both proteins were incubated with Ni-NTA beads in the absence of nucleotides (Figure 3.9D), washed

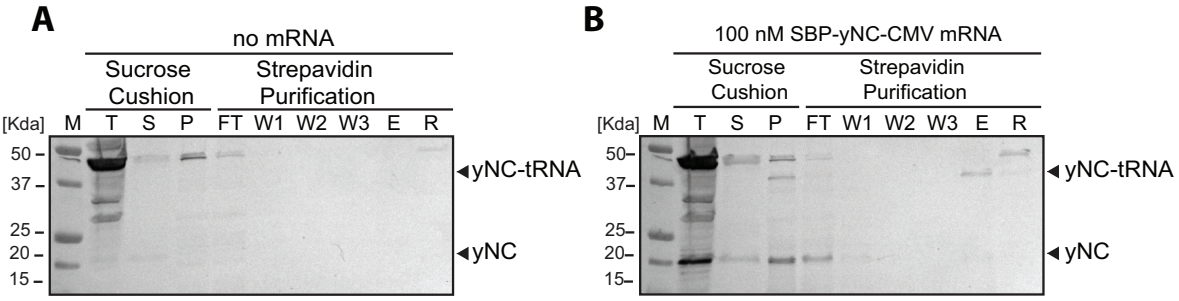

Figure 3.8: Further Optimization of RNC purification. A. B. *RNC purification using BSA and total yeast RNA treatment of the streptavidin beads with or without SBP-yNC mRNA as indicated. Western blot using streptavidin HRP (1/4,000 dilution). Two bands can be detected for the SBP tagged yNC: a lower band at 20 kDa indicating free protein (yNC) and a higher band at 40 kDa corresponding to the yNC still attached to P-site tRNA (tRNA-yNC). M: Marker; T: total reaction, S: supernatant; P: pellet Fraction; FT: flow-through; W1, W2, W3: washes; E: elution and R: resin. M: protein molecular weight standards (kDa).*

extensively and the bound proteins were eluted with imidazole. Untagged Upf1p was found in the elution fractions suggesting unspecific binding. However, Upf1p bound very slightly to eRF3 alone or to eRF1-eRF3 complexes (Figure 3.9D, lanes 5-7). The subsequent question to be answered was whether Pab1p could bind to eRF3 in pulldown assays (Figure 3.9E). However, binding of Pab1p to eRF3 alone or in presence of Upf1p could not be detected under the conditions tested (Figure 3.9E, lanes 5-7). Our results are thus ambiguous and additional techniques must be used to validate the interaction between the release factors and Upf1p and Pab1p. Either these interactions are transient by nature or additional factors are required to stabilize the interactions.

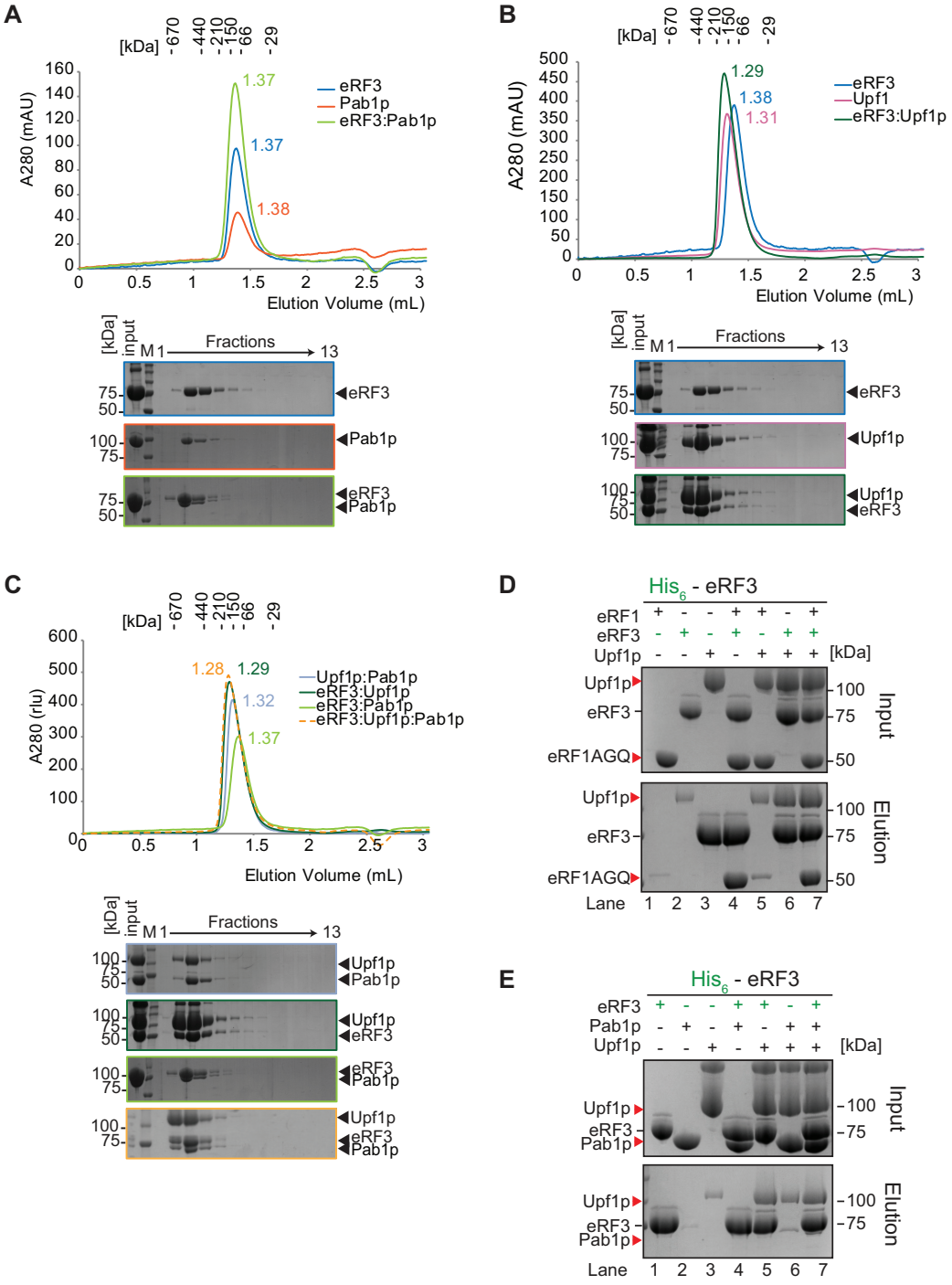

Figure 3.9: Binding assays between yeast Upf1p, Pab1p and the release factors. ***A.*** *Size exclusion chromatography (SEC) elution profile of eRF3 (blue) or Pab1p (orange) or both (light green) (left). 20 µM of each protein was loaded onto a Superdex 200 column. The elution volume (in mL) is indicated for each experiment. Calibration of the column was performed with globular proteins (shown above). Eluate fractions were analyzed by SDS-PAGE (below). M: protein molecular weight standards (kDa)* ***B.*** *Same as A. but with eRF3 (blue), Upf1p (purple) and both (green).* ***C.*** *Same as A. but with Upf1:Pab1p (purple), eRF3:Upf1 (green), eRF3:Pab1p (light green) and eRF3:Upf1:Pab1p (light orange)* ***D.*** *Pulldown with hexahistidine-tagged eRF3 mixed with eRF1 or Upf1p or both. Protein mixtures loaded (input) onto the beads (above) and after elution (below) were separated by SDS-PAGE followed by Coomassie staining.* ***E.*** *Same as D. but with untagged Pab1p (10 µM protein input).*

3.3 Discussion

The aim of this study was to gain insights into the mechanism of the termination of translation by solving the structure of terminating ribosomes bound to the release factors and Upf1p or Pab1p. To achieve this, a yeast cell-free lysate system for *in vitro* translation was established in our laboratory. This allowed the purification of stalled translating ribosomes still with the nascent chain bound in the exit tunnel (RNC) by a two-step procedure. First, ribosomes were separated from associated factors by ultracentrifugation through a high salt sucrose cushion. Second, an affinity purification step allowed the separation of non-translating from translating ribosomes which contain a SBP tag at the N-terminal end of the nascent chain. To reconstitute the translation termination complexes, it was decided to use a fusion protein approach to promote complex formation by physically linking eRF3 with Upf1p or Pab1p. This strategy allowed the purification of a complex containing eRF1AGQ and eRF3 linked to Pab1p. The complex was able to bind to purified RNCs and a cryo-EM dataset of the reconstituted complex was collected. However, the test reconstruction showed only a small fraction of ribosomes containing a P-site tRNA and density for the release factors. No density could be observed for the Pab1p despite being linked to eRF3. This indicates that Pab1p does not interact with the release factors, ribosomal proteins or rRNA when tethered to the A-site of the ribosome.

3.3.1 Optimization of yeast translational extract

It was found that 5' end mRNA capping was critical for the cell-free translation system. *In vitro* transcribed mRNAs were capped using purified VCE. The optimal ratio between capping enzyme and mRNAs was determined to be 1:2 (Figure 3.2A-C). The mRNA concentration in the system was also optimized and the addition of 100 nM mRNA to the translation reaction resulted in the maximal detection of yNC peptide after ultracentrifugation. This indicates that the nascent chain remained bound to the ribosome through the sucrose cushion and thus is part of a ribosome-nascent chain complex (Figure 3.2D). Cap-independent mechanisms using CrPV IRES elements have been reported in yeast (Iizuka et al., 1994) and have been successfully used to generate ribosome-nascent chain complexes (Matheisl et al., 2015). Under the conditions tested, IRES-mediated translation did not occur efficiently (Figure 3.12A). The yNC sequence was verified to be correct and therefore it was concluded that the yeast strain or the cell extract preparation protocol used in this study was not optimal for IRES-mediated translation initiation. In agreement with this statement, it has been shown that CrPV-IRES functions more efficiently in mutant yeast strains which result in enhanced phosphorylation of translation initiation factor eIF2α, which is critical for

IRES-mediated translation initiation (Thompson et al., 2001).

3.3.2 Preparation of yeast ribosome-nascent chain complexes

The *in vitro* translation reaction was loaded onto a high salt sucrose cushion and subjected to ultracentrifugation. This separated the ribosomal complexes from the remaining cell extract components. The presence of an N-terminal tag on the yNC allowed the purification of translating ribosomes. The translation system was optimized to stall ribosomes using a mutant of eRF1 which cannot trigger the nascent chain release during the *in vitro* translation reaction (Figure 3.3). Moreover, a CMV stalling motif was introduced in the coding sequence of the synthetic mRNA in order to efficiently stall the translating ribosomes and stabilize them during the purification procedure. Subsequently, a larger fraction of tRNA-bound nascent chain in the ribosomal pellet was detected after ultracentrifugation (Figure 3.3). The possibility cannot be excluded that tRNA-yNC failed to be detected on Western blots during earlier experiments, due to sensitivity of our detection technique. In fact, the peptidyl-tRNA is usually detected radioactively after RNC purification according to published protocols (Beckmann et al., 2001; Brown et al., 2015), which is more sensitive than Western blotting.

3.3.3 Purification of termination complexes

eRF1AGQ, eRF3 and Pab1p full length proteins were purified from *E. coli* (BL21(DE3)*) using a C-terminal hexahistidine tag. Upf1p full length with an N-terminal hexahistidine tag was produced in insect cells (*Sf21*). Whereas eRF1AGQ and eRF3 formed a stable complex, we could not detect a ternary complex after addition of Pab1p or Upf1p under the tested conditions (Figure 3.4). It was thus decided to fuse Pab1p or Upf1p to eRF3 in order to promote complex formation and enrich the presence of Upf1p / Pab1p at the ribosome. The fusion proteins Pab1p-eRF3 and Upf1p-eRF3 could be purified (Figure 3.5). However, only Pab1p-eRF3 could form a complex with eRF1AGQ during the SEC experiments (Figure 3.5). It can be speculated that the eRF1:Upf1p-eRF3 interaction is too transient, possibly due to steric problems, and thus dissociates during gel filtration. In addition, we cannot exlude that, despite being long and flexible, the linker could interfere witht the protein interactions.

3.3.4 Reconstitution of termination complexes and single particle analysis

Using co-sedimentation experiments, it was revealed that eRF1AGQ:Pab1p-eRF3 complexes interacted with 80S ribosomes, and that this interaction was sensitive to high salt

concentrations in the buffer (Figure 3.6). The reconstitution of RNC:eRF1AGQ:Pab1p-eRF3 complexes were conducted in presence of GMPPNP to block eRF3's GTPase activity. These complexes were used for cryo-grid preparation and a test cryo-EM data set was collected (Figure 3.6). Image processing of a small dataset of 42,239 ribosomal particles resulted in a structure from a subpool of 2,480 particles (5% of the dataset) that contained a P-site tRNA and density in the A-site corresponding to eRF1AGQ and eRF3. However, no density could be observed for Pab1p (Figure 3.7). The number of particles was insufficient when compared to the other published ribosomal complex structures (Becker et al., 2011; Preis et al., 2014), indicating that the *in vitro* translation protocol required further improvement. Overall, these observations indicated that the RNC preparation could be further optimized to increase the fraction of translating ribosomes. Peptide-tRNA is sensible to pH and thus buffers at pH7.0 instead of pH7.5 should be used for the purification. In addition, the RNCs probably decay over time and therefore, the RNCs should be prepared freshly before sample freezing. At this point, the possibility that the absence of Pab1p density was due to the addition of release factors during the *in vitro* translation cannot be excluded. It is possible that the eRFs could not be efficiently removing during sucrose cushion centrifugation and thus addition of a ten-fold excess of eRF1AGQ:Pab1p-eRF3 was not sufficient. The interaction between and eRF1AGQ and Pab1p-eRF3 may be transient. It is possible that this complex is too weak to survive the vitrification procedure, resulting in a complex that lacks density for Pab1p in our final reconstruction because this part of the complex is flexibly attached to eRF3. In fact, eRF1AGQ is not completely inactive and retains 5 % activity in peptidyl-tRNA hydrolysis (Alkalaeva et al., 2006). So it is possible that, in the presence of the ribosome, the basal activity of the release factors could have been stimulated by Pab1p and resulted in nascent peptide hydrolysis and factor release. Last but not least, the previously published ribosomal volumes used at least 20,000 particles for the final reconstruction (Brown et al., 2015; Matheisl et al., 2015). In order to build an atomic model of a terminating ribosome in the presence of the release factors and Pab1p a significantly larger cryo dataset must be collected.

3.3.5 Final experiments and eRF3 interaction with Upf1 and Pab1p

Our experiments have shown that the purity of RNC could be further improved by the pre-incubation of the streptavidin resin with yeast total RNA and BSA (Figure 3.8). In addition, the interaction between eRF3, Upf1p and Pab1p was investigated (Figure 3.9). The results have hinted toward the formation of a eRF3:Upf1p complex when high protein concentrations were used but this result is yet to be confirmed by additional biochemical techniques such as surface plasmon resonance and isothermal

titration calorimetry. eRF3 complexes with Pab1p could not be isolated. Nevertheless, the binding of Upf1p and Pab1p to eRF3 has been reported previously in yeast (Wang et al., 2001; Cosson et al., 2002a; Kobayashi et al., 2004; Cosson et al., 2002b) and humans (Hoshino et al., 1999; Kashima et al., 2006; P. V. Ivanov et al., 2008; Kozlov & Gehring, 2010). Using yeast two-hybrid and co-immunoprecipitations, the interaction between the two proteins could be mapped to the N and the M domains of eRF3 and the C-terminal part of Pab1p (comprising amino acids 406-577) (Roque et al., 2014). It is worth noting that the N terminal domain of eRF3 is not conserved between yeast and humans. In this thesis work, unlike previously published studies (Kervestin et al., 2012; Roque et al., 2014), no direct *in vitro* interaction between eRF3 and Pab1p could be observed. As different experimental settings were tested compared to these studies, it cannot be excluded that the binding between eRF3 and Pab1p requires conditions similar to those in previously published work. Despite using a very high concentration (40 µM) of purified Pab1p and His_6-eRF3 for our binding assay (Figure 3.9), an interaction was not confirmed. Taken together, these observations indicate that the affinity between yeast Pab1p and eRF3 is very low under the tested conditions. Further work is required to determine whether this interaction could be detected in a different buffer or if it is mediated by other proteins.

3.3.6 Concluding remarks

During this doctoral research study, a yeast *in vitro* translation system was established in our laboratory and provided a framework for the reconstitution of RNC complexes and their examination by cryo-EM single particle analysis. Biochemical experiments were also established to study protein-protein interactions which were critical for the second part of this work (see Chapter 4).

Furthermore, attempts were made to study the interplay of yeast Upf2p and Upf3p with the release factors. Despite our efforts, only high-purity full length Upf3p could be obtained (Figure 3.13). Since full length as well as fragments of human UPF3B were already available in our laboratory, we decided to switch our focus to the human model. The following section details the work done during this doctoral thesis to investigate the role of human UPF3B in NMD and termination of translation.

3.4 Methods

3.4.1 Molecular Biology Techniques

3.4.1.1 Cloning of yeast nascent chain and protein constructs

Sequence and ligation independent cloning (SLIC) and self-SLIC.

Sequence and ligation independent cloning (SLIC) was performed as described previously (M. Z. Li & Elledge, 2007). SLIC reactions without an insert were performed in order to introduce mutations or generate truncations of the sequence of interest. This is referred as to self-SLIC (Figure 3.10). Briefly, the vector was amplified by PCR using primers carrying mutations. 40 U of *DpnI* enzyme was added to 100 µL of PCR reaction and incubated at 37°C for 1 h. The DNA was purified using via a PCR purification and a DNA extraction kit (Qiagen). Subsequently, 1 µg of plasmid was treated with 0.5 U of T4 DNA polymerase in T4 ligase buffer in 20 µL at RT for 30 min. The reaction was stopped by adding 1/10 volume of 10mM dCTP and left on ice. Annealing reactions were set up with 150 ng of linearized plasmid with 1x T4 ligase buffer at a final volume of 10 µL and incubated at 37°C for 30 min. 5 µL of the annealed mixture was used to transform chemically competent TOP10 *E. coli* cells (Thermo Scientific).

yNC mRNA cloning.

The yeast Nascent Chain (yNC) plasmid construct was ordered from Clontech and sub-cloned into pUC19 through the *Eco*RI and *Nco*I restriction sites. The boxB and poly(A) sequence was inserted via the *Not*I and *Hind*III restriction sites from pBS-BMS_EF3_3boxBpA73 to generate pUC19-SBP-yNC-BoxB-pA plasmid (Duncan et al., 2006). The 3Strep-tag was amplified by PCR from pUC19-3Strep-FtsQ-SecM (Schaffitzel & Ban, 2007) and subcloned into pUC19-SBP-yNC-BoxB-pA plasmid via *Eco*RI and *Spe*I. A CMV stalling motif was inserted by PCR using the T7 primer and a reverse primer containing the CMV sequence (see primers in Appendix A). The resulting PCR fragment was subcloned into pUC19-SBP-yNC-BoxB-pA using *Eco*RI and *Nco*I restriction enzymes. The IRES motif was amplified from pUC18-CPV-UAA_mRNA (kind gift of Elena Alkalaeva) and sub-cloned into yNC plasmid using *Eco*RI and *Nhe*I.

yNC plasmid production and linearization.

yNC plasmids were transformed into XL1-Blue competent cells. A Lysogeny broth (LB) medium culture with 200 µg/mL ampicillin were started from 10 colonies. Incubation was completed overnight in an orbital shaker incubator at 37°C and 150 rotations per

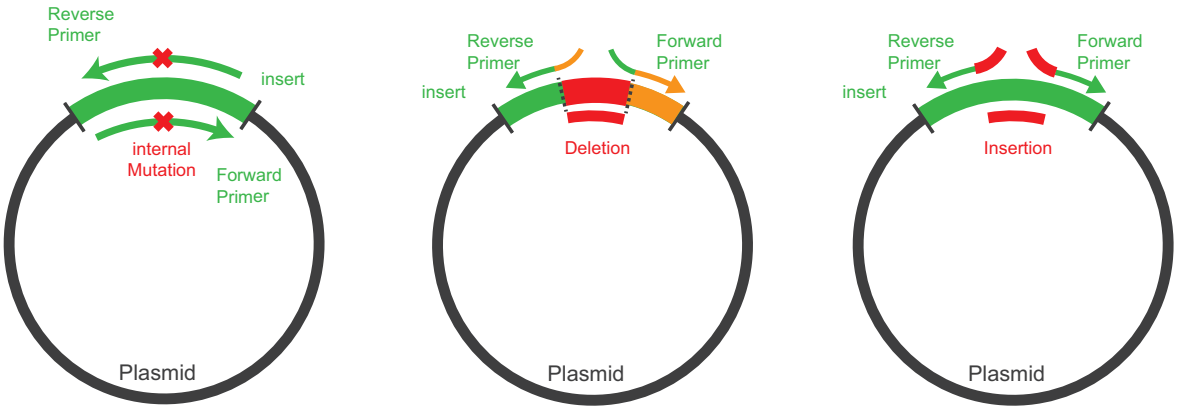

Figure 3.10: Vector modification using self-SLIC. *Scheme representing different mutagenic primers (arrows) allowing the introduction of mutations (left), or deletions (middle) or insertions (right) within the sequence of interest (green thick line). Modifications are indicated in red, primers as arrows, and the remaining plasmid is represented as a black circle.*

minute (rpm). Cultures were stopped when OD_{600} was above 1. For plasmid production, 1 L of LB with 100 µg/mL ampicillin was inoculated with 1 mL of an overnight culture. Bacteria were grown overnight at 30°C and 150 rpm in a shaking incubator and stopped when OD_{600} reached 1. Cells were pelleted at 5,500 rpm for 20 minutes at 4°C using a JA8.1000 rotor and aliquots from 2 L culture were stored at -80°C if not used immediately. DNA plasmid extraction was performed under RNAse-free conditions using the Qiagen MaxiPrep Kit according to the manufacturer's protocol. *HindIII* was used in an overnight digestion to linearize the vector. 100 µg of DNA was digested with 292 U of *HindIII* in buffer 2 (New England Biolabs) overnight at 37°C. Linearization was verified by comparison with undigested plasmid by the addition of 4 µL of 4x loading DNA dye followed by electrophoresis on a 1 % agarose gel . *In vitro* transcription was performed as described in section 3.4.1.2.

eRF1AGQ, eRF3, Pab1p and Upf1p and fusion proteins cloning.

S. cerevisiae eRF1AGQ and eRF3 sequences containing a C-terminal hexahistidine tag were ordered from GenScript and and inserted into pET21. pET22-Pab1p with a C-terminal hexahistidine tag was kindly donated by Bertrand Seraphin. The gene encoding Upf1p was ordered from GenScript and subcloned into pFastBac-Htb (N-terminal hexahistidine tag). In order to generate fusion-proteins, inserts were subcloned into a pFastBac plasmid engineered by Lahari Yeramala, the pFastBac-11linker (*Nco*I - *Sal*I - *Not*I - [GGGGS]x11 - *Nhe*I - *Sac*I - *Kpn*I - TEV - StrepTag - stop - *Nsi*I - *Hind*III). For Upf1p/Pab1p-eRF3 fusion proteins, the eRF3 sequence was amplified by PCR and subcloned into the pFastBac-11linker using *Nhe*I and *Sac*I restriction enzymes. Upf1p and Pab1p inserts were then, after PCR amplification, subcloned into the plasmid containing eRF3 using *Sal*I / *Not*I and *Nco*I / *Sal*I restriction sites, respectively. To generate eRF3-Upf1p/Pab1p fusion proteins, the eRF3 sequence was

amplified by PCR and subcloned into the pFastBac-11linker plasmid using *Xho*I and *Not*I restriction enzymes. Upf1p and Pab1p were amplified by PCR and subcloned into the plasmid containing eRF3 using *NheI* and *SacI* restriction sites.

3.4.1.2 RNA Techniques

In vitro transcription with T7 RNA polymerase.

100 µg of linearized plasmid was transcribed *in vitro* with 37.5 µg of T7 RNA polymerase in 200 mM HEPES/KOH, pH 7.6, 30 mM $Mg(OAc)_2$, 2 mM spermidine, 40 nM DTT, 8.75 mM dNTPs, 0.4 mg/mL RNAsin (Promega). Reactions were incubated for 4 hours at 37°C.

In vitro transcription with T3 RNA polymerase.

Luciferase mRNA was transcribed from the pUC19-CA_fireflyLUC (Promega) plasmid using the mMESSAGE mMACHINE® High Yield Capped RNA Transcription Kit (Ambion).

RNA purification.

In order to purify mRNA from DNA and proteins, lithium chloride precipitations were performed by the addition of 800 µL of 6 M LiCl into a final volume of 1,600 µL. Reactions were vortexed and kept on ice for at least 30 min. After 30 minutes of centrifugation at 14,000 x g at 4°C, the pellet was washed with 500 µL of 70 % ethanol. The pellet was resuspended in 100 µL RNAse-free water. Ethanol precipitations were carried out by the addition of 100 µL 97 % ethanol and 4 µL of 3 M sodium acetate. Reactions and wash steps were performed as for the LiCl precipitation. Finally, the pellet was resuspended in 20 µL of RNAse-free water.

mRNA concentration determination.

mRNA concentration was determined as follows: 1 µL of sample was diluted 1/10 into RNAse-free water and the absorbance at 260 nm was determined. RNA concentration was calculated on the basis that an OD_{260} of 1 corresponds to 40 µg/mL RNA.

RNA agarose gel electrophoresis.

Analytic RNA agarose gels were run to assess the mRNA quality. RNA molecules were separated on agarose gels containing 1.5 % agarose in freshly prepared RNAse free 1 x TBE. Guanidinium isothiocyanate and ethidium bromide were added to the agarose gel to a final concentration of 20 mM and 0.05 µL/mL respectively. Before loading, samples were mixed in a 1:2 [v/v] ratio with RNA loading dye (ThermoFisher Scientific) and incubated for 10 min at 70°C to dissolve secondary structures. Electrophoresis was

carried out at 70 V for 45 min.

RNAse contamination test.

To test proteins for contaminating RNases, 100 ng of mRNA was incubated alone or with 2 - 5 pmoles of protein in a final volume of 10 µL at 37 °C for 1h, followed by RNA agarose gel electrophoresis, as described above. The presence of RNases in the protein sample would result in degradation of the mRNA, as indicated by a diminution of the full size mRNA band and the appearance of lower molecular weight bands (smear) after electrophoresis.

mRNA capping.

To dissolve potential secondary structures, the uncapped mRNA was denatured at 65 °C for 10 minutes and transferred onto ice immediately. VCE and mRNA were mixed in a 1:2 ratio in 1x script capping buffer (Epicentre Biotechnologies) supplemented with 1 mM GTP and 0.1 mM S-adenosylmethionine (SAM) (final concentration). The reactions were incubated for 45 min at 37 °C, frozen in liquid nitrogen and stored at -80°C, if not used immediately.

3.4.2 Cell Culture

Yeast cultures.

Yeast extracts were prepared from the RH2585 strain (*MATa, ura3-52, trp1::hisG, his3::hisG* - kind gift of Prof. Altmann). A second strain was designed with Robbie Loewith's laboratory in Geneva where eRF1 (sup45 in yeast) was TAP-tagged in order to deplete it from the cell extract. This yeast strain background is the following: *TB50 sup45-TAP: a leu2 ura3 rme1 trp1 his3Δ GAL+ HMLa.* A few µL of the glycerol stock of yeast were streaked out onto yeast extract peptone dextrose (YPD - 2 % [w/v] tryptone, 1 % [w/v] yeast extract, 2 % [w/v] glucose) agar-agar plates and incubated for 48h at 30°C. 10 colonies from each plate were used to start 20 mL precultures in YPD media at 30°C and 150 rpm overnight. The overnight pre-cultures were used to start 5 L cultures by dilution 1:1,000. Cultures were stop when the OD_{600} reached 1 in order to avoid overgrowth. The cells were pelleted at 5,000 rpm for 5 min at 4°C using a JA8.1000 rotor.

***E. coli* expression: eRF1AGQ, eRF3, Pab1p, VCE.**

Plasmids were transformed into chemically competent BL21(DE3)* cells. 20 mL cultures were grown overnight at 37°C from a single colony in LB medium containing 100 µg/ml ampicillin. 1 liter of TB medium containing 100 µg/ml ampicillin was inoculated with 10 ml of overnight culture and grown until an OD_{600} of 0.8 was

reached. The expression was induced by addition of 0.5 mM IPTG (Isopropyl β-D-1-thiogalactopyranoside) at 20°C and continued incubation overnight. The cells were harvested by centrifugation at 5,500 rpm and 4°C for 20 min using a JA8.1000 rotor.

Insect cell culture: Upf1p and fusion proteins expression.

Proteins were expressed in the cell line *Spodoptera frugiperda* (*Sf*21 - Invitrogen) using the MultiBac system as previously described (Fitzgerald et al., 2006). Briefly, *Sf21* insect cells were transfected with a recombinant bacmid isolated from DH10-EMBacY cells and grown in Sf-900 media (ThermoFisher Scientific) (Bieniossek et al., 2008). V0 was produced in a 6-well plate with 3 mL of culture per well. This virus was used to generate a higher titer V1 by infection of 25 mL *Sf21* cell cultures in a shaker flask. The V1 was used for large scale protein production by infection of 400 mL of Hi5 insect cells (ThermoFisher Scientific) in Express-Five medium (ThermoFisher Scientific) in 2 L flasks. The cells were harvested 72 - 96 h following the day of proliferation arrest (DPA) when the expression of the internal expression reporter, yellow fluorescent protein (YFP), plateaued. The cells were harvested by centrifugation at 1,000 x g in a JA8.1000 rotor for 10 min at 4°C.

3.4.3 Protein Biochemistry

3.4.3.1 Protein biochemistry techniques

Western blotting.

The PVDF membrane (Millipore) was activated in 100 % methanol for a few seconds. Proteins from the SDS-PAGE were transferred to the membrane soaked in transfer buffer (25 mM Tris-Base, 192 mM Glycine, 20 % EtOH) at 25 V for 1 h using a Trans-Blot SD Semi-Dry Transfer Cell (Bio-Rad). Non-specific interactions were reduced by blocking buffer consisting of 3 % BSA in PBS buffer (137 mM NaCl, 2.7 mM KCl, 1 mM Na_2HPO_4, 1.8 mM KH_2PO_4, pH 7.4) supplemented with 0.05 % [v/v] Tween-20 for at least 1 h at room temperature. The membrane was incubated with the appropriate dilution of antibody or Streptavidin or Strep-Tactin in PBS + 0.05 % Tween-20 with 0.75 % BSA. Streptavidin coupled with Horseradish Peroxidase (HRP) (Sigma) and Strep-Tactin coupled with Alkaline Phosphatase (AP) (IBA Lifesciences) were diluted 1/4,000 and incubated with the membrane for 1 h. His-tagged proteins were detected using 1/10,000 dilution of mouse monoclonal anti-polyHistidine antibody coupled to AP. After washing in PBS + 0.05 % Tween-20 for 3 x 15 minutes, blots with AP were developed using BCIP/NBT photoreaction solution (100 mM Tris, 100 mM NaCl, 5 mM $MgCl_2$, 1 % [v/v] BCIP/NBT (Roche), pH 8.8). Western blots with HRP were developed using 3,3´-Diaminobenzidine tablets (Sigma) in 1 mL of ultrapure water.

3.4.3.2 Protein purification

Yeast eRF1AGQ, eRF3, Pab1p and Upf1p purification.

Cell pellets were lysed in buffer B (20 mM HEPES/KOH pH 7.5, 300 mM KOAc, 10 % [v/v] glycerol, 5 mM β-Mercaptoethanol) and 10 mM imidazole by 2 passages in a French press cell with a pressure of 20,000 psi. The lysed cells were centrifuged for 30 min at 31,000 rpm at 4°C using a Type 70Ti rotor (Beckmann Coulter). The lysate was applied to 10 ml of 50 % slurry Ni-NTA resin (Qiagen) and washed with buffer B plus 1 M KOAc and 50 mM imidazole. The protein was eluted with buffer B containing 200 mM imidazole. If required, the hexahistidine tag was cleaved by the addition of TeV protease [1/50] during overnight dialysis into buffer C (20 mM HEPES/KOH pH 7.5, 2.5 mM $Mg(OAC)_2$, 5 % [v/v] glycerol, 100 mM KOAc) at 4°C supplemented with 5 mM β-Mercaptoethanol. Subsequently, the sample was incubated with Ni-NTA resin and the flow-through collected. The sample was loaded onto a MonoQ 5/50GL column (GE Healthcare), pre-equilibrated with buffer C plus 2 mM DTT. The proteins were eluted by a 40 ml gradient from 100 mM – 1 M KOAc. The proteins were further purified by size-exclusion chromatography using a Superdex 200 column (GE Healthcare) pre-equilibrated with buffer C plus additional 50 mM KOAc and 2 mM DTT.

Purification of vaccinia capping enzyme (VCE).

Cell pellets were lysed in buffer D (40 mM HEPES/KOH pH 8.0, 200 mM NaCl) and 40 mM imidazole by sonication. The lysed cells were centrifuged at 30,000 rpm for 20 min at 4°C using a Type 70Ti rotor (Beckmann Coulter). The lysate was applied to 10 ml Ni-NTA resin (Qiagen) and washed with buffer D supplemented with 1 M NaCl and 60 mM imidazole. The proteins were eluted with buffer D, plus 300 mM imidazole. The His tag was cleaved by the addition of 1/100 TeV protease [w/w] at 4°C during overnight dialysis in buffer D supplemented with 3 mM β-Mercaptoethanol. The sample was loaded onto a 5 ml pre-packed Heparin column (GE Healthcare), pre-equilibrated with buffer D containing 3 mM β-Mercaptoethanol. VCE was eluted by a 20 ml gradient from 200 mM – 1 M NaCl. The protein was further purified by size-exclusion chromatography using a Superdex 200 column (GE Healthcare) equilibrated with buffer D and 3 mM DTT (Kyrieleis et al., 2014).

3.4.3.3 Yeast Extract preparation and purification

After harvesting, the yeast cell pellets were washed in DEPC (Diethylpyrocarbonate) water and subsequently with buffer A (30 mM HEPES/KOH pH7.4, 100 mM KOAc, 2 mM $Mg(OAc)_2$, 2 mM DTT, 0.1 mM PMSF) supplemented with 8.5 % [v/v] mannitol. The cells were frozen in liquid nitrogen and grinded using a mortar and a pestle until a

homogenous paste was obtained. The reactions were pelleted twice at 13,000 rpm for 15 min at 4°C using a tabletop centrifuge (Eppendorf). Subsequently, the supernatant was further purified using a Sephadex G25 column equilibrated with buffer A. Fractions with A_{260} close to 100 rlu were frozen in liquid nitrogen and stored at -80°C.

3.4.3.4 *In vitro* translation and RNC preparation

Luciferase assay using the yeast cell-free translation system.

Capped and polyadenylated Renilla luciferase (Rluc) mRNA was used to measure translational activity in an untreated cell extract (exogenously added mRNA will compete with endogenous mRNA for translation). 20 ng Rluc mRNA was translated with 50 % [v/v] yeast extract, 0.04 mM amino acids (-methionine), 25 mM creatine phosphate, 0. 5 mg/mL creatine phosphokinase, 1 U RNAsin (Promega) in a final volume of 10 µL. Samples were incubated for 45 min in a 25°C water bath. Reactions were stopped by the addition of 12 µL of 1x passive lysis buffer (Promega Dual-Luciferase). 20 µL samples were supplemented with 50 µl luciferase assay reagent (Promega), and luminescence was read out from a 96 well plate on a plate reading luminometer (Mithras, Berthold Technologie). The luminescence was detected 1.6 sec after injection of the substrate solution for 10 sec.

***in vitro* translation of yNC mRNA.**

100 nM yNC mRNA was translated in 50 % [v/v] yeast cell extract (~100 OD_{260}/mL) for 60 minutes at 25°C in 20 mM HEPES/KOH, pH 7.5, 150 mM KOAc, 1.5 mM $Mg(OAc)_2$, 2 mM DTT, 25 mM creatine phosphate, 0.5 mg/mL creatine phosphokinase, 0.75 mM ATP, 0.1 mM GTP, 0.4 mM amino acids (-methionine), 1 U/µL RNAsin (Promega). 4 µM of eRF1AGQ and eRF3 were added to the reaction. The *in vitro* translation reaction was stopped by 0.2 µg/µL cycloheximide, a translocation inhibitor. Subsequently, the ribosomes were pelleted through a 3 mL high salt sucrose cushion (50 mM HEPES/KOH pH7.5, 220 mM KOAc, 25 mM $Mg(OAc)_2$, 2 mM DTT, 10 µg/mL cycloheximide, 1 M sucrose and protease inhibitors) by ultracentrifugation using a TLA-55 rotor (Beckmann Coulter) at 4°C, 3 h at 55,000 rpm. The ribosomal pellets were resuspended in RNC buffer (50 mM HEPES/KOH pH7.5, 2 mM DTT, 10 µg/mL cycloheximide) supplemented with 50 mM KOAc and 5 mM $Mg(OAc)_2$.

RNC affinity purification.

Subsequently, non-translating ribosomes were removed by an affinity purification step. Resuspended pellets were added to 500 µL of streptavidin beads (Fisher Scientific) in RNC buffer supplemented with 50 mM KOAc and 5 mM $Mg(OAc)_2$ and 0.05 % [v/v] Tween20. The beads were washed with 5 volumes (cv) of RNC buffer with

220 mM KOAc and 25 mM $Mg(OAc)_2$. RNCs were eluted with 1 cv of RNC buffer supplemented with 100 mM KOAc and 2.5 mM $Mg(OAc)_2$ and 2 mM biotin. The final RNC concentration was measured using A_{260} and the purity of the RNCs was evaluated by coomassie stained SDS-PAGE gel and Western blot using an appropriate antibody against the yNC tag.

Ribosome binding experiments.

For co-sedimentation experiments, 2 pmol of yeast total ribosomes were mixed with a ten-fold molar excess of eRF1AGQ and eRF3 or fusion protein in 20 µL of RNC buffer with 100 mM KOAc and 2.5 mM $Mg(OAc)_2$ and incubated for 1 hour on ice. Subsequently, the reaction mixtures were applied on a sucrose cushion (same buffer containing 1 M sucrose) and centrifuged for 3 h at 55,000 rpm at 4°C using a TLA-55 rotor (Beckman). Supernatant and pellet fractions were analyzed by SDS-PAGE followed by SYPRO Ruby (Thermo Scientific) staining and Western blot using the appropriate antibody against the yNC tag, or the hexahistidine tag fused to the release factors.

***In vitro* pulldown assays.**

All experiments were performed with 20 mM of each protein in a final reaction volume of 20 µL in buffer D (20 mM HEPES/KOH pH 7.5, 100 mM KCl, 10 mM imidazole, 0.05 % [v/v] Tween20, 5 mM β-Mercaptoethanol, 5 % [v/v] glycerol, 5 mM $Mg(OAC)_2$), if not indicated otherwise. The protein mixtures were incubated for 1 hour on ice; subsequently 20 µL of Ni-NTA agarose (Qiagen) was added to the reaction mix and incubated for 1 hour on ice. The reaction mixtures were washed 5 times with 200 µL of buffer D, and proteins were eluted using buffer D supplemented with 200 mM imidazole by centrifugation at 2,000 rpm for 2 minutes in a tabletop centrifuge (Eppendorf). 8 µL of SDS loading dye were mixed with either 2 µL of input reactions or 20 µL of the eluted complexes. 10 µL of the input sample and 10 µL of the elution sample were loaded onto a 10 or 12 % SDS-PAGE gel.

Size exclusion chromatography.

For SEC, 7 µM of each protein was added to a final reaction volume of 60 µL in buffer E (20 mM HEPES/KOH pH 7.5, 150 mM KCl, 5 mM $Mg(OAc)_2$, 2 mM DTT). The protein mixtures were incubated for 1 hour on ice before loading onto a Superdex 200 PC3.2/30 column (AEKTA micro system, GE Healthcare). 10 µL of each elution fraction was loaded onto a 10 % SDS-PAGE gel. The SEC runs in section 3.2.4.2 were performed with 40 µM instead of 7 µM.

3.4.4 Electron microscopy

Negative staining electron microscopy.

Samples were applied to a carbon film deposited on a 300 mesh copper grid (Quantifoil), followed by staining with 2 % uranyl acetate solution. Grids were dried and then inserted into the microscope. Image acquisition was performed at room temperature in a JEOL JEM-1200EX II microscope using high magnification (30 k – 50 k) and a Gatan ORIUS CCD camera .

Cryo-grid preparation.

2 pmol of RNCs were incubated with 10x molar excess of purified eRF1:eRF3-Pab1p in RNC buffer supplemented with 100 mM KOAc, 2.5 mM $Mg(OAc)_2$ and 200 µM GMPPNP. 3.5 µL of this sample were applied to Quantifoil grids R 2/2 type with a thin continuous carbon foil. The grids were previously glow discharged (for 1 min at 25 mA and at 1 x 10 1 mbar). Subsequently, the grids were vitrified using a Vitrobot Mark IV (FEI Company) at 5 °C and 100 % relative humidity with a 2 min incubation before blotting.

Cryo-electron microscopy and single particle reconstruction.

Data collection was performed by Manikandan Karuppasamy on a Tecnai POLARA F30 (FEI Company) equipped with 4k x 4k CCD camera (Gatan Inc), operated at 300 keV using the EPU software (FEI). 1,740 micrographs were collected at a magnification of 50,000 x and a nominal defocus between -2.5 and -3.5 µm. The pixel size was 1.93 Å. 575 micrographs were discarded after contrast transfer function (CTF) correction (bctf, Bsoft Package; (Heymann, 2001)) and 42,239 ribosomal particles were manually picked with EMAN2 (Tang et al., 2007). The particles were aligned and refined using the RELION autorefine procedure (S. H. W. Scheres, 2012) and an *S. cerevisiae* 80S empty ribosome (EMDB 2275 (Bai et al., 2013)) was used as an initial model. 3D classification was performed to sort out the particles into 5 classes. From the 5 resulting reconstructions, one reconstruction contained a ribosome with P-Site t-RNA. This reconstruction contained 27 % of the dataset (11,700 particles). It was further autorefined with RELION and subjected to a new round of classification using the same parameters. From the five new reconstructions, one class showed P-Site tRNA and density in the A-site, this class contained 2,480 particles (5.8 % of the dataset).

3.4.5 Acknowledgements

We are much obliged to Prof. Karl Altmann for generously introducing us to the reconstituted *in vitro* translation system and for providing the RH2585 yeast strain, Robbie

Loewith for TB50 engineered strain, Bertrand Seraphin for the Pab1p expression plasmid and Elena Alkalaeva for providing the CrPV construct. This work is supported by an European Research Council Starting Grant (ComplexNMD, 281331)

3.5 Supplemental information

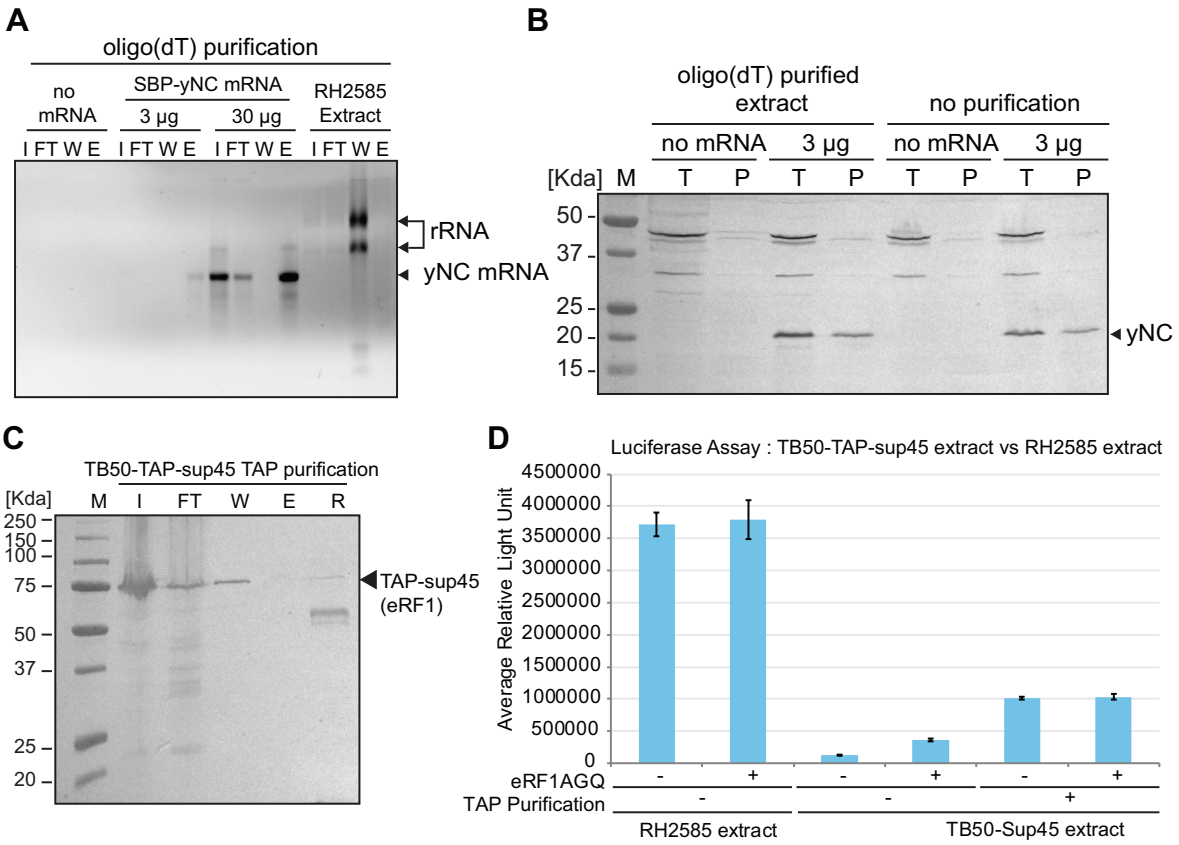

Figure 3.11: mRNA depletion of the yeast extract for in vitro translation. A. *RNA gel analysis of the endogenous mRNA depletion experiment using oligo(dT) resin, showing input (I), flow-through (FT), last wash (W) and elution (E) fractions. SBP-yNC contains a poly(A) tail and was used as a positive control* ***B.*** *Western blot analysis of 100 µL of in vitro translation with depleted extract (Oligo(dT) purified) and un-depleted (no purification) using 1/4,000-diluted streptavidin-HRP for the total reaction (T) and after sucrose cushion ultracentrifugation (Pellet - P). eRF1 (TAP-sup45) depletion of the TB50-TAP-sup45 cell extract for in vitro translation.* ***C.*** *Western blot analysis of eRF1 TAP purification using dynabeads (Invitrogen) coupled with IgG, showing input (I), flow-through (FT), last wash (W), elution (E) fractions and resin (R).* ***D.*** *Luciferase assay using the yeast in vitro translation system and wildtype yeast extract or TB50-Sup45 yeast extract with or without TAP purification and addition of exogenous eRF1AGQ. M: protein molecular weight standards (kDa).*

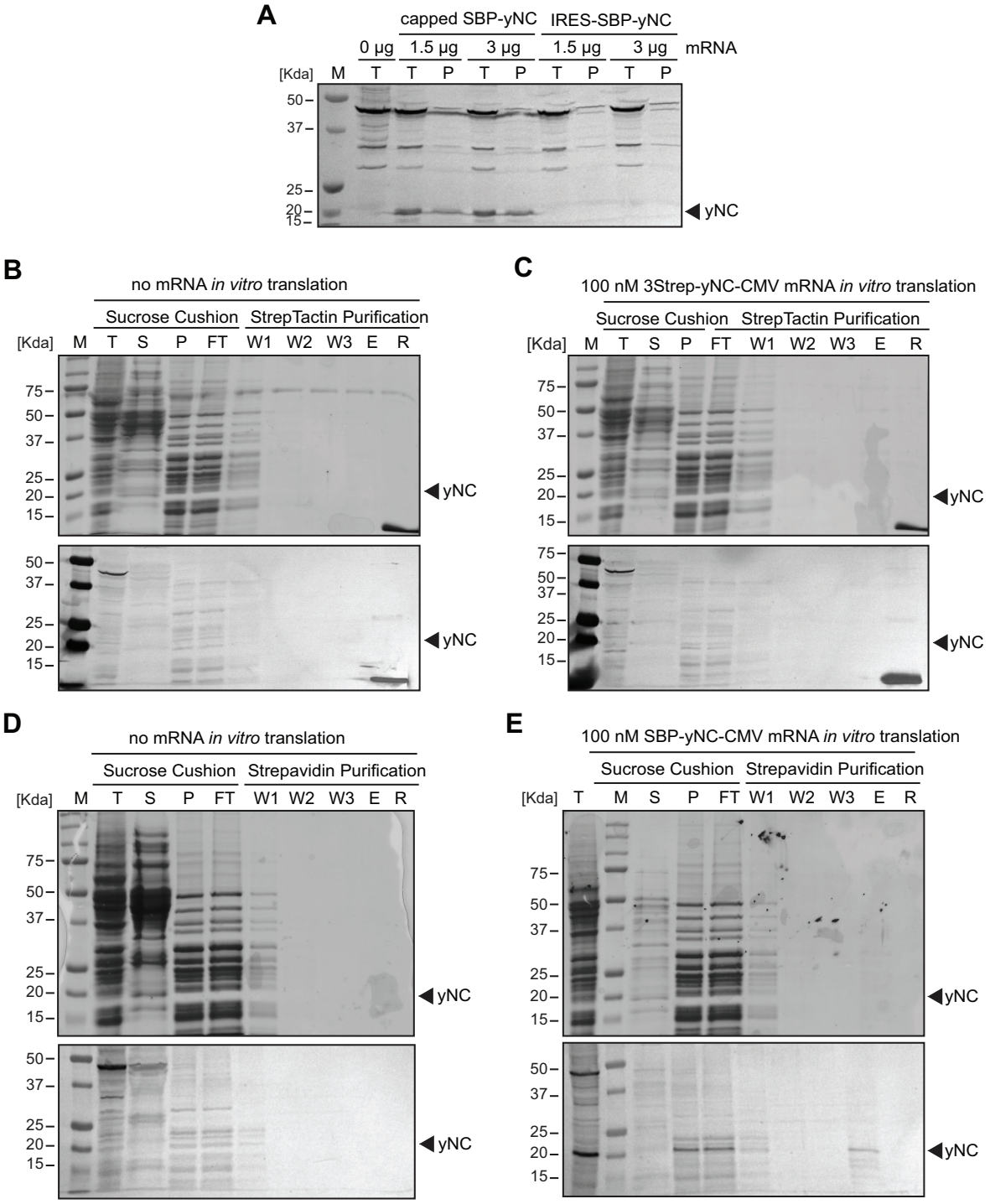

Figure 3.12: yNC mRNA construct optimization. ***A.*** *Western blot analysis of in vitro translation using capped SBP-yNC or IRES-SBP-yNC. Two mRNA concentrations were used for in vitro translation. Western blot was performed with streptavidin-HRP for the total reaction (T) and after sucrose cushion ultracentrifugation (Pellet – P). 100 µL translation reaction.* ***B.*** *Western blot analysis of RNC purifications without mRNA using Strep-Tactin resin.* ***C.*** *RNC Purification using 3Strep tagged yNC mRNA using Strep-Tactin resin.* ***D.*** *Same as A. using strepavidin resin.* ***E.*** *Same as B. using SBP tagged yNC and strepavidin resin. Western blots were performed using streptavidin-HRP or Strep-Tactin-AP. Total reaction (T), Supernatant (S), pellet (P), flow-through (FT), washes (W1-3) and elution (E). M: protein molecular weight standards (kDa).*

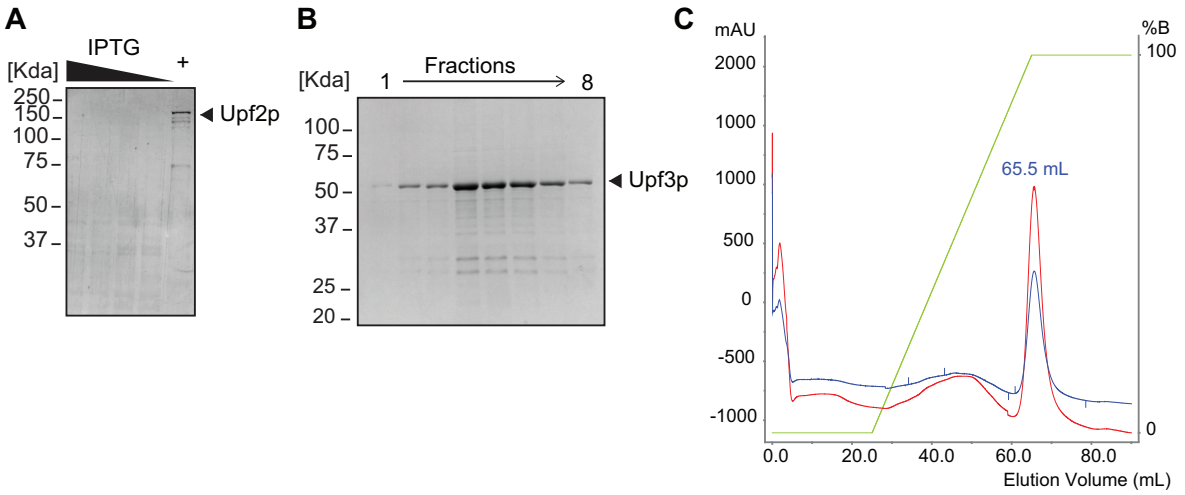

Figure 3.13: Upf2p and Up3p Purification. ***A.*** *SDS-PAGE followed by a Western Blot, using 1/4,000-diluted anti-hexahistidine antibody coupled to alkaline phosphatase, analysis of Upf2p expression in BL21 using different concentrations of IPTG. Human UPF2L (121-1227) was used as a positive control (+).* ***B.*** *SDS-PAGE analysis of Upf3p purification by anion exchange (SP/HP - GE Healthcare).* ***C.*** *Chromatogram of Upf3p purification by anion exchange (SP/HP - GE Healthcare). Absorbance at 280 nm and 245 nm (mAU) is displayed in blue and red, respectively. Elution in mL is indicated for each elution peak. Elution following a KCl gradient (%B) from 150 mM to 1 M is indicated as a green line and the secondary axis.*

4. Double-tasking of UPF3B in early and late phases of translation termination

Resumé en français

L'objectif du travail présenté dans ce chapitre était d'obtenir des informations biochimiques sur les interactions entre les facteurs de terminaison et ceux de la NMD au cours de la terminaison, afin de mettre à l'épreuve le modèle actuel de discrimination des PTCs. Dans cette optique, nous avons utilisé une approche combinant un système de traduction *in vitro*, établi dans notre laboratoire, ainsi que des analyses d'interactions *in vitro* et *in vivo*. Nous avons montré que UPF3B, et non UPF1 ou UPF2, est le seul facteur capable de se lier à eRF1 et eRF3a. D'après nos résultats, UPF1 ne joue aucun rôle significatif dans la terminaison de la traduction *in vitro*. De plus, UPF3B peut s'associer à l'ARN, au ribosome et à UPF1. UPF3B retarde la reconnaissance du codon stop si les facteurs de terminaison sont limitants. Dans le cas où les facteurs de terminaison sont saturants, UPF3B favorise la dissociation des sous-unités ribosomales une fois que le codon stop est reconnu. UPF1 n'a pas d'influence dans cette activité mais la présence de UPF2 abolit le délai de la terminaison et la dissociation du ribosome par UPF3B.

Double-tasking of UPF3B in early and late phases of translation termination

Manuscript under review in Molecular Cell

Authors

Gabriele Neu-Yilik* and Etienne Raimondeau*, Boris Eliseev, Lahari Yeramala, Beate Amthor, Aurélien Deniaud, Karine Huard, Kathrin Kerschgens, Matthias Hentze**, Christiane Schaffitzel**, Andreas Kulozik**

* co-first authors

** corresponding authors

Affiliations

- European Molecular Biology Laboratory, Grenoble Outstation, 71 Avenue des Martyrs, 38042 Grenoble, France
- School of Biochemistry, University of Bristol, Bristol, BS8 1TD, United Kingdom
- Department of Pediatric Oncology, Hematology and Immunology, University of Heidelberg, Im Neuenheimer Feld 430, 69120 Heidelberg, Germany
- Molecular Medicine Partnership Unit, University of Heidelberg and European Molecular Biology Laboratory, Im Neuenheimer Feld 350, 69120 Heidelberg,
- Germany European Molecular Biology Laboratory, Meyerhofstr. 1, 69117 Heidelberg, Germany

Abstract

Nonsense-mediated mRNA decay (NMD) is a cellular surveillance pathway that recognizes and degrades mRNAs with premature termination codons (PTCs). The mechanisms underlying translation termination are key to the understanding of RNA surveillance mechanisms such as NMD and crucial for the development of therapeutic strategies for NMD-related diseases. Here, we have used a fully reconstituted *in vitro* translation system to probe the currently prevailing model of how NMD proteins interact with the termination apparatus. We discovered that UPF3B (1) delays translation termination and (2) dissociates post-termination ribosomal complexes that are devoid of the nascent peptide. These previously unknown functions of UPF3B in early and late phases of translation termination position UPF3B at a central mechanistic step of RNA surveillance and suggest that it may function as a dedicated NMD ribosome rescue factor.

4.1 Introduction

Nonsense-mediated mRNA decay (NMD) is a eukaryotic surveillance mechanism that controls the expression of aberrant mRNAs, degrading transcripts with premature termination codons (PTCs). PTCs can be introduced into mRNAs by mutations, transcriptional errors, and aberrant splicing, but are also contained in 5 -15 % of normal transcripts. By modulating the expression of physiological target mRNAs, NMD serves as a posttranscriptional regulator of gene expression and thus controls important cellular and organismal processes in development, cellular stress responses, immunity, and neuronal differentiation (Kurosaki & Maquat, 2016; Linder et al., 2015; Ottens & Gehring, 2016). NMD is also of medical importance as it limits the production of truncated proteins that may otherwise exert dominant negative functions but can also result in loss of function when mRNAs encoding (partially) functional truncated proteins are degraded (Bhuvanagiri et al., 2010; Nguyen et al., 2014). Mutations or copy number variations in NMD factors are linked to genetic diseases, specifically to neurodevelopmental disorders and intellectual disabilities (Linder et al., 2015; Nguyen et al., 2014).

Conceptually, NMD can be divided into a translation termination phase and an mRNA degradation phase. During the past two decades a wealth of information has accumulated concerning the interplay between the core NMD factors and decay enzymes that enable the recognition and degradation of NMD substrates (Schweingruber et al., 2013; Fatscher et al., 2015). However, the mechanism by which translation termination at a PTC is distinguished from termination at a normal termination codon (NTC) is still poorly understood. Two prevailing models, the "downstream marker model" and the "faux 3'UTR model", have been proposed to explain the difference between normal and aberrant termination as well as the interaction between the terminating ribosome and the NMD machinery (reviewed in (Bhuvanagiri et al., 2010; He & Jacobson, 2015b)). The "downstream marker model" posits the formation of an aberrant termination complex at a PTC consisting of the terminating ribosome, the central NMD effector UPF1, the UPF1 kinase complex SMG1-8-9, and the release factors eRF1 and eRF3. This so-called SURF complex (Kashima et al., 2006) is thought to delay translation termination and to sense the presence of an mRNP complex on the extended 3'UTR which in mammalian cells is represented by an exon junction complex (EJC) downstream of the PTC. The premature termination complex and the EJC are thought to be bridged by UPF2 that, according to this model, interacts with UPF1 at the termination site and EJC-bound UPF3B, leading to the formation of a decay inducing complex that remodels the 3' mRNP and recruits mRNA decay enzymes.

In contrast, the faux 3'UTR model posits that NMD can be induced by an aberrant 3'UTR mRNP, which is characterized by the absence of at least one termination-

enhancing factor that is associated with a normal 3' UTR. Consequently, termination at a PTC is decelerated and inefficient. Such an aberrant 3' UTR mRNP can be defined by the inappropriate distance between the termination codon and the poly(A) tail thus preventing the termination promoting interaction between eRF3a and poly(A) binding protein and instead allowing the recruitment of UPF1.

Both models converge on the central NMD effector UPF1 that interacts with the release factors (eRFs) at the terminating ribosome. For yeast NMD, all three UPF proteins are essential, whereas in higher eukaryotes, UPF2-independent, UPF3B-independent, and EJC-independent NMD branches have been described (Bühler et al., 2006; Chan et al., 2007; Gehring et al., 2005). UPF1 can be recruited to the termination site by the NMD-stimulating EJC, by an aberrant 3' UTR mRNP, or by an inefficient termination event. How UPF2 and UPF3 are recruited to the termination site in EJC-independent NMD is unknown. UPF2 and UPF3B are thought to stimulate the phosphorylation of UPF1 and to activate UPF1's ATPase and helicase functions that are necessary to remodel the 3'UTR mRNP and to recruit mRNA degradation enzymes (Chamieh et al., 2008; P. V. Ivanov et al., 2008; Kashima et al., 2006; Fiorini et al., 2015).

Although the necessity of an interaction between the UPF proteins and the translation termination apparatus is generally accepted, the sequence and timing of NMD factor recruitment to the termination site has not been addressed experimentally. Recent studies revealed that UPF1 is bound along the entire length of transcripts and that this binding occurs in a translation-independent fashion (Hogg & Goff, 2010; Hurt et al., 2013; Zünd et al., 2013). These findings have challenged the hypothesis, proposed by both the downstream marker model and the faux 3'UTR model, that UPF1 is specifically recruited to aberrant termination events as an anchor point for the assembly of an NMD-mRNP.

Translation termination, whether regular or aberrant, needs to recycle ribosomes to avoid deleterious consequences for the translation apparatus (Graille & Séraphin, 2012; J. Lykke-Andersen & Bennett, 2014). In ribosome recycling of normal and different forms of abnormal termination, the ATPase ABCE1/Rli1 is needed for the ultimate dissociation of post-termination ribosomes from the mRNA (Dever & Green, 2012; Franckenberg et al., 2012; Graille & Séraphin, 2012; Jackson et al., 2012). In yeast and human cells, depletion of the UPF proteins induces readthrough at PTCs *in vivo* as well as delayed termination *in vitro* (Amrani et al., 2004; Peixeiro et al., 2012). A recent attempt to reconcile all available data into a new NMD model posits that UPF1, UPF2, and UPF3 have roles in both, the early and late phases of premature termination (He & Jacobson, 2015b). Accordingly, UPF1's initially weak association with elongating ribosomes is proposed to be stabilized by UPF2 and UPF3 when a ribosome terminates prematurely. The UPF1-UPF2-UPF3 complex stimulates the initially de-

layed termination at a PTC by either recruiting the release factors or by enhancing peptide release. Subsequently, UPF2 and UPF3 promote ATP hydrolysis by UPF1 to fuel the dissociation of post-terminating ribosomal complexes. UPF1, still bound to the 40S ribosomal subunit, then recruits mRNA decay enzymes to initiate mRNA degradation.

To shed light on these critical aspects of translation, we adopted an approach that combines a fully reconstituted cell-free *in vitro* translation termination system with *in vitro* and *in vivo* interaction studies to decipher the UPF-eRF interactome in translation termination. We find that UPF3B, rather than UPF1 interacts with eRF3a and forms a trimeric complex with both eRF3a and eRF1. Moreover, UPF3B binds to RNA, the ribosome, and to UPF1. UPF1 plays no discernible functional role in this context, suggesting that it acts downstream to promote NMD. In contrast, UPF3B delays translation termination when release factors are limiting and dissolves post-termination complexes after peptidyl-tRNA hydrolysis by the release factors.

4.2 Results

Validation of the experimental system

During termination at a PTC, the UPF1-eRF interaction is thought to stall translation termination (P. V. Ivanov et al., 2008; Kashima et al., 2006). Here, we set out to analyze whether UPF1 alone or together with UPF2 and/or UPF3B affects the efficiency of mammalian translation termination *in vitro*.

We produced full-length eRF1, eRF3a, UPF1, and UPF3B and a UPF2 variant (UPF2L) comprising amino acids (aa) 121–1227 (Supplemental Figure 4.8A). Ribosomal pre-termination complexes (translating ribosomes stalled at a stop codon; preTCs) were assembled on a model mRNA using ribosomal subunits, aminoacylated tRNAs, and purified initiation, elongation and release factors. The model mRNA (MVHC-STOP) contained the β-globin 5'-UTR and a short open reading frame encoding a MVHC tetrapeptide followed by a UAA stop codon and a 3'UTR of ~400 nt (Figure 4.1A) (Alkalaeva et al., 2006; Fan-Minogue et al., 2008). The formation of defined ribosomal complexes was analyzed by sucrose density gradient (SDG) centrifugation and primer extension inhibition (toeprinting). PreTCs containing the peptidyl-tRNA^{Cys} in the ribosomal P-site and the stop codon in the A-site are characterized by specific toeprints at position +16 nt 3' to the U of the UGC (Cys) codon (Figure 4.1B, lane 1, Supplemental Figure 4.8B).

During translation termination, eRF1 in complex with eRF3a binds to the stop codon (Brown et al., 2015) inducing conformational rearrangements. The formation of such post-termination complexes (postTCs) is manifested by a +1-2 nt forward shift relative to the preTC toeprint (Figure 4.1B, lane 2; Supplemental Figure 4.8B) (Shirokikh et al., 2009). GTP hydrolysis by eRF3a leads to accommodation of the GGQ motif of eRF1 in the peptidyl transferase centre of the large ribosomal subunit, resulting in rapid peptide release. eRF1 (together with eRF3a or after dissociation of eRF3a) remains associated with postTCs, thus maintaining the +2 nt shift of their toeprint (Alkalaeva et al., 2006).

To confirm the biological activity of purified UPF1, UPF2L, and UPF3B, we performed ATP hydrolysis experiments. In previous studies (Chakrabarti et al., 2011; Chamieh et al., 2008). Maximal ATP hydrolysis by UPF1 was achieved at low pH (6-6.5) using N- and C-terminally truncated UPF1 fragments (Supplemental Figure 4.8C). UPF1LΔCH (aa 295-914) lacks the CH domain and exhibits high ATPase activity that cannot be further stimulated, whereas UPF1L (aa 115-914) contains the CH domain and exhibits similar ATPase activity but requires stimulation by UPF2 and UPF3B (Chamieh et al., 2008). In full-length UPF1 (UPF1) the C-terminus contributes to maintaining UPF1 in an inactive state (Fiorini et al., 2013). Using UPF1L

and UPF1ΔCH as controls, we first tested ATP hydrolysis by UPF1 in end-point experiments at pH 6.5 (Supplemental Figure 4.8D). UPF1 exhibited only modest ATPase activity at 30°C and pH 6.5 which was doubled in the presence of UPF2L/3B (Supplemental Figure 4.8D, lanes 2 and 3). In contrast, the ATPase activity of UPF1L was about fourfold compared to that of UPF1 and was strongly enhanced by UPF2L/3B (lanes 4 and 5). The ATPase activity of UPF1LΔCH was comparable to that of UPF1L/2L/3B and could not be further stimulated (lanes 6 and 7). Notably, at a physiological pH 7.5 the activity of all proteins was lower, but followed a similar pattern (Supplemental Figure 4.8D, lanes 8-13). We further investigated the ATPase activity of UPF1, either alone or in the presence of UPF2L, UPF3B or both, under *in vitro* translation conditions at pH 7.5 and 37°C (Supplemental Figure 4.8E). We found that neither UPF2L (lane 5) nor UPF3B (lane 6) have a significant effect on the ATPase function of UPF1. By contrast, when used in combination the ATPase function of UPF1 was slightly enhanced (lane 7). Taken together, these data show that our UPF proteins are biologically active.

UPF3B delays inefficient translation termination in a fully reconstituted translation termination system

According to current models, termination at a PTC contrasts with termination at an NTC by being slow and inefficient, possibly caused by inefficient recruitment of the eRFs (He & Jacobson, 2015b). To simulate this situation *in vitro*, we used limiting concentrations of eRFs for our termination experiments as judged by the retention of a faint but discernible preTC toeprint in addition to the appearance of postTC signals after termination (Figure 4.1B, lane 2).

To test if UPF proteins affect the efficiency of translation termination, preTCs were incubated with excess UPF1, UPF2L, UPF3B or combinations of these proteins (Figure 4.1B, lanes 3-9). As controls, preTCs were either left untreated (lane 1) or the UPF proteins were replaced by BSA (lane 2). Subsequently, limiting amounts of eRFs were added to the reactions (except in lane 1), and translation termination was allowed to proceed for 5 min, followed by toeprinting analysis.

Neither UPF1 nor UPF2L individually (Figure 4.1B, lanes 3, 4) or together (lane 6) affected the intensity of pre- or postTC bands, compared to the control sample (lane 2). These findings indicate that when the eRFs are limiting, neither UPF1 nor UPF2L have a direct effect on translation termination *in vitro*.

By contrast, UPF3B (lane 5) substantially reduced the preTC to postTC transformation rate to about 40 % of the rate observed in the control reaction (lane 2) as estimated by calculating the ratio between the preTC and postTC signal intensities using a phosphorimager. Notably, the addition of UPF1 to UPF3B resulted in a similar delay of termination (lane 7) and did not have an additive, synergistic or reversing

effect. Addition of UPF2L abolished the effect of UPF3B on translation termination (lane 7, 8), indicating that binding to UPF2L may prevent UPF3B from interfering with the termination reaction. We observed that the toeprint signals corresponding to the full length RNA and to the termination complexes as well as to the traces of initiating and elongating ribosomes present in preTC preparations were always stronger in the presence of UPF3B than in reactions without UPF3B. Therefore, we performed toeprinting of preTCs that had been incubated with UPF3B but without eRFs. We found that here, too, all toeprint signals were stronger than in the absence of UPF3B (Figure 4.1B, lanes 1 and 10), which is likely to be caused by a more efficient recovery of ribosomal complexes and RNA.

UPF3B reduces the efficiency of peptidyl-tRNA hydrolysis at low concentrations of release factors

To investigate if UPF3B delays translation termination by impairing peptidyl-tRNA hydrolysis, preTCs assembled on the MVHC-STOP mRNA using ^{35}S-labeled initiator-tRNA were incubated with or without UPF3B, and with limiting amounts of eRFs. In comparison to the maximal rate of peptidyl-tRNA hydrolysis achieved within the observed time window, peptide release efficiency was reduced in the presence of UPF3B by ~40-50 % (Figure 4.1C). We conclude that UPF3B impairs stop codon recognition and peptidyl-tRNA hydrolysis by the eRFs and thereby reduces termination efficiency.

Translation termination *in vitro* is independent of ATP-binding or the ATPase activity of UPF1

ATP binding and hydrolysis by UPF1 are essential for NMD. UPF2 and UPF3B have been shown to stimulate this ATPase function (Chakrabarti et al., 2011; Chamieh et al., 2008). Therefore, we repeated the toeprinting experiment described above in the presence of either ATP (Supplemental Figure 4.9, lanes 2-8) or its non-hydrolyzable analogue AMPPNP (lanes 9-15). Under these conditions, neither UPF1 nor UPF2L individually (lanes 3, 4, 10, 11) or together (lanes 6, 13) affected the intensity of pre- or postTC signals compared to the control samples (lanes 2, 9). By contrast, UPF3B both alone and following addition of UPF1 reduced termination efficiency. These findings were independent of the presence of ATP or AMPPNP, indicating that neither the ATP-binding nor the ATPase function of UPF1 influences the transition of preTCs to postTCs.

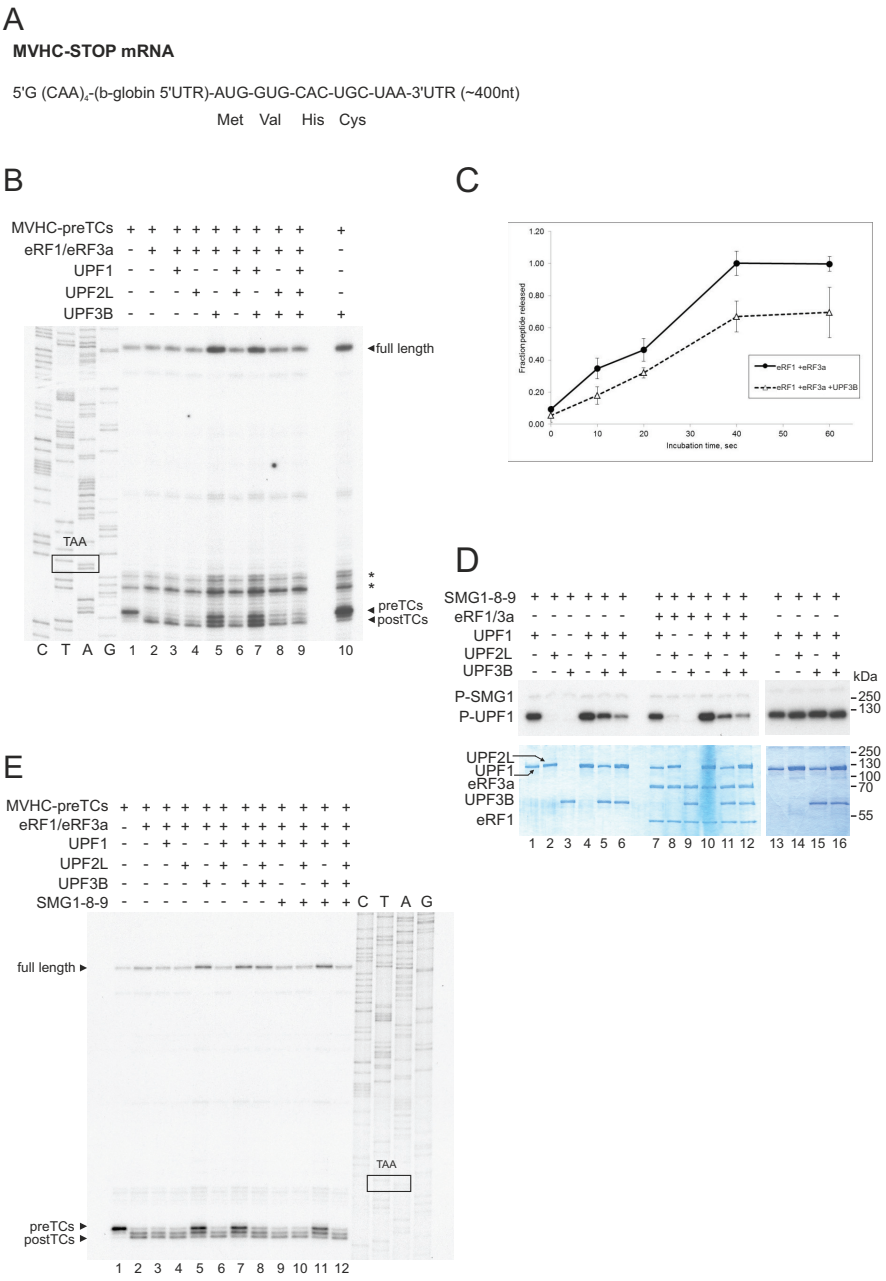

Figure 4.1: UPF3B delays translation termination in vitro. ***A.*** *Structure of the MVHC-STOP mRNA.* ***B.*** *Toeprinting analysis of ribosomal complexes obtained by incubating preTCs assembled on MVHC-STOP mRNA (MVHC-preTCs) with UPF1, UPF2L, UPF3B, or BSA at 1 mM free Mg^{2+} followed by termination with limiting amounts of eRF1 and eRF3a. The positions of preTCs, postTCs, and full length cDNA are indicated. Asterisks mark initiation and elongation complexes.* ***C.*** *Kinetics of [^{35}S]-peptidyl-tRNA hydrolysis in the presence of eRF1 and eRF3a (black circles) or eRF1, eRF3a, and UPF3B (white triangles). A value equal to 1 corresponds to the maximum value for peptide release triggered by eRF1 and eRF3a.* ***D.*** *UPF1 in vitro phosphorylation by SMG1-8-9 in the presence of UPF2L and/or UPF3B and in the presence (lanes 7-12) or absence (lanes 1-6) of the eRFs. In lanes 13-16 UPF2L and/or UPF3B were added after UPF1 phosphorylation. Samples were analysed by SDS-PAGE, Coomassie-stained to control for equal loading (lower panel) and autoradiographed (upper panel). SMG1 autophosphorylation (P-SMG1) confirms equal SMG1-activity in all samples. UPF1 is represented by the lower and UPF2L by the upper of the two closely migrating bands between 125 and 130 kDa in the Coomassie stained gel.* ***E.*** *Toeprinting analysis of ribosomal complexes obtained by incubating MVHC-preTCs with UPF1, UPF2L, UPF3B, SMG1-8-9, or BSA as indicated followed by translation termination by eRF1 and eRF3a. See also Supplemtental Figure 4.9.*

Translation termination is independent of UPF1 phosphorylation and the presence of the SMG1-8-9 complex

According to current models, UPF1, the eRFs, and the SMG1-8-9 complex form the termination-stalling SURF complex (Kashima et al., 2006). UPF1 phosphorylation by SMG1 is thought to trigger UPF1's release from the eRFs (Kashima et al., 2006; Okada-Katsuhata et al., 2012). Here, we explored whether *in vitro* phosphorylation of UPF1 in the absence or in the presence of UPF2L and/or UPF3B influences translation termination. Maximal *in vitro* phosphorylation of UPF1 by SMG1 or SMG1-8-9 is achieved at pH 9.0, corresponding to the pH-optimum of the kinase (Chakrabarti et al., 2014; Deniaud et al., 2015; Morita et al., 2007). We examined phosphorylation of UPF1 by SMG1-8-9 at physiological pH in the absence or presence of UPF2L, UPF3B and the eRFs (Figure 4.1D). UPF2L only slightly stimulates UPF1 phosphorylation (Figure 4.1D, lanes 4, 10) by SMG1-8-9. In contrast, UPF3B alone (lanes 5, 11) moderately and together with UPF2L (lanes 6, 12) strongly inhibits UPF1 phosphorylation by SMG1-8-9 irrespective of the presence of equimolar concentrations of the eRFs. We confirmed that our UPF2L or UPF3B preparations do not contain a phosphatase by co-incubating the phosphorylated UPF1 (P-UPF1) with the preparations of UPF2L and UPF3B for 15 min at 37°C (lanes 13-16), which did not affect the abundance of the phosphorylated UPF1.

We next investigated whether UPF1 phosphorylation or the presence of SMG1-8-9 per se affects *in vitro* translation termination. UPF1 alone or together with either UPF2L, UPF3B, or both was incubated with SMG1-8-9 and ATP for 30 min and subsequently mixed with preTCs for another 10 min at 37°C (Figure 4.1E, lanes 9-12) followed by termination with eRF1 and eRF3a and toeprint analysis. Reactions without SMG1-8-9 served as controls (lanes 3-8). We found that irrespective of the presence of either UPF2L or UPF2L and UPF3B, neither UPF1 phosphorylation nor the presence of SMG1-8-9 have a detectable influence on termination efficiency as judged by the rate of transformation of preTCs to postTCs (compare lanes 3 and 9, lanes 6 and 10, lanes 8 and 12). Importantly, the inhibitory effect of UPF3B on this transformation was independent of the presence of SMG1-8-9 and UPF1 (compare lanes 7 and 11).

UPF1 and UPF3B are part of release factor-containing complexes *in vivo*

We next analyzed the interaction of the UPF proteins with the termination complex *in vivo*. Based on co-immunoprecipitation (co-IP) experiments, human UPF1 has been suggested to interact with both eRF1 and eRF3a, and thereby physically link the NMD apparatus with translation termination (P. V. Ivanov et al., 2008; Kashima et al., 2006; Singh et al., 2008). In yeast, all three Upf proteins were reported to bind to eRF3 (Sup35) (Wang et al., 2001). We thus transiently co-transfected HeLa cells with FLAG-tagged eRF1 or eRF3a and full length versions of V5-tagged UPF1, UPF2, or

UPF3B, and immunoprecipitated on FLAG-antibody beads in the presence of RNase A. Co-IPs of FLAG-eRF1 with V5-eRF3a and of FLAG-eRF3a with V5-eRF1 served as positive controls and yielded strong eRF1-eRF3a interactions (Figure 4.2A, B, lanes 2). Co-IPs of FLAG-eRFs with the EJC-disassembly factor PYM (Gehring et al., 2009) served as specificity controls (Figure 4.2A, B, lanes 10).

Using FLAG-eRF1 as bait, UPF1 (Figure 2A, lane 3), but not UPF2 (lanes 4, 6, 8, 9) or UPF3B (lane 5, 7-9) was co-immunoprecipitated with eRF1. Importantly, co-transfection of UPF3B and UPF1 prevented the formation of a complex containing eRF1 and UPF1 (lane 7) indicating that UPF3B either directly or indirectly competes with eRF1 for UPF1 binding.

When we co-expressed V5-tagged UPF proteins with FLAG-eRF3a the complex contained only little UPF2 (Figure 4.2B, lane 4) but considerably more UPF1 and UPF3B (lanes 3 and 5). Interestingly, we found UPF3B in FLAG-eRF3a immunoprecipitates together with UPF1 (lanes 7 and 9), indicating that UPF1 and UPF3B can bind both, individually and together, but that these proteins do not compete for eRF3a-binding. Although co-transfection of UPF2 strongly enhanced the ability of UPF1 to co-immunoprecipitate with eRF3a (compare lane 3 to lane 6), UPF2 was excluded from these complexes as well as from complexes containing eRF3a and UPF3B (lanes 6, 8 and 9). We conclude that UPF2 stimulates the direct or indirect interaction between UPF1 and eRF3a, but does not partake in complexes containing eRF3a together with UPF1, UPF3B, or both.

UPF3B directly interacts with eRF3a in a magnesium-sensitive manner forming a ternary complex with eRF1

Co-IP experiments do not reveal whether the interactions identified are direct or indirect. Therefore, we performed *in vitro* pulldown assays to analyse whether purified UPF proteins and release factors interact directly.

We incubated reaction mixtures containing His-tagged UPF1, UPF2L or UPF3B and one or both untagged eRF(s) (Figure 4.3A) with Ni-NTA beads, washed extensively and eluted the bound proteins with imidazole. We found that neither eRF1 nor eRF3a individually, nor the eRF1-eRF3a complex, detectably bound to UPF1 (Figure 4.3B, lanes 5-7), or UPF2L (Figure 4.3C, lanes 5-7). UPF2 has recently been reported to directly interact with eRF3a. However, UPF2L did not bind to eRF3a, although it contains the part that has been reported to interact with eRF3a (López-Perrote et al., 2015). In contrast, eRF3a and, to a lesser extent, eRF1 co-eluted with UPF3B individually (Figure 4.3D, lanes 5, 6) as well as simultaneously (lane 7) indicating that UPF3B directly interacts with both release factors.

Reciprocal control experiments using His-eRF3a as a bait for both UPF1 and UPF3B (Supplemental Figure 4.10) corroborated the eRF3a-UPF3B interaction (Sup-

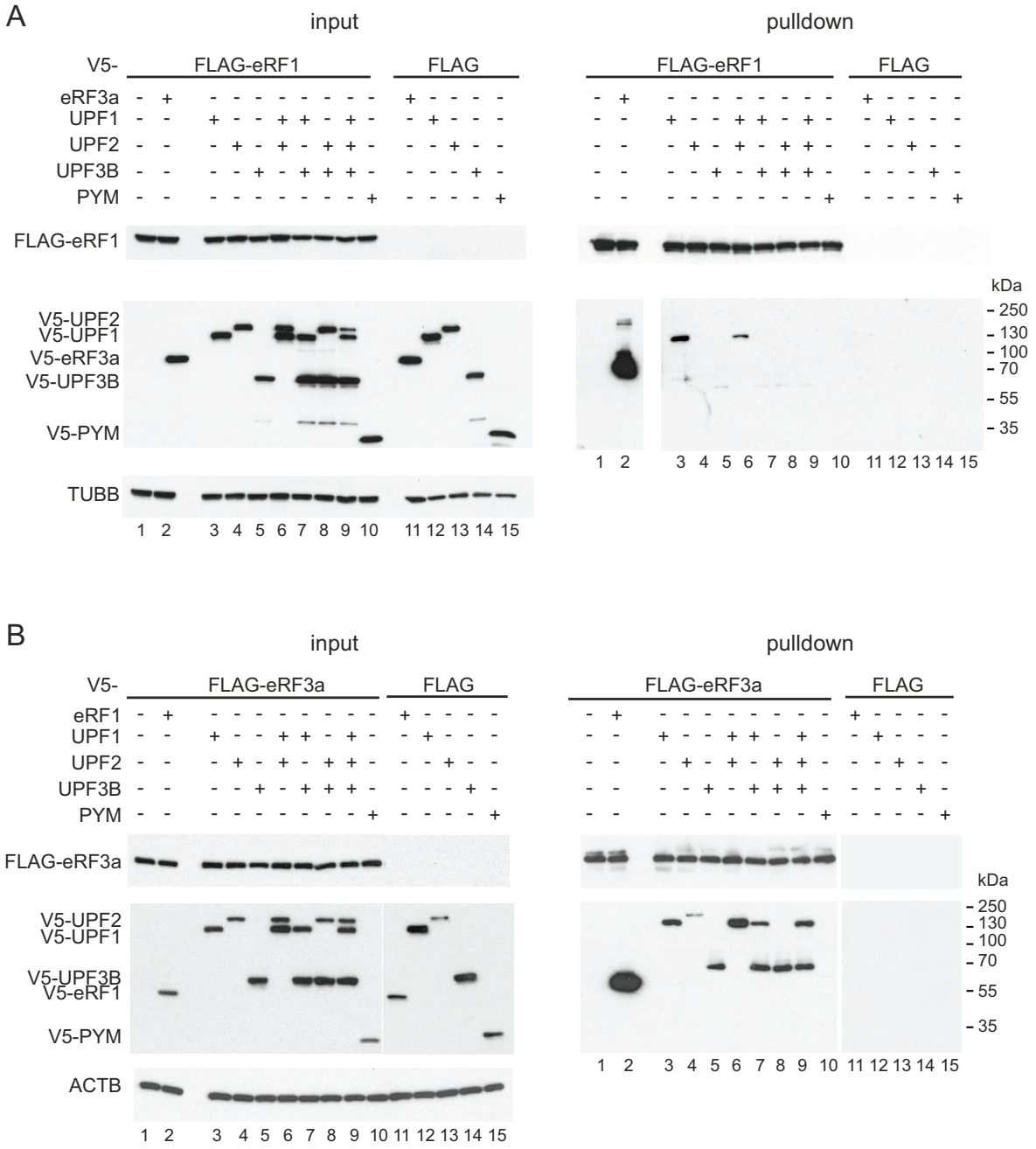

Figure 4.2: In vivo interaction between release factors and UPF proteins. ***A.*** *Co-immunoprecipitation from RNase A-treated lysates of Hela cells transfected with FLAG-eRF1 (lanes 1-10) or unfused FLAG (lanes 11-15) and V5-eRF3a, V5-UPF1, V5-UPF2, V5-UPF3B, or V5-PYM. Co-precipitated proteins were detected using an anti-V5 antibody. Lysate used for the immunoprecipitations was loaded in the input lanes (left). Re-probing with anti-TUBB antibody served as loading control.* ***B.*** *Co-IP experiment as in (A) with FLAG-eRF3a. Re-probing with anti-ACTB served as loading control.*

plemental Figure 4.10) and confirmed that UPF1 does not co-elute with eRF3a irrespective of the presence of eRF1 (Supplemental Figure 4.10A).

Translation is modulated by the Mg^{2+} concentration both *in vivo* and *in vitro*. In our *in vitro* translation termination assays (Figure 4.1) we used 1mM free Mg^{2+} which corresponds to the physiological intracellular level of unbound Mg^{2+} (MacDermott, 1990; Veloso et al., 1973). We explored the impact of Mg^{2+} on the UPF3B-eRF interaction. At physiological [Mg^{2+}] a substantial amount of UPF3B bound to eRF3a, whereas at >5 mM Mg^{2+} the interaction between UPF3B and eRF3a was considerably weaker (Figure 4.3E, lanes 4-6). Notably, UPF1 did not directly interact with the eRFs at all Mg^{2+} concentrations tested (Supplemental Figure 4.10C).

To assess UPF3B-eRF complex formation independently, we performed size exclusion chromatography (SEC). Co-incubation of equimolar amounts of eRF3a and UPF3B resulted in a complex eluting in earlier fractions at a higher apparent molecular weight than the individual proteins (Figure 4.3F), corroborating a direct interaction between eRF3a and UPF3B. Because UPF3B alone eluted at a higher apparent molecular weight than expected (Figure 4.3F), indicating possible oligomerisation or a deviation from the globular shape, we subjected UPF3B to SEC-MALLS and found that UPF3B is monomeric thus suggesting a non-globular shape of this protein (Supplemental Figure 4.10D).

In contrast, after co-incubation of eRF1 and UPF3B the proteins eluted in two peaks (Supplemental Figure 4.10E). The first peak eluted at the same volume as UPF3B when analysed individually and thus corresponds to UPF3B. The second peak eluted at a higher apparent molecular weight than eRF1 alone (1.55 ml vs. 1.50 ml). Accordingly, in the SDS-PAGE analysis a slight shift of the eRF1 containing fractions can be observed in the gel analysing co-migration of UPF3B and eRF1 in SEC as compared to the gel analysing the eRF1-SEC fractions (Supplemental Figure 4.10E) suggesting a weak interaction between eRF1 and UPF3B.

When UPF3B was mixed with both eRF1 and eRF3a, a single peak containing all three proteins eluted at a higher apparent molecular weight than each individual protein (Figure 4.3G) demonstrating that UPF3B, eRF1, and eRF3a can form a stable trimeric complex. The complex is likely stabilized by eRF3a, which can bind both UPF3B and eRF1, indicating that UPF3B does not compete with eRF1 for eRF3a-binding. These findings suggest that the effect of UPF3B on translation termination can be fully or partially mediated by a direct interaction of UPF3B with either eRF3a or the eRF1-eRF3a complex.

UPF3B and UPF1 interact directly

In EJC-dependent NMD, UPF2 is thought to bridge the termination complex and the EJC by simultaneously binding to UPF1 at the termination site and UPF3B at the EJC

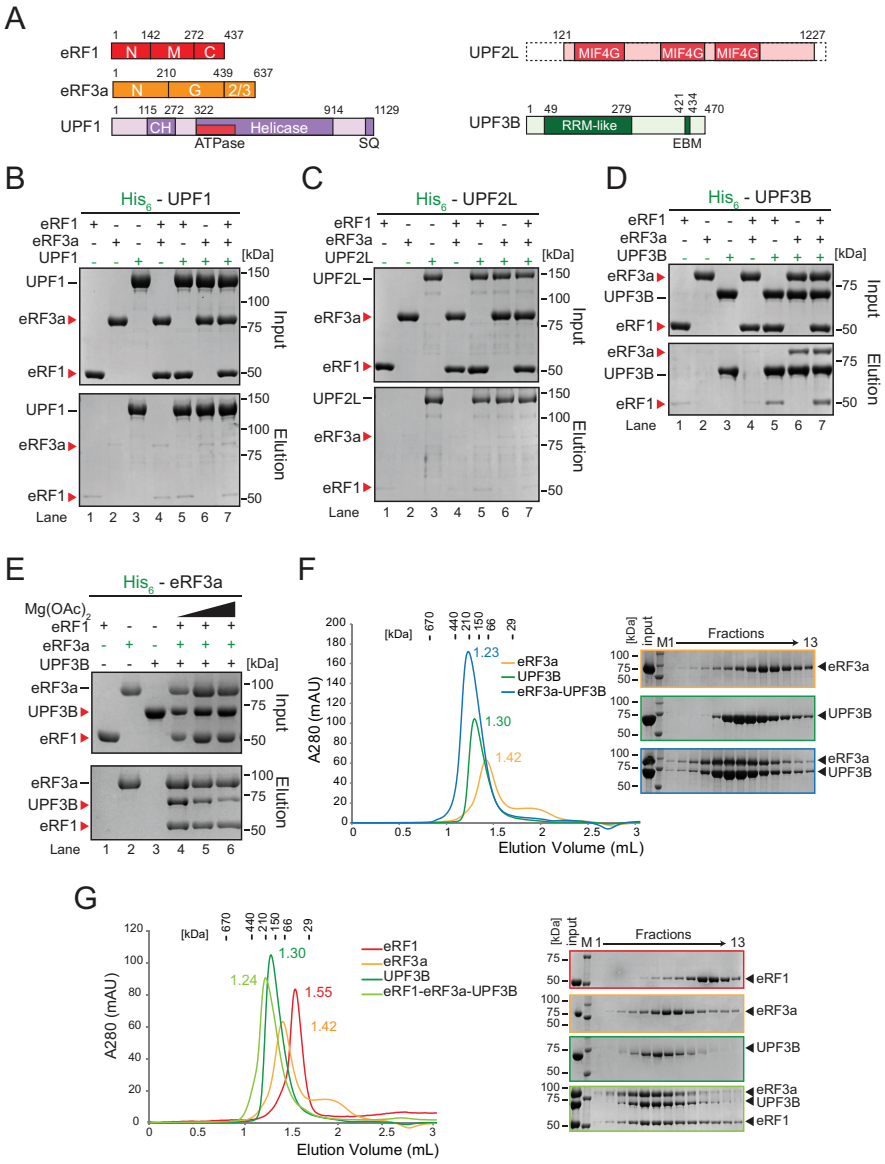

Figure 4.3: UPF3B forms a complex with eRF3a and eRF1. ***A.*** *Schematic representation of eRFs, UPF1, UPF2L and UPF3B proteins. Domains of known function and structural motifs are indicated. N, M, C, G, CH stand for N-terminal, middle, C-terminal, GTP-binding- and cysteine-histidine-rich domain, respectively. 2/3: domains 2 and 3. MIF4G: middle fragment of eIF4G, RRM: RNA-recognition motif, EBM: EJC-binding motif.* ***B.*** *In vitro pulldown of eRF1 and/or eRF3a with His-UPF1. Protein mixtures before loading onto the beads (input) or after elution (eluate) were separated by SDS-PAGE.* ***C.*** *Pulldown as in B, with His-UPF2L as bait.* ***D.*** *Pulldown as in B, with His-UPF3B as bait.* ***E.*** *Pulldown of eRF1, UPF3B, or both with His-eRF3a at 0, 2.5, or 5 mM Mg^{2+} respectively.* ***F.*** *Left: SEC elution profile of eRF3a (yellow), UPF3B (green), or both (blue). The elution volume (in mL) is indicated for each experiment. Column calibration was performed with globular proteins (shown above). Right: SDS-PAGE analysis of eluate fractions. M: protein molecular weight standards (kDa).* ***G.*** *SEC elution profile and SDS-PAGE analysis as in (F) of eRF1 (red), eRF3a, UPF3B or all three (light green). See also Supplemental Figure 4.10.*

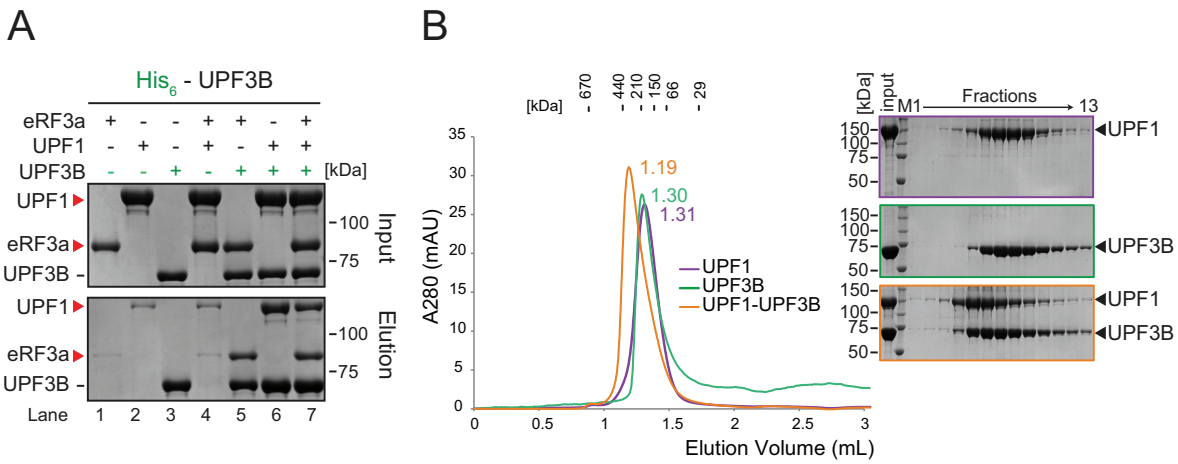

Figure 4.4: UPF3B can directly interact with UPF1. A. *In vitro pulldown of eRF3a, UPF1, or both with His-UPF3B. Protein mixtures before loading onto the beads (input) or after elution (eluate) were separated by SDS-PAGE.* ***B.*** *Left: SEC elution profile of UPF1 (purple), UPF3B (green) or both (red). Right: SDS-PAGE analysis of eluate fractions.*

(Chamieh et al., 2008; Kashima et al., 2006). However, UPF3B but not UPF1 binds to eRF3a *in vitro* and UPF2, in contrast to UPF1 and UPF3B, is excluded from eRF3a-bound complexes *in vivo* (Figures 4.2, 4.3). Although earlier *in vitro* binding studies using a truncated UPF1 variant revealed no direct interaction (Chamieh et al., 2008), we tested full length UPF1 binding to UPF3B. We incubated His-UPF3B with UPF1 either in the presence or in the absence of eRF3a and found that UPF1 directly interacts with UPF3B (Figure 4.4A, lanes 6). Binding of eRF3a to UPF3B was not affected by UPF1, suggesting that the two proteins can bind to UPF3B independently (lanes 5 and 7). In SEC analysis, a single peak containing both UPF1 and UPF3B eluted earlier than UPF1 and UPF3B alone. SDS-PAGE analysis revealed that the elution profile of UPF1 and UPF3B within this peak was not fully symmetric, indicating that the UPF1-UPF3B complex partly dissociates during SEC (Figure 4.4B).

The eRF3a-UPF3B interaction requires the N-terminus of eRF3a in-vitro and in-vivo

The N-terminus of eRF3a is not required for the function of eRF3a in translation termination (Ter-Avanesyan et al., 1993). We explored whether an eRF3a variant lacking the first 138 aa (eRF3aΔN) (Figure 4.5A) can bind UPF3B and found that in contrast to eRF3a (Figure 4.5B, lanes 4), eRF3aΔN was not co-eluted with His-UPF3B (lane 5). In the reciprocal experiment using His-eRF3a or His-eRF3aΔN as bait, UPF3B co-eluted with eRF3a (Figure 4.5C, lanes 4) but not with eRF3aΔN (lanes 5).

We further characterized the eRF3a-UPF3B interaction and generated truncated versions of His-UPF3B comprising the RNA recognition motif (RRM) domain (aa 42-

217, UPF3B-N) (Kadlec et al., 2004), the middle domain (aa 147-419, UPF3B-M), part of the RRM-like domain (aa 147-256, UPF3B-SM), or the EJC-binding motif (EBM) (aa 380-470, UPF3B-C) (Figure 4.5D). UPF3B-N and UPF3B-C did not bind eRF3a, indicating that neither the RRM domain which binds UPF2 nor the EBM are sufficient to interact with eRF3a (Figure 4.5E, lanes 8, 11).In contrast, UPF3B-M and UPF3B-SM, comprising the hitherto uncharacterized middle domain of UPF3B, bound to eRF3a, albeit less efficiently than the full length protein (lanes 9, 10). The protein-protein contact between eRF3a and UPF3B is thus established by binding between the eRF3a N-terminus and the middle domain of UPF3B. Notably, most UPF3B mutations linked to neurodevelopmental disorders are located in this region (Alrahbeni et al., 2015).

To examine if the interaction between UPF3B and N-terminally truncated eRF3a was also impaired *in vivo*, we transiently co-transfected HeLa cells with plasmids encoding a FLAG-tagged version of eRF3a lacking the first 199 aa (FLAG-eRF3aΔ199) and with V5-eRF1 or V5- UPF1, -UPF2, or -UPF3B, either individually or simultaneously (Figure 4.5F). We found that UPF1 still co-precipitated with eRF3aΔ199 when it was co-transfected individually or with UPF2 (Figure 4.5F, lanes 3, 6). In contrast, only trace amounts of UPF3B were found in FLAG-eRF3aΔ199 complexes (lanes 5, 7-9), illustrating that the eRF3a N-terminus is necessary for the interaction with UPF3B *in vivo*.

Next, we examined if the inability of eRF3aΔN to interact with UPF3B affects the termination-delaying function of UPF3B (Figure 4.5G). However, the pre- and postTC toeprints generated in the presence of UPF3B and eRF3a (lanes 3, 5) or eRF3aΔN (lanes 4, 6), respectively, were very similar. We thus examined whether the effect of UPF3B in delaying translation termination may involve direct binding to the ribosome, and whether its potential role in eRF3a recruitment can be bypassed by eRF1 in the *in vitro* translation system. With an isoelectric point of 9.4, UPF3B is positively charged at physiological pH, and may interact with negatively charged rRNAs or ribosomal proteins. However, previous studies using truncated UPF2 and UPF3B protein fragments found that UPF3B's RRM binds to UPF2 instead of RNA (Kadlec et al., 2004). Here, we used a 24 nt RNA oligomer in SEC to analyse the RNA-binding capacity of full length UPF3B (Supplemental Figure 4.11A). The first of two peaks from the SEC column contained UPF3B, eluted earlier than UPF3B alone (1.22 ml vs 1.30 ml), and had a higher OD_{260nm} signal, indicating the presence of nucleic acids. The second peak contained unbound RNA oligomer. The majority of the RNA oligonucleotide shifted to the position of the UPF3B peak, demonstrating that full length UPF3B binds RNA, a finding that is consistent with recent iCLIP and RNA interactome data (Sieber et al., 2016).

To explore the ability of UPF3B, UPF1, and UPF2L to interact with ribosomes

we performed co-sedimentation assays. Centrifugation without ribosomes served as controls (Supplemental Figure 4.11B). UPF1 and UPF3B individually and simultaneously co-sedimented with 80S ribosomes (Supplemental Figure 4.11C, lanes 2, 6, 8), indicating that both proteins can bind independently to ribosomes. In contrast, the minor ribosome binding of UPF2L alone (lane 4) was considerably enhanced in the presence of UPF3B (lane 10). This finding indicates that UPF2L can be recruited to the ribosome by UPF3B, and that the interaction with UPF2L on the ribosome may interfere with the function of UPF3B in termination.

UPF3B triggers disassembly of post-termination complexes

The ability of UPF3B to form complexes with UPF1 and the release factors suggests the existence of a previously unknown dynamic UPF-eRF protein network. We reasoned that the influence of the UPF proteins on translation termination might differ from what we had observed with limiting amounts of the eRFs at equimolar and saturating amounts of eRFs and UPF proteins, allowing free interplay of all factors.

We thus complemented the experiments described in Figure 4.1B, E and Supplemental Figure 4.9 with saturating amounts of eRFs (Figure 4.6A, Supplemental Figure 4.12A, B). Addition of the eRFs induced the transformation of all preTCs to postTCs as indicated by a shift of the toeprint by +1-2 nt relative to the preTC toeprint (Figure 4.6A, Supplemental Figure 4.12A, B, lanes 2). Irrespective of the presence of ATP or AMPPNP, this pattern was essentially the same when preTCs were pre-incubated with either UPF1, UPF2L, both of these proteins (lanes 3, 4, and 6), with UPF2L and UPF3B (lanes 8), or with all three UPF proteins (lanes 9). We also investigated whether the phosphorylation of UPF1 either alone (Figure S4.5C, lane 7), in presence of UPF2L and/or UPF3B (8-10), or before (lanes 11-14) addition of UPF2L and/or UPF3B influenced UPF1 function. We found that irrespective of the phosphorylation status, toeprints generated by termination with phosphorylated UPF1 (lanes 7-14) were indistinguishable from those generated with non-phosphorylated UPF1 (lanes 3-6) Thus, independent of its functions in ATP-binding or ATP-hydrolysis or of its phosphorylation status, UPF1 has no impact on translation termination even when eRFs are present at saturating concentrations.

In termination reactions including UPF3B either alone or together with UPF1 a small amount of preTCs was retained, suggesting that here, too, UPF3B delayed termination. However, most preTCs were transformed to postTCs in the presence of either UPF3B alone or in the presence of both, UPF1 and UPF3B, when eRFs were not limiting (Figure 4.6A, Supplemental Figure 4.12A, B, lanes 5, 7, 4.12C lane 5, 9, 13). Importantly, the postTC toeprints resulting from termination reactions in the presence of UPF3B (or of UPF1 and UPF3B; Figures 4.6A, S4.12A,B, lanes 5 and 7) were considerably weaker and the readthrough full length signal considerably stronger

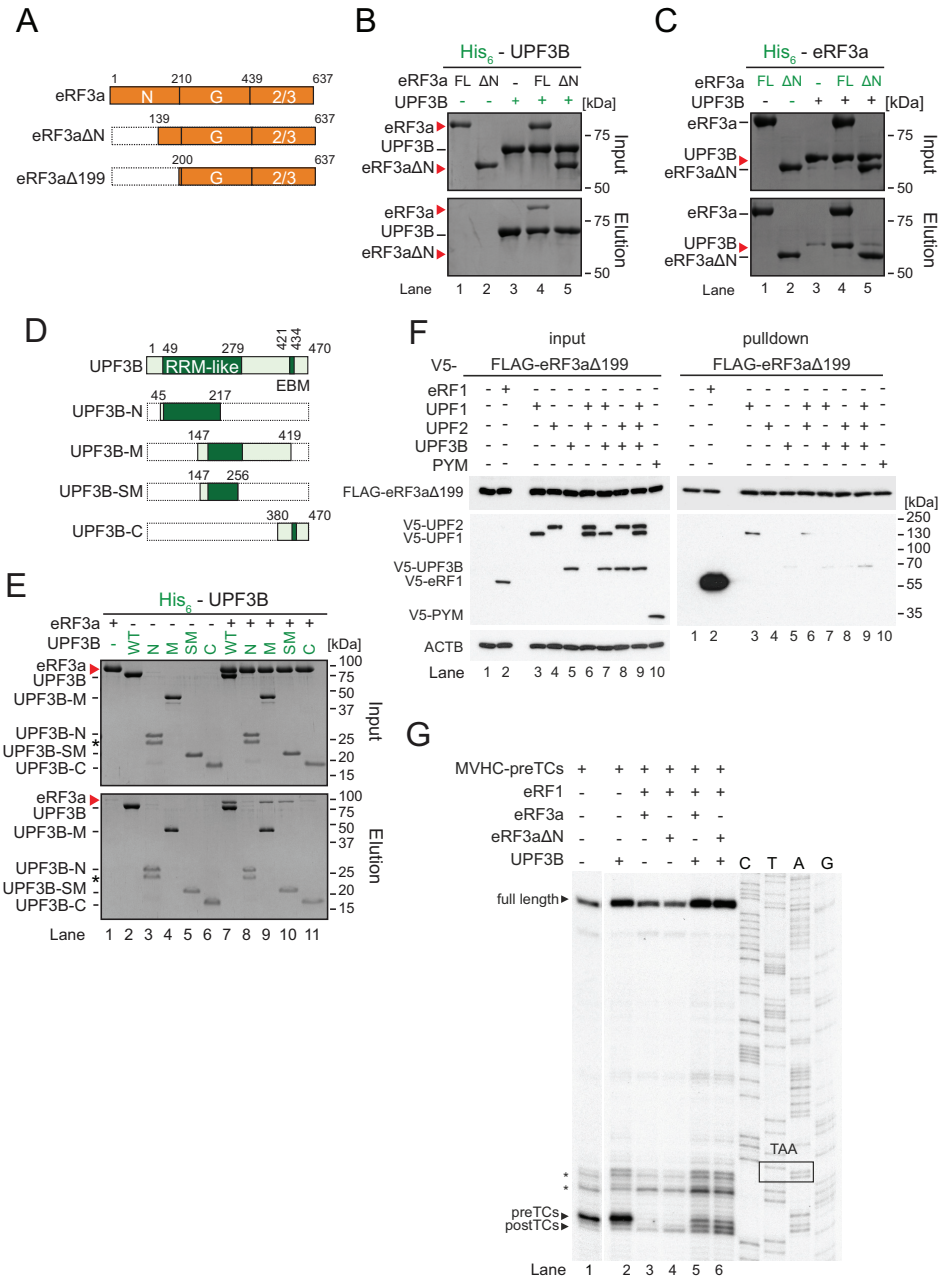

Figure 4.5: UPF3B interacts with the eRF3a N-terminus. ***A.*** *Schematic representation of eRF3a constructs used for this figure. eRF3aΔN, eRF3aΔN199: eRF3a variants lacking amino acids 1-100 and 1-199, respectively.* ***B.*** *In vitro pulldown as in Figure 3 of eRF3a or eRF3aΔN with His-UPF3B.* ***C.*** *Pulldown of UPF3B with His-eRF3a or His-eRF3aΔN.* ***D.*** *Co-IP experiment as in Figure 2 with FLAG-eRF3aΔ199 and V5-UPF1, -UPF2L, -UPF3B, or -PYM.* ***E.*** *Schematic representation of UPF3B constructs.* ***F.*** *Pulldown of eRF3a with His-UPF3B variants.* ***G.*** *Toe-printing analysis of ribosomal complexes obtained by incubating MVHC-preTCs with BSA or with UPF3B as indicated. Termination was completed with limiting amounts of eRF1 and either eRF3a (lanes 3,5) or eRF3aΔN (lanes 4,6), respectively.*

than toeprints resulting from termination reactions without UPF3B (Figures 4.6A, 4.12A,B, lanes 2-4, 6, 8, 9; S4.12C, lanes 3, 4, 7, 8, 11, 12). This finding indicates that UPF3B induced the release of postTCs from the mRNA. We thus conclude that UPF3B destabilizes postTCs when release factors are abundant. This activity is independent of UPF1 and is prevented by UPF2L (Figures 4.6A, S4.12A, B, lanes 8, 9; S4.12C, lanes 6, 10, 14).

To explore if UPF3B exerts its postTC-dissociating activity before or after peptide release, we interfered with the termination reaction by adding GMPPNP, eRF1AGQ, or the peptide-releasing reagent puromycin to the preTCs, or by omitting eRF3a (Supplemental Figure 4.12C, lane 7), in presence of UPF2L and/or UPF3B (8-10) or before (lanes 11-14) addition of UPF2L and/or UPF3B influenced its function in this experimental setting. We found that irrespective of the phosphorylation mode, toeprints generated by termination with phosphorylated UPF1 (lanes 7-14) were indistinguishable from those generated with unphosphorylated UPF1 (lanes 3-6) and that UPF3B dissociated postTCs both in the presence of phosphorylated and unphosphorylated UPF1 (lanes 5, 9, 13).

To explore if UPF3B exerts its postTC-dissociating activity before or after peptide release, we interfered with the termination reaction by adding GMPPNP, eRF1AGQ, or the peptide-releasing reagent puromycin to the preTCs, or by omitting eRF3a (Figure 4.6B). eRF1AGQ (Figure S4.8A, lane 2) carries a G183A mutation in the GGQ motif. eRF1AGQ is inactive in peptide release, but can bind ribosomes, stimulate the GTPase activity of eRF3a, and together with eRF3a can induce the ribosomal rearrangements reflected by the +1-2 nt shift in the toeprint (Figure 4.6B, lane 4, 5)(Alkalaeva et al., 2006; Frolova et al., 1999). Likewise, eRF3a supports ribosomal rearrangements in the presence of GMPPNP (lane 3), but impairs peptidyl-tRNA hydrolysis by eRF1. eRF1 alone can induce termination and ribosomal rearrangements as well as peptide release, but the reaction is considerably less efficient than in the presence of eRF3a and GTP (Alkalaeva et al., 2006). UPF3B efficiently dissociated postTCs generated in the presence of eRF1, eRF3a and GTP (Figure 4.6B, lane 10) but not ribosomal complexes that were deficient in peptide release either due to blocking the activity of eRF3a by GMPPNP (lane 12), the peptide-hydrolysis defective eRF1AGQ (lane 13), or the absence of eRF3a (lane 15). When peptide release was enforced by the addition of puromycin, UPF3B effectively dissociated the resulting postTCs (lanes 14, 16), which was also reflected by a concomitant increase of the toeprint corresponding to the ribosome-free full length mRNA. Notably, UPF3B was unable to dissociate preTCs in the absence of eRFs (Figure 4.6B, lane 9) or residual preTCs in reactions that were incubated with eRF1 or puromycin alone (lanes 15, 16). These data indicate that UPF3B dissociates postTCs after both GTP and peptidyl-tRNA hydrolysis, but not preTCs or postTCs before peptide hydrolysis. UPF3B also dissociates postTCs that

have been generated in the absence of eRF3a (Figure 4.6B, lane 9) herefore, the eRF3a-UPF3B interaction is not required for the function of UPF3B in ribosome dissociation.

The ability of UPF3B to promote the dissociation of postTC is reminiscent of the energy-free ribosome recycling activity mediated by eIF3, eIF1, and eIF1A (Pisarev et al., 2007), which is apparent only at low Mg^{2+} concentrations. Furthermore, ribosomal inter-subunit association is dynamic and more flexible at physiological rather than at higher Mg^{2+} concentrations (Shenvi et al., 2005). Therefore, we investigated the ability of UPF3B to dissociate postTCs at Mg^{2+} concentrations higher than 1 mM (Figure 4.6C). Whereas incubation of preTCs with eRFs and UPF3B at 1 mM free Mg^{2+} resulted in the dissociation of postTCs (Figure 4.6C, lane 7), no dissociation occurred at 2.5 or 5 mM Mg^{2+} (lanes 8, 9), respectively. These findings suggest that UPF3B dissociates postTCs with flexible subunit association, possibly by accessing the inter-subunit surfaces of one or both ribosomal subunits.

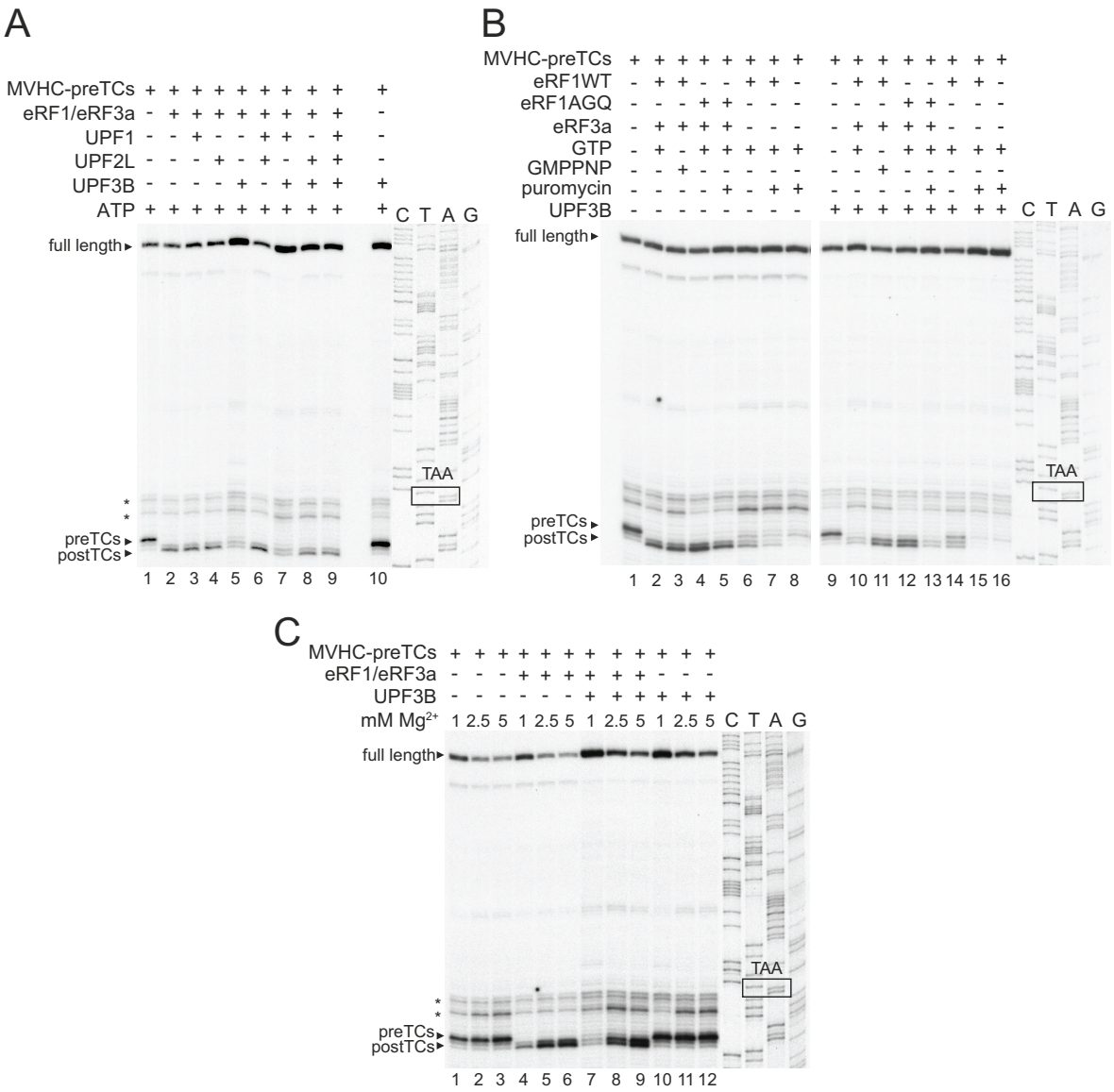

Figure 4.6: UPF3B dissociates postTCs. ***A.*** *Toeprinting analysis of ribosomal complexes obtained by incubating MVHC-preTCs with UPF1, UPF2L, UPF3B, or BSA at 1 mM free Mg^{2+} and 1 mM ATP followed by termination with saturating amounts of eRF1 and eRF3a.* ***B.*** *Toeprinting analysis of ribosomal complexes obtained by incubating preTCs as in (A) with UPF3B or BSA and combinations of eRF1, eRF1AGQ, eRF3a, and puromycin in the presence of GTP or GMPPNP. Gel on the left was exposed 2x longer than gel on the right. Note that puromycin-treated preTCs are relatively unstable at low Mg^{2+} (**Skabkin et al., 2013**).* ***C.*** *Mg^{2+} sensitivity of postTC dissociation by UPF3B. Toe-printing analysis of ribosomal complexes obtained by incubating MVHC-preTCs with BSA (lanes 1-6) or UPF3B (lanes 7-12) and at the indicated concentrations of free Mg^{2+} . Termination was completed by adding eRF1 and eRF3a to the samples in lanes 4-9. See also Supplemental Figure 4.12.*

4.3 Discussion

How translation termination at a premature termination codon differs from termination at a normal termination codon has long been a matter of debate. All prevailing models from yeast to man ascribe a critical role to UPF1 not only in the mRNA degradation phase, but already in the translation termination phase of NMD. These hypotheses are founded on the interaction of UPF1 with eRF1 and eRF3a, which were identified in co-IP experiments (P. V. Ivanov et al., 2008; Wang et al., 2001; Singh et al., 2008) (Figure 4.2). UPF1 is thought to recruit the eRFs to ribosomes that are stalled at a PTC in an early phase of termination and to promote ribosome disassembly in a late phase of termination via its ATPase function that is activated by UPF2- and UPF3 binding (reviewed in (Celik et al., 2015; He & Jacobson, 2015b; Brogna et al., 2016)). However, it has not been possible to address the hypothetical functions of NMD factors in translation termination in cells and organisms, because no adequate *in vivo* termination assay is available to date. Deletion of the *UPF* genes in yeast leads to increased stop codon suppression (Keeling et al., 2004; Wang et al., 2001), whereas RNAi-mediated depletion of UPF1 in human cells reduces stop codon readthrough (P. V. Ivanov et al., 2008). Yet, it is unclear, if these manipulations disturb or reflect direct interactions of NMD proteins with the translation termination machinery.

Here, we tested the functional interactions of key NMD factors *in vitro* using a fully reconstituted translation termination system that has been demonstrated to faithfully mirror all phases of eukaryotic translation (Alkalaeva et al., 2006; Pisarev et al., 2007; Pisareva et al., 2008). We discover that neither UPF1 per se nor its biochemical functions such as ATP-binding, ATP–hydrolysis or its phosphorylation play a discernable role in early or late phases of translation termination. We also find that UPF2L and UPF3B do not substantially stimulate the ATPase activity of UPF1 at physiological pH, and that UPF3B inhibits UPF1 phosphorylation (Figures 4.1D, 4.8E, F). Furthermore, UPF1 does not appear to bind eRF1 and eRF3a directly, and the previously described interactions between UPF1 and the eRFs, found in co-IP experiments, are likely to be indirect. Cumulatively, our data demonstrate that UPF1 remains inactive or functionally dispensable during translation termination, and that the role of both, UPF1 and UPF2, may be restricted to the post-termination phase of NMD. This conclusion is supported by findings that show UPF1 phosphorylation and its ATPase and helicase activities to be important for its functions in 3'UTR mRNP remodeling and the recruitment of mRNA decay factors (Fiorini et al., 2015; Franks et al., 2010; Kurosaki et al., 2014; Okada-Katsuhata et al., 2012).

We discover that UPF3B binds eRF3a *in vivo* and *in vitro*, and exerts the bifunctional influence on translation termination that has hitherto been attributed to UPF1. When release factors are limiting and translation termination is inefficient, UPF3B

further delays termination and inhibits peptide release. After GTP hydrolysis and release of the nascent peptide UPF3B promotes the dissociation of post-termination ribosomal complexes. Both activities are prevented by UPF2L, which is likely caused by either sequestration of UPF3B from the termination reaction or by interference with its function at the termination site. This dual function of UPF3B is in excellent accord with the observation that termination at PTCs is considerably slower than termination at NTCs (Amrani et al., 2004; Peixeiro et al., 2012), and that deletion of any of the UPF genes in yeast causes defects in ribosome release both *in vitro* and *in vivo* (Ghosh et al., 2010).

Because UPF3B impairs the large structural rearrangement induced by stop codon recognition by eRF1 complexed with GTP-bound eRF3a, we incorporate the central role of UPF3B into a new model for NMD. According to this model, UPF3B binds in the vicinity of the A site of the ribosome and assists in the recruitment of eRF1-eRF3a during the initial slow phase of termination at a PTC (Figure 4.7, phase 1). In the light of recent findings that UPF1 binds along the entire 3'UTR of translated mRNAs (Hogg & Goff, 2010; Hurt et al., 2013; Zünd et al., 2013) UPF1 molecules bound nearby may interact with terminating ribosomes but remain inactive in the proceedings of termination. As our eRF3a co-IP experiments indicate (Figure 4.2B), UPF2 could assist with this interaction, but is not itself part of a complex that contains both, UPF1 and the terminating ribosome. After both GTP and peptidyl-tRNA hydrolysis (Figure 4.7, phase 2). UPF3B, possibly promoted by a conformational or positional change at the ribosome, contributes to the rescue of ribosomes stalled at a PTC and dissolves the postTC (Figure 4.6A, B, Figure 4.7, phase 3). This phase is independent of UPF3B-eRF binding and may be promoted by electrostatic interactions of UPF3B with the solvent-exposed inter-subunit surface of the ribosomal subunits. Because UPF2 is not detected in complexes that contain both UPF3B and eRF3a (Figure 4.2B) UPF2 is proposed to be recruited to postTCs after the release of eRF3a and dissociation of the ribosome by UPF3B. Subsequently UPF1, supported by UPF2 and UPF3B, engages in 3'UTR remodeling and the recruitment of decay enzymes triggering the decay phase of NMD. Since UPF2 does not elicit a strong stimulation of the ATPase function of UPF1 or of its phosphorylation at physiological pH, additional factors may well be involved (Figure 4.7, phase 4).

Importantly, UPF3B can neither destabilize preTCs nor postTCs, when either GTP hydrolysis by eRF3a or peptidyl-tRNA hydrolysis are inhibited (Figure 4.6B). Ribosome recycling after proper or faulty translation termination is crucial for the protein synthesis machinery to avoid sequestration of essential components of the translation apparatus. In normal termination, no-go decay (NGD) and non-stop decay (NSD) postTCs or stalled ribosomes are dissociated by ABCE1 (reviewed in (Graille & Séraphin, 2012; S. Lykke-Andersen & Jensen, 2015)). A specific mechanism for ribo-

some rescue in NMD has not yet been identified. UPF1 has been proposed to dissolve ribosomes stalled at a PTC, possibly because eRF3a is not able to leave the complex and therefore prevents the interaction of ABCE1 with eRF1 (Celik et al., 2015). Here, we uncover that UPF3B dissociates postTCs and may, therefore, function as a dedicated NMD ribosome rescue factor. However, since UPF3B is not an ATPase, its activity is reminiscent of the energy-free activity of initiation factors that can recycle post-termination complexes only at a narrow range of low Mg^{2+} (Pisarev et al., 2007, 2010). Dissociation of postTCs by eIF3 alone is relatively inefficient and is enhanced by eIF1, eIF1A, and eIF3j. Similarly, UPF3B does not dissolve all postTCs (Figure 4.6)) even when in large excess over the preTCs. Hence, future work will determine whether UPF3B-mediated ribosome dissociation is simply slower than ribosome release in normal termination as has been suggested (He & Jacobson, 2015b), or if it can be stimulated by other proteins reminiscent of the cooperation of initiation factors and ABCE1 (Pisarev et al., 2010).

There still remain to be questions answered concerning the role of UPF3B both in NMD and in NMD-related diseases. Loss-of-function mutations of the UPF3B gene result in X-linked intellectual disability disorders. However, their underlying molecular mechanisms are unknown (Jolly et al., 2013; Tarpey et al., 2007). Most of these mutations impair NMD and have been mapped to the functionally uncharacterized middle domain of UPF3B (Alrahbeni et al., 2015). We show here that this domain mediates the interaction with eRF3a (Figure 4.5E). This finding will enable investigation of whether disruption of the UPF3B-eRF3a interaction leads to the deregulation of genes that are required for normal neurodevelopment.

Upf3 is essential for NMD in yeast, but both UPF2-independent and UPF3B-independent branches have been reported for human NMD (Chan et al., 2007; Gehring et al., 2005). Our discovery that UPF1 can directly interact with UPF3B contributes to the understanding of the UPF2-independent NMD branch, since UPF2 was assumed to bridge between UPF1 and UPF3B. However, if the major role of UPF3B in NMD is confined to translation termination, it remains to be investigated how ribosomes stalled at a PTC are recognized in the UPF3B-independent branch. Notably, UPF3 exists in two paralogs in higher eukaryotes, UPF3A and UPF3B. UPF3A has hitherto been considered to be a "backup molecule" that can substitute for UPF3B in NMD (Chan et al., 2009). By contrast, UPF3A has recently been shown to also act as an antagonist of UPF3B and to function as a suppressor of NMD (Shum et al., 2016). Therefore, it will be interesting to probe if UPF3A can either substitute or antagonize the role of UPF3B in translation termination.

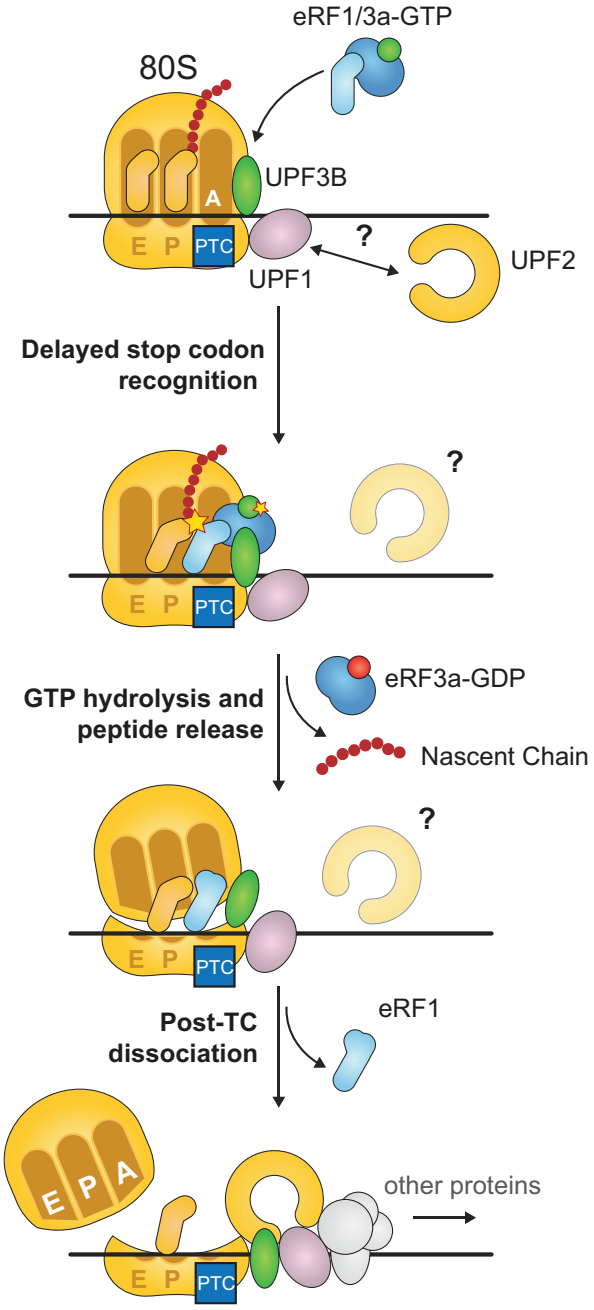

Figure 4.7: Model for early and late UPF3B function in translation termination. *During termination at a PTC ribosome-bound UPF3B recruits the eRF1/eRF3a-GTP complex by interacting with the eRF3a N-terminus. UPF1 bound to the 3'UTR and stimulated by UPF2 contacts the termination complex, but remains inactive. The presence of UPF3B or lack of a termination-enhancing factor delay stop codon recognition. After GTP hydrolysis and nascent peptide release UPF3B destabilizes the post-termination ribosomal complex. Subsequently, UPF3B, UPF1, UPF2 and other factors form a complex that activates UPF1 ATPase and helicase functions to remodel the 3' UTR mRNP and attract decay enzymes.*

4.4 Methods

Plasmids.

The pPROExHtb_eRF1 plasmid was generated by subcloning the PCR-amplified gene encoding from pQE30_eRF1 (Frolova et al., 1999) into pPROExHtb (Life Technologies) using restriction enzymes *Nco*I and *Not*I. The plasmid pET21d_UPF2L (121-1227) was generated by subcloning pPROExHtb_UPF2 (121-1227) into pET21d (EMD Biosciences) using restriction enzymes *Nco*I and *Not*I. pFastBacHtb_eRF3a was generated by subcloning the *Nco*I/*Hind*III fragment encoding full-size wildtype eRF3a from pET15b-eRF3a into pFastBacHtb (Life Technologies). Deletion constructs for pFastBacHtb_UPF3B or pFastBacHtb_eRF3a were engineered by Self-SLIC, an insert-free SLIC reaction (M. Z. Li & Elledge, 2007). Plasmids encoding human UPF1, UPF2L, UPF3A and UPF3B were generated by subcloning *Nco*I/*Not*I digested fragments from the respective pCI Neo / pcDNA vectors (Promega) into pFastBacHtb. Plasmids pCIneo-FLAG-eRF1, -eRF3a, and eRF3a variant plasmids as well as pCIneo-V5-UPF1, -UPF2, and -UPF3B plasmids for eukaryotic expression have been described previsouly (P. V. Ivanov et al., 2008).

Protein production and purification.

UPF1(115-914) and UPF1(295-914) were expressed from plasmids pET28-UPF1(115-914) and pET28a-UPF1(295-914) and purified as described (Chamieh et al., 2008). His-tagged human eRF3a, UPF1, UPF2L and UPF3B were expressed using the Multibac expression system (Fitzgerald et al., 2006). His-tagged eRF1 and UPF2L were expressed in the *E. coli* strain BL21-Gold(DE3) (Life Technologies). Cells were lysed in buffer A (25 mM HEPES-KOH, 10 mM imidazole, 300 mM KCl, 5 mM 2-mercaptoethanol, 5% [v/v] glycerol, pH 7.5) supplemented with protease inhibitor cocktail (Roche) and 0.1% [v/v] NP40 for the insect cell expressed proteins. Lysed cells were centrifuged at 30,000 x g, 30 min. The supernatant was subjected to Ni-NTA affinity chromatography (QIAGEN). After removal of the His-tag with Tobacco Etch Virus (TEV) protease, proteins were further purified using a HiTrap QXL column (GE Healthcare); followed by cation exchange chromatography using a HiTrap SP/HP column (GE Healthcare) for UPF3B. UPF1, eRF1 and eRF3a were further purified by size-exclusion chromatography (SEC) using a Superdex 200 column (GE Healthcare) equilibrated with buffer B (25 mM HEPES-KOH, 300 mM KCl, 5 mM Dithiothreitol (DTT), 5% [v/v] glycerol, pH 7.5). The SMG1-8-9 complex was expressed in HEK-293T cells and purified via its streptavidin-binding tag and SEC as described (Deniaud et al., 2015). For *in vitro* termination, ATPase and *in vitro* phosphorylation assays all proteins used were diluted to 3 µM in the protein storage buffer (25 mM Tris, pH 7.5, 150 mM NaCl,

1mM $Mg(OAc)_2$, 1 µM ZnSO4, 1mM DTT, 10% [v/v] glycerol). Aliquots were stored at -80°C.

Pulldown assays to probe protein-protein interaction using purified proteins.

All experiments were performed with 20 µM of each protein in the final reaction volume of 20 µL in buffer C (25 mM HEPES/KOH, 150 mM KCl, 10 mM imidazole, 0.05% [v/v] Tween20, 5 mM DTT, 5% [v/v] glycerol, pH 7.5), if not indicated otherwise. The protein mixtures were incubated for 1 hour on ice, subsequently 20 µL of Ni-NTA agarose (QIAGEN) was added to the mix and incubated for 1 hour on ice. The reaction mixtures were washed 4 times with 200 µL of buffer C, and proteins were eluted using buffer C supplemented with 200 mM imidazole. 8 µL of SDS loading dye were mixed with either 2 µL of input reactions or 20 µL for the eluted complexes. 5 µL of the input sample and 10 µL of the elution sample were loaded onto a 10 or 12% SDS-PAGE gel.

Size Exclusion Chromatography.

For SEC, 40 µM of each protein was added in a final reaction volume of 60 µL in buffer D (25 mM HEPES/KOH, 200 mM KCl, 3 mM $Mg(OAc)_2$, 0.05% [v/v]Tween20, 5 mM DTT, 5% [v/v] glycerol, pH 7.5). The protein mixtures were incubated for 1 hour on ice before loading onto a Superdex 200 PC3.2/30 column (AEKTA micro system, GE Healthcare). 10 µL of each elution fraction was loaded onto a 10% SDS-PAGE gel. For the UPF3B-RNA interaction experiment, 40 µM of a 24-nucleotide long RNA oligonucleotide (5'-CCCAGGTGCTGCCGTCAGCTCAGGG-3') was mixed with 40 µM UPF3B.

Size Exclusion Chromatography coupled to Multiple Angle Laser Light Scattering (SEC-MALLS).

SEC-MALLS of UPF3B was performed with a Superdex-200 increase column (GE Healthcare) equilibrated with 25 mM HEPES-KOH, 300 mM KCl, 5 mM DTT, 5% [v/v] glycerol, pH 7.5. The column was calibrated with globular standard proteins. The experiments were performed at 20°C with a flowrate of 0.5 $mL.min^{-1}$. A DAWN-HELEOS II detector (Wyatt Technology Corp.) with a laser emitting at 690 nm was used for detection. The protein concentration was determined on-line by differential refractive index measurements, using an Optilab T-rEX detector (Wyatt Technology Corp.) and a refractive index increment, dn/dc, of 0.185 $mL.g^{-1}$. The weight-averaged molar masses were calculated using the ASTRA software (Wyatt Technology Corp.).

Ribosome binding experiments.

For co-sedimentation experiments, 5 pmol of rabbit 80S ribosomes were mixed with a ten-fold molar excess of UPF1, UPF2L and UPF3B in 20 µL of 25 mM HEPES-KOH pH 7.5, 100 mM KOAc, 2.5 mM $Mg(OAc)_2$, 2 mM DTT and incubated for 1 hour on ice. Subsequently, the reaction mixtures were applied on a sucrose cushion (same buffer containing 250 mM KOAc and 750 mM sucrose) and spun for 3 h at 55,000 x g at 4°C using a TLA-55 rotor (Beckman). Supernatant and pellet fractions were analysed by SDS-PAGE followed by SYPRO Ruby (Thermo Scientific) staining.

ATPase assays.

ATPase assays were performed in a total volume of 20 µL essentially as described (Chamieh et al., 2008). Briefly, 1.5 pmol UPF1 either alone or in presence of 3 pmol UPF2L and/or 3 pmol UPF3B were mixed with 4 µL 5x MES buffer (250 mM MES pH 6.5, 250 mM KOAc, 25 mM $Mg(OAc)_2$, 10 mM DTT, 0.5 mg/mL BSA) or 5 x translation buffer (100 mM Tris pH 7.5, 500 mM KCl, 12.5 mM $MgCl_2$, 10 mM DTT, 1.25 mM spermidine), 2 µL Poly(U) RNA (Sigma, 2 mg/mL in H_2O) and H_2O to a final volume of 16 µL. When variable protein compositions were tested, the total volume of proteins added was adjusted to equal using protein storage buffer. The reaction was started by adding 3.9 µL 10 mM ATP and 0.1 µL γ^{32}P-ATP (Hartmann Analytic, 3000Ci/mmol). Reactions proceeded for 1 h at 30 or 37°C. 1.5 µL per sample were spotted on PEI cellulose TLC plates (Merck) that had been pre-run in water. Plates were developed in 0.4 M LiCl, 0.8 M acetic acid, dried and visualized by autoradiography.

***In vitro* phosphorylation.**

1.2 pmol UPF1 either alone or in presence of various combinations of 2.4 pmol of UPF2L, UPF3B, eRF1/eRF3a and 40 fmol of SMG1-8-9 were mixed with 4 µL 5 x translation buffer and H_2O to a final volume of 16 µL. When variable protein compositions were tested, the total volume of proteins added was adjusted to equal using protein storage buffer. The reaction was started by adding 2.5 µL 10 mM ATP and 1.5 µL γ^{32}P-ATP and was allowed to proceed for 30 min at 37°C. Samples were separated by SDS-PAGE and visualized by autoradiography.

Cell culture and transfections.

HeLa cells were grown in DMEM and transfected in 10 cm plates using JetPrime transfection reagent (Polyplus), 1 – 4.5 µg of the test plasmids, and 0.4 µg of a YFP-plasmid. Empty pGEMG 3z vector (Promega) was used to adjust total amounts of transfected DNA.

Co-immunoprecipitation assays from transfected cells.

24 hours after transfection, cells were harvested in 400 µL/10 cm plate of buffer E (20 mM Tris pH 7.5, 150 mM KCl, 0.1% [v/v] NP40) supplemented with 0.3 mM $MgCl_2$ and EDTA-free complete (Sigma-Aldrich) and lyzed 30 min on ice. Magnetic M2 anti-FLAG beads (Sigma-Aldrich) were used to immunoprecipitate FLAG-tagged complexes from RNaseA-treated (30 µg/mL) cell lysates after 1 h incubation with the beads at 4°C. Beads were washed 8 times with buffer E supplemented with 0.6 mM $MgCl_2$. Tubes were changed before the last wash. FLAG-complexes were eluted with 25 µL 0.1 M glycine (pH 3.0) added to 6 µL 5 x loading buffer and neutralized with 1.5 µL 1 M Tris pH 7.5. 6 µL of the samples were loaded for anti-FLAG detection and 20 µL for anti-V5 detection, separated by SDS-PAGE and analysed by immunoblotting using anti-FLAG and anti-V5-antibodies (both Sigma-Aldrich).

Pre-termination complex assembly and purification.

Pre-termination complexes (preTC) were assembled as described (Alkalaeva et al., 2006) with the following modifications. The translation reaction performed in translation buffer D (20 mM Tris–HCl, pH 7.5, 50 mM KOAc, 1.3 mM $MgCl_2$, 2 mM DTT, 0.25 mM spermidine) supplemented with 200 U RNase inhibitor (RiboLock, Fermentas), 1 mM ATP , 0.2 mM GTP, 35 pmol of MVHC-stop mRNA, 35 pmol initiator-$tRNA_t$ (acylated with [^{35}S]-methionine for peptide release assays), 75 µg total tRNA (acylated with individual amino acids), 50 pmol purified human ribosomal subunits (40S and 60S), 100 pmol eIF2, 50 pmol eIF3, 80 pmol eIF4GΔ, eIF4A, eIF4B, eIF1, eIF1A, eIF5, eIF5BΔ each, 200 pmol eEF1H and 50 pmol eEF2 in the volume of 500 µL. The reaction mix was incubated for 40 min at 37°C. Subsequently, the reaction mix was loaded onto a 10–30 % [w/w] linear sucrose density gradient (SDG) prepared in buffer D with 5 mM $MgCl_2$ and centrifuged for 115 min at 4°C at 50 000 rpm using a Beckman SW60 rotor. The fractions corresponding to preTC complexes according to optical density and the presence of [^{35}S]-methionine were combined and used for toe-printing and peptide release assays.

***In vitro* translation and toe-printing analysis of pre- and post-termination complexes.**

In vitro translation termination was performed essentially as described (Alkalaeva et al., 2006). Briefly, SDG-purified preTCs assembled on MVHC-STOP mRNA (0.1 pmol) were incubated for 10 minutes at 37°C with 3 pmol of UPF proteins or BSA in a total volume of 35 µL translation buffer E (10 mM Tris pH 7.5, 100 mM KCl, 1 mM free $MgCl_2$, 2 mM DTT, 0.25 mM spermidine) supplemented with 0.5 mM GTP and 1 mM ATP or AMPPNP as indicated. Protein storage buffer was used to compensate for

varying amounts of proteins. The amounts of eRF1 and eRF3a required to limit the termination rate were determined for each batch of preTCs. eRF1 and eRF3a were added to the reaction mix, and termination was allowed to proceed for 5 minutes at 37°C. Ribosomal complexes were analyzed by primer extension inhibition using AMV reverse transcriptase and a [^{32}P]-labelled primer (5'-GCAATGAAAATAAATTTCC-3') complementary to a coding region of β-globin mRNA. For the experiment described in Figure 4.1E 3 pmol of UPF1 were incubated in ATP-supplemented translation buffer either alone or the presence of equal amounts of UPF2L and/or UPF3B and with or without 50 fmol SMG1-8-9 as indicated for 30 min at 37°C. After the addition of preTCs the mixture was incubated for 10 min at 37°C. The termination reaction was initiated by the addition of eRF1 and eRF3a and allowed to proceed for 5 min.

Peptide release assays.

The termination efficiency was determined as described(Alkalaeva et al., 2006) with the following modifications. Aliquots containing 0.01 pmol of [^{35}S]-methionine containing preTCs were incubated for 10 minutes at 37°C with 0.3 pmol BSA or UPF3B in translation buffer E supplemented with 1 mM ATP and 0.5 mM GTP. The peptide release reaction was started by addition of termination-rate limiting amounts eRF1 and eRF3a. Subsequently, the reaction was allowed to proceed for 0-60 sec at 37°C. The ribosomal complexes were pelleted with ice-cold 5% [v/v] trichloroacetic acid and centrifuged for 30 min at 4°C and 14,000 x g. The amount of released [^{35}S]-methionine-containing tetrapeptide was determined by scintillation counting of the supernatants using a Wallac 1504 liquid scintillation spectrometer.

Author contributions

GN-Y, CS, AEK, and MWH designed the study and wrote the manuscript with input from ER, BE, and LY; GN-Y, BA, and KK performed toeprinting experiments, ATPase assays, *in vitro* phosphorylation, and Co-IPs; ER, BE, LY, AD, and KH produced proteins; ER performed *in vitro* pulldown, co-sedimentation, and SEC (SEC-MALLS) experiments; BE generated preTCs and performed peptide release experiments.

Acknowledgements

We are much obliged to Tatyana Pestova for generously introducing K.K. to the reconstituted *in vitro* translation system and for providing the MVHC-STOP plasmid. We thank Hervé Le Hir for the UPF1L and UPF1ΔCH expression plasmids and providing protocols for their production as well as for the ATPase assay, Ludmila Frolova for providing the plasmid pET15b-eRF3a, and Stephen Cusack for plasmids pPROEx-Htb_UPF2 (121-1227), pPROExHtb_UPF3B-N, and the RNA oligonucleotide for

RNA interaction assays. We thank Elena Alkalaeva for providing Met-tRNA and the plasmids for initiation factors used for *in vitro* translation Alain Miller. AD is supported by an EC-EMBL CoFUNDS EIPOD fellowship, CS is supported by a European Research Council Starting Grant (ComplexNMD, 281331). The experimental work of MWH and AEK is supported by the DFG through the SFB 1036 grant and together with GN-Y through the SPP1935 grant.

4.5 Supplemental information

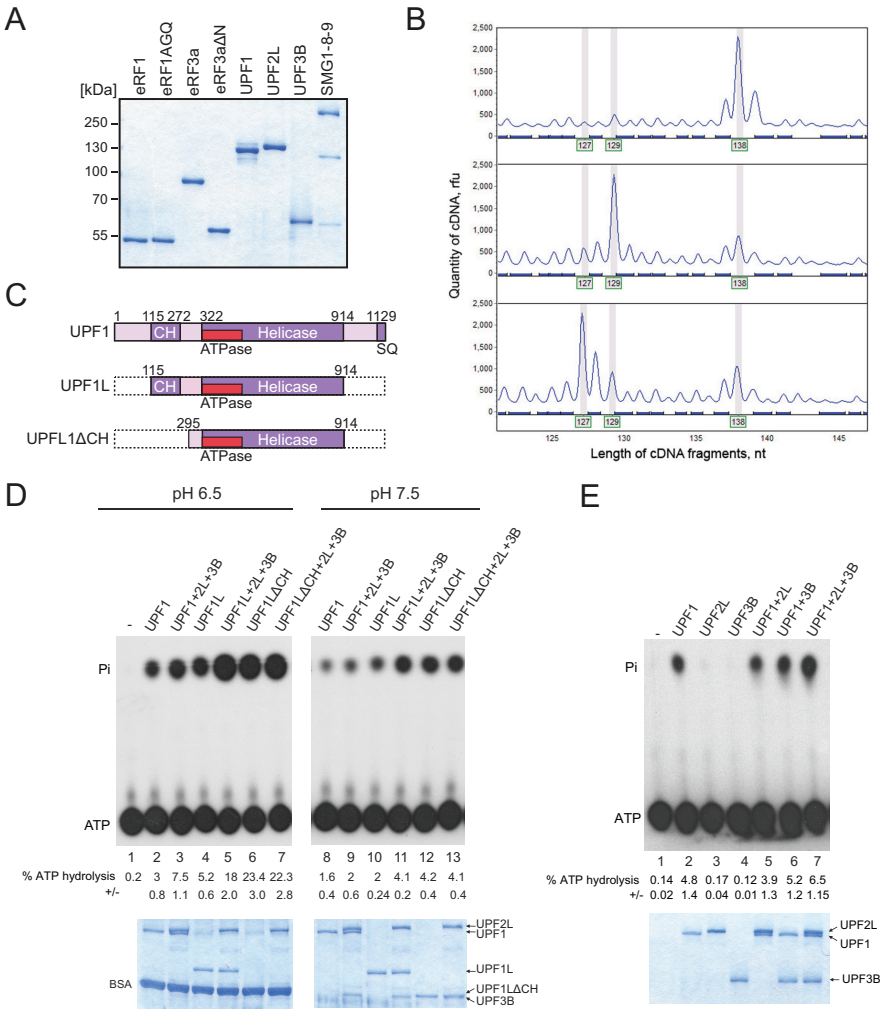

Figure 4.8: Supplemental Figure related to Figure 4.1. ***A.*** *SDS-PAGE analysis of purified recombinant proteins used in the toe-printing experiments as indicated.* ***B.*** *Toe-print analysis of translation complexes prepared by the reconstituted in vitro translation system. Above: 80S initiation complex; middle: pre-termination complex (preTC); below: termination complex formed in presence of eRF1, eRF3a and GTP. Peaks at 138 nt indicate the position of the 80S initiation complex on mRNA, peaks at 129 nt indicate the position of preTC and peaks at 127 nt correspond to the termination complex (postTC). Rfu – relative fluorescence units.* ***C.*** *Schematic representation of UPF1 variants used in (D).* ***D.*** *Thin layer chromatography (TLC) analysis of the ATPase activity of UPF1 variants in the absence or presence of UPF2L and/or UPF3B at 30 °C in MES buffer (pH 6.5, lanes 1-7) or translation buffer (pH 7.5, lanes 8-13), respectively. 1.5 µl of the samples were spotted on the TLC plates and the residual 18.5 µl were analysed on SDS-PAGE gels for loading control (lower panels). The positions of γ^{32}P-ATP and γ^{32}P-Pi are indicated. % ATP hydrolysis was calculated using a phosphorimager and displays the means ± SEM of 4 independent experiments.* ***E.*** *ATP hydrolysis experiment as in (D) at 37 °C in translation buffer.*

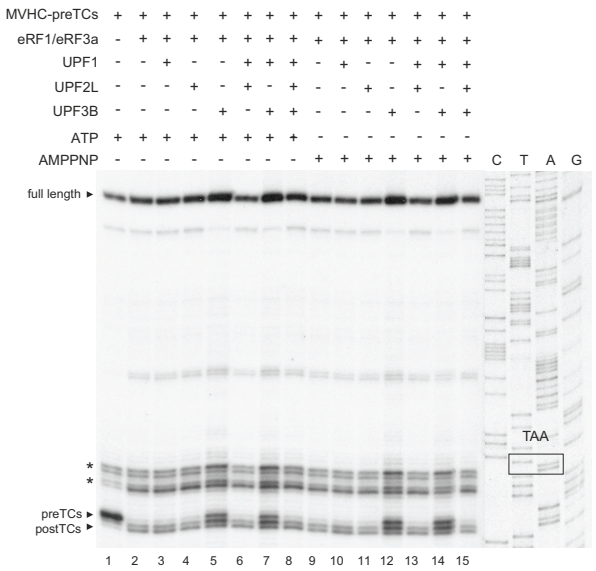

***Figure 4.9: Supplemental Figure related to Figure** 4.1**B.** Toe-printing analysis of ribosomal complexes obtained as in Figure 4.1B in the presence of 1 mM ATP or AMPPNP, respectively.*

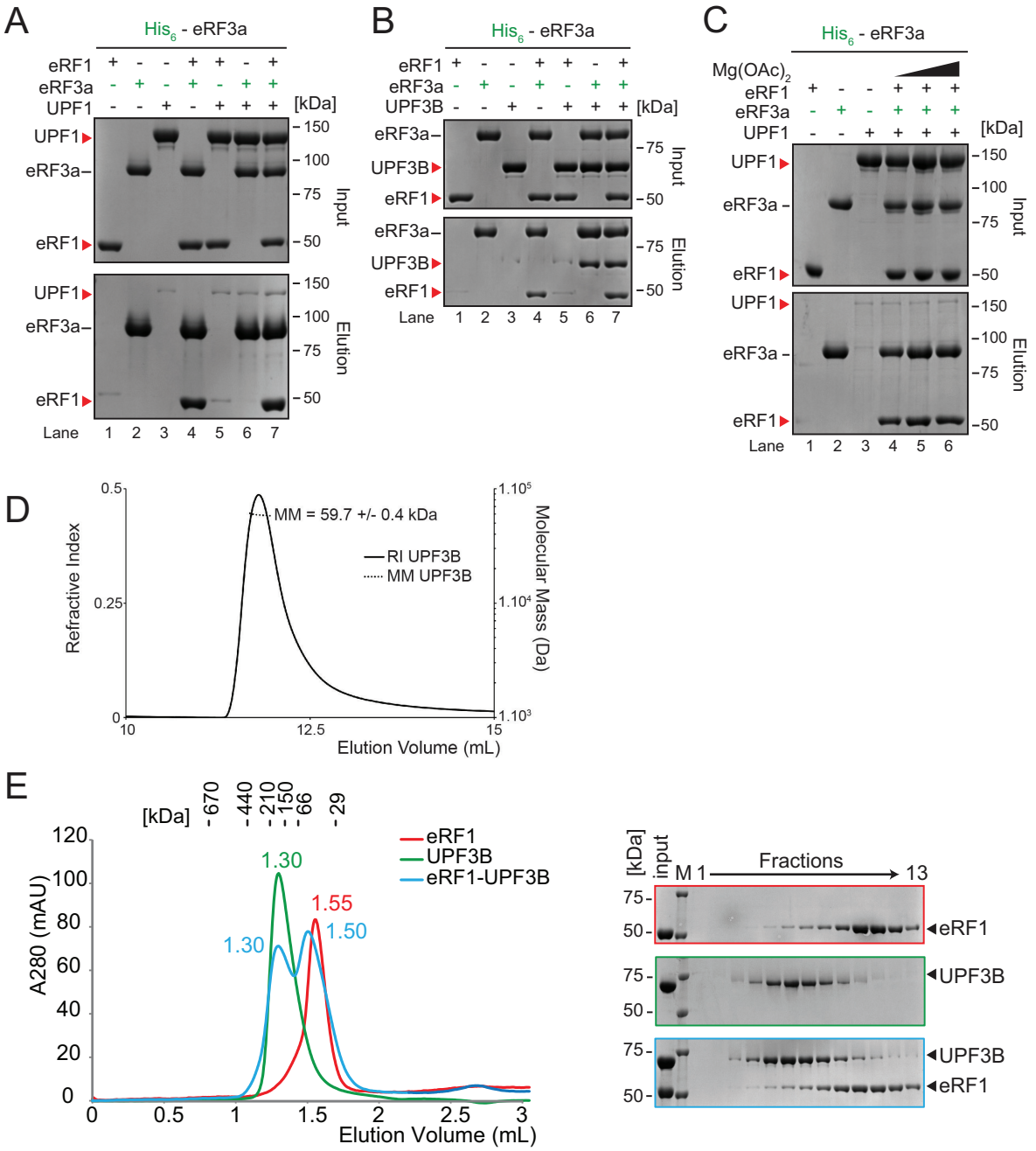

Figure 4.10: Supplemental Figure related to Figure** 4.3.* ***A. *In vitro pulldown of eRF1 and/or UPF1 with His-eRF3a. Protein mixtures before loading onto the beads (input) or after elution (eluate) were separated by SDS-PAGE.* ***B.*** *Pulldown experiment as in (A) with eRF1, UPF3B, and His-eRF3a.* ***C.*** *Pulldown experiment as in (B) with eRF1, UPF1, and His-eRF3a and at 0, 2.5, and 5 mM of Mg^{2+} (lanes 4-6), respectively.* ***D.*** *Molecular mass of UPF3B determined by size-exclusion chromatography using a Superdex 200 column combined with detection by multiangle laser light scattering and refractometry (SEC-MALLS-RI). The SEC elution profiles as monitored by refractometry (RI) are represented for UPF3B. The molecular mass (MM) of UPF3B calculated from light scattering and refractometry data is indicated.* ***E.*** *SEC elution profile of eRF1 (red), UPF3B (green), or both (blue). The elution volume (in mL) is indicated for each experiment. Calibration of the column was performed with globular proteins (shown above). Lower panel: SDS-PAGE analysis of eluate fractions. M: protein molecular weight standards (kDa).*

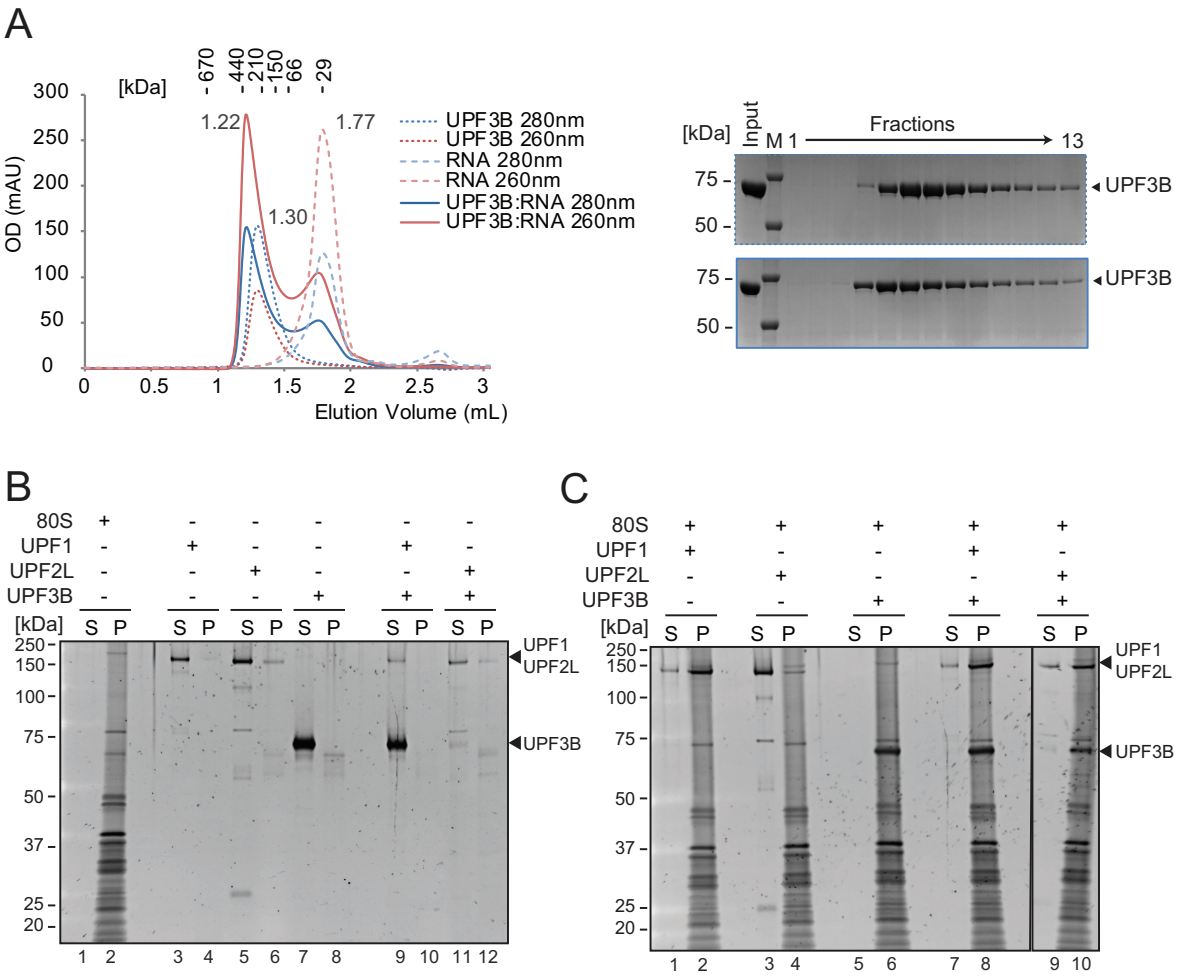

Figure 4.11: Supplemental Figure related to Figure** 4.5.* ***A. *Left: SEC elution profile of UPF3B (dotted lines), RNA (dashed lines) and the mix (solid lines). Optical density was recorded at 280 nm (blue) and at 260 nm (red). 40 µM of UPF3B or RNA oligonucleotide (24 mer) or both were loaded onto the Superdex200 column. The elution volumes are indicated next to the curves. Right: Eluate fractions of UPF3B alone (upper) and UPF3B-RNA mixes (lower) were analysed by SDS-PAGE. M: protein molecular weight standards (kDa).* ***B.*** *Sucrose cushion co-sedimentation analysis of UPF1, UPF2L, or UPF3B or in combinations as indicated. After ultracentrifugation, the supernatant (S) and pellet (P) fractions were analysed by SDS-PAGE.* ***C.*** *Sucrose cushion co-sedimentation analysis of UPF1, UPF2L, or UPF3B as in (B) but with 80S ribosomes as indicated.*

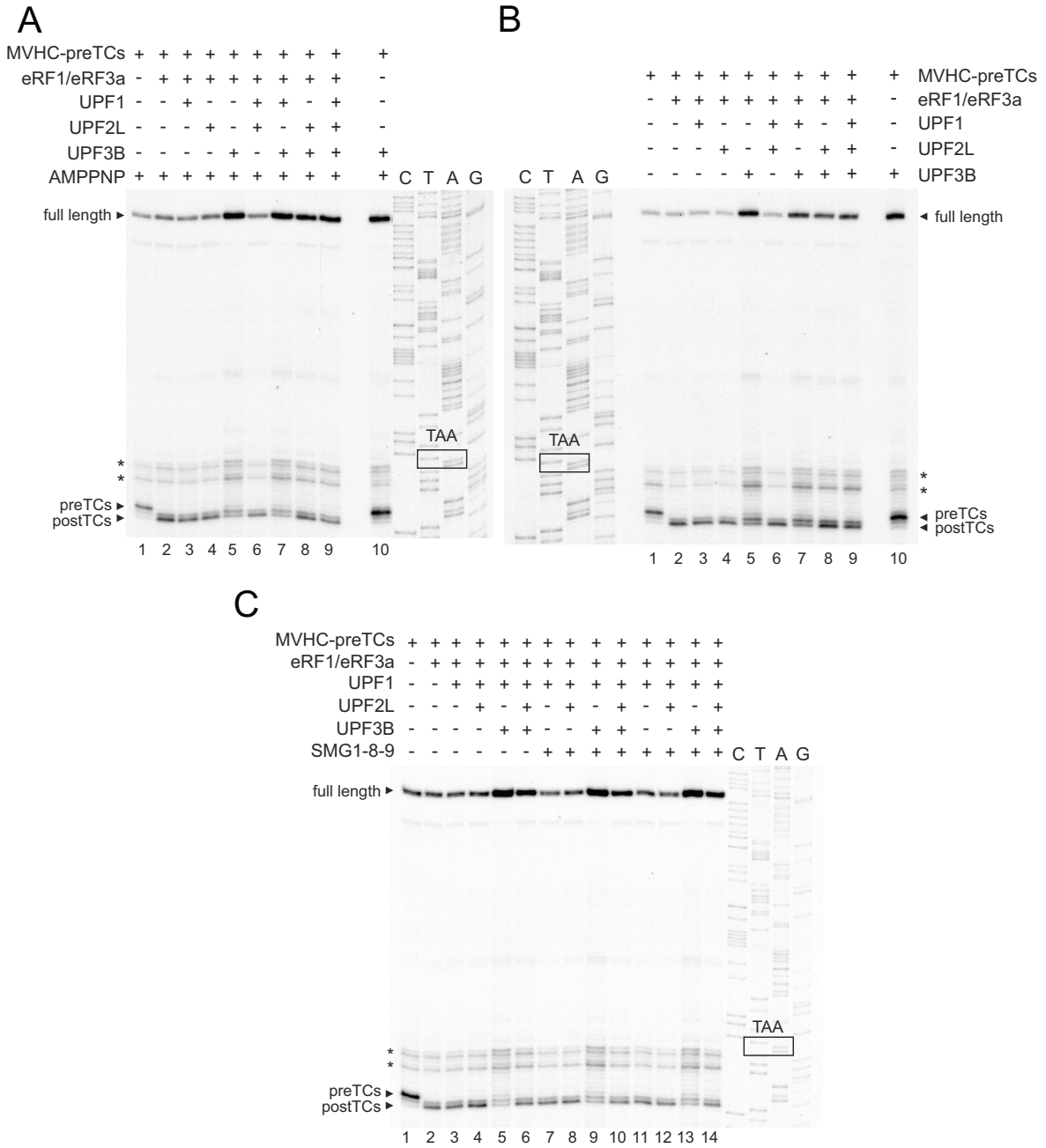

***Figure 4.12: Supplemental Figure related to Figure** 4.6. **A. B.** Toe-printing analysis of ribosomal complexes as in Figure 4.6A, but in the presence of 1 mM AMPPNP (A) or without nucleotide (B). **C.** Impact of UPF1-phosphorylation on efficient translation termination and on ribosome dissociation by UPF3B. Toe-printing analysis of ribosomal complexes obtained by incubating preTCs formed on MVHC-STOP mRNA (MVHC-preTCs) with UPF1, UPF2L, UPF3B, or BSA at 1 mM free Mg^{2+} and 1 mM ATP. In lanes 7-10 UPF1 was incubated with SMG1-8-9 and ATP for 30 min at 37 °C either alone (lane 7) or in the presence of UPF2L, UPF3B, or both (lanes 8-10) before preTCs were added to the mixture and again incubated for 10 min. In lanes 11-14 UPF1 was incubated with ATP and SMG1-8-9 for 30 min. Then, UPF2L and /or UPF3B were added for additional 15 min (lanes 12-14). Finally, MVHC-preTCs were added to the mixtures for 10 min followed by translation termination by eRF1 and eRF3a.*

4.6 Additional results

This section describes additional result, which were generated, on the interplay between the human release factors and UPF proteins, but which were not included in the submitted manuscript.

Full length UPF2 interacts with the release factors

In order to further investigate the binding of UPF proteins to the release factors, full length UPF2 was purified from insect cells (Figure 4.13A) and additional binding assays were performed. Complexes were resolved by incubating the sample with NiNTA affinity resin (see the method section 4.4). After extensive washing, proteins were eluted with imidazole and subsequently were visualized on Coomassie stained SDS-PAGE.

Immobilized full-length UPF1, UPF2 and UPF3B were tested against eRF3a (Figure 4.13B). UPF3B co-purified with eRF3a as described previously (figure 4.3, 4.13B lane 7). Surprisingly, UPF2 also co-eluted with eRF3a but to a lesser degree than UPF3B, suggesting that UPF3B might have a higher affinity for eRF3a than UPF2 (Figure 4.13B, lane 5-7). Using full-length His-tagged UPF2 for binding assays with both release factors, eRF3a, but not eRF1AGQ alone, co-eluted with UPF2 (Figure 4.13C, lane 5-7). However, a ternary complex could be formed when both release factors were mixed with UPF2 indicating that eRF1AGQ might be recruited to the complex through eRF3a (Figure 4.13C, lane 5-7). This result is consistent with a recent study showing that the MIF4G-3 domain of UPF2 forms a stable complex with eRF3a but not with eRF1 (López-Perrote et al., 2015). In our previous binding assays, we did not isolate a strong complex with UFP2L indicating that the binding site might be an overlap between the C-terminal part of UPF2 and the MIF4G-3 (Figure 4.3). Alternatively, UPF2L was purified from *E. coli* and thus could lack some important post-translational modifications promoting the interaction with eRF3a. It was tested if the interaction between UPF2 and the release factors was dependent on the Mg^{2+} concentration, similarly to UPF3B. It was found that UPF2 interacted with the release factors in a Mg^{2+}-independent manner (Figure 4.13).

To further investigate the interaction network, combinations of NMD factors were mixed in the presence of eRF3a. UPF2 interaction with eRF3a appear to be disturbed in presence of UFP1 (Figure 4.13D, lane 5-7). This is consistent with the *in vivo* pull-downs performed in Figure 4.2 where a complex comprising eRF3a, UPF1 and UPF2 could not be isolated. In contrast, UPF2 interaction with eRF3a was not affected by the presence of UPF3B (Figure 4.13E, lane 6-7). However, It is unclear at the moment whether a ternary complex is formed or whether UPF2-UPF3 and UPF2-eRF3a complexes are coeluted. These results should be confirmed by performing pulldowns experiments with untagged UPF2 and by alternative methods.

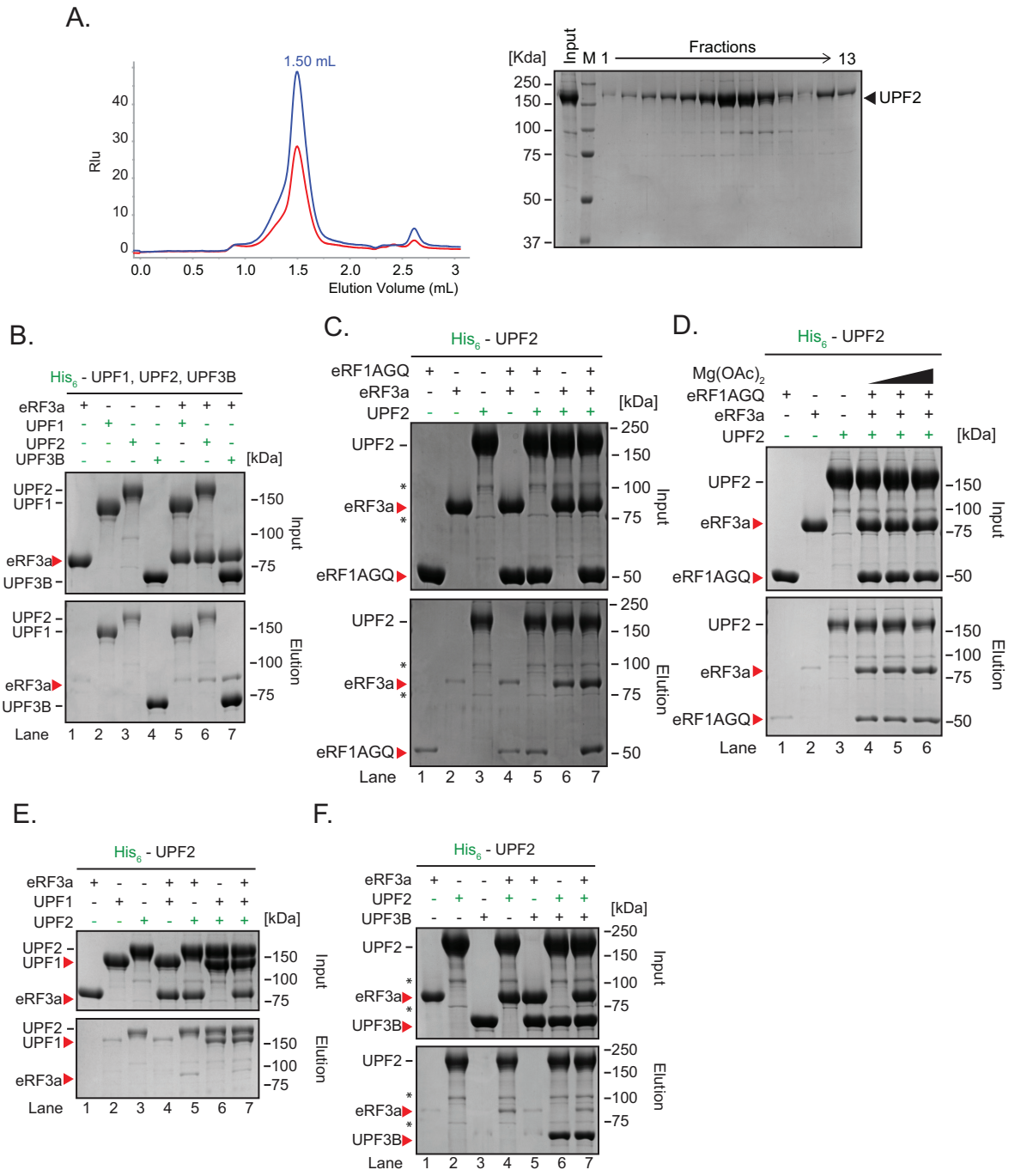

Figure 4.13: UPF2 interacts with eRF3a. ***A.*** *Full length UPF2 size exclusion profile using Superdex 6 16/60 (GE Healthcare).* ***B.*** *Pulldown with hexahistidine-tagged UPF1, UPF2 or UPF3B with untagged eRF3a. Protein mixtures loaded (input) onto the beads (above) and after elution (below) were separated by SDS-PAGE followed by Coomassie staining.* ***C.*** *Pulldown with hexahistidine-tagged UPF2 mixed with eRF1 or eRF3a or both.* ***D.*** *Same as C. but with increasing $Mg(OAc)_2$ concentrations from 0 to 2.5 to 5 mM.* ***E.*** *Pulldown as C. but with untagged eRF3a or UPF1.* ***F.*** *Pulldown as C. but with untagged eRF3a or UPF3B.*

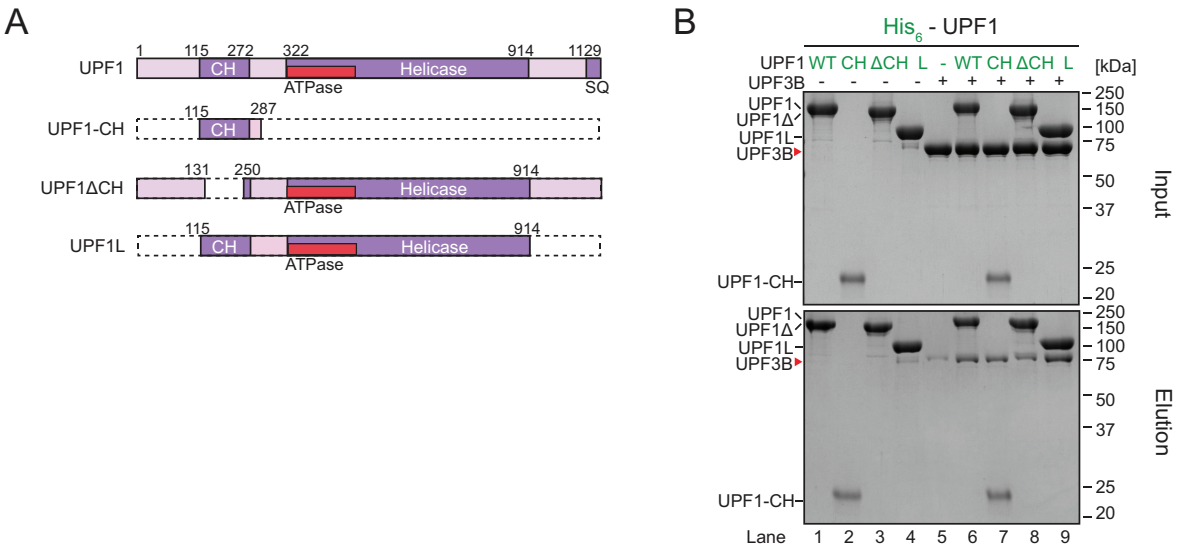

Figure 4.14: UPF3B interacts with UPF1 CH domain A. *Schematic representation of UPF1 constructs used in B.* ***B.*** *Pulldown with hexahistidine-tagged UPF1, UPF1-CH, UPF1ΔCH or UPF1L untagged UPF3B. Protein mixtures loaded (input) onto the beads (above) and after elution (below) were separated by SDS-PAGE followed by Coomassie staining.*

UPF3B interacts with UPF1 CH domain

Surprisingly, UPF1 and UPF3B co-eluted in the absence of eRF3a (Figure 4.4). Previously, this interaction has been tested with purified human UPF1L (aa115-914) and UPF3B but was not observed (Chamieh et al., 2008). In order to map the UPF1 interaction domain, different His-tagged UPF1 constructs were generated (Figure 4.14A). UPF1-CH comprises the CH domain of UPF1 (aa115-287) whereas UPF1ΔCH lacks most of this domain (aa1-131 and 250-1129); UPF1L is described in section 4.2 and lacks both N- and C-terminal ends (aa115-314). These constructs were used in *in vitro* pulldown assays and it was found that full length UPF1, UPF1L and UPF1-CH fragment co-eluted with a similar amount with UPF3B, indicating that the UPF1 CH domain might mediate the interaction (Figure 4.14B, lane 6,7,9). However, UPF1ΔCH could still interact with UPF3B, albeit less efficiently, suggesting the possibility of a second binding site (Figure 4.14B, lane 8).

UPF3B is a phosphorylated protein

Using mass spectrometry, our collaborators identified 4 phosphorylation sites in UPF3B: Y160, T169, S320 and T413 (Figure 4.15A). Interestingly, Y160 has been linked to autistic features when the tyrosine is mutated to an aspartic acid (UPF3B-Asp160) (Tarpey et al., 2007). This residue is conserved between UPF3A, and UPF3B in higher eukaryotes (Figure in Appendix B.3). The UPF3B-Asp160 mutant was found to increase the expression of NMD targets indicating that it may reduce UPF3B activity (Alrahbeni et al., 2015). In addition, patients with UPF3B-Asp160 have higher levels

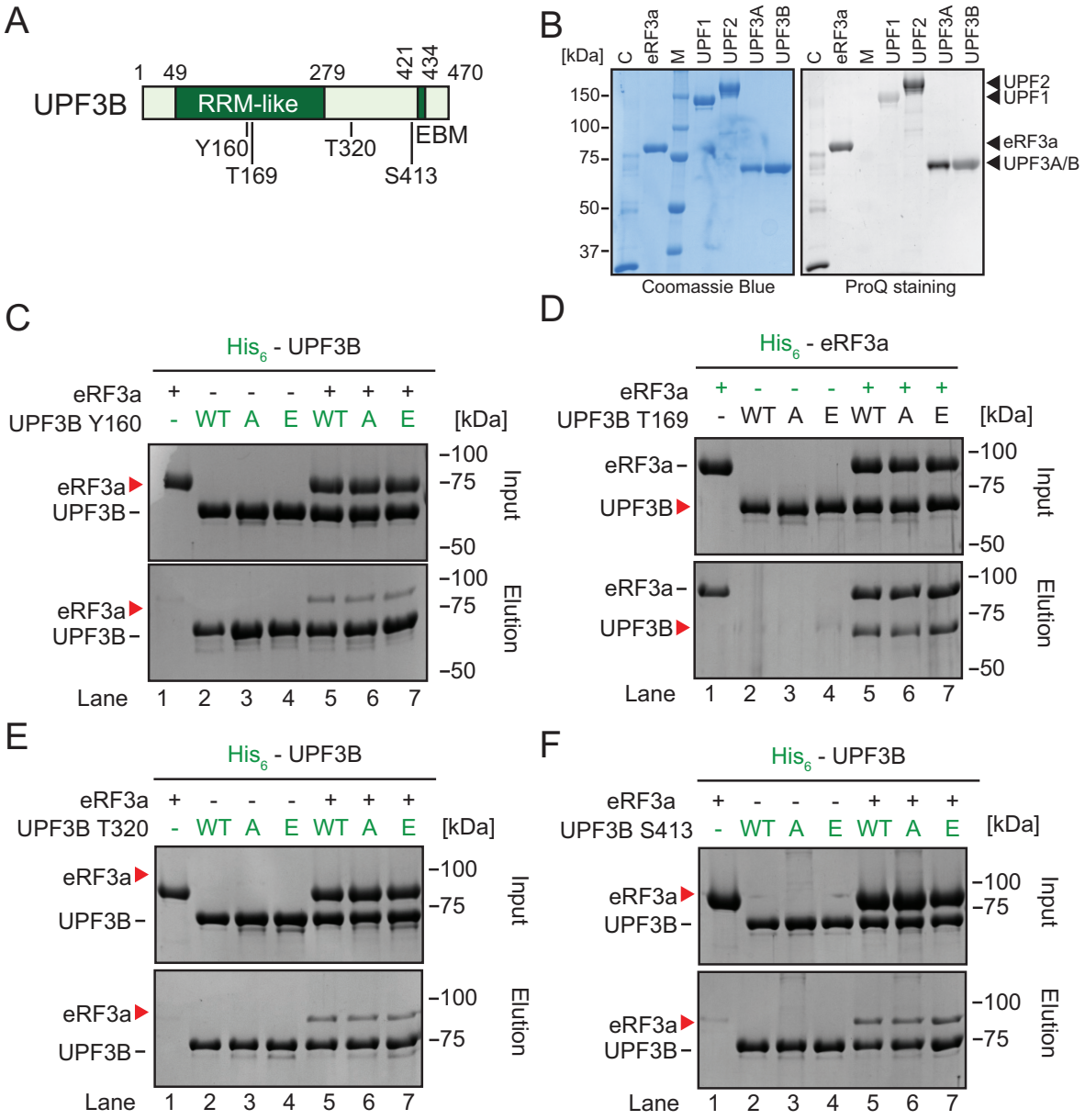

Figure 4.15: UPF3B phosphorylation does not impair eRF3a binding A. *Schematic representation of UPF3B. 4 phosphorylation sites identified by mass spectrometry are mapped to the sequence with their respective amino acids and position. RRM-like: RNA-recognition motif-like, EBM: EJC-binding motif.* ***B.*** *SDS-PAGE analysis of purified recombinant proteins. Left and right panels were stained with Coomassie blue or ProQ (Thermo scientific) staining respectively.* ***C.*** *Pulldown with hexahistidine-tagged WT or Y160A or Y160E mutant UPF3B and eRF3 alone or mixed together. Protein mixtures loaded (input) onto the beads (above) and after elution (below) were separated by SDS-PAGE followed by Coomassie staining.* ***D.*** *Pulldown with hexahistidine-tagged eRF3 and untagged WT or T169A or T169E mutant UPF3B alone or mixed together.* ***E.*** *Same as C. but with T320A or T320E UPF3B mutants.* ***F.*** *Same as C. but with S413A or S413E UPF3B mutants.*

of UPF3A, similarly to patients lacking UPF3B. The T169 site was found to be a casein kinase 2 (ck2) substrate motif (TDNE). Interestingly, ck2 has already been reported as a putative kinase for yeast Upf2p (Wang et al., 2006). No information was found for S320 and T413 except that T413 phosphorylation was only observed in the presence of UPF2. The phosphorylation status of the UPF proteins were assessed by ProQ staining (Thermo Scientific) (Figure 4.15B). Surprisingly, it was found that eRF3a, UPF2, UPF3A and UPF3B all showed strong signals after ProQ staining indicative of phosphorylation during protein expression in insect cell. However, following purification, UPF1 did not appear to be hyperphosphorylated (Figure 4.15B). In order to assess the effect of the phosphorylation on UPF3B interactions, the amino acids Y160, T169, S320 and T413 were mutated to either glutamic acid (mimicking a phosphorylated form) or an alanine residue. Thus, 8 UPF3B mutants were generated recombinantly and probed for binding to eRF3a. Using the same *in vitro* binding assays as described in section 4.2, we found that none of these mutations alone could impair the binding of UPF3B to eRF3a (Figure 4.15C-F). However, these binding assays are rather insensitive and cannot discriminate between small changes in dissociation constants. It would be interesting to measure the Kds of different UPF3B mutants for eRF3a. Alternatively, these amino acids could be important for another function of UPF3B, for example binding to the ribosome or to another partner.

UPF3B could bridge UPF2 to the ribosome

To explore the ability of UPF3B to interact with ribosomes, co-sedimentation assays were performed (Figure 4.16). Briefly, the protein was added to the 80S ribosome and centrifuged through a sucrose cushion. Only the proteins interacting with the ribosome will sediment to the pellet fraction. Firstly, the buffer conditions were optimized. Centrifugation of UPF proteins without 80S ribosome served as controls to confirm that the proteins remained in the supernatant fraction. Two different volume of sucrose layer and two different buffer combinations were tested (Figure 4.16A). Subsequently, ribosome pelleting assays were performed using 10-fold molar excess of UPF proteins. It was found that UPF3B co-sediments with 80S ribosomes indicating that UPF3B can bind ribosomes (Figure 4.16A). Conditions were further optimized to 400 µL of sucrose cushion in HEPES/KOH buffer with KOAc as it allowed only a fraction of UPF3B to bind to 80S, thus minimizing unspecific binding. Magnesium levels have previously been shown to be critical for ribosomal subunits stability,(Shenvi et al., 2005). In addition, it was already found that UPF3B interaction with the release factors was dependent on the Mg^{2+} level (Figure 4.10). Thus, the binding of UPF3B to the ribosome was next assessed at different Mg^{2+} concentration (Figure 4.16B). The binding of UPF3B to the 80S ribosome was only slightly depending on the Mg^{2+} concentration and UPF3B binding could still be observed above 5 mM $Mg(OAc)_2$. It was decided

to keep 2.5 mM Mg^{2+} which allowed stable association of UPF3B with 80S ribosome during sedimentation. Following these experiments it was investigated whether the interaction was depending on the salt concentration (Figure 4.16C). UPF3B binding to the ribosome was lost at increasing salt concentrations (Figure 4.16C lanes 6 vs 10 vs 14). It was decided to use 250 mM KOAc for further experiments as UPF3B could only partially bind to the 80S as indicated by UPF3B presence in the supernatant fraction (Figure 4.16C lane 10). Next, the influence of full length UPF2 on UPF3B ribosomal binding was investigated[1]. Similarly to UPF2L, full length UPF2 only weakly bound to the 80S ribosome. The ribosomal binding of UPF2 was increased in presence of UPF3B, indicating that UPF3B may recruit full length UPF2 to the 80S ribosome (Figure 4.16D lane 10 vs 14). Subsequently, the ability of UPF2 to co-sediment with the ribosome in the presence of UPF1 was assessed. In contrast to UPF3B, UFP1 presence did not significantly increase UPF2 co-sedimentation with the 80S ribosome (Figure 4.16D lane 10 vs 14). This result suggests that only UPF3B could bridge UPF2 to the ribosome. In future experiments, UPF3B binding to either ribosomal subunits should be assessed.

[1]UPF3B binding to the 80S ribosome in the presence of UPF1 was tested in the manuscript. Please refer to section 4.2

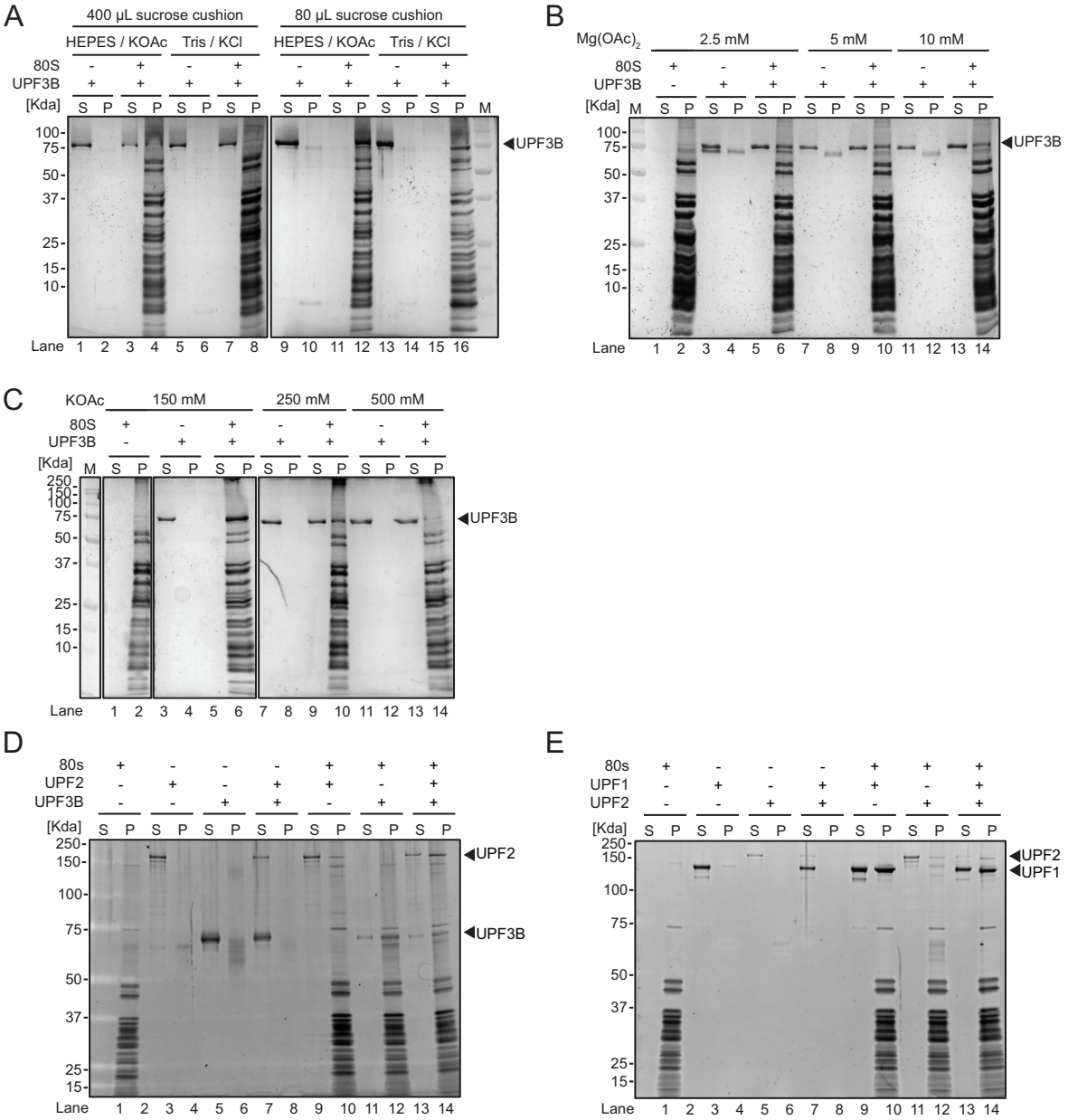

Figure 4.16: UPF3B bridges UPF2 to the 80S ribosome A. *Sucrose cushion co-sedimentation analysis of UPF3B with different volume cushion and buffer/salt concentrations as indicated. After ultracentrifugation, the supernatant (S) and pellet (P) fractions were analyzed by 12 % SDS-PAGE followed by silver staining (Bio-Rad).* ***B.*** *Same as A. but with increasing concentration of $Mg(OAc)_2$ as indicated.* ***C.*** *Same as A. but with increasing concentration of KOAc as indicated.* ***D.*** *Sucrose cushion co-sedimentation analysis of UPF2 and UPF3B alone or together as indicated.* ***E.*** *Same as D. but with UPF1 and UPF2. The fractions were analyzed by SDS-PAGE on 4-12 % Bis-Tris (Invitrogen) following by SYPRO Ruby staining (Invitrogen)*

5. Discussion

Resumé en français

Les travaux effectués durant cette thèse ont pour but de fournir des informations biochimiques et structurales sur la termination de la traduction lors de la dégradation d'ARNm non-sens (NMD). Ceux-ci se basent sur des systèmes de traduction *in vitro* de levure et d'homme. Nos systèmes nous ont permis de reconstruire des complexes de termination de levure ainsi que de tester l'impact de différents facteurs NMD sur la termination chez l'homme. De tels systèmes sont essentiels pour l'enrichissement des connaissances sur le rôle des facteurs NMD dans la termination de la traduction.

Ce travail de thèse apporte pour la première fois l'évidence que UPF3B, et non UPF1, a un effet dans la termination et le recyclage de la traduction, contrairement au courant de pensée établi. Nos résultats suggèrent un nouveau mécanisme pour la reconnaissance des PTCs et soulignent aussi une implication directe de la NMD dans le recyclage des ribosomes positionnés au niveau d'un PTC. De nombreuses questions restent à élucider notamment sur le fonctionnement de la NMD dans la branche indépendante de UPF3B ou sur le rôle de UPF3A dans la termination. Nos travaux sont un point de départ solide pour de futures études fonctionnelles et structurales sur des complexes de terminations en levure et en humain.

La NMD est un mécanisme de contrôle complexe qui connecte différents processus cellulaires dans l'espace et le temps. Sa compréhension représente un challenge formidable en particulier pour le développement de nouvelles stratégies thérapeutiques dans le traitement des maladies associées au NMD.

Despite decades of investigation, the interplay between translation and NMD factors allowing the discrimination between NTCs and PTCs remained unclear. Multiples models have been proposed for the mechanism of premature translation termination and activation of NMD, but all failed to restitute complexity of the pathway. This PhD work was aiming at providing biochemical and structural information on the termination of translation in the presence of NMD factors. *In vitro* translation systems for yeast and human were established in our laboratory, which permitted the reconstruction of termination complexes and functional probing of the different factors. This work yielded the first evidence that UPF3B and not UPF1 has an activity in termination of translation and dissociation of PTC-stalled ribosomes. In the following sections, I discuss the implications of our results in our understanding of the various steps from termination to ribosome recycling during NMD. The final section will discuss the repercussion of our understanding of NMD.

5.1 Binding of NMD and termination factors at a PTC

5.1.1 Interplay between eRF1-3a and the NMD factors

In contrast to other surveillance pathways, NMD requires the canonical release factors and additional factors to terminate translation and rescue ribosomes stalled at a premature termination codon (Figure 5.1). However, toeprint experiments suggest that termination is slower at a PTC than at a NTC in yeast (Amrani et al., 2004). This delay was attributed to the absence of Pab1p, which would allow the recruitment of Upf1 by the release factors. In yeast, Upf1p was shown to interact with eRF1 and eRF3 (Wang et al., 2001; Kervestin et al., 2012; Roque et al., 2014). Yet we were not able to confirm a direct *in vitro* interaction between eRF3a and UPF1 from both human and yeast as our experiments showed ambiguous results (Figure 3.9, 4.3). Human UPF2, in contrast, interacted directly with eRF3a, but not with eRF1 in our pulldown experiments, confirming the result from (López-Perrote et al., 2015). However, no complexes between the release factors and UPF2 were isolated by *in vivo* immunoprecipitations, indicating that UPF2 might bridge the release factors with other factors. Yet, it might not partake in the resulting interactions and thus it remain unclear which UPF protein could interact with the release factors both *in vivo* and *in vitro*. In our experiments, UPF3B was the only NMD factor, able to bind directly to eRF1 and to eRF3a both *in vitro* and *in vivo* and thus potentially able to interfere with termination (Figure 4.3).

UPF1 is thought to associate with NMD-target mRNAs and possibly the elongating ribosomes (He & Jacobson, 2015b). This would explain the co-immunoprecipitation of

UPF1 with the release factors in an RNA-independent manner (Figure 4.2). However, it remains unclear whether UPF1 can mark stop codons as aberrant or if additional factors are involved in the decision (He & Jacobson, 2015b). In the toeprint assays, we could not detect any effect of UPF1 or UPF2 alone on the stop codon recognition process, indicating that they may not be active on their own during termination of translation as previously proposed (Figure 4.1) (He & Jacobson, 2015b). Our results indicate that UPF3B is the only NMD factor which could, in addition to interacting with both release factors, impair the stop codon recognition and peptide release. We propose that the presence of UPF3B nearby a terminating ribosome could form the basis of a molecular mechanism signaling aberrant termination to the NMD machinery. Our results challenge the prevailing NMD models, which place UPF1 at center stage, and shed light on previously unknown functions of UPF3B in PTC recognition and ribosome rescue after termination at a PTC.

However, in the cell, additional mRNP factors, such as the EJC or PABPC1, are likely to be involved. The effect of UPF3B in stop codon recognition and release factors binding remains to be investigated *in vivo*. Such an endeavor will require the development and application of new techniques such as real time *in vivo* imaging (Yan et al., 2016) and innovative transcriptome-wide approaches (Pelechano et al., 2015; Archer et al., 2016). The latter approach has already revolutionized our view of NMD but remains to be extended to other NMD factors(Zünd et al., 2013; Hogg & Goff, 2010; S. R. Lee et al., 2015; Hauer et al., 2016).

5.1.2 eRF3a as a node for the integration of termination signals

5.1.2.1 Possible competition between PABPC1 and UPF3B during termination

The N-terminal part of Hbs1 interacts with the 40S subunit proteins S3 and S30 near the mRNA entry site and might have a regulatory activity in no-go decay (NGD) activation, an RNA surveillance mechanism for mRNAs stalled in translation elongation (Becker et al., 2012). Consistent with this idea, ribosomal subunit dissociation in NGD is sensitive to mRNA length in the presence of Hbs1 (Pisareva et al., 2011). As Hbs1 and eRF3 share homology, it has been hypothesized that the eRF3 N-terminal was able to bind the same ribosomal surface and to help to regulate termination efficiency (Franckenberg et al., 2012). In support of this idea, the yeast eRF3 N-terminal region was proposed to regulate the binding of eRF1 binding site in a competitive manner (Kong et al., 2004). In addition, the Faux 3' UTR model postulates that Pab1p could promote termination and antagonize nonsense mediated mRNA decay by associating with the eRF3 N-terminal (Amrani et al., 2004; Kervestin et al., 2012; A. Ivanov et

al., 2016).

However, in our biochemistry and cryo-EM studies of yeast proteins, we could not reproduce the direct binding of Pab1p to eRF3 observed previously (Figure 3.9) (Kervestin et al., 2012; Roque et al., 2014). Since these interactions have been reported (Wang et al., 2001; Cosson et al., 2002a), only the interaction between human eRF3a and PABPC1 has been solved by x-ray crystallography (Kozlov & Gehring, 2010). We reasoned that the competition model between Upf1p and Pab1p for the binding of eRF3 should be investigated more thoroughly in yeast. In our experiments, a stable binding of yeast Upf1p or Pab1p to the yeast release factors could not be confirmed. This may be explained by a rather transient nature of their interaction. Alternatively, it cannot be excluded that these interactions may be promoted by other mRNP factors in yeast. In mammalian NMD, the interaction between UPF3B and the eRF3a N-terminal domain raises the possibility of competition between human UPF3B and PABPC1 for the binding of eRF3a (Figure 4.3). Competition *in vitro* binding assays can be performed to investigate possible competition between UPF3B and PABPC1 for the eRF3a N-terminal domain. Additionally, further mapping of UPF3B interaction with eRF3a N-terminal by peptide spot arrays could be performed to find out whether the PABPC1-binding motifs of eRF3a overlap with the UPF3B-interacting region. In contrast, recent studies have proposed that the PABPC1 interaction with eRF3a N-terminal may be important for post-termination and reinitiation but not for mRNA decay (Joncourt et al., 2014; Durand & Lykke-Andersen, 2013; Roque et al., 2014). Thus, competition between UPF3B and PABPC1 for the eRF3a N-terminal region would be difficult to reconcile with these recent observations. However, it could also be a sign of partially overlapping roles for both proteins in recycling and reinitiation of translation.

5.1.2.2 Possible competition between eI3j and UPF3B following termination

In yeast, the j subunit of eukaryotic initiation factor 3 (eIF3j) has been shown to bind to the ribosomal protein S30 on the small subunit (40S) and eRF3 (Beznosková et al., 2013; Aylett et al., 2015). It was proposed that eIF3j could promote eRF3-GDP dissociation from the ribosome to allow efficient recycling by ABCE1 in a 'termination-initiation' complex (Beznosková et al., 2013). Our work is consistent with the facts that UPF3B associates with the eRF3a N-terminal part and with the ribosome and slows down peptide release. Interestingly, in tethering experiments, the deletion of the UPF3B RRM-like domain and the first predicted coiled coil (aa 49-279) impaired the activation of translation observed by wild-type UPF3B (Appendix B.3) (Kunz et al., 2006). Based on these observations it is tempting to speculate that UPF3B could influence the eRF3a GTP hydrolysis rate or the dissociation rate from the ribosome

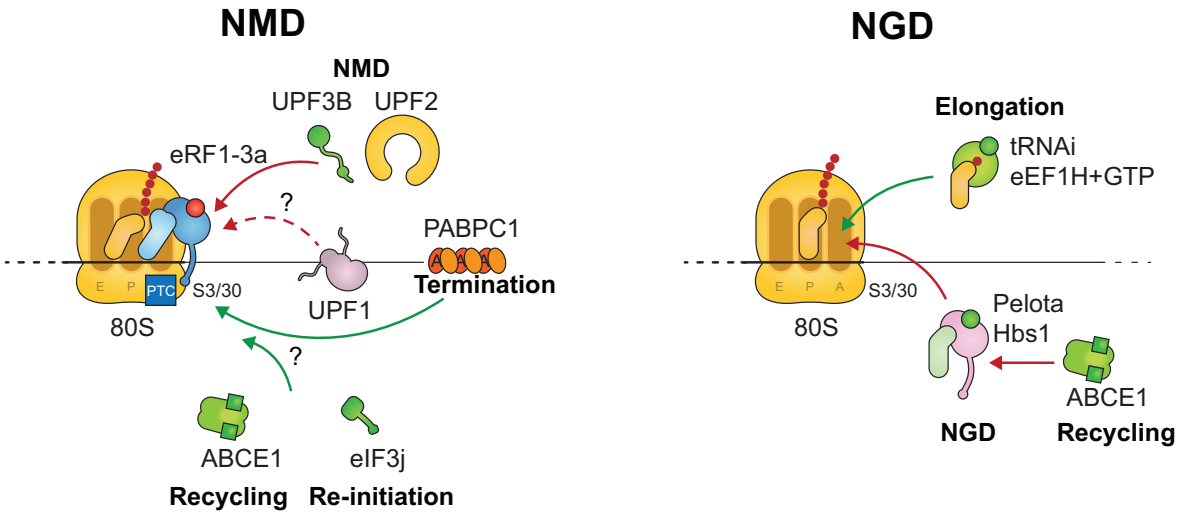

Figure 5.1: eRF3a and the ribosome integrate signals for mRNA quality control. *Left panel: during recognition of a premature termination codon (PTC in blue box) by nonsense mediated mRNA decay (NMD), eRF3a N-terminal could integrate stimulatory and inhibitory signals (green and red arrows respectively) from various factors: poly(A) binding protein PABPC1, recycling factor ABCE1, initiation factor eIF3j and the NMD factors UPF1, UPF2 and UPF3B; in order to decide if the quality control pathway should be activated. Right panel: similarly, during no-go decay (NGD) activation, NGD factor Pelota compete with elongation factors bound to tRNA. Subsequent to translation termination, Pelota recruits ABCE1 to rescue the stalled ribosome.*

through a mechanism reminiscent of eIF3j. However, our toeprints assays suggest that UPF3B's activity could be independent of the eRF3a N-terminal domain (Figure 4.5). To shed light on UPF3B's action in termination and ribosome recycling, the influence of UPF3B on eRF3a-ribosome association and GTP hydrolysis should be determined (Figure 5.1). Atomic resolution structures of terminating ribosomes in the presence of full length eRFs and/or UPF3B would yield additional insights into the impact of UFP3B on translation termination.

In summary, the role of the eRF3a N-terminal domain remains obscure. It could be critical to integrate the different inhibitory or stimulatory signals during the termination-recycling-initiation (Figure 5.1).

5.2 NMD factors control the recycling and initiation of ribosomes

5.2.1 Ribosome dissociation following PTC recognition

The importance of proper recycling of the translation components in mRNA surveillance was illustrated by Young and colleagues who found that in the absence of ABCE1/Rli1 and Pelota/Dom34, yeast 80S ribosomes accumulated at stop codons and

in the 3'UTR of mRNAs, possibly due to aberrant reinitiation (Young et al., 2015). eRF1-eRF3a were reported to destabilize the association between the P-site tRNA and the 60S subunit following peptide release (Shoemaker et al., 2010). When the release factors were saturating, our results indicate that UPF3B could dissolve postTCs following peptide hydrolysis (Figure 4.6B, 5.2). This energy-free mechanism was reminiscent of eIF3, eIF3j, eIF1, and eIF1A mediated ribosome recycling which operates only at low Mg^{2+} concentrations (1 mM Mg^{2+}) (Pisarev et al., 2007). We found that at Mg^{2+} concentration higher than 5 mM, UPF3B could not dissolve postTCs nor interact with the release factors (Figure 4.3, 4.6) indicating that UPF3B's role in termination is highly sensitive to Mg^{2+} concentrations and possibly providing a molecular reason for the Mg^{2+} homeostasis by NMD (Johansson & Jacobson, 2010). Previous toeprint studies have suggested that ribosomes dissociate slower at PTCs than NTCs (Amrani et al., 2004). Concordantly, our data indicate that UPF3B cannot dissociate all the postTCs indicating that the process is likely to be less efficient than ABCE1-mediated ribosome dissociation (Figure 4.6). Moreover, UPF2 appears to inhibit UPF3B's capacity to delay termination and to dissolve postTCs. At the same time, our sedimentation assays indicate that UPF2 could associate with the ribosomes more efficiently in the presence of UPF3B. These two observations appear to be contradicting, but may represent different activities of the UPF proteins at different stages during NMD. One possible explanation is that UPF3B could be recruited to the terminating ribosome in an inactive form bound to UPF2 and other mRNPs (Figure 5.2). This idea is consistent with the fact that UPF3B interaction with UPF2 is not required to activate NMD, but UPF3B is required to dissociate from the UPF1-UPF2-EJC complexes after UPF1 phosphorylation and activation of NMD, for subsequent mRNA decay (Gehring et al., 2003; Ohnishi et al., 2003; Kashima et al., 2010). In addition, UPF3B activity could be fine-tuned by the competition with UPF3A in mammals (Shum et al., 2016) and Mg^{2+} levels (Johansson & Jacobson, 2010). Peptide release assays and sedimentation on a sucrose gradient with differently labeled components of the termination machinery would yield insight into the UPF3B mechanism of action on the ribosome.

5.2.2 Translation repression and reinitiation

In contrast to eRF1, Pelota cannot trigger peptide release (Brandman & Hegde, 2016). Thus, following ribosome dissociation by ABCE1 bound to Pelota in NGD, the 60S subunit is still bound to the peptidyl-tRNA and is then recognized by the ribosome quality control factors NEMF and Listerin (Figure 5.2) (Shao & Hegde, 2014; Shao et al., 2015). These factors inhibit reassociation of the 60S subunit with the 40S subunit and thus prevent reinitiation of translation on faulty mRNAs (Brandman & Hegde, 2016). Similarly, *in vitro* re-initiation following termination was shown to be less

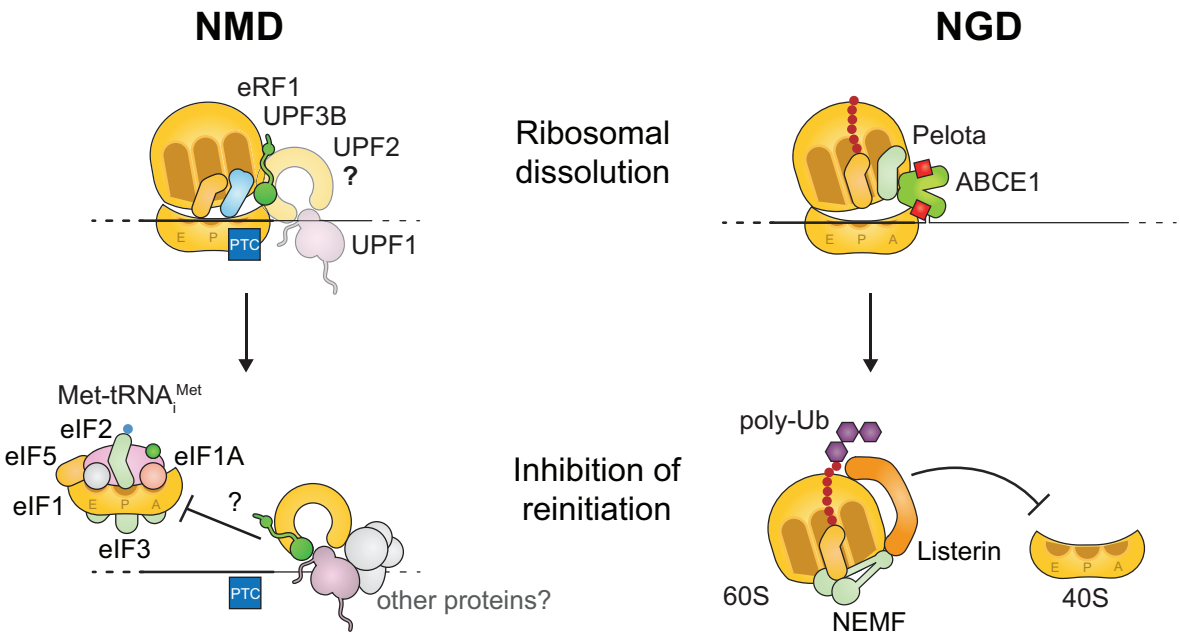

Figure 5.2: mRNA surveillance mechanisms and recycling and initiation control. *Left panel: following translation termination, UPF3B promotes ribosomal dissociation. It remains to be unclear whether UPF1 and UPF2 participate in this activity. NMD activation also triggers inhibition of reinitiation by 40S bound to initiation factors eIF3, eIF1, eIF1A, eIF2 and eIF5 though phosphorylated UPF1 binding to eIF3a subunit (Isken et al., 2008) Right panel: during no-go decay (NGD), ABCE1 bound to Pelota mediates the dissociation of the ribosome using ABCE1's ATPase activity (Red squares). Subsequently, ribosome quality control factors Listerin and NEMF mediate nascent chain ubiquitination (poly-Ub) resulting in inhibition of 60S association with the 40S subunit. Adapted from (Brandman & Hegde, 2016)*

efficient following termination at a PTC compared to normal termination (Ghosh et al., 2010). Moreover, reinitiation was suggested to inhibit NMD (Zhang & Maquat, 1997). This indicates that NMD factors could directly repress the reinitiation of translation of PTC-containing mRNAs (Figure 5.2). Protein association during scanning, initiation and the first few rounds of elongation is controlled by the largest initiation factor eIF3, consisting of 13 subunits (eIF3a-m) (Hinnebusch, 2014; des Georges et al., 2015; A. S. Y. Lee et al., 2015). In addition to a role in recycling identified for eIF3g, eIF3i and eIF3j, evidence exists that eIF3 has a critical role in NMD (Pisarev et al., 2010; Beznosková et al., 2013). Phosphorylated UPF1 might prohibit 80S assembly by interacting with eIF3a (Isken et al., 2008). eIF3f and eIF3h appear to prevent NMD while subunit eIF3e appears to be required for NMD and interaction with UPF2 (Morris et al., 2007; Peixeiro et al., 2012). It is thus possible that eIF3 promotes the transition from termination to initiation while the UPF factors control the kinetics of the overall process for each stop codon. Therefore, mRNAs failing to reinitiate efficiently would trigger the activation of the NMD factors. This is consistent with the hypothesis that all mRNAs are primed for NMD and the fact that UPF1 and UPF3B are also bound in the 3'UTR of normal mRNAs (Hogg & Goff, 2010; Zünd et al., 2013; S. R. Lee et al., 2015; Hauer et al., 2016). Following this logic, Brogna and colleagues suggested a new NMD model in which NMD is the result of a premature release of ribosomes from the mRNA rather than a discrimination mechanism between normal and aberrant stop codons (Brogna et al., 2016). The model predicts that translating ribosomes would passively stabilize transcripts. Premature release of the ribosomes and blocking of reinitiation by NMD factors would leave large regions of the mRNA exposed to nucleolytic attacks. However, co-translational 5' to 3' decay has been reported and challenges the idea that ribosomes would significantly stabilize and prevent mRNAs from decay (Pelechano et al., 2015). Thus, the interplay between eIF3 and the UPFs proteins during the different initiation complex conformations (see introduction 2.1.2.1) and termination remains to be further investigated in order to understand its significance (Figure 5.2).

5.3 mRNA and nascent chain degradation

Following ribosomal dissociation during NGD rescue, a mechanism allows NEMF and Listen to access the nascent chain by binding to the 60S interface and next to the ribosomal tunnel exit (Figure 5.2) (Shao & Hegde, 2014). NEMF and Listerin are responsible for the ubiquitination of the nascent chain, resulting in its degradation by the proteasome (Figure 5.2). In contrast, little is known about the degradation of nascent chains following NMD. UPF1 has been shown to promote the degradation of nonsense peptides and to act as an E3 Ligase. In fact, the CH domain of UPF1 shares

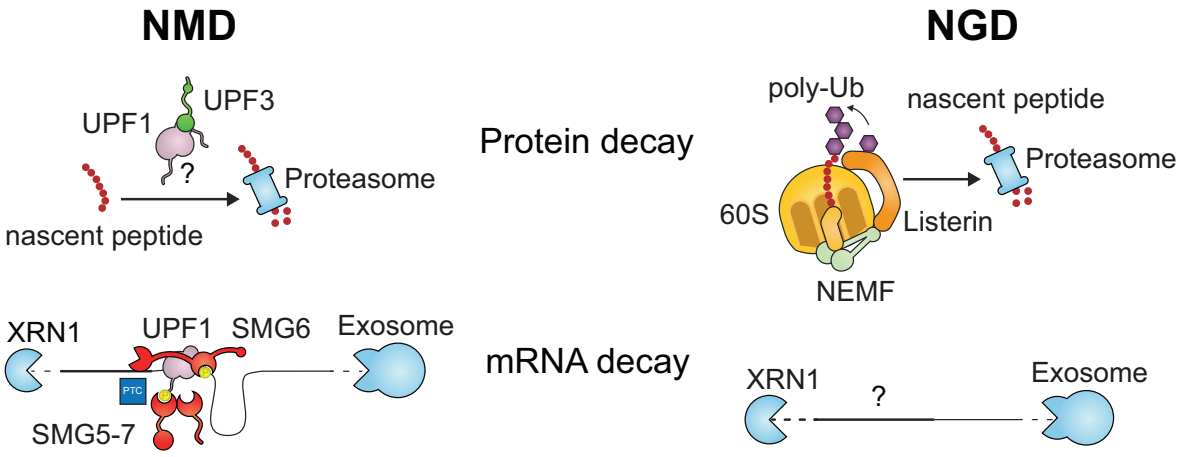

Figure 5.3: mRNA surveillance mechanisms and protein and mRNA decay control. *Left panel: the proteasome is responsible for the degradation of ubiquitinylated proteins. Evidence exists that in nonsense mediated mRNA decay (NMD), UPF3B could activate UPF1 E3 ligase activity to promote nascent chain degradation (Takahashi et al., 2008). Decay of premature termination codon (PTC) containing mRNAs by XRN1 and the exosome is accelerated by SMG6 and SMG5-7 which recruit these factors to the mRNA as described in Figure 2.8. Right panel: During no-go decay (NGD), Listerin and NEMF are responsible for the poly-ubiquitination (poly-Ub) and the targeting of the nascent chain to the proteasome (Shao et al., 2015). The molecular mechanisms of recruitment of mRNA decay factors during NGD remain unclear.*

homologies with E3 RING finger domains. Yeast Upf1p has been reported to self-ubiquitylate *in vitro* in an Upf3p-dependant manner (Kuroha et al., 2009; Takahashi et al., 2008). Supporting this idea, our results indicate that the CH domain of human UPF1 binds to UPF3B, but additional regions of UPF1 might further stabilize the interaction (Figure 4.14). The toeprint assays from chapter 4 indicate that UPF1 did not influence the activity of UPF3B during termination of translation. Hence, the functional roles of UPF1 association with UPF3B and the ubiquitination of UPF1 remain unclear. UPF1's ubiquitinylation activity could be assessed using an *in vitro* reconstituted ribosome-associated ubiquitination system (Shao & Hegde, 2014). It is tempting to speculate that UPF3B could not only bridge UPF1 to downstream mRNPs, as proposed by the EJC model, but also be involved in the regulation of UPF1 activity in a later stage of aberrant termination to promote efficient nascent peptide degradation.

mRNA decay is well documented for NMD (see introduction section 2.3.7) compared to NGD (J. Lykke-Andersen & Bennett, 2014) (Figure 5.3). However, this work rises the question of why and how UPF3B may interfere with UPF1 phosphorylation by the SMG1-8-9 complex (Figure 4.1) which is the critical step during NMD activation and subsequent mRNA decay. Binding affinity and phosphorylation kinetic measurements coupled with mass spectrometry (to identify specific phospho-sites) would allow the probing of the influence of UPF3B on UPF1 phosphorylation. These experiments

have already been performed for UPF1 alone (Deniaud et al., 2015). Using mass spectrometry, we identified 4 phosphorylation sites on recombinant UPF3B purified from insect cells (Y160, T169, S320 and T413). The mutation of Y160 has been previously reported to fail to activate NMD in tethering experiments (Alrahbeni et al., 2015). In our assays, it was not possible to observe any impact of such modifications hence the physiological significance remains to be investigated (Figure 4.15).

5.4 Regulation of NMD and outlook

Helicases play a critical role in coordinating the various steps during mRNA metabolism, processing and quality control (Bourgeois et al., 2016). As discussed in the introduction (see section 2.2), mRNA processing and degradation are in direct kinetic competition. This is exemplified by the spliceosome assembly, which is a succession of defined conformations. Transitions between steps are coupled in time with ATP hydrolysis by helicases (Query & Konarska, 2006). Aberrant mRNPs which are too slow to transition between conformational states within the ATP hydrolysis rate will be targeted for degradation (Villa et al., 2008). Most likely, the same principle applies to translation termination and NMD. Over recent years, multiple helicases involved in termination of translation and NMD have been identified, of which initiation factor eIF4A and NMD factor UPF1 are the best characterized (Bourgeois et al., 2016). Recently, several newly discovered helicases have been linked to termination and NMD (Figure 5.4). For example, yeast Dbp5/DDX19B has been shown to mediate eRF1 stop codon recognition (Gross et al., 2007), DHX34 and MOV10 were identified as a helicases contributing to UPF1 activity in NMD (Gregersen et al., 2014; Hug & Cáceres, 2014). Human DDX5 has been shown to bind to UPF3B *in vivo* (Geißler et al., 2013). The impact of these helicases on kinetically coordinating mRNP remodeling steps remains to be established. Evidence has accumulated on the critical role of ATPase activity of UPF1, but its function, site of action and time of activation in the NMD pathway remains to be elucidated (He & Jacobson, 2015b).

Lastly, a critical achievement in the field would be to improve the current *in vitro* translation system in order to recapitulate the NMD pathway *in vitro*. There is currently no reconstituted *in vitro* NMD assay. Here we performed experiments with terminating ribosomes, release factors, UPFs and SMGs proteins but new techniques must be developed to dissect the recruitment of the NMD machinery and its activation to trigger mRNA decay. Moreover, it will now be important to corroborate our finding that UPF3B has a direct impact on translation termination *in vivo*, using mutational studies (UPF3B variants) and ribosome profiling (Ingolia et al., 2012; Archer et al., 2016), in addition to the classical *in vivo* NMD and stop codon readthrough assays with reporter mRNAs.

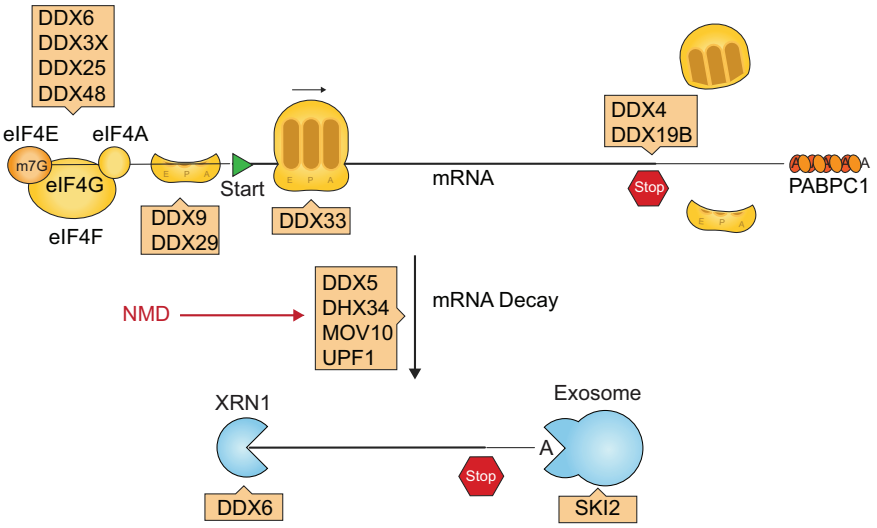

Figure 5.4: mRNA translation and decay regulation by helicases. *The eIF4F complex (eIF4A, E and G) regulates 43S loading onto the mRNA and scanning for the start codon. This process is regulated and depends on several DEAD box helicases that help to unwind the 5'UTR. Ribosomal subunits are represented in yellow. DDX4 and DDX19 helicases have been shown to impact translation termination. Following translation, mRNA decay is carried out by exonucleases XRN1 and the exosome; both complexes contain subunits with helicase function. Nonsense mediated mRNA decay (NMD) has been shown to be regulated by DDX5, DHX34 and MOV10 helicases. All helicases identified in the regulation of the different steps from translation to decay are indicated in orange boxes. Adapted from (Bourgeois et al., 2016)*

5.5 Concluding remarks

There has been much effort has been made to investigate NMD and the role of UPF1 in aberrant termination. In recent years, several studies have expanded and superseded our view of the NMD pathway mechanism and shed light on its complexity and the implication of numerous additional factors involved in PTC discrimination and downstream events. The main achievement of this thesis work was to probe the activity of the NMD factors, alone or in combination, in a reconstituted *in vitro* translation system. The finding that UPF3B has a role in termination *in vitro* may constitute a major step forward in our understanding of the NMD pathway. It is the first time that a NMD factor has been shown to directly influence the stop codon recognition and peptide release during *in vitro* termination of translation. NMD links multiple steps within the mRNA life cycle, from splicing in the nucleus to translation and degradation in the cytoplasm. The pathway thus constitutes a densely meshed interactome network which must be tightly regulated in time and space in the cell. Its understanding constitutes a formidable challenge.

Classic *in vitro* biochemistry and genome-wide approaches in combination in with innovative single molecule imaging techniques (Yan et al., 2016) and advanced ribosome

profiling technologies (Archer et al., 2016) are required to further our understanding of the complex interplay of NMD factors and the translation machinery. Recent advances in cryo-EM regarding direct electron detectors (Veesler et al., 2013) and image processing (S. H. W. Scheres, 2012; S. H. w. Scheres, 2014) have revolutionized the structural biology field and allowed solving high-resolution structures from sparse and heterogeneous samples. There is no doubt that cryo-EM structures will provide critical insights into the interplay between the translational machinery with the NMD factors once the relevant ribosomal complexes have been identified.

A mechanistic understanding of the recognition of premature stop codons would facilitate the development of new therapeutic strategies to treat NMD-associated diseases. Current treatments rely on stop codon read through approaches. An improved mechanistic understanding of NMD could allow the targeting of early NMD steps rather than the translation machinery in general (Martin et al., 2014). The future of healthcare is moving towards personalized medicine and the identification of particular mutations will determine an appropriate treatment. As CRISPR/Cas9 technology is improving, understanding of the rules that govern NMD activation will offer the possibility to amend mutations leading to a PTC by specific replacement of faulty genes with correct DNA sequences (Popp & Maquat, 2016).

In conclusion, despite many years of study, translation termination at a PTC and NMD activation remain enigmatic. The future expansion of our understanding of NMD holds promises for both technique development to elucidate its mechanism and for the treatment of NMD-associated diseases.

References

Addington, A. M., Gauthier, J., Piton, A., Hamdan, F. F., Raymond, a., Gogtay, N., ... Rouleau, G. a. (2011). A novel frameshift mutation in UPF3B identified in brothers affected with childhood onset schizophrenia and autism spectrum disorders. *Molecular Psychiatry*, *16*(3), 238–239.

Alexandrov, A., Colognori, D., Shu, M.-D., & Steitz, J. A. (2012). Human spliceosomal protein CWC22 plays a role in coupling splicing to exon junction complex deposition and nonsense-mediated decay. *Proceedings of the National Academy of Sciences of the United States of America*, *109*(52), 21313–8.

Alkalaeva, E. Z., Pisarev, A. V., Frolova, L. Y., Kisselev, L. L., & Pestova, T. V. (2006). In Vitro Reconstitution of Eukaryotic Translation Reveals Cooperativity between Release Factors eRF1 and eRF3. *Cell*, *125*(6), 1125–1136.

Allmang, C., Petfalski, E., Podtelejnikov, A., Mann, M., Tollervey, D., & Mitchell, P. (1999). The yeast exosome and human PM-Scl are related complexes of 3' - 5' exonucleases. *Genes and Development*, *13*(16), 2148–2158.

Alrahbeni, T., Sartor, F., Anderson, J., Miedzybrodzka, Z., McCaig, C., & Müller, B. (2015). Full UPF3B function is critical for neuronal differentiation of neural stem cells. *Molecular brain*, *8*(1), 33.

Amrani, N., Ganesan, R., Kervestin, S., Mangus, D. A., Ghosh, S., & Jacobson, A. (2004). A faux 3'-UTR promotes aberrant termination and triggers nonsense-mediated mRNA decay. *Nature*, *432*(7013), 112–118.

Archer, S. K., Shirokikh, N. E., Beilharz, T. H., & Preiss, T. (2016). Dynamics of ribosome scanning and recycling revealed by translation complex profiling. *Nature*, 1–17.

Atkin, A. L., Schenkman, L. R., Eastham, M., Dahlseid, J. N., Lelivelt, M. J., & Culbertson, M. R. (1997). Relationship between yeast polyribosomes and Upf proteins required for nonsense mRNA decay. *Journal of Biological Chemistry*, *272*(35), 22163–22172.

Avery, P., Vicente-Crespo, M., Francis, D., Nashchekina, O., Alonso, C. R., & Palacios, I. M. (2011). Drosophila Upf1 and Upf2 loss of function inhibits cell growth and causes animal death in a Upf3-independent manner. *RNA (New York, N.Y.)*, *17*(4), 624–638.

Aylett, C. H. S., Boehringer, D., Erzberger, J. P., Schaefer, T., & Ban, N. (2015). Structure of a yeast 40S-eIF1-eIF1A-eIF3-eIF3j initiation complex. *Nature structural & molecular biology*, *22*(3), 269–71.

Bai, X. C., Fernandez, I. S., McMullan, G., & Scheres, S. H. W. (2013). Ribosome structures to near-atomic resolution from thirty thousand cryo-EM particles. *eLife*, *2013*(2),

2–13.

Becker, T., Armache, J.-P., Jarasch, A., Anger, A. M., Villa, E., Sieber, H., ... Beckmann, R. (2011). Structure of the no-go mRNA decay complex Dom34-Hbs1 bound to a stalled 80S ribosome. *Nature structural & molecular biology*, *18*(6), 715–20.

Becker, T., Franckenberg, S., Wickles, S., Shoemaker, C. J., Anger, A. M., Armache, J.-P., ... Beckmann, R. (2012). Structural basis of highly conserved ribosome recycling in eukaryotes and archaea. *Nature*, *482*(7386), 501–6.

Beckmann, R., Spahn, C. M. T., Eswar, N., Helmers, J., Penczek, P. A., Sali, A., ... Blobel, G. (2001). Architecture of the protein-conducting channel associated with the translating 80S ribosome. *Cell*, *107*(3), 361–372.

Bentley, D. L. (2014). Coupling mRNA processing with transcription in time and space. *Nature reviews. Genetics*, *15*(3), 163–75.

Beznosková, P., Cuchalová, L., Wagner, S., Shoemaker, C. J., Gunišová, S., von der Haar, T., & Valášek, L. S. (2013). Translation Initiation Factors eIF3 and HCR1 Control Translation Termination and Stop Codon Read-Through in Yeast Cells. *PLoS Genetics*, *9*(11).

Bhattacharya, A., Czaplinski, K., Trifillis, P., He, F., Jacobson, A., & Peltz, S. W. (2000). Characterization of the biochemical properties of the human Upf1 gene product that is involved in nonsense-mediated mRNA decay. *RNA (New York, N.Y.)*, *6*(9), 1226–1235.

Bhushan, S., Meyer, H., Starosta, A. L., Becker, T., Mielke, T., Berninghausen, O., ... Beckmann, R. (2010). Structural basis for translational stalling by human cytomegalovirus and fungal arginine attenuator peptide. *Molecular Cell*, *40*(1), 138–146.

Bhuvanagiri, M., Schlitter, A. M., Hentze, M. W., & Kulozik, A. E. (2010). NMD: RNA biology meets human genetic medicine. *The Biochemical journal*, *430*(3), 365–77.

Bieniossek, C., Richmond, T. J., & Berger, I. (2008). MultiBac: Multigene baculovirus-based eukaryotic protein complex production. *Current Protocols in Protein Science*, *Chapter 5*(SUPPL. 51), Unit 5.20.

Boehm, V., Haberman, N., Ottens, F., Ule, J., & Gehring, N. H. (2014). 3' UTR length and messenger ribonucleoprotein composition determine endocleavage efficiencies at termination codons. *Cell Reports*, *9*(2), 555–568.

Bourgeois, C. F., Mortreux, F., & Auboeuf, D. (2016). The multiple functions of RNA helicases as drivers and regulators of gene expression. *Nature Reviews Molecular Cell Biology*.

Brandman, O., & Hegde, R. S. (2016). Ribosome-associated protein quality control. *Nature Structural & Molecular Biology*, *23*(1), 7–15.

Brogna, S., McLeod, T., & Petric, M. (2016). The Meaning of NMD: Translate or Perish. *Trends in Genetics*, *xx*, 1–13.

Brown, A., Shao, S., Murray, J., Hegde, R. S., & Ramakrishnan, V. (2015). Structural basis for stop codon recognition in eukaryotes. *Nature*, *524*(7566), 493–6.

Buchwald, G., Ebert, J., Basquin, C., Sauliere, J., Jayachandran, U., Bono, F., ... Conti, E.

(2010). Insights into the recruitment of the NMD machinery from the crystal structure of a core EJC-UPF3b complex. *Proceedings of the National Academy of Sciences of the United States of America*, *107*(22), 10050–10055.

Bühler, M., Steiner, S., Mohn, F., Paillusson, A., & Mühlemann, O. (2006). EJC-independent degradation of nonsense immunoglobulin-mu mRNA depends on 3' UTR length. *Nature structural & molecular biology*, *13*(5), 462–464.

Burkard, K. T., & Butler, J. S. (2000). A nuclear 3'-5' exonuclease involved in mRNA degradation interacts with Poly(A) polymerase and the hnRNA protein Npl3p. *Molecular and cellular biology*, *20*(2), 604–16.

Casadio, A., Longman, D., Hug, N., Delavaine, L., Vallejos Baier, R., Alonso, C. R., & Cáceres, J. F. (2015). Identification and characterization of novel factors that act in the nonsense-mediated mRNA decay pathway in nematodes, flies and mammals. *EMBO reports*, *16*(1), 71–8.

Cazzola, M., Della Porta, M. G., & Malcovati, L. (2013). The genetic basis of myelodysplasia and its clinical relevance. *Blood*, *122*(25), 4021–4034.

Celik, A., Kervestin, S., & Jacobson, A. (2015). NMD: At the crossroads between translation termination and ribosome recycling. *Biochimie*, *114*, 2–9.

Chakrabarti, S., Bonneau, F., Schüssler, S., Eppinger, E., & Conti, E. (2014). Phospho-dependent and phospho-independent interactions of the helicase UPF1 with the NMD factors SMG5-SMG7 and SMG6. *Nucleic Acids Research*, *42*(14), 9447–9460.

Chakrabarti, S., Jayachandran, U., Bonneau, F., Fiorini, F., Basquin, C., Domcke, S., ... Conti, E. (2011). Molecular Mechanisms for the RNA-Dependent ATPase Activity of Upf1 and Its Regulation by Upf2. *Molecular Cell*, *41*(6), 693–703.

Chamieh, H., Ballut, L., Bonneau, F., & Le Hir, H. (2008). NMD factors UPF2 and UPF3 bridge UPF1 to the exon junction complex and stimulate its RNA helicase activity. *Nature structural & molecular biology*, *15*(1), 85–93.

Chan, W.-K., Bhalla, A. D., Le Hir, H., Nguyen, L. S., Huang, L., Gécz, J., & Wilkinson, M. F. (2009). A UPF3-mediated regulatory switch that maintains RNA surveillance. *Nature structural & molecular biology*, *16*(7), 747–753.

Chan, W.-K., Huang, L., Gudikote, J. P., Chang, Y.-F., Imam, J. S., MacLean, J. a., & Wilkinson, M. F. (2007). An alternative branch of the nonsense-mediated decay pathway. *The EMBO journal*, *26*(7), 1820–1830.

Chauvin, C., Salhi, S., Le Goff, C., Viranaicken, W., Diop, D., & Jean-Jean, O. (2005). Involvement of human release factors eRF3a and eRF3b in translation termination and regulation of the termination complex formation. *Molecular and cellular biology*, *25*(14), 5801–11.

Chazal, P.-E., Daguenet, E., Wendling, C., Ulryck, N., Tomasetto, C., Sargueil, B., & Le Hir, H. (2013). EJC core component MLN51 interacts with eIF3 and activates translation. *Proceedings of the National Academy of Sciences of the United States of America*, *110*(15), 5903–8.

Chen, M., & Manley, J. L. (2009). Mechanisms of alternative splicing regulation: insights from

molecular and genomics approaches. *Nature reviews. Molecular cell biology*, *10*(11), 741–54.

Cheng, Z., Saito, K., Pisarev, A. V., Wada, M., Pisareva, V. P., Pestova, T. V., ... Song, H. (2009). Structural insights into eRF3 and stop codon recognition by eRF1. *Genes and Development*, *23*(9), 1106–1118.

Cho, H., Kim, K. M., & Kim, Y. K. (2009). Human Proline-Rich Nuclear Receptor Coregulatory Protein 2 Mediates an Interaction between mRNA Surveillance Machinery and Decapping Complex. *Molecular Cell*, *33*(1), 75–86.

Clerici, M. (2009). *Etudes structurales du mécanisme d'interaction des protéines UPF1 et UPF2, impliquées dans le "Nonsense Mediated mRNA Decay"* (Unpublished doctoral dissertation). Université Joseph Fourier (Grenoble).

Clerici, M., Deniaud, A., Boehm, V., Gehring, N. H., Schaffitzel, C., & Cusack, S. (2014). Structural and functional analysis of the three MIF4G domains of nonsense-mediated decay factor UPF2. *Nucleic Acids Research*, *42*(4), 2673–2686.

Clerici, M., Mourão, A., Gutsche, I., Gehring, N. H., Hentze, M. W., Kulozik, A., ... Cusack, S. (2009). Unusual bipartite mode of interaction between the nonsense-mediated decay factors, UPF1 and UPF2. *The EMBO journal*, *28*(15), 2293–2306.

Colak, D., Ji, S.-J., Porse, B. T., & Jaffrey, S. R. (2013). Regulation of axon guidance by compartmentalized nonsense-mediated mRNA decay. *Cell*, *153*(6), 1252–65.

Cosson, B., Couturier, A., Chabelskaya, S., Kiktev, D., Inge-vechtomov, S., Philippe, M., & Zhouravleva, G. (2002a). Poly (A) -Binding Protein Acts in Translation Termination via Eukaryotic Release Factor 3 Interaction and Does Not Influence [PSI +] Propagation Poly (A) -Binding Protein Acts in Translation Termination via Eukaryotic Release Factor 3 Interaction an. *Molecular and cellular biology*, *22*(10), 3301–3315.

Cosson, B., Couturier, A., Chabelskaya, S., Kiktev, D., Inge-vechtomov, S., Philippe, M., & Zhouravleva, G. (2002b). Poly (A) -Binding Protein Acts in Translation Termination via Eukaryotic Release Factor 3 Interaction and Does Not Influence [PSI +] Propagation Poly (A) -Binding Protein Acts in Translation Termination via Eukaryotic Release Factor 3 Interaction an. *Molecular and cellular biology*, *22*(10), 3301–3315.

Cramer, P., Bushnell, D. a., & Kornberg, R. D. (2001). Structural basis of transcription: RNA polymerase II at 2.8 angstrom resolution. *Science (New York, N.Y.)*, *292*(5523), 1863–1876.

Culbertson, M. R., & Leeds, P. F. (2003). Looking at mRNA decay pathways through the window of molecular evolution. *Current Opinion in Genetics and Development*, *13*(2), 207–214.

Danckwardt, S., Hentze, M. W., & Kulozik, A. E. (2008). 3' end mRNA processing: molecular mechanisms and implications for health and disease. *Embo J*, *27*(3), 482–498.

Deniaud, A., Karuppasamy, M., Bock, T., Masiulis, S., Huard, K., Garzoni, F., ... Schaffitzel, C. (2015). A network of SMG-8, SMG-9 and SMG-1 C-terminal insertion domain regulates UPF1 substrate recruitment and phosphorylation. *Nucleic Acids Research*, *43*(15), 7600–7611.

Des Georges, A., Hashem, Y., Unbehaun, A., Grassucci, R. A., Taylor, D., Hellen, C. U. T., ... Frank, J. (2014). Structure of the mammalian ribosomal pre-termination complex associated with eRF1.eRF3.GDPNP. *Nucleic Acids Research*, *42*(5), 3409–3418.

des Georges, A., Dhote, V., Kuhn, L., Hellen, C. U. T., Pestova, T. V., Frank, J., & Hashem, Y. (2015). Structure of mammalian eIF3 in the context of the 43S preinitiation complex. *Nature*, *525*(7570), 491–5.

Dever, T. E., & Green, R. (2012). The elongation, termination, and recycling phases of translation in eukaryotes. *Cold Spring Harbor Perspectives in Biology*, *4*(7), 1–16.

Doma, M. K., & Parker, R. (2007). RNA Quality Control in Eukaryotes. *Cell*, *131*(4), 660–668.

Duncan, K., Grskovic, M., Strein, C., Beckmann, K., Niggeweg, R., Abaza, I., ... Hentze, M. W. (2006). Sex-lethal imparts a sex-specific function to UNR by recruiting it to the msl-2 mRNA 3' UTR: Translational repression for dosage compensation. *Genes and Development*, *20*(3), 368–379.

Durand, S., Franks, T. M., & Lykke-Andersen, J. (2016). Hyperphosphorylation amplifies UPF1 activity to resolve stalls in nonsense-mediated mRNA decay. *Nature communications*, *7*, 12434.

Durand, S., & Lykke-Andersen, J. (2013). Nonsense-mediated mRNA decay occurs during eIF4F-dependent translation in human cells. *Nature structural & molecular biology*, *20*(6), 702–9.

Eberle, A. B., Lykke-Andersen, S., Mühlemann, O., & Jensen, T. H. (2009). SMG6 promotes endonucleolytic cleavage of nonsense mRNA in human cells. TL - 16. *Nature structural & molecular biology*, *16 VN - r*(1), 49–55.

Estrozi, L. F., Boehringer, D., Shan, S.-O., Ban, N., & Schaffitzel, C. (2011). Cryo-EM structure of the E. coli translating ribosome in complex with SRP and its receptor. *Nature structural & molecular biology*, *18*(1), 88–90.

Eulalio, A., Behm-Ansmant, I., & Izaurralde, E. (2007). P bodies: at the crossroads of post-transcriptional pathways. *Nature Reviews Molecular Cell Biology*, *8*(1), 9–22.

Fan-Minogue, H., Du, M., Pisarev, A. V., Kallmeyer, A. K., Salas-Marco, J., Keeling, K. M., ... Bedwell, D. M. (2008). Distinct eRF3 Requirements Suggest Alternate eRF1 Conformations Mediate Peptide Release during Eukaryotic Translation Termination. *Molecular Cell*, *30*(5), 599–609.

Fanourgakis, G., Lesche, M., Akpinar, M., Dahl, A., & Jessberger, R. (2016). Chromatoid Body Protein TDRD6 Supports Long 3' UTR Triggered Nonsense Mediated mRNA Decay. *PLOS Genetics*, *12*(5), e1005857.

Fatscher, T., Boehm, V., & Gehring, N. H. (2015). Mechanism, factors, and physiological role of nonsense-mediated mRNA decay. *Cellular and Molecular Life Sciences*, *72*(23), 4523–4544.

Fatscher, T., Boehm, V., Weiche, B., & Gehring, N. H. (2014). The interaction of cytoplasmic poly(A)-binding protein with eukaryotic initiation factor 4G suppresses nonsense-mediated mRNA decay. *RNA (New York, N.Y.)*, *20*(10), 1579–92.

Fiorini, F., Bagchi, D., Le Hir, H., & Croquette, V. (2015). Human Upf1 is a highly processive RNA helicase and translocase with RNP remodelling activities. *Nature Communications*, *6*(May 2015), 7581.

Fiorini, F., Boudvillain, M., & Hir, H. L. (2013). Tight intramolecular regulation of the human Upf1 helicase by its N- and C-terminal domains. *Nucleic Acids Research*, *41*(4), 2404–2415.

Fitzgerald, D. J., Berger, P., Schaffitzel, C., Yamada, K., Richmond, T. J., & Berger, I. (2006). Protein complex expression by using multigene baculoviral vectors. *Nature methods*, *3*(12), 1021–1032.

Franckenberg, S., Becker, T., & Beckmann, R. (2012). Structural view on recycling of archaeal and eukaryotic ribosomes after canonical termination and ribosome rescue. *Current Opinion in Structural Biology*, *22*(6), 786–796.

Franks, T. M., Singh, G., & Lykke-Andersen, J. (2010). Upf1 ATPase-dependent mRNP disassembly is required for completion of nonsense-mediated mRNA decay. *Cell*, *143*(6), 938–950.

Frolova, L. Y., Tsivkovskii, R. Y., Sivolobova, G. F., Oparina, N. Y., Serpinsky, O. I., Blinov, V. M., ... Kisselev, L. L. (1999). Mutations in the highly conserved GGQ motif of class 1 polypeptide release factors abolish ability of human eRF1 to trigger peptidyl-tRNA hydrolysis. *RNA (New York, N.Y.)*, *5*(8), 1014–1020.

Fukuhara, N., Ebert, J., Unterholzner, L., Lindner, D., Izaurralde, E., & Conti, E. (2005). SMG7 is a 14-3-3-like adaptor in the nonsense-mediated mRNA decay pathway. *Molecular Cell*, *17*(4), 537–547.

Gardner, L. B. (2010). Nonsense-mediated RNA decay regulation by cellular stress: implications for tumorigenesis. *Molecular cancer research : MCR*, *8*(3), 295–308.

Garneau, N. L., Wilusz, J., & Wilusz, C. J. (2007). The highways and byways of mRNA decay. *Nature reviews. Molecular cell biology*, *8*(2), 113–126.

Gatfield, D., Unterholzner, L., Ciccarelli, F. D., Bork, P., & Izaurralde, E. (2003). Nonsense-mediated mRNA decay in Drosophila: At the intersection of the yeast and mammalian pathways. *EMBO Journal*, *22*(15), 3960–3970.

Gehring, N. H., Kunz, J. B., Neu-Yilik, G., Breit, S., Viegas, M. H., Hentze, M. W., & Kulozik, A. E. (2005). Exon-junction complex components specify distinct routes of nonsense-mediated mRNA decay with differential cofactor requirements. *Molecular Cell*, *20*(1), 65–75.

Gehring, N. H., Lamprinaki, S., Kulozik, A. E., & Hentze, M. W. (2009). Disassembly of Exon Junction Complexes by PYM. *Cell*, *137*(3), 536–548.

Gehring, N. H., Neu-Yilik, G., Schell, T., Hentze, M. W., & Kulozik, A. E. (2003). Y14 and hUpf3b form an NMD-activating complex. *Molecular Cell*, *11*(4), 939–949.

Geißler, V., Altmeyer, S., Stein, B., Uhlmann-Schiffler, H., & Stahl, H. (2013). The RNA helicase Ddx5/p68 binds to hUpf3 and enhances NMD of Ddx17/p72 and Smg5 mRNA. *Nucleic Acids Research*, *41*(16), 7875–7888.

Ghosh, S., Ganesan, R., Amrani, N., & Jacobson, A. (2010). Translational competence of

ribosomes released from a premature termination codon is modulated by NMD factors. *RNA (New York, N.Y.)*, *16*(9), 1832–1847.

Giorgi, C., Yeo, G. W., Stone, M. E., Katz, D. B., Burge, C., Turrigiano, G., & Moore, M. J. (2007). The EJC Factor eIF4AIII Modulates Synaptic Strength and Neuronal Protein Expression. *Cell*, *130*(1), 179–191.

Glavan, F., Behm-Ansmant, I., Izaurralde, E., & Conti, E. (2006). Structures of the PIN domains of SMG6 and SMG5 reveal a nuclease within the mRNA surveillance complex. *Embo J*, *25*(21), 5117–5125.

Gloggnitzer, J., Akimcheva, S., Srinivasan, A., Kusenda, B., Riehs, N., Stampfl, H., ... Riha, K. (2014). Nonsense-mediated mRNA decay modulates immune receptor levels to regulate plant antibacterial defense. *Cell Host and Microbe*, *16*(3), 376–390.

Graille, M., & Séraphin, B. (2012). Surveillance pathways rescuing eukaryotic ribosomes lost in translation. *Nature reviews. Molecular cell biology*, *13*(11), 727–35.

Gregersen, L. H., Schueler, M., Munschauer, M., Mastrobuoni, G., Chen, W., Kempa, S., ... Landthaler, M. (2014). MOV10 Is a 5' to 3' RNA Helicase Contributing to UPF1 mRNA Target Degradation by Translocation along 3' UTRs. *Molecular Cell*, *54*(4), 573–585.

Gross, T., Siepmann, A., Sturm, D., Windgassen, M., Scarcelli, J. J., Seedorf, M., ... Krebber, H. (2007). The DEAD-box RNA helicase Dbp5 functions in translation termination. *Science (New York, N.Y.)*, *315*(5812), 646–9.

Guan, Q., Zheng, W., Tang, S., Liu, X., Zinkel, R. A., Tsui, K. W., ... Culbertson, M. R. (2006). Impact of nonsense-mediated mRNA decay on the global expression profile of budding yeast. *PLoS Genetics*, *2*(11), 1924–1943.

Gulsuner, S., Walsh, T., Watts, A. C., Lee, M. K., Thornton, A. M., Casadei, S., ... McClellan, J. M. (2013). Spatial and temporal mapping of de novo mutations in schizophrenia to a fetal prefrontal cortical network. *Cell*, *154*(3), 518–529.

Halic, M., Becker, T., Pool, M. R., Spahn, C. M. T., Grassucci, R. A., Frank, J., & Beckmann, R. (2004). Structure of the signal recognition particle interacting with the elongation-arrested ribosome. *Nature*, *427*(6977), 808–14.

Hall, G. W., & Thein, S. (1994). Nonsense codon mutations in the terminal exon of the beta-globin gene are not associated with a reduction in beta-mRNA accumulation: a mechanism for the phenotype of dominant beta-thalassemia. *Blood*, *83*(8), 2031–7.

Hauer, C., Sieber, J., Schwarzl, T., Alleaume, A.-m., Hentze, M. W., Kulozik, A. E., ... Alleaume, A.-m. (2016). Exon Junction Complexes Show a Distributional Bias toward Alternatively Spliced mRNAs and against mRNAs Coding for Ribosomal Proteins Article Exon Junction Complexes Show a Distributional Bias toward Alternatively Spliced mRNAs and against mRNAs Coding fo. *CellReports*, 1–16.

He, F., Brown, A. H., & Jacobson, A. (1997). Upf1p, Nmd2p, and Upf3p are interacting components of the yeast nonsense-mediated mRNA decay pathway. *Molecular and cellular biology*, *17*(3), 1580–94.

He, F., & Jacobson, a. (2001). Upf1p, Nmd2p, and Upf3p regulate the decapping and

exonucleolytic degradation of both nonsense-containing mRNAs and wild-type mRNAs. *Molecular and cellular biology*, *21*(5), 1515–1530.

He, F., & Jacobson, A. (2015a). Control of mRNA decapping by positive and negative regulatory elements in the Dcp2 C-terminal domain. *RNA (New York, N.Y.)*, 1633–1647.

He, F., & Jacobson, A. (2015b). Nonsense-Mediated mRNA Decay: Degradation of Defective Transcripts Is Only Part of the Story. *Annual Review of Genetics*, *49*(1), annurev–genet–112414–054639.

He, F., Li, X., Spatrick, P., Casillo, R., Dong, S., & Jacobson, A. (2003). Genome-Wide Analysis of mRNAs Regulated by the Nonsense-Mediated and 5' to 3' mRNA Decay Pathways in Yeast. *Molecular Cell*, *12*(6), 1439–1452.

Heymann, J. B. (2001). Bsoft: image and molecular processing in electron microscopy. *Journal of structural biology*, *133*(2-3), 156–69.

Hinnebusch, A. G. (2014). The scanning mechanism of eukaryotic translation initiation. *Annual review of biochemistry*, *83*(1), 779–812.

Hir, H. L., Saulière, J., & Wang, Z. (2015). The exon junction complex as a node of post-transcriptional networks. *Nature reviews. Molecular cell biology*, *17*(1), 41–54.

Hocine, S., Singer, R. H., & Grünwald, D. (2010). RNA processing and export. *Cold Spring Harbor perspectives in biology*, *2*(12), 1–20.

Hogg, J. R., & Goff, S. P. (2010). Upf1 senses 3'UTR length to potentiate mRNA decay. *Cell*, *143*(3), 379–389.

Hoshino, S. I., Imai, M., Kobayashi, T., Uchida, N., & Katada, T. (1999). The eukaryotic polypeptide chain releasing factor (eRF3/GSPT) carrying the translation termination signal to the 3'-poly(A) tail of mRNA. Direct association of eRF3/GSPT with polyadenylate-binding protein. *Journal of Biological Chemistry*, *274*(24), 16677–16680.

Huang, Y., & Steitz, J. A. (2005). SRprises along a messenger's journey. *Molecular Cell*, *17*(5), 613–615.

Hug, N., & Cáceres, J. F. (2014). The RNA Helicase DHX34 Activates NMD by promoting a transition from the surveillance to the decay-inducing complex. *Cell Reports*, *8*(6), 1845–1856.

Huntzinger, E., Kashima, I., Fauser, M., Saulière, J., & Izaurralde, E. (2008). SMG6 is the catalytic endonuclease that cleaves mRNAs containing nonsense codons in metazoan. *RNA (New York, N.Y.)*, *14*(12), 2609–17.

Hurt, J. A., Robertson, A. D., & Burge, C. B. (2013). Global analyses of UPF1 binding and function reveal expanded scope of nonsense-mediated mRNA decay. *Genome Research*, *23*(10), 1636–1650.

Hussain, T., Llácer, J. L., Fernández, I. S., Munoz, A., Martin-Marcos, P., Savva, C. G., ... Ramakrishnan, V. (2014). Structural changes enable start codon recognition by the eukaryotic translation initiation complex. *Cell*, *159*(3), 597–607.

Iizuka, N., Najita, L., Franzusoff, a., & Sarnow, P. (1994). Cap-dependent and cap-

independent translation by internal initiation of mRNAs in cell extracts prepared from Saccharomyces cerevisiae. *Molecular and cellular biology*, *14*(11), 7322–7330.

Ingolia, N. T., Brar, G. A., Rouskin, S., McGeachy, A. M., & Weissman, J. S. (2012). The ribosome profiling strategy for monitoring translation in vivo by deep sequencing of ribosome-protected mRNA fragments. *Nature protocols*, *7*(8), 1534–50.

Isken, O., Kim, Y. K., Hosoda, N., Mayeur, G. L., Hershey, J. W. B., & Maquat, L. E. (2008). Upf1 Phosphorylation Triggers Translational Repression during Nonsense-Mediated mRNA Decay. *Cell*, *133*(2), 314–327.

Ito-Harashima, S., Kuroha, K., Tatematsu, T., & Inada, T. (2007). Translation of the poly(A) tail plays crucial roles in nonstop mRNA surveillance via translation repression and protein destabilization by proteasome in yeast. *Genes and Development*, *21*(5), 519–524.

Ivanov, A., Mikhailova, T., Eliseev, B., Yeramala, L., Sokolova, E., Susorov, D., ... Alkalaeva, E. (2016). PABP enhances release factor recruitment and stop codon recognition during translation termination. *Nucleic Acids Research*, gkw635.

Ivanov, P. V., Gehring, N. H., Kunz, J. B., Hentze, M. W., & Kulozik, A. E. (2008). Interactions between UPF1, eRFs, PABP and the exon junction complex suggest an integrated model for mammalian NMD pathways. *The EMBO journal*, *27*(5), 736–747.

Izumi, N., Yamashita, A., Iwamatsu, A., Kurata, R., Nakamura, H., Saari, B., ... Ohno, S. (2010). AAA+ proteins RUVBL1 and RUVBL2 coordinate PIKK activity and function in nonsense-mediated mRNA decay. *Science signaling*, *3*(116), ra27.

Jackson, R. J., Hellen, C. U. T., & Pestova, T. V. (2010). The mechanism of eukaryotic translation initiation and principles of its regulation. *Nature reviews. Molecular cell biology*, *11*(2), 113–127.

Jackson, R. J., Hellen, C. U. T., & Pestova, T. V. (2012). *Termination and post-termination events in eukaryotic translation* (1st ed., Vol. 86). Elsevier Inc.

Jiao, X., Chang, J. H., Kilic, T., Tong, L., & Kiledjian, M. (2013). A Mammalian Pre-mRNA 5' End Capping Quality Control Mechanism and an Unexpected Link of Capping to Pre-mRNA Processing. *Molecular Cell*, *50*(1), 104–115.

Johansson, M. J. O., & Jacobson, A. (2010). Nonsense-mediated mRNA decay maintains translational fidelity by limiting magnesium uptake. *Genes and Development*, *24*(14), 1491–1495.

Johnson, J. M. (2003). Genome-Wide Survey of Human Alternative Pre-mRNA Splicing with Exon Junction Microarrays. *Science*, *302*(5653), 2141–2144.

Jolly, L. A., Homan, C. C., Jacob, R., Barry, S., & Gecz, J. (2013). The UPF3B gene, implicated in intellectual disability, autism, ADHD and childhood onset schizophrenia regulates neural progenitor cell behaviour and neuronal outgrowth. *Human Molecular Genetics*, *22*(23), 4673–4687.

Joncourt, R., Eberle, A. B., Rufener, S. C., & Mühlemann, O. (2014). Eukaryotic initiation factor 4G suppresses nonsense-mediated mRNA decay by two genetically separable mechanisms. *PloS one*, *9*(8), e104391.

Kadlec, J., Izaurralde, E., & Cusack, S. (2004). The structural basis for the interaction between nonsense-mediated mRNA decay factors UPF2 and UPF3. *Nature structural & molecular biology*, *11*(4), 330–337.

Karam, R., Carvalho, J., Bruno, I., Graziadio, C., Senz, J., Huntsman, D., ... Oliveira, C. (2008). The NMD mRNA surveillance pathway downregulates aberrant E-cadherin transcripts in gastric cancer cells and in CDH1 mutation carriers. *Oncogene*, *27*(30), 4255–4260.

Kashima, I., Jonas, S., Jayachandran, U., Buchwald, G., Conti, E., Lupas, A. N., & Izaurralde, E. (2010). SMG6 interacts with the exon junction complex via two conserved EJC-binding motifs (EBMs) required for nonsense-mediated mRNA decay. *Genes and Development*, *24*(21), 2440–2450.

Kashima, I., Yamashita, A., Izumi, N., Kataoka, N., Morishita, R., Hoshino, S., ... Ohno, S. (2006). Binding of a novel SMG-1-Upf1-eRF1-eRF3 complex (SURF) to the exon junction complex triggers Upf1 phosphorylation and nonsense-mediated mRNA decay. *Genes and Development*, *20*(3), 355–367.

Katahira, J. (2012). MRNA export and the TREX complex. *Biochimica et Biophysica Acta - Gene Regulatory Mechanisms*, *1819*(6), 507–513.

Keeling, K., Lanier, J., Du, M., Salas-marco, J. O. E., Gao, L. I. N., Kaenjak-angeletti, A., & Bedwell, D. M. (2004). Leaky termination at premature stop codons antagonizes nonsense-mediated mRNA decay in S . cerevisiae Leaky termination at premature stop codons antagonizes nonsense-mediated mRNA decay in S . cerevisiae. *Rna*, *10*(4), 691–703.

Kerr, T. P., Sewry, C. A., Robb, S. A., & Roberts, R. G. (2001). Long mutant dystrophins and variable phenotypes: Evasion of nonsense-mediated decay? *Human Genetics*, *109*(4), 402–407.

Kervestin, S., & Jacobson, A. (2012). NMD: a multifaceted response to premature translational termination. *Nature Reviews Molecular Cell Biology*, *13*(11), 700–712.

Kervestin, S., Li, C., Buckingham, R., & Jacobson, A. (2012). Testing the faux-UTR model for NMD: Analysis of Upf1p and Pab1p competition for binding to eRF3/Sup35p. *Biochimie*, *94*(7), 1560–1571.

Kim, V. N. (2001). Role of the Nonsense-Mediated Decay Factor hUpf3 in the Splicing-Dependent Exon-Exon Junction Complex. *Science*, *293*(5536), 1832–1836.

Kobayashi, T., Funakoshi, Y., Hoshino, S. I., & Katada, T. (2004). The GTP-binding release factor eRF3 as a key mediator coupling translation termination to mRNA decay. *Journal of Biological Chemistry*, *279*(44), 45693–45700.

Köhler, A., & Hurt, E. (2007). Exporting RNA from the nucleus to the cytoplasm. *Nature Reviews Molecular Cell Biology*, *8*(10), 761–773.

Kong, C., Ito, K., Walsh, M. A., Wada, M., Liu, Y., Kumar, S., ... Song, H. (2004). Crystal structure and functional analysis of the eukaryotic class II release factor eRF3 from S. pombe. *Molecular Cell*, *14*(2), 233–245.

Kozlov, G., & Gehring, K. (2010). Molecular basis of eRF3 recognition by the MLLE domain

of poly(A)-binding protein. *PLoS ONE*, *5*(4), e10169.

Kryuchkova, P., Grishin, A., Eliseev, B., Karyagina, A., Frolova, L., & Alkalaeva, E. (2013). Two-step model of stop codon recognition by eukaryotic release factor eRF1. *Nucleic Acids Research*, *41*(8), 4573–4586.

Kunz, J. B., Neu-Yilik, G., Hentze, M. W., Kulozik, A. E., & Gehring, N. H. (2006). Functions of hUpf3a and hUpf3b in nonsense-mediated mRNA decay and translation. *RNA (New York, N.Y.)*, *12*(6), 1015–1022.

Kuroha, K., Tatematsu, T., & Inada, T. (2009). Upf1 stimulates degradation of the product derived from aberrant messenger RNA containing a specific nonsense mutation by the proteasome. *EMBO reports*, *10*(11), 1265–71.

Kurosaki, T., Li, W., Hoque, M., Popp, M. W. L., Ermolenko, D. N., Tian, B., & Maquat, L. E. (2014). A Post-Translational regulatory switch on UPF1 controls targeted mRNA degradation. *Genes and Development*, *28*(17), 1900–1916.

Kurosaki, T., & Maquat, L. E. (2016). Nonsense-mediated mRNA decay in humans at a glance. *Journal of cell science*(January), 461–467.

Kyrieleis, O. J. P., Chang, J., De La Peña, M., Shuman, S., & Cusack, S. (2014). Crystal structure of vaccinia virus mRNA capping enzyme provides insights into the mechanism and evolution of the capping apparatus. *Structure*, *22*(3), 452–465.

Laumonnier, F., Shoubridge, C., Antar, C., Nguyen, L. S., Van Esch, H., Kleefstra, T., ... Raynaud, M. (2010). Mutations of the UPF3B gene, which encodes a protein widely expressed in neurons, are associated with nonspecific mental retardation with or without autism. *Molecular Psychiatry*, *15*(7), 767–776.

Le Hir, H., Gatfield, D., Izaurralde, E., & Moore, M. J. (2001). The exon-exon junction complex provides a binding platform for factors involved in mRNA export and nonsense-mediated mRNA decay. *EMBO Journal*, *20*(17), 4987–4997.

Lee, A. S. Y., Kranzusch, P. J., & Cate, J. H. D. (2015). eIF3 targets cell-proliferation messenger RNAs for translational activation or repression. *Nature*, *522*, 111–114.

Lee, S. R., Pratt, G. A., Martinez, F. J., Yeo, G. W., & Lykke-Andersen, J. (2015). Target Discrimination in Nonsense-Mediated mRNA Decay Requires Upf1 ATPase Activity. *Molecular Cell*, *59*(3), 413–425.

Leeds, P., Wood, J. M., Lee, B. S., & Culbertson, M. R. (1992). Gene products that promote mRNA turnover in Saccharomyces cerevisiae. *Molecular and cellular biology*, *12*(5), 2165–77.

Lejeune, F., Li, X., & Maquat, L. E. (2003). Nonsense-mediated mRNA decay in mammalian cells involves decapping, deadenylating, and exonucleolytic activities. *Molecular Cell*, *12*(3), 675–687.

Lewis, B. P., Green, R. E., & Brenner, S. E. (2003). Evidence for the widespread coupling of alternative splicing and nonsense-mediated mRNA decay in humans. *Proceedings of the National Academy of Sciences of the United States of America*, *100*(1), 189–92.

Li, M. Z., & Elledge, S. J. (2007). Harnessing homologous recombination in vitro to generate recombinant DNA via SLIC. *Nature methods*, *4*(3), 251–256.

Li, T., Shi, Y., Wang, P., Guachalla, L. M., Sun, B., Joerss, T., ... Wang, Z.-Q. (2015). Smg6/Est1 licenses embryonic stem cell differentiation via nonsense-mediated mRNA decay. *The EMBO Journal*, *34*(12), 1630–1647.

Linder, B., Fischer, U., & Gehring, N. H. (2015). MRNA metabolism and neuronal disease. *FEBS Letters*, *589*(14), 1598–1606.

Liu, C., Karam, R., Zhou, Y., Su, F., Ji, Y., Li, G., ... Lu, Y. (2014). The UPF1 RNA surveillance gene is commonly mutated in pancreatic adenosquamous carcinoma. *Nature medicine*, *20*(6), 596–599.

Loh, B., Jonas, S., & Izaurralde, E. (2013). The SMG5-SMG7 heterodimer directly recruits the CCR4-NOT deadenylase complex to mRNAs containing nonsense codons via interaction with POP2. *Genes and Development*, *27*(19), 2125–2138.

Longman, D., Hug, N., Keith, M., Anastasaki, C., Patton, E. E., Grimes, G., & Cáceres, J. F. (2013). DHX34 and NBAS form part of an autoregulatory NMD circuit that regulates endogenous RNA targets in human cells, zebrafish and Caenorhabditis elegans. *Nucleic Acids Research*, *41*(17), 8319–8331.

López-Perrote, A., Castaño, R., Melero, R., Zamarro, T., Kurosawa, H., Ohnishi, T., ... Llorca, O. (2015). Human nonsense-mediated mRNA decay factor UPF2 interacts directly with eRF3 and the SURF complex. *Nucleic Acids Research*, *44*(4), 1909–1923.

Losson, R., & Lacroute, F. (1979). Interference of nonsense mutations with eukaryotic messenger RNA stability. *Proceedings of the National Academy of Sciences of the United States of America*, *76*(10), 5134–5137.

Lou, C. H., Shao, A., Shum, E. Y., Espinoza, J. L., Huang, L., Karam, R., & Wilkinson, M. F. (2014). Posttranscriptional Control of the Stem Cell and Neurogenic Programs by the Nonsense-Mediated RNA Decay Pathway. *Cell Reports*, *6*(4), 748–764.

Lykke-Andersen, J., & Bennett, E. J. (2014). Protecting the proteome: Eukaryotic cotranslational quality control pathways. *Journal of Cell Biology*, *204*(4), 467–476.

Lykke-Andersen, J., Shu, M. D., & Steitz, J. A. (2000). Human Upf proteins target an mRNA for nonsense-mediated decay when downstream of a termination codon. *Cell*, *103*(7), 1121–1131.

Lykke-Andersen, J., Shu, M. D., & Steitz, J. a. (2001). Communication of the position of exon-exon junctions to the mRNA surveillance machinery by the protein RNPS1. *Science (New York, N.Y.)*, *293*(5536), 1836–1839.

Lykke-Andersen, S., & Jensen, T. H. (2015). Nonsense-mediated mRNA decay: an intricate machinery that shapes transcriptomes. *Nature reviews. Molecular cell biology*, *16*(11), 665–677.

Lynch, S. A., Nguyen, L. S., Ng, L. Y., Waldron, M., McDonald, D., & Gecz, J. (2012). Broadening the phenotype associated with mutations in UPF3B: Two further cases with renal dysplasia and variable developmental delay. *European Journal of Medical Genetics*, *55*(8-9), 476–479.

MacDermott, M. (1990). The intracellular concentration of free magnesium in extensor

digitorum longus muscles of the rat. *Experimental physiology*, *75*(6), 763–769.

Maderazo, A. B., He, F., Mangus, D. A., & Jacobson, A. (2000). Upf1p control of nonsense mRNA translation is regulated by Nmd2p and Upf3p. *Molecular and cellular biology*, *20*(13), 4591–603.

Maquat, L. E., Kinniburgh, a. J., Rachmilewitz, E. a., & Ross, J. (1981). Unstable beta-globin mRNA in mRNA-deficient beta o thalassemia. *Cell*, *27*(3 Pt 2), 543–553.

Martin, L., Grigoryan, A., Wang, D., Wang, J., Breda, L., Rivella, S., ... Gardner, L. B. (2014). Identification and characterization of small molecules that inhibit nonsense-mediated rna decay and suppress nonsense p53 mutations. *Cancer Research*, *74*(11), 3104–3113.

Matheisl, S., Berninghausen, O., Becker, T., & Beckmann, R. (2015). Structure of a human translation termination complex. *Nucleic acids research*, *1*(18), 1–12.

Mazza, C., Ohno, M., Segref, A., Mattaj, I. W., & Cusack, S. (2001). Crystal structure of the human nuclear cap binding complex. *Molecular Cell*, *8*(2), 383–396.

Melero, R., Buchwald, G., Castaño, R., Raabe, M., Gil, D., Lázaro, M., ... Llorca, O. (2012). The cryo-EM structure of the UPF-EJC complex shows UPF1 poised toward the RNA 3' end. *Nature structural & molecular biology*, *19*(5), 498–505, S1–2.

Melero, R., Hug, N., López-Perrote, A., Yamashita, A., Cáceres, J. F., & Llorca, O. (2016). The RNA helicase DHX34 functions as a scaffold for SMG1-mediated UPF1 phosphorylation. *Nature communications*, *7*, 10585.

Melero, R., Uchiyama, A., Castaño, R., Kataoka, N., Kurosawa, H., Ohno, S., ... Llorca, O. (2014). Structures of SMG1-UPFs complexes: SMG1 contributes to regulate UPF2-dependent activation of UPF1 in NMD. *Structure*, *22*(8), 1105–1119.

Mendell, J. T., Sharifi, N. a., Meyers, J. L., Martinez-Murillo, F., & Dietz, H. C. (2004). Nonsense surveillance regulates expression of diverse classes of mammalian transcripts and mutes genomic noise. *Nature genetics*, *36*(10), 1073–1078.

Min, E. E., Roy, B., Amrani, N., He, F., & Jacobson, A. (2013). Yeast Upf1 CH domain interacts with Rps26 of the 40S ribosomal subunit. TL - 19. *RNA (New York, N.Y.)*, *19 VN - r*(8), 1105–1115.

Moore, M. J., & Proudfoot, N. J. (2009). Pre-mRNA Processing Reaches Back toTranscription and Ahead to Translation. *Cell*, *136*(4), 688–700.

Morita, T., Yamashita, A., Kashima, I., Ogata, K., Ishiura, S., & Ohno, S. (2007). Distant N- and C-terminal domains are required for intrinsic kinase activity of SMG-1, a critical component of nonsense-mediated mRNA decay. *Journal of Biological Chemistry*, *282*(11), 7799–7808.

Morris, C., Wittmann, J., Jäck, H.-M., & Jalinot, P. (2007). Human INT6/eIF3e is required for nonsense-mediated mRNA decay. *EMBO reports*, *8*(6), 596–602.

Muhlrad, D., & Parker, R. (1999). Aberrant mRNAs with extended 3' UTRs are substrates for rapid degradation by mRNA surveillance. *RNA (New York, N.Y.)*, *5*, 1299–1307.

Nagy, E., & Maquat, L. E. (1998). A rule for termination-codon position within intron-containing genes: When nonsense affects RNA abundance. *Trends in Biochemical*

Sciences, *23*(6), 198–199.

Nguyen, L. S., Wilkinson, M. F., & Gecz, J. (2014). Nonsense-mediated mRNA decay: Inter-individual variability and human disease. *Neuroscience and Biobehavioral Reviews*, *46*(P2), 175–186.

Nott, A., Le Hir, H., & Moore, M. J. (2004). Splicing enhances translation in mammalian cells: An additional function of the exon junction complex. *Genes and Development*, *18*(2), 210–222.

Ohnishi, T., Yamashita, A., Kashima, I., Schell, T., Anders, K. R., Grimson, A., ... Ohno, S. (2003). Phosphorylation of hUPF1 induces formation of mRNA surveillance complexes containing hSMG-5 and hSMG-7. *Molecular Cell*, *12*(5), 1187–1200.

Okada-Katsuhata, Y., Yamashita, A., Kutsuzawa, K., Izumi, N., Hirahara, F., & Ohno, S. (2012). N-and C-terminal Upf1 phosphorylations create binding platforms for SMG-6 and SMG-5:SMG-7 during NMD. *Nucleic Acids Research*, *40*(3), 1251–1266.

Ottens, F., & Gehring, N. H. (2016). Physiological and pathophysiological role of nonsense-mediated mRNA decay. *Pflügers Archiv - European Journal of Physiology*.

Palacios, I. M., Gatfield, D., St Johnston, D., & Izaurralde, E. (2004). An eIF4AIII-containing complex required for mRNA localization and nonsense-mediated mRNA decay. *Nature*, *427*(6976), 753–7.

Peixeiro, I., Inácio, Â., Barbosa, C., Silva, A. L., Liebhaber, S. A., & Romão, L. (2012). Interaction of PABPC1 with the translation initiation complex is critical to the NMD resistance of AUG-proximal nonsense mutations. *Nucleic Acids Research*, *40*(3), 1160–1173.

Pelechano, V., Wei, W., & Steinmetz, L. M. (2015). Widespread co-translational RNA decay reveals ribosome dynamics. *Cell*, *161*(6), 1400–1412.

Pisarev, A. V., Hellen, C. U. T., & Pestova, T. V. (2007). Recycling of Eukaryotic Posttermination Ribosomal Complexes. *Cell*, *131*(2), 286–299.

Pisarev, A. V., Skabkin, M. A., Pisareva, V. P., Skabkina, O. V., Rakotondrafara, A. M., Hentze, M. W., ... Pestova, T. V. (2010). The Role of ABCE1 in Eukaryotic Posttermination Ribosomal Recycling. *Molecular Cell*, *37*(2), 196–210.

Pisareva, V. P., Pisarev, A. V., Hellen, C. U. T., Rodnina, M. V., & Pestova, T. V. (2006). Kinetic analysis of interaction of eukaryotic release factor 3 with guanine nucleotides. *Journal of Biological Chemistry*, *281*(52), 40224–40235.

Pisareva, V. P., Pisarev, A. V., Komar, A. A., Hellen, C. U. T., & Pestova, T. V. (2008). Translation Initiation on Mammalian mRNAs with Structured 5'UTRs Requires DExH-Box Protein DHX29. *Cell*, *135*(7), 1237–1250.

Pisareva, V. P., Skabkin, M. A., Hellen, C. U. T., Pestova, T. V., & Pisarev, A. V. (2011). Dissociation by Pelota, Hbs1 and ABCE1 of mammalian vacant 80S ribosomes and stalled elongation complexes. *The EMBO journal*, *30*(9), 1804–17.

Popp, M., & Maquat, L. (2016). Leveraging Rules of Nonsense-Mediated mRNA Decay for Genome Engineering and Personalized Medicine. *Cell*, *165*(6), 1319–1322.

Porrua, O., & Libri, D. (2015). Transcription termination and the control of the transcrip-

tome: why, where and how to stop. *Nat Rev Mol Cell Biol*, *16*(3), 190–202.

Preis, A., Heuer, A., Barrio-Garcia, C., Hauser, A., Eyler, D. E., Berninghausen, O., ... Beckmann, R. (2014). Cryoelectron microscopic structures of eukaryotic translation termination complexes containing eRF1-eRF3 or eRF1-ABCE1. *Cell Reports*, *8*(1), 59–65.

Query, C. C., & Konarska, M. M. (2006). Splicing fidelity revisited. *Nature structural & molecular biology*, *13*(6), 472–4.

Rajavel, K. S., & Neufeld, E. F. (2001). Nonsense-mediated decay of human HEXA mRNA. *Molecular and cellular biology*, *21*(16), 5512–5519.

Reed, R., & Cheng, H. (2005). TREX, SR proteins and export of mRNA. *Current Opinion in Cell Biology*, *17*(3), 269–273.

Rehwinkel, J., Raes, J., & Izaurralde, E. (2006). Nonsense-mediated mRNA decay: target genes and functional diversification of effectors. *Trends in Biochemical Sciences*, *31*(11), 639–646.

Roque, S., Cerciat, M., Gaugué, I., Mora, L., Floch, A. G., de Zamaroczy, M., ... Kervestin, S. (2014). eukaryotic release factor eRF3 regulates translation termination but not mRNA decay in Saccharomyces cerevisiae Interaction between the poly (A) -binding protein Pab1 and the eukaryotic release factor eRF3 regulates translation termination but not mRNA . *RNA (New York, N.Y.)*, *21*(1), 124–134.

Sainsbury, S., Bernecky, C., & Cramer, P. (2015). Structural basis of transcription initiation by RNA polymerase II. *Nature reviews. Molecular cell biology*, *16*(3), 129–143.

Sakaki, K., Yoshina, S., Shen, X., Han, J., DeSantis, M. R., Xiong, M., ... Kaufman, R. J. (2012). RNA surveillance is required for endoplasmic reticulum homeostasis. *Proceedings of the National Academy of Sciences of the United States of America*, *109*(21), 8079–84.

Saulière, J., Murigneux, V., Wang, Z., Marquenet, E., Barbosa, I., Le Tonquèze, O., ... Le Hir, H. (2012). CLIP-seq of eIF4AIII reveals transcriptome-wide mapping of the human exon junction complex. TL - 19. *Nature structural & molecular biology*, *19 VN - r*(11), 1124–1131.

Schaffitzel, C., & Ban, N. (2007). Reprint of "Generation of ribosome nascent chain complexes for structural and functional studies" [J. Struct. Biol. 158 (2007) 463-471]. *Journal of Structural Biology*, *159*(2 SPEC. ISS.), 302–310.

Scheres, S. H. W. (2012). RELION: Implementation of a Bayesian approach to cryo-EM structure determination. *Journal of Structural Biology*, *180*(3), 519–530.

Scheres, S. H. w. (2014). Beam-induced motion correction for sub-megadalton cryo-EM particles. *eLife*, *3*, e03665.

Schoenberg, D. R., & Maquat, L. E. (2012). Regulation of cytoplasmic mRNA decay. *Nature reviews. Genetics*, *13*(4), 246–59.

Schweingruber, C., Rufener, S. C., Zünd, D., Yamashita, A., & Mühlemann, O. (2013). Nonsense-mediated mRNA decay - Mechanisms of substrate mRNA recognition and degradation in mammalian cells. *Biochimica et Biophysica Acta - Gene Regulatory*

Mechanisms, *1829*(6-7), 612–623.

Serin, G., Gersappe, A., Black, J. D., Aronoff, R., & Maquat, L. E. (2001). Identification and characterization of human orthologues to Saccharomyces cerevisiae Upf2 protein and Upf3 protein (Caenorhabditis elegans SMG-4). *Molecular and cellular biology*, *21*(1), 209–23.

Shao, S., Brown, A., Santhanam, B., & Hegde, R. S. (2015). Structure and assembly pathway of the ribosome quality control complex. *Molecular Cell*, *57*(3), 433–445.

Shao, S., & Hegde, R. S. (2014). Reconstitution of a Minimal Ribosome-Associated Ubiquitination Pathway with Purified Factors. *Molecular Cell*, *55*(6), 880–890.

Shenvi, C. L., Dong, K. C., Friedman, E. M., Hanson, J. A., & Cate, J. H. D. (2005). Accessibility of 18S rRNA in human 40S subunits and 80S ribosomes at physiological magnesium ion concentrations–implications for the study of ribosome dynamics. *RNA (New York, N.Y.)*, *11*(12), 1898–908.

Shibuya, T., Tange, T. Ø., Sonenberg, N., & Moore, M. J. (2004). eIF4AIII binds spliced mRNA in the exon junction complex and is essential for nonsense-mediated decay. *Nature Structural & Molecular Biology*, *11*(4), 346–351.

Shirokikh, N. E., Alkalaeva, E. Z., Vassilenko, K. S., Afonina, Z. A., Alekhina, O. M., Kisselev, L. L., & Spirin, A. S. (2009). Quantitative analysis of ribosome-mRNA complexes at different translation stages. *Nucleic Acids Research*, *38*(3), e15.

Shoemaker, C. J., Eyler, D. E., & Green, R. (2010). Dom34:Hbs1 promotes subunit dissociation and peptidyl-tRNA drop off to initiate no-go decay. *Science*, *330*(6002), 369–372.

Shoemaker, C. J., & Green, R. (2011). Kinetic analysis reveals the ordered coupling of translation termination and ribosome recycling in yeast. *Proceedings of the National Academy of Sciences of the United States of America*, *108*(51), E1392–8.

Shoemaker, C. J., & Green, R. (2012). Translation drives mRNA quality control. *Nature structural & molecular biology*, *19*(6), 594–601.

Shum, E. Y., Jones, S. H., Shao, A., Dumdie, J., Krause, M. D., Chan, W. K., ... Wilkinson, M. F. (2016). The Antagonistic Gene Paralogs Upf3a and Upf3b Govern Nonsense-Mediated RNA Decay. *Cell*, *165*(2), 382–395.

Sieber, J., Hauer, C., Bhuvanagiri, M., Leicht, S., Krijgsveld, J., Neu-Yilik, G., ... Kulozik, A. E. (2016). Proteomic analysis reveals branch-specific regulation of the unfolded protein response by nonsense-mediated mRNA decay. *Molecular & cellular proteomics : MCP*, *15*(5), 1584–1597.

Singh, G., Kucukural, A., Cenik, C., Leszyk, J. D., Shaffer, S. A., Weng, Z., & Moore, M. J. (2012). The cellular EJC interactome reveals higher-order mRNP structure and an EJC-SR protein nexus. *Cell*, *151*(4), 750–764.

Singh, G., Rebbapragada, I., & Lykke-Andersen, J. (2008). A competition between stimulators and antagonists of Upf complex recruitment governs human nonsense-mediated mRNA decay. *PLoS Biology*, *6*(4), 860–871.

Skabkin, M., Skabkina, O., Hellen, C. T., & Pestova, T. (2013). Reinitiation and other unconventional posttermination events during eukaryotic translation. *Molecular Cell*,

51(2), 249–264.

Subtelny, A. O., Eichhorn, S. W., Chen, G. R., Sive, H., & Bartel, D. P. (2014). Poly(A)-tail profiling reveals an embryonic switch in translational control. *Nature*, *508*(7494), 66–71.

Takahashi, S., Araki, Y., Ohya, Y., Sakuno, T., Hoshino, S.-I., Kontani, K., ... Katada, T. (2008). Upf1 potentially serves as a RING-related E3 ubiquitin ligase via its association with Upf3 in yeast. *RNA (New York, N.Y.)*, *14*(9), 1950–8.

Tang, G., Peng, L., Baldwin, P. R., Mann, D. S., Jiang, W., Rees, I., & Ludtke, S. J. (2007). EMAN2: An extensible image processing suite for electron microscopy. *Journal of Structural Biology*, *157*(1), 38–46.

Tani, H., Imamachi, N., Salam, K. A., Mizutani, R., Ijiri, K., Irie, T., ... Akimitsu, N. (2012). Identification of hundreds of novel UPF1 target transcripts by direct determination of whole transcriptome stability. *RNA biology*, *9*(11), 1370–9.

Tarpey, P. S., Raymond, F. L., Nguyen, L. S., Rodriguez, J., Hackett, A., Vandeleur, L., ... Gécz, J. (2007). Mutations in UPF3B, a member of the nonsense-mediated mRNA decay complex, cause syndromic and nonsyndromic mental retardation. *Nature genetics*, *39*(9), 1127–33.

Ter-Avanesyan, M. D., Kushnirov, V. V., Dagkesamanskaya, a. R., Didichenko, S. a., Chernoff, Y. O., Inge-Vechtomov, S. G., & Smirnov, V. N. (1993). Deletion analysis of the SUP35 gene of the yeast Saccharomyces cerevisiae reveals two non-overlapping functional regions in the encoded protein. *Molecular microbiology*, *7*(5), 683–692.

Thein, S. L., Hesketh, C., Taylor, P., Temperley, I. J., Hutchinson, R. M., Old, J. M., ... Weatherall, D. J. (1990). Molecular basis for dominantly inherited inclusion body beta-thalassemia. *Proceedings of the National Academy of Sciences of the United States of America*, *87*(10), 3924–3928.

Thermann, R., Neu-Yilik, G., Deters, A., Frede, U., Wehr, K., Hagemeier, C., ... Kulozik, A. E. (1998). Binary specification of nonsense codons by splicing and cytoplasmic translation. *EMBO Journal*, *17*(12), 3484–3494.

Thompson, S. R., Gulyas, K. D., & Sarnow, P. (2001). Internal initiation in Saccharomyces cerevisiae mediated by an initiator tRNA/eIF2-independent internal ribosome entry site element. *Proceedings of the National Academy of Sciences of the United States of America*, *98*(23), 12972–12977.

Tian, B., Hu, J., Zhang, H., & Lutz, C. S. (2005). A large-scale analysis of mRNA polyadenylation of human and mouse genes. *Nucleic Acids Research*, *33*(1), 201–212.

Unterholzner, L., & Izaurralde, E. (2004). SMG7 acts as a molecular link between mRNA surveillance and mRNA decay. *Molecular Cell*, *16*(4), 587–596.

Veesler, D., Campbell, M. G., Cheng, A., yu Fu, C., Murez, Z., Johnson, J. E., ... Carragher, B. (2013). Maximizing the potential of electron cryomicroscopy data collected using direct detectors. *Journal of Structural Biology*, *184*(2), 193–202.

Veloso, D., Guynn, R., Oskarsson, M., & RL. (1973). The concentrations of free and bound magnesium in rat tissues. *Journal of Biological Chemistry*, *248*(13), 4811–4819.

Venkatesh, S., & Workman, J. L. (2015). Histone exchange, chromatin structure and the regulation of transcription. *Nature Reviews. Molecular Cell Biology*, *16*(3), 178–189.

Villa, T., Rougemaille, M., & Libri, D. (2008). Nuclear quality control of RNA polymerase II ribonucleoproteins in yeast: Tilting the balance to shape the transcriptome. *Biochimica et Biophysica Acta - Gene Regulatory Mechanisms*, *1779*(9), 524–531.

Wang, W., Cajigas, I. J., Peltz, S. W., Wilkinson, M. F., & González, C. I. (2006). Role for Upf2p phosphorylation in Saccharomyces cerevisiae nonsense-mediated mRNA decay. *Molecular and cellular biology*, *26*(9), 3390–3400.

Wang, W., Czaplinski, K., Rao, Y., & Peltz, S. W. (2001). The role of Upf proteins in modulating the translation read-through of nonsense-containing transcripts. *EMBO Journal*, *20*(4), 880–890.

Waters, M. G., & Blobel, G. (1986). Secretory protein translocation in a yeast cell-free system can occur posttranslationally and requires ATP hydrolysis. *Journal of Cell Biology*, *102*(5), 1543–1550.

Weischenfeldt, J., Damgaard, I., Bryder, D., Theilgaard-Mönch, K., Thoren, L. A., Nielsen, F. C., ... Porse, B. T. (2008). NMD is essential for hematopoietic stem and progenitor cells and for eliminating by-products of programmed DNA rearrangements. *Genes and Development*, *22*(10), 1381–1396.

Wells, S. E., Hillner, P. E., Vale, R. D., & Sachs, a. B. (1998). Circularization of mRNA by eukaryotic translation initiation factors. *Molecular cell*, *2*(1), 135–140.

Xie, J., Kozlov, G., & Gehring, K. (2014). The "tale" of poly(A) binding protein: The MLLE domain and PAM2-containing proteins. *Biochimica et Biophysica Acta - Gene Regulatory Mechanisms*, *1839*(11), 1062–1068.

Xu, X., Zhang, L., Tong, P., Xun, G., Su, W., Xiong, Z., ... Hu, Z. (2013). Exome sequencing identifies UPF3B as the causative gene for a Chinese non-syndrome mental retardation pedigree. *Clinical Genetics*, *83*(6), 560–564.

Yamashita, A., Ohnishi, T., Kashima, I., Taya, Y., & Ohno, S. (2001). Human SMG-1, a novel phosphatidylinositol 3-kinase-related protein kinase, associates with components of the mRNA surveillance complex and is involved in the regulation of nonsense-mediated mRNA decay. *Genes and Development*, *15*(17), 2215–2228.

Yan, X., Hoek, T., Vale, R., & Tanenbaum, M. (2016). Dynamics of Translation of Single mRNA Molecules In Vivo. *Cell*, *165*(4), 976–989.

Young, D. J., Guydosh, N. R., Zhang, F., Hinnebusch, A. G., & Green, R. (2015). Rli1/ABCE1 Recycles Terminating Ribosomes and Controls Translation Reinitiation in 3'UTRs In Vivo. *Cell*, *162*(4), 872–84.

Zhang, J., & Maquat, L. E. (1997). Evidence that translation reinitiation abrogates nonsense-mediated mRNA decay in mammalian cells. *EMBO Journal*, *16*(4), 826–833.

Zünd, D., Gruber, A. R., Zavolan, M., & Mühlemann, O. (2013). Translation-dependent displacement of UPF1 from coding sequences causes its enrichment in 3' UTRs. TL - 20. *Nature structural & molecular biology*, *20 VN - r*(8), 936–943.

Acknowledgements

All this work would not have been possible without the support, patience of the people around me. Thank you to all of them.

First, I would like to thank my supervisor Prof. Christiane Schaffitzel for giving me the opportunity to work on fascinating problems in a great environment and for the guidance and helpful discussions during these four years.

I also would like to thank my jury members : Dr. Niels Gehring, Prof. Sven Danckwardt, Dr. André Verdel and Prof. Winfried Wissenhorn for taking their time to evaluate my thesis.

I am also thankful to the members of my thesis advisory committee : Dr. Ramesh Pillai, Dr. Carsten Sachse and Dr. Guy Schoehn for their input and advice throughout our annual reports.

I am very grateful to the people involved in the project and more especially our collaborators Gabriele Neu-Yilik, Beate Amthor, Matthias Hentze and Andreas Kulozik (MMU, Heidelberg, Germany) for their help and sharing their knowledge about NMD. Gabriele has been essential for pushing the project foward and I am thankful for the helpful discussions.

I am thankful for the support by EMBL, IBS and PSB core facilities : the EEF, the Biophysical Platform for their great work. I would like to give special thanks to the past and present members of the Berger and Schaffitzel laboratories for the great working environment in the lab. Especially I would like to especially thank Lahari my 'sister in arms', Boris, Mani and Aurelien and Karine without who nothing would have be possible. A very big thanks to Miriam for reading and giving suggestions to improve this manuscript. Special thanks for the following people : Sara, Jorge, Matze, Taiana, Simon, Sarah, Kyle, Jelger, Mathieu, Paul, Petra, Kapil, Martin. I am grateful for the predoc course and all the great people I met there especially these crazy ones: Pietro Il magnifico, Simone, Ana Rita, Hernando, Nick, Alex and Florian.

Merci Georgia (B.S) pour ton aide précieuse, ta patience et pour reussir à me supporter depuis tout ce temps!

Enfin j'aimerai remercier mes parents sans qui rien n'aurait été possible. Je tiens aussi à les remercier ainsi que Guillaume, Anne, Jojo et Tintin pour leurs enouragements et leur soutien! Je souhaiterai remercier mes amis en particulier ceux de la promo Biotech 2010 de l'ESIL.

Lastly, this is for Jorge : Like a boss!

A. Primer and plasmid list

All the oligonucleotides and plasmids used in this study are listed in the following tables. For more information please refer to the Materiel and methods section of the appropriate Chapter.

Table A.1: *Oligonucleotides used in Chapter 3*

	Name	Sequence (5' - 3')	Insert	Vector	Tag	Restriction
1	pUC19Strep3_EcoRI_For	GCCAGTGAATTCGAGCTCGGTAC	3Strep for yNC	pUC19	3Strep	EcoRI
2	pUC19Strep3_SpeI_Rev	GCCTGACCcatgagACTAGTTTTTTTCG	3Strep for yNC	pUC19	3Strep	SpeI
3	pUC19Strep3_EcoRI_For	GCCAGTGAATTCGAGCTCGGTAC	CMV for yNC	pUC19		EcoRI
4	pUC19_CMV_NcoI_Rev	TTCAATCCATGGTTAAGGAGGAATATATT-TGCAGGTCAGCAGGCTGCTCAGTTTTTTG-CACTCAGCACCAGCGGTTCAATTTTATTG-TCACTAATCCAT	CMV for yNC	pUC19		NcoI
5	pUC18-CPV_IRES_T7_EcoRI_For	GCCAGTGAATTCtaatacgactcactatagcaaaaatgt-gatcttgc	T7-IRES for yNC	pUC19		EcoRI
6	pUC18-CPV_IRES_NheI_Rev	GCCAGTGCTAGCaggtaaatttcttaggtttttcgactacct-aatctg	T7-IRES for yNC	pUC19		NheI
7	RF_Linker_XhoI_For	catggc ctcgaga AGCTCGGATTCAAACCAAGGCAAC	eRF3	pFastBac 11Linker		XhoI
8	RF_Linker_NotI_Rev	cat atg gcggccgc CTCGAGCTCGGCAATTTTAACAATTTTACC	eRF3	pFastBac 11Linker		NdeI, NotI, SacI, XhoI
9	Linker_RF_NheI_For	CAT ATG GCT AGC TCG GAT TCA AAC CAA G	eRF3	pFastBac 11Linker		NdeI, NheI
10	Linker_RF_SacI_Rev	cat atg gagctcgcCTCGGCAATTTTAACAATTTTACC	eRF3	pFastBac 11Linker		NdeI, SacI, XhoI
11	Linker_Upf_NheI_For	cat atg gct agc GTC GGT TCC GGT TCT CAC ACT C	Upf1p	pFastBac 11Linker		NdeI, NheI
12	Linker_Upf_SacI_Rev	cat atg gagctcgcTATTCCCAAATTGCTGAAGTCTT-TTGACAATTCATGC	Upf1p	pFastBac 11Linker		SacI, XhoI
13	Upf_Linker_SalI_For	catggc gtcgaca GTC GGT TCC GGT TCT CAC ACT C	Upf1p	pFastBac 11Linker		SalI
14	Upf_Linker_NotI_Rev	cat atg gcggccgcTATTCCCAAATTGCTGAAGTCTT-TTGACAATTCATGC	Upf1p	pFastBac 11Linker		NdeI, NotI, XhoI
15	Pab_Linker_NcoI	cat atg ccatggaa GCT GAT ATT ACT GAT AAG ACA GCT GAA CAA TTG G	Pab1p	pFastBac 11Linker		NcoI
16	Pab_Linker_SalI_Rev	catggc gtcgaCGCAGC TTG CTC AGT TTG TTG TTC TTG CTC	Pab1p	pFastBac 11Linker		SalI
17	Linker_Pab_NheI_For	cat atg gct agc GCT GAT ATT ACT GAT AAG ACA GCT GAA CAA TTG G	Pab1p	pFastBac 11Linker		NheI
18	Linker_Pab_SacI_Rev	cat atg gagctCGCAGC TTG CTC AGT TTG TTG TTC TTG CTC	Pab1p	pFastBac 11Linker		SacI
19	pFast11_yupf2_SalI_For	GATCCGGTCGACGgacgatggacggaaaaaagaattgca	Upf2p	pFastBac 11Linker		SalI
20	pFast11_yupf2_SacI_Rev	GATATAGAGCTCCAgtcgaaagaacgttttaaaacaa-tctttttaatc	Upf2p	pFastBac 11Linker		SacI
21	pProEx Htb_yupf2_NcoI_For	GATCCGCCATGGGCgacgatggacggaaaaaagaattgca	Upf2p	pPROEx Htb	His6-Tag	NcoI
22	pProEx Htb_yupf2_NotI_Rev	GATATAgcggccGCTCATTTTTCGAACTGCG-GGTGGCTCCAGCCCTGAAAATACAGGTT-TTCGagctcgtcgaaagaacgttttaaaacaatcttttttaatc	Upf2p	pPROEx Htb	Strep-Tag	NotI
23	pFast1_yupf2_SalI_For	GATCCGGTCGACatgTGGAGCCACCCGCAG-TTCGAAAAAGAAAACCTGTATTTTCAGG-GCCATATGgacgatggacggaaaaaagaattgca	Upf2p	pFastBac	Strep-Tag	SalI

	Name	Sequence (5' - 3')	Insert	Vector	Tag	Restriction
24	pFast1_yupf2_SacI_Rev	GATATAGAGCTCtcagtgatggtgatggtgatggtagtac-gactgaaaatacaggttttcggtcgttgggatatcgtaatcCCA-TGGgtcgaaagaacgttttaaaacaatctttttaatc	Upf2p	pFastBac	His6-Tag	SacI
25	pET21d_yupf2_NdeI_For	GATATACATATGTGGAGCCACCCGCAGTT-CGAAAAAGAAAACCTGTATTTTCAGGGC-gagctCgacgatggacggaaaaaagaattgca	Upf2p	pET21d	Strep-Tag	NdeI
26	pET21d_yupf2_XhoI_Rev	GATATACTCGAGgtcgaaagaacgttttaaaacaatctttttaatc	Upf2p	pET21d	His6-Tag	XhoI
27	pFast_yupf3_BamHI_For	GATCCGGGATCCagcaatgtggctggggaattg	Upf3p	pFastBac	His6-Tag	BamHI
28	pFast_yupf3_XhoI_Rev	GATATACTCGAGCActacttcttggtatcatcacgatgca	Upf3p	pFastBac	His6-Tag	XhoI
29	pET21a_yupf3_NdeI_For	GATATACATATGagcaatgtggctggggaattg	Upf3p	pET21a	His6-Tag	NdeI
30	pET21a_yupf3_XhoI_Rev	GATATACTCGAGcttcttggtatcatcacgatgca	Upf3p	pET21a	His6-Tag	XhoI
31	pPRO_U3_For	ctgtattttcagggcgccatggtgagcaatgtggctggggaattg	Upf3p	pPROEx Htb	His6-Tag	SLIC
32	pPRO_U3_Rev	aattttgcatcgtgatgataccaagaagtgagatccggaattcaaa-ggcct	Upf3p	pPROEx Htb	His6-Tag	SLIC
33	pPRO_U3_Rev_Plsm	caattccccagccacattgctcaccatggcgccctgaaaatacag	pPROEx Htb	pPROEx Htb	His6-Tag	SLIC
34	pPRO_U3_For_Plsm	aattttgcatcgtgatgataccaagaagtgagatccggaattcaaa-ggcct	pPROEx Htb	pPROEx Htb	His6-Tag	SLIC
35	pACEBac1_U1_BamHI_For	agatccGGATCCGGAATTATGGTCGGTTCC	Upf1p	pAceBac		BamHI
36	pACEBac1_U1_XhoI_Rev	gagctcCTCGAGTTATATTCCCAAATTGCTG-AAGTCTTTTG	Upf1p	pAceBac		XhoI/SalI
37	pACEBac1_U1_SLIC_For	tcccaccatcgggcgcGGATCCGGAATTATGGTC-GGTTCC	Upf1p	pAceBac		SLIC
38	pACEBac1_U1_SLIC_Plsm_R	GGAACCGACCATAATTCCGGATCCgcgcccg-atggtggga	pAceBac	pAceBac		SLIC
39	pACEBac1_U1_SLIC_Rrev	gccgcgacaagtgagctcgTCGAGTTATATTCCCA-AATTGCTGAAGTC	Upf1p	pAceBac		SLIC
40	pACEBac1_U1_SLIC_Plsm_For	GACTTCAGCAATTTGGGAATATAACTCGA-cgagctcacttgtcgcggc	pAceBac	pAceBac		SLIC
41	pIDC_His_U2_RsrII_For	gcctaccggtccgaaaccatgtcgtactac	Upf2p	pIDC	His6-Tag	RsrII
42	pIDC_U2_SalI_For	gcctacGTCGACgatggacgatggacg	Upf2p	pIDC		SalI
43	pIDC_U2_SacI_Rev	actagtGagctcTcagtcgaaagaacgttttaaaac	Upf2p	pIDC		SacI
44	PIDC_His_U2_SLIC_Fore	ccatcgggcgcggatcccggtccgaaaccatgtcgtactac	Upf2p	pIDC	His6-Tag	SLIC
45	PIDC_His_U2_SLIC_Plsm_Rev	gtagtacgacatggtttcggaccgggatccgcgcccgatgg	Upf2p	pIDC	His6-Tag	SLIC
46	PIDC_U2_SLIC_For	gcgcggaattcaaaggcctacGTCGACgatggacgatggacgg	Upf2p	pIDC		SLIC
47	PIDC_U2_SLIC_Plsm_Rev	ccgtccatcgtccatcGTCGACgtaggcctttgaattccgcgc	Upf2p	pIDC		SLIC
48	pIDC_U2_SLIC_Rev	gaaagcggccgcgactagtGagctcTcagtcgaaagaacgttt-taaaac	Upf2p	pIDC		SLIC
49	PIDC_U2_SLIC_Plsm_For	gttttaaaacgttctttcgactgAgagctCactagtcgcggccgctttc	Upf2p	pIDC		SLIC
50	PET21a_Pab1_XbaI_F	TAATTCTCTAGATAAGGAGGTGACTATG-AATGGCTGATATTACTGATAAGACAGCTGAAC	Pab1p	pET21a	His6-Tag	XbaI
51	PET21a_Pab1_BamHI_R	ATAGTCGGATCCAGCTTGCTCAGTTTGTT-GTTCTTG	Pab1p	pET21a	His6-Tag	BanHI
52	eRF3_52	CAGAACGGTAACCAACAACAAG	eRF3			
53	eRF3_846	CTTGACTGGCTCTGTGGATAAG	eRF3			
54	eRF3_1708	ACATCGCCAAAGAACCCTATC	eRF3			
55	Upf1p_440	GTAGAATACCTTGTGCCCAGAC	Upf1p			
56	Upf1p_874	GTTGCCATCGGTGATGAAATG	Upf1p			
57	Upf1p_1287	CCACCAGGCACTGGTAAAAC	Upf1p			

	Name	Sequence (5' - 3')	Insert	Vector	Tag	Restriction
58	Upf1p_2061	GGTAGAGAGGAGATTTCTGCTA	Upf1p			
59	Upf1p_874	GTTGCCATCGGTGATGAAATG	Upf1p			
60	Upf1p_1657	TGTGTTGGTGCTGGTGATAAG	Upf1p			
61	Upf1p_2389	GGTCTAACCCGTGCCAAATA	Upf1p			
62	Pab1p_678	CTCCGAAACTACTGACGAACAA	Pab1p			
63	Pab1p_1456	CAAGGTGGTTTCCCAAGAAATG	Pab1p			
64	Upf2p_744	GGCCACAGAACTGCATAAGA	Upf2p			
65	Upf2p_1356	GGCTTCAGGAGTCAATTACAT	Upf2p			
66	Upf2p_2147	ACTACTCAGATCCACCGGATAA	Upf2p			
67	Upf2p_744	GGCCACAGAACTGCATAAGA	Upf2p			
68	Upf2p_1356	GGCTTCAGGAGTCAATTACAT	Upf2p			
69	Upf2p_2147	ACTACTCAGATCCACCGGATAA	Upf2p			
70	PIDK_For	cactcgacgaagacttgat		pIDK		
71	Upf3p_533	cctacgtaaagaaattcactcaa	Upf3p			
72	PIDK_Rev	ccgtgtttcagttagcct		pIDK		

Table A.2: *Oligonucleotides used in Chapter 4*

	Name	Sequence (5' - 3')	Insert	Vector	Tag	Restriction
72	pPRO_hRF1m_NcoI_For	GATCCGCCATGGTAATGGCGGACG	eRF1AGQ	pPROEx	TeV-Site	NcoI
73	pPRO_hRF1m_NotI_Rev	GATCCGgcggccgcCTAgtagtcatcaaggtc	eRF1AGQ	pPROEx	TeV-Site	NotI
74	PPRO_Strep_RsrII_For	GATAtAcggtccgtataatctgtggaattgtgagcggataaca-atttcacacaggaaacagaccatgtcgtactacTGGAGCC-ACCCGCAGTTCGAAAAAgattacgatatcccaacga	-	pPROEx	Strep-tag	RsrII
75	PPRO_Strep_NcoI_Rev	cggatcccatggcgccctgaaaatacaggtttt	-	pPROEx	Strep-tag	NcoI
76	PPRO_Strep_For	gaaacagaccatgtcgtactacTGGAGCCACCCGCA-GTTCGAAAAAgattacgatatcccaacga	eRF1AGQ	pPROEx	His6-Strep-Tag	RsrII
77	PPRO_Strep_Rev	cggatcccatggcgccctgaaaatacaggtttt	eRF1AGQ	pPROEx	His6-Strep-Tag	NcoI
78	PPRO_Strep_Nest_RsrII_For	GATAtAcggtccgtataatctgtggaattgtgagcggataaca-atttcacacaggaaacagaccatg	eRF1AGQ	pPROEx	His6-Strep-Tag	RsrII
79	PPRO_Strep_Nest_NcoI_Rev	cctttgaattccggatcccatggcgccctg	eRF1AGQ	pPROEx	His6-Strep-Tag	NcoI
80	PPRO_eRF1_A183G_For	aacacggtagagGaggtcagtcagcc	eRF1	pPROEx	His6-Tag	Self-SLIC
81	PPRO_eRF1_A183G_Rev	ggctgactgacctCctctaccgtgtt	eRF1	pPROEx	His6-Tag	Self-SLIC
81	pFast11_hRF3_FL_NcoI_For	GATCCGccATGGATCCGGGCAGTG	eRF3a	pFastBac 11linker	His6-Strep-Tag	NcoI
82	pFast11_hRF3_FL_KpnI_Rev	GATCCGagcttggtaccGTCTTTCTCTGGAACCAGT	eRF3a	pFastBac 11linker	His6-Strep-Tag	KpnI
83	PET23c_RF3A_208_For	GATATACATATGAAGAAAGAGCATGTAA-ATGTAGTATTC	eRF3a ΔNM (208-636)	pET23c	His6-Tag	NdeI
84	PET23c_RF3A_256_Rev	CATGCTCTTTCTTCATATGTATATCTCCTT-CTTAAAGTTAAAC	eRF3a ΔNM (208-636)	pET23c	His6-Tag	XhoI
85	PET23c_RF3A_439_For	gatataCATATGATCAGGCTGCCAATTGTGG-ATAAGTACAAGGATATG	eRF3A 23 (439-636)	pET23c	His6-Tag	NdeI
86	PET23c_RF3A_636_Rev	TGGCAGCCTGATCATATGtatatctccttcttaaagttaa	eRF3A 23 (439-636)	pET23c	His6-Tag	XhoI
87	PET23c_RF3A_139_For	TCAATAGATCAGCTCGAGcaccaccaccacc	eRF3a MG (139-434)	pET23c	His6-Tag	NdeI
88	PET23c_RF3A_434_Rev	gtggtgCTCGAGCTGATCTATTGAAGTTCGG-CAAATTAT	eRF3a MG (139-434)	pET23c	His6-Tag	XhoI
89	PET23c_RF3A_G_208_NdeI_For	GATATACATATGAAGAAAGAGCATGTAA-ATGTAGTATTCATTGG	eRF3a G (208-434)	pET23c	His6-Tag	NdeI
90	PET23c_RF3A_G_434_XhoI_Rev	GATATACTCGAGTCATGATCTATTGAAGT-TCGGCA	eRF3a G (208-434)	pET23c	His6-Tag	XhoI
91	pPRO_3A_1_NcoI_For	catcatccatggcaATGGATCCGGGCAGTG	eRF3a NM (1-203)	pPROEx	His6-Tag	NcoI
92	pPRO_3A_203_NotI_Rev	catcatGCGGCCGCtcaCGGTGCAACCACAGA-CTTAG	eRF3a NM (1-203)	pPROEx	His6-Tag	NotI
93	pPRO_3A_1_NcoI_For	catcatccatggcaATGGATCCGGGCAGTG	eRF3A NMG (1-453)	pPROEx	His6-Tag	NcoI
94	pPRO_3A_453_NotI_Rev	catcatGCGGCCGCtcaCACAGTGCCCATATCC-TTG	eRF3A NMG (1-453)	pPROEx	His6-Tag	NotI
95	pPRO_3A_dN_1_For	TGAAAGTTCCATGGCGCCCTGAAAATAC	eRF3A ΔN (Δ1-138)	pPROEx	His6-Tag	Self-SLIC
96	pPRO_3A_dN_138_Rev	CAGGGCGCCATGGAACTTTCAGAACCTAT-TGTAGA	eRF3A ΔN (Δ1-138)	pPROEx	His6-Tag	Self-SLIC
97	Pfast_RF3a_1_For	AagcttggtaccTTAGCTAACAGCTGAATTTGA-ACCTTC	eRF3a N (1-138)	pFastBac	His6-Tag	Self-SLIC
98	Pfast_RF3a _138_Rev	GCTGTTAGCTAAggtaccaagcttgtcgagaagtact	eRF3a N (1-138)	pFastBac	His6-Tag	Self-SLIC
99	pETM13_Strep_hU2_B31_NcoI_For	GATATACCATGGGAATGAAAGAAAAAG-AAGAATCCATTCAGCTTCATCAGGAAG	UPF2-B31	pETM13	TeV-Site	NcoI
100	pETM13_Strep_hU2_B31_XhoI_Rev	GTGGTGCTCGAGgccctgaaaatacaggttttcTGCG-GCCGcttcttgttcttg	UPF2-B31	pETM13	TeV-Site	XhoI
101	Fast11_U2_NcoI_For	AGGGCGCCATGGGGATCC	UPF2	pFastBac 11linker	His6-Strep-Tag	NcoI

	Name	Sequence (5' - 3')	Insert	Vector	Tag	Restriction
102	Fast11_U2_NHe_Rev	TCGAAAGCTAGCACGTCTCCTCCCA	UPF2	pFastBac 11linker	His6-Strep-Tag	NheI
103	U2_B31_1_NcoI_For	GATATACCATGGgaatgaaagaaaaag	UPF2 B31 (121-1227)	pFastBac 11linker	His6-Strep-Tag	NcoI
104	U2_B31_NotI_Rev	TTTTCTGCGGCCGCTTATTCTT	UPF2 B31 (121-1227)	pFastBac 11linker	His6-Strep-Tag	NotI
105	U2_1_NcoI_For	GATATACCATGGgaATGCCAGCTGAGCGT-AAAAAGC	UPF2 B70 (1-1227)	pFastBac 11linker	His6-Strep-Tag	NcoI
106	U2_1227_NotI_Rev	GATATAGCGGCCGCTCATTCTTGTTCTTGC-CGTTCATTGA	UPF2 B70 (1-1227)	pFastBac 11linker	His6-Strep-Tag	NotI
107	U2_B31_121_NcoI_For	GATATACCATGGgaATGAAAGAAAAAGA-AGAATCCATTCA	UPF2 B71 (121-1272)	pFastBac 11linker	His6-Strep-Tag	NcoI
108	U2_NotI_Rev	GATATAGCGGCCGCTGCTGGATCAA	UPF2 B71 (121-1272)	pFastBac 11linker	His6-Strep-Tag	NotI
109	pFast11_hU3_FL_NcoI_For	GATCCGCCATGGAGATGAAGGAAGAG	UPF3B	pFastBac 11linker	His6-Strep-Tag	NcoI
110	pFast11_hU3_FL_KpnI_Rev	GATCCGggtaccCTCCTCTCCTCCTTC	UPF3B	pFastBac 11linker	His6-Strep-Tag	KpnI
111	Pfast_His_Strep_RsrI_For	ggatctcggtccgaaaccatgtcgtactaccatcaccatcaccat-cacgctagcTGGAGCCACCCGCAGTTCGAAA-AAgattacgatatcccaacgaccg	UPF3B	pFastBac	His6-Strep-Tag	RsrII
112	Pfast_Strep_NcoI_Rev	GATCCGCCATGGCgccctgaaaatacaggttttcggtc	UPF3B	pFastBac	His6-Strep-Tag	NcoI
113	Pfast_Strep_RsrI_For	ggatctcggtccgaaaccatgtcgtactacTGGAGCCACC-CGCAGTTCGAAAAAgattacgatatcccaacgaccgaaa	-	pFastBac	His6-Strep-Tag	RsrII
114	Pfast_Strep_NcoI_Rev	GATCCGCCATGGCgccctgaaaatacaggttttcggtc	-	pFastBac	His6-Strep-Tag	NcoI
115	hU3B2_Y160F_For	TCGATGATGATCCAGAATTTAGAAAGTTT-TTGGAAAGTT	UPF3B Y160F	-	-	Self-SLIC
116	hU3B2_Y160F_Rev	AACTTTCCAAAAACTTTCTAAATTCTGGA-TCATCATCGA	UPF3B Y160F	-	-	Self-SLIC
117	hU3B2_Y160A_For	TCGATGATGATCCAGAAGCTAGAAAGTT-TTTGGAAAGTT	UPF3B Y160A	-	-	Self-SLIC
118	hU3B2_Y160A_Rev	AACTTTCCAAAAACTTTCTAGCTTCTGGA-TCATCATCGA	UPF3B Y160A	-	-	Self-SLIC
119	hU3B2_Y160D_For	TCGATGATGATCCAGAAGATAGAAAGTT-TTTGGAAAGTT	UPF3B Y160D	-	-	Self-SLIC
120	hU3B2_Y160D_Rev	AACTTTCCAAAAACTTTCTATCTTCTGGAT-CATCATCGA	UPF3B Y160D	-	-	Self-SLIC
121	hU3B2_Y160E_For	TCGATGATGATCCAGAAGAAAGAAAGTT-TTTGGAAAGTT	UPF3B Y160E	-	-	Self-SLIC
122	hU3B2_Y160E_Rev	AACTTTCCAAAAACTTTCTTTCTTCTGGAT-CATCATCGA	UPF3B Y160E	-	-	Self-SLIC
123	hU3B2_T320A_For	GCCAGTGGGCAAAGTTGTGCCTTGCCCAA-GCGTTCTGAT	UPF3B T320A	-	-	Self-SLIC
124	hU3B2_T320A_Rev	ATCAGAACGCTTGGGCAAGGCACAACTTT-GCCCACTGGC	UPF3B T320A	-	-	Self-SLIC
125	hU3B2_T320E_For	GCCAGTGGGCAAAGTTGTGAATTGCCCA-AGCGTTCTGAT	UPF3B T320E	-	-	Self-SLIC
126	hU3B2_T320E_Rev	ATCAGAACGCTTGGGCAATTCACAACTTT-GCCCACTGGC	UPF3B T320E	-	-	Self-SLIC
127	hU3B2_S412A_For	AAGGCTGAAAGTACAGAAGCCATAGGCA-GCTCAGAAAAA	UPF3B S413A	-	-	Self-SLIC
128	hU3B2_S412A_Rev	TTTTTCTGAGCTGCCTATCCGTTCTGTACT-TTCAGCCTT	UPF3B S413A	-	-	Self-SLIC
129	hU3B2_S412E_For	AAGGCTGAAAGTACAGAAGAAATAGGC-AGCTCAGAAAAA	UPF3B S413E	-	-	Self-SLIC

	Name	Sequence (5' - 3')	Insert	Vector	Tag	Restriction
130	hU3B2_S412E_Rev	TTTTTCTGAGCTGCCTATTTCTTCTGTACT-TTCAGCCTT	UPF3B S413E	-	-	Self-SLIC
131	PPRO_U3B_42_NcoI_F	AgggcgccatggAAAACAAGGAGAAGAAAGA-AGCGC	UPF3B (42-x)	pPROEx	His6-Tag	NcoI
132	PPRO_U3B_256_NotI_R	tcgaaagcggccgcTCAAATTCTGTCTATCTTCT-TTAGCTTTTCTATATCTTTCC	UPF3B (x-256)	pPROEx	His6-Tag	NotI
133	PPRO_U3B_303_NotI_R	TcgaaagcggccgcTCACCCACTGGCTCTTTCATCA	UPF3B (x-303)	pPROEx	His6-Tag	NotI
134	PPRO_U3B_402_NotI_R	tcgaaagcggccgcTCAGCTGCCTATTGATTCTG-TACTTTCAGC	UPF3B (x-402)	pPROEx	His6-Tag	NotI
135	PPRO_U3B_179_NcoI_F	agggcgccatggAAGAGACACTGCTAGAGGAA-ATAGAAGCA	UPF3B (179-x)	pPROEx	His6-Tag	
136	PPRO_U3B_1_NcoI_F	catcatccatggcaATGAAGGAAGAGAAGGAGCAC	UPF3B (1-x)	pPROEx	His6-Tag	NcoI
137	PPRO_U3B_143_NotI_R	catcatGCGGCCGCtcaCTTCTTTTTTGCAGCT-TTTTG	UPF3B (x-143)	pPROEx	His6-Tag	NotI
138	Pfast_U3B_147_NcoI_F	AgggcgccatggAAAAAAGAGATACCAAAGT-CGGGACTATCG	UPF3B (147 - x)	pFastBac	His6-Tag	NcoI
139	Pfast_U3B_419_NotI_R	tcgaaagcggccgcTCATCGATCTCTCTTGACCA-CTTCTTCTT	UPF3B (x-419)	pFastBac	His6-Tag	NotI
140	Pfast_U3B_294_NotI_R	tcgaaagcggccgcTCACTCTTTGTCCAATTTCT-TGGCTTTTTCT	UPF3B (x-294)	pFastBac	His6-Tag	NotI
141	Pfast_U3B_439_NotI_R	tcgaaagcggccgcTCAATTTCGGCTTCGAGCTCC	UPF3B (x-439)	pFastBac	His6-Tag	NotI
142	pFB_U3B_380_NcoI_F	AgggcgccatggAAATGAAAAAAGAGAAAGA-CACACTTC	UPF3B (380-x)	pFastBac	His6-Tag	NcoI
143	pFB_U3B_470_NotI_R	tcgaaagcggccgcTCACTCCTCTCCTCCTTCTTT	UPF3B (x-470)	pFastBac	His6-Tag	NotI
144	hU3B2_d421_For	TCGATTTCGGCTGTTTCTTATTCGATCTCT-CTTGACC	UPF3B ΔEBM (Δ421-434)	-	-	Self-SLIC
145	hU3B2_d434_Rev	CGAATAAGAAACAGCCGAAATCGACTCTGTC	UPF3B ΔEBM (Δ421-434)	-	-	Self-SLIC

Table A.3: *Plasmids used in this study*

ID	Name	Species	Resistance	Insert	Comment	Tag	Source
1	CA_fireflyLUC	S. cerevisiae	Amp	Luciferase	firefly Luciferase mRNA with polyA tail, T3 promoter		Hentze/Kulozik Group
2	pBS-BMS_EF3_3boxBpA73	S. cerevisiae	Amp	BoxB	BoxB and 70nt poly(A)	BoxB	Hentze/Kulozik Group
3	pUC19_Strep3_FtsQ_SecM	S. cerevisiae	Amp	3Strep-FtsQ-SecM		3Strep	Schaffitzel Group
4	pUC18-CPV-UAA_mRNA	S. cerevisiae	Amp	CrPV	CrPV-IRES, MVHL-UAA and globin ORF		Alkalaeva Group
5	pUC19-SBP-yNC-BoxB-pA	S. cerevisiae	Amp	SBP-yNC	SBP, DPAPB-1, PGK1 3'UTR , BoxB and 70nt poly(A)	N-SBP	This study
6	pUC19-3Strep-yNC-BoxB-pA	S. cerevisiae	Amp	3Strep-yNC	3Strep tags, DPAPB-1, PGK1 3'UTR , BoxB and 70nt poly(A)	N-3xStrep	This study
7	pUC19-SBP-CMV-yNC-BoxB-pA	S. cerevisiae	Amp	SBP-yNC-CMV	SBP, DPAPB-1 with CMV stalling motif, PGK1 3'UTR , BoxB and 70nt poly(A)	N-SBP	This study
8	pUC19-IRES-SBP-yNC-BoxB-pA	S. cerevisiae	Amp	IRES-SBP-yNC	IRES, SBP, DPAPB-1, PGK1 3'UTR , BoxB and 70nt poly(A)	N-SBP	This study
9	pET21a yRF1 AGQ His	S. cerevisiae	Amp	eRF1AGQ	sup35	C-His6	This study
10	pET21b yRF3 His	S. cerevisiae	Amp	eRF3	sup45	C-His6	This study
11	pET22_PAB1 / pBS2188	S. cerevisiae	Amp	Pab1p		C-His6	Seraphin Group
12	pFastbac Htb 11Linker	S. cerevisiae	Amp		NcoI-SalI-NotI-[GGGGS]x11-NheI-SacI--KpnI-TEV-StrepTag-stop-NsiI-HindIII).	N-His6, C-Strep	Schaffitzel Group
13	pFastbac Htb eRF3 11Linker	S. cerevisiae	Amp	eRF3-linker-		N-His6, C-Strep	This study
14	pFastbac Htb Upf1p 11Linker	S. cerevisiae	Amp	Upf1p-linker-		N-His6, C-Strep	This study
15	pFastbac Htb Pab1p 11Linker	S. cerevisiae	Amp	Pab1p-linker-		N-His6, C-Strep	This study
16	pFastbac Htb eRF3 11Linker Upf1p	S. cerevisiae	Amp	eRF3-linker-Upf1p		N-His6, C-Strep	This study
17	pFastbac Htb eRF3 11Linker Pab1p	S. cerevisiae	Amp	eRF3-linker-Pab1p		N-His6, C-Strep	This study
18	pFastbac Htb Upf1p 11Linker eRF3	S. cerevisiae	Amp	Upf1p-linker-eRF3		N-His6, C-Strep	This study
19	pFastbac Htb Pab1p 11Linker eRF3	S. cerevisiae	Amp	Pab1p-linker-eRF3		N-His6, C-Strep	This study
20	pFastBac Htb yUpf1p	S. cerevisiae	Amp	Upf1p	Acceptor vector for MultiBac with yeast UPF1	N-His6	This study
21	pACEBac1 Htb yUpf1p	S. cerevisiae	Amp	Upf1p	Acceptor vector for MultiBac with yeast UPF1	N-His6	This study
22	pFastBac1 Strep yUpf2p His	S. cerevisiae	Amp	Upf2p		N-His6, C-Strep	This study
23	pFastBac1 Htb yUpf3p	S. cerevisiae	Amp	Upf3p		N-His6	This study
24	pACEBac1 Htb yUpf3	S. cerevisiae	Amp	Upf3p	Acceptor vector for MultiBac with yeast UPF3	N-His6	This study
25	pIDC yUPF2p	S. cerevisiae	Amp	Upf2p	Donor vector for MultiBac with yeast UPF2	No	This study
26	pFastBac1 His yUpf3 +pIDC yUPF2p (crelox)	S. cerevisiae	Amp		Crelox His tag on yeast UPF3, untagged UPF2	N-His6	This study
27	pQE30-eRF1 AGQ	H. sapiens	Amp	eRF1AGQ		N-His6	Hentze/Kulozik Group
28	pProEx Htb eRF1a (183G)	H. sapiens	Amp	eRF1AGQ		N-His6	This study
29	pProEx Htb eRF1 WT	H. sapiens	Amp	eRF1		N-His6	This study
30	pFastbac Htb eRF3a iso2	H. sapiens	Amp	eRF3a		HisatN-Terminus	Schaffitzel Group
31	pFastBac Strep eFR3a isoform2	H. sapiens	Amp	eRF3a	eRF3a FL isoform2	N-His-Strep	This study
32	pFastBac Stb eFR3a iso2	H. sapiens	Amp	eRF3a	eRF3a FL isoform2	N-Strep	This study
33	pProEx Htb heRF3a ΔN	H. sapiens	Amp	eRF3a (1-138)	eRF3a Fragment missing aa1-138	N-His6	This study
34	pProEx Htb heRF3a 1-143	H. sapiens	Amp	eRF3a (1-143)	eRF3a Fragment (1-143)	N-His6	This study
35	pProEx Htb heRF3a 1-217	H. sapiens	Amp	eRF3a (1-217)	eRF3a Fragment (1-217)	N-His6	This study
36	pProEx Htb hUPF3a 1-256	H. sapiens	Amp	eRF3a (1-256)	eRF3a Fragment (1-256)	N-His6	This study
37	pProEx Htb heRF3a 1-203	H. sapiens	Amp	eRF3a (1-203)	eRF3a Fragment (1-203)	N-His6	This study
38	pFast Bac Htb eRF3a N	H. sapiens	Amp	eRF3a (1-138)	eRF3a Fragment (1-138)	N-His6	This study
39	pFastBac-HTc-UPF1-WT	H. sapiens	Amp	UPF1	UPF1 isoform2 FL	N-His6	Hentze/Kulozik Group
40	PfastBac-HTc-UPF1 deltaCHR domain	H. sapiens	Amp	UPF1 (Δ131-250)	UPF1 isoform2 Fragment missing aa131-250	N-His6	Hentze/Kulozik Group
41	PfastBac-HTc-UPF1 stop at 975	H. sapiens	Amp	UPF1 (1-986)	UPF1 isoform2 Fragment stop at aa986	N-His6	Hentze/Kulozik Group
42	PfastBac-HTc-UPF1 stop at 1084	H. sapiens	Amp	UPF1 (1-1047)	UPF1 isoform2 Fragment stop at aa1084	N-His6	Hentze/Kulozik Group
43	pFastBac-HTc-UPF1-delta N-ter	H. sapiens	Amp	UPF1 (40-1118)	UPF1 isoform2 Fragment missing aa1-40	N-His6	Schaffitzel Group
44	pFastBac HTC_UPF2	H. sapiens	Amp	UPF2	UPF2 FL		Hentze/Kulozik Group
45	pETM13_upf2(120-1227)	H. sapiens	Kan	UPF2 (120-1227)	UPF2 Fragment (120-1227)	N-His6	Cusack Group
46	pProEX Htb UPF2 (120-757)	H. sapiens	Amp	UPF2 (120-757)	UPF2 Fragment (120-757)	N-His6	Cusack Group
47	pET21d UPF2 B31 TeV His	H. sapiens	Amp	UPF2 (120-1227)	UPF2 Fragment (120-1227)	C-His6	This study

ID	Name	Species	Resistance	Insert	Comment	Tag	Source
75	pFastBac hUPF3B FL S413E	H. sapiens	Amp	UPF3B	UPF3B FL isoform2 S413E mutant	N-His6	This study
48	pFastBac11 hUPF2 FL	H. sapiens	Amp	UPF2	UPF2 FL	N-Strep, C-His	This study
49	pFastBac Stc hUPF2 FL	H. sapiens	Amp	UPF2	UPF2 FL	N-Strep	This study
50	pFastBac Stc hUPF2 B70	H. sapiens	Amp	UPF2 (121-1227)	UPF2 Fragment (121-1227)	N-Strep	This study
51	pFastBac Stc hUPF2 B71	H. sapiens	Amp	UPF2 (1-1227)	UPF2 Fragment (1-1227)	N-Strep	This study
52	pFastBac Stc hUPF2 B31	H. sapiens	Amp	UPF2 (121-1272)	UPF2 Fragment (121-1272)	N-Strep	This study
53	pFastbac Htc UPF3B	H. sapiens	Amp	UPF3B	UPF3B FL isoform2	N-His6	Hentze/Kulozik Group
54	pFastBac Htb hUPF3B	H. sapiens	Amp	UPF3B	UPF3B FL isoform2	N-His6	This study
55	pFastBac Htb Strep UPF3B	H. sapiens	Amp	UPF3B	UPF3B FL isoform2	N-His6-Strep	This study
56	pFastBac Stc UPF3B FL	H. sapiens	Amp	UPF3B	UPF3B FL isoform2	N-Strep	This study
57	pProEX Htb UPF3B D1	H. sapiens	Amp	UPF3B (42-143)	UPF3B fragment (42-143)	N-His6	Cusack Group
58	pProEX Htb UPF3B D2	H. sapiens	Amp	UPF3B (42-143)	UPF3B fragment (42-143)	N-His6	Cusack Group
59	pFast Bac Htb hUPF3B D22	H. sapiens	Amp	UPF3B (42-402)	UPF3B fragment (42-402)	N-His6	This study
60	pFastBac Htb hUPF3B D24	H. sapiens	Amp	UPF3B (179-402)	UPF3B fragment (179-402)	N-His6	This study
61	pFastBac Htb hUPF3B D25	H. sapiens	Amp	UPF3B (1-143)	UPF3B fragment (1-143)	N-His6	This study
62	pFastBac Htb hUPF3B D26	H. sapiens	Amp	UPF3B (1-217)	UPF3B fragment (1-217)	N-His6	This study
63	pFastBac Htb hUPF3B D27	H. sapiens	Amp	UPF3B (1-256)	UPF3B fragment (1-256)	N-His6	This study
64	pFastBac Htb hUPF3B D28	H. sapiens	Amp	UPF3B (147-419)	UPF3B fragment (147-419)	N-His6	This study
65	pFastBac Htb hUPF3B D29	H. sapiens	Amp	UPF3B (147-256)	UPF3B fragment (147-256)	N-His6	This study
66	pFastBac Htb hUPF3B D30	H. sapiens	Amp	UPF3B (147-284)	UPF3B fragment (147-284)	N-His6	This study
67	pFastBac Htb hUPF3B D31	H. sapiens	Amp	UPF3B (42-419)	UPF3B fragment (42-419)	N-His6	This study
68	pFastBac Htb hUPF3B D32	H. sapiens	Amp	UPF3B (380-470)	UPF3B fragment (380-470)	N-His6	This study
69	pFastBac hUPF3B FL Δ421-434	H. sapiens	Amp	UPF3B (Δ421-434)	UPF3B fragment missing EBM (421-434)	N-His6	This study
70	pFastBac hUPF3B FL Y160A	H. sapiens	Amp	UPF3B	UPF3B FL isoform2 Y160A mutant	N-His6	This study
71	pFastBac hUPF3B FL Y160E	H. sapiens	Amp	UPF3B	UPF3B FL isoform2 Y160E mutant	N-His6	This study
72	pFastBac hUPF3B FL T320A	H. sapiens	Amp	UPF3B	UPF3B FL isoform2 T320A mutant	N-His6	This study
73	pFastBac hUPF3B FL T320E	H. sapiens	Amp	UPF3B	UPF3B FL isoform2 T320E mutant	N-His6	This study
74	pFastBac hUPF3B FL S413A	H. sapiens	Amp	UPF3B	UPF3B FL isoform2 S413A mutant	N-His6	This study

B. Second Appendix

B.1 Secondary structure prediction of human UPF3B

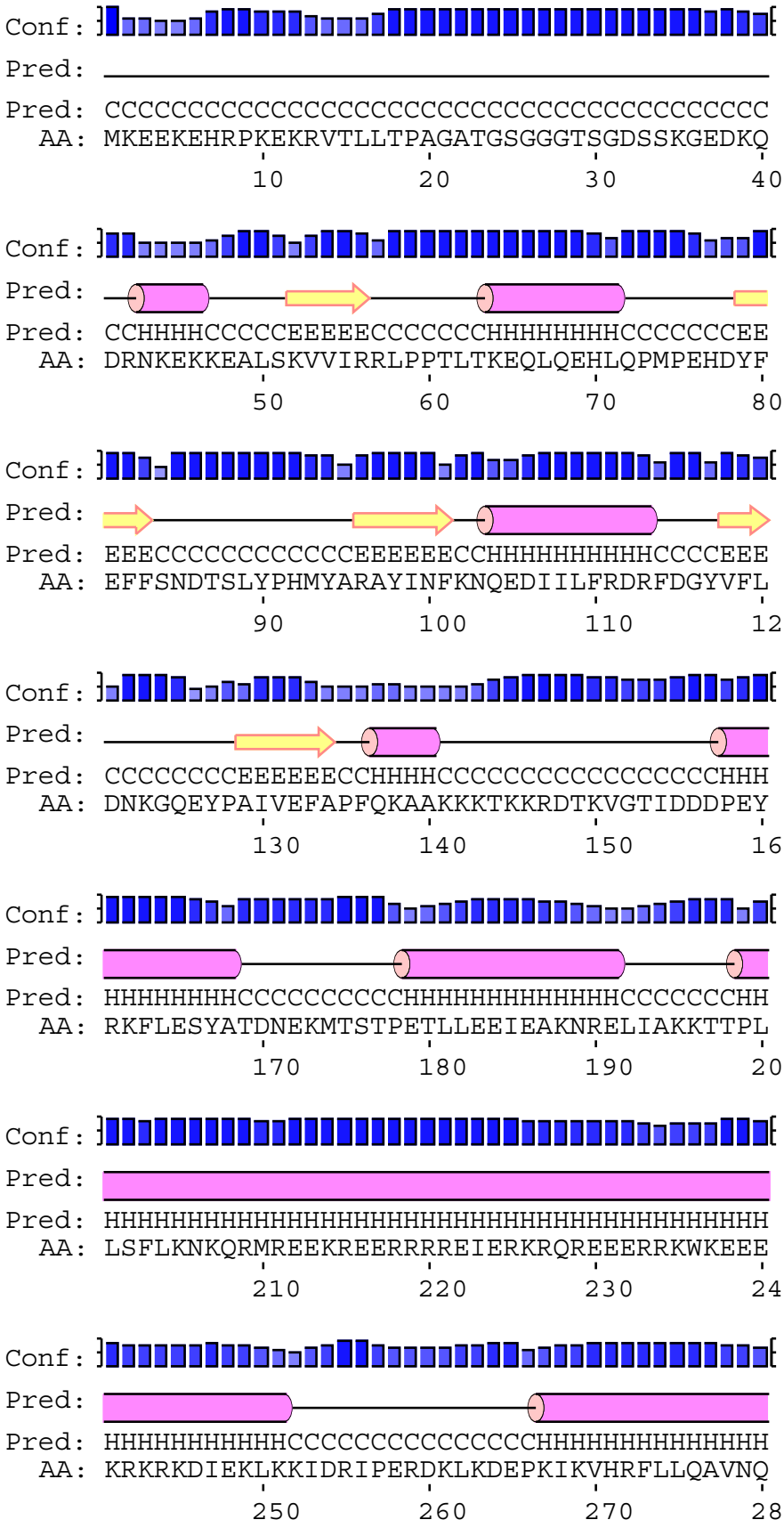
Conf:
Pred:
Pred: CCCCCCCCCCCCCCCCCCCCCCCCCCCCCCCCCCCCCCCC
AA: MKEEKEHRPKEKRVTLLTPAGATGSGGGTSGDSSKGEDKQ
10 20 30 40
Conf:
Pred:
Pred: CCHHHHCCCCCEEEEECCCCCCCHHHHHHHHHCCCCCCCEE
AA: DRNKEKKEALSKVVIRRLPPTLTKEQLQEHLQPMPEHDYF
50 60 70 80
Conf:
Pred:
Pred: EEECCCCCCCCCCCCEEEEEECCHHHHHHHHHHCCCCEEE
AA: EFFSNDTSLYPHMYARAYINFKNQEDIILFRDRFDGYVFL
90 100 110 120
Conf:
Pred:
Pred: CCCCCCCCEEEEEECCHHHHCCCCCCCCCCCCCCCCHHH
AA: DNKGQEYPAIVEFAPFQKAAKKKTKKRDTKVGTIDDDPEY
130 140 150 160
Conf:
Pred:
Pred: HHHHHHHHCCCCCCCCCCHHHHHHHHHHHHHCCCCCCCHH
AA: RKFLESYATDNEKMTSTPETLLEEIEAKNRELIAKKTTPL
170 180 190 200
Conf:
Pred:
Pred: HHHHHHHHHHHHHHHHHHHHHHHHHHHHHHHHHHHHHHHH
AA: LSFLKNKQRMREEKREERRRREIERKRQREEERRKWKEEE
210 220 230 240
Conf:
Pred:
Pred: HHHHHHHHHHHCCCCCCCCCCCCCCCHHHHHHHHHHHHHH
AA: KRKRKDIEKLKKIDRIPERDKLKDEPKIKVHRFLLQAVNQ
250 260 270 280

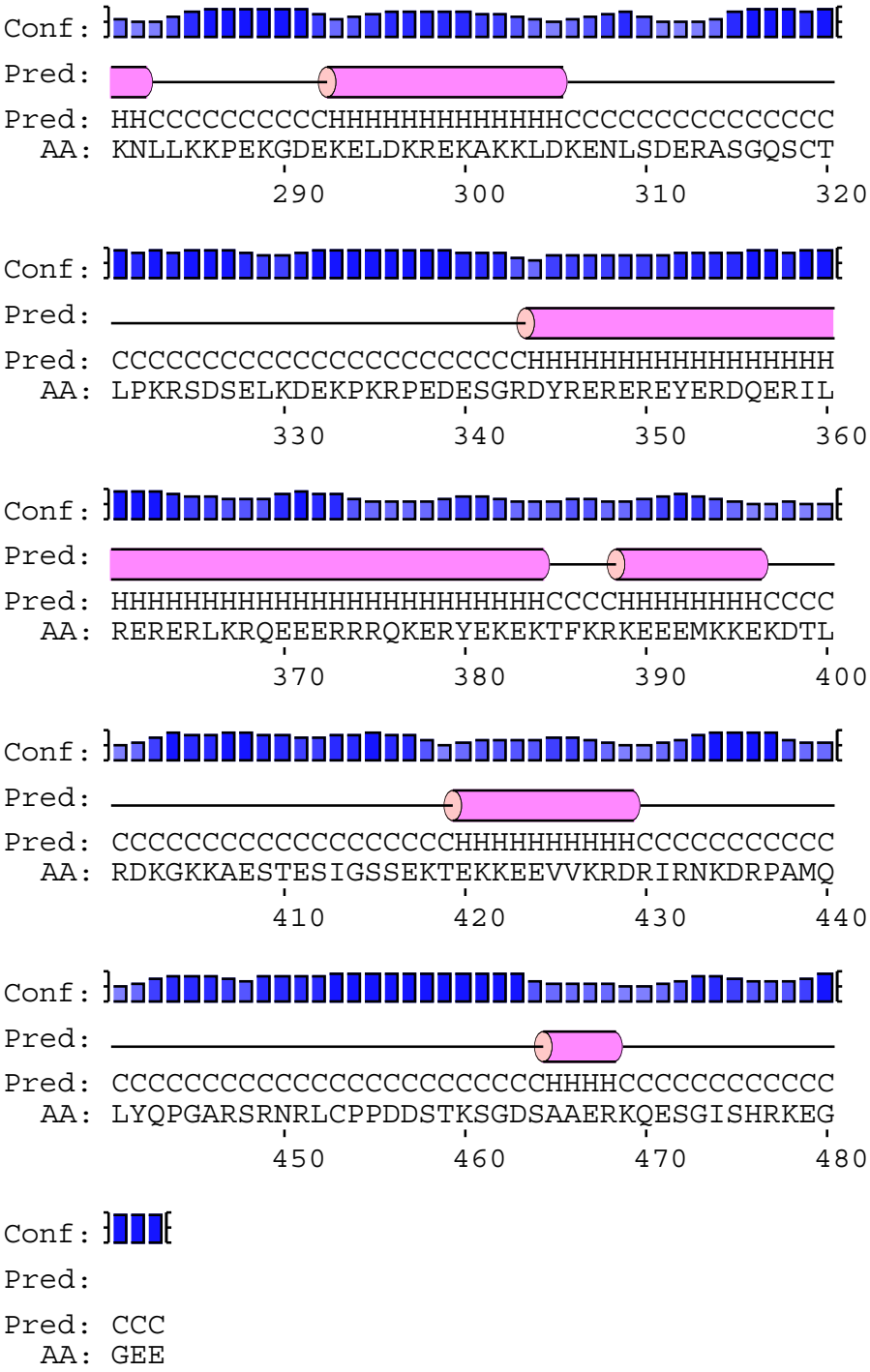

Legend:

= helix

= strand

= coil

Conf: = confidence of prediction

\- +

Pred: predicted secondary structure

AA: target sequence

B.2 Multispecies alignment of UPF3

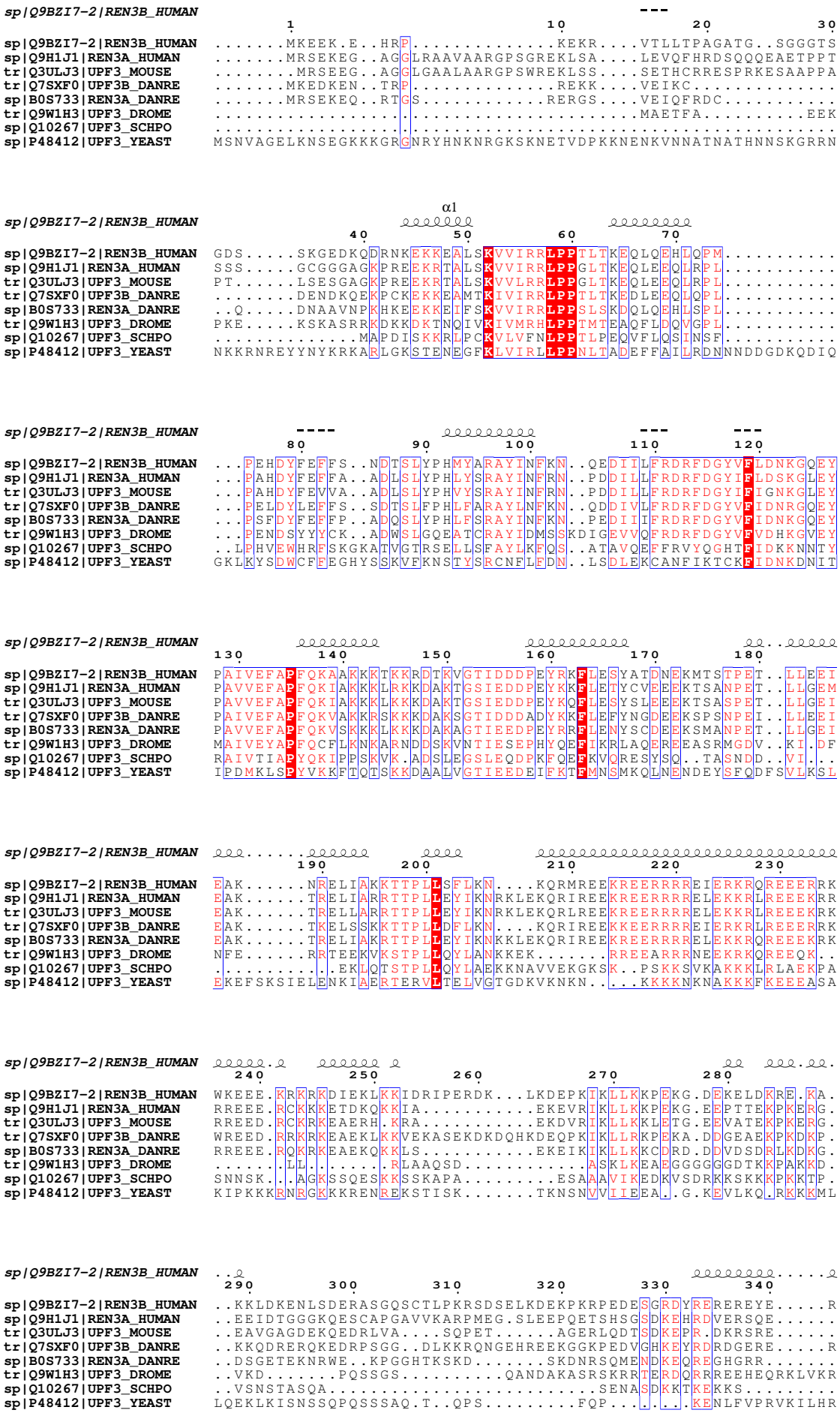
sp|Q9BZI7-2|REN3B_HUMAN
sp|Q9H1J1|REN3A_HUMAN
tr|Q3ULJ3|UPF3_MOUSE
tr|Q7SXF0|UPF3B_DANRE
sp|B0S733|REN3A_DANRE
tr|Q9W1H3|UPF3_DROME
sp|Q10267|UPF3_SCHPO
sp|P48412|UPF3_YEAST
α1

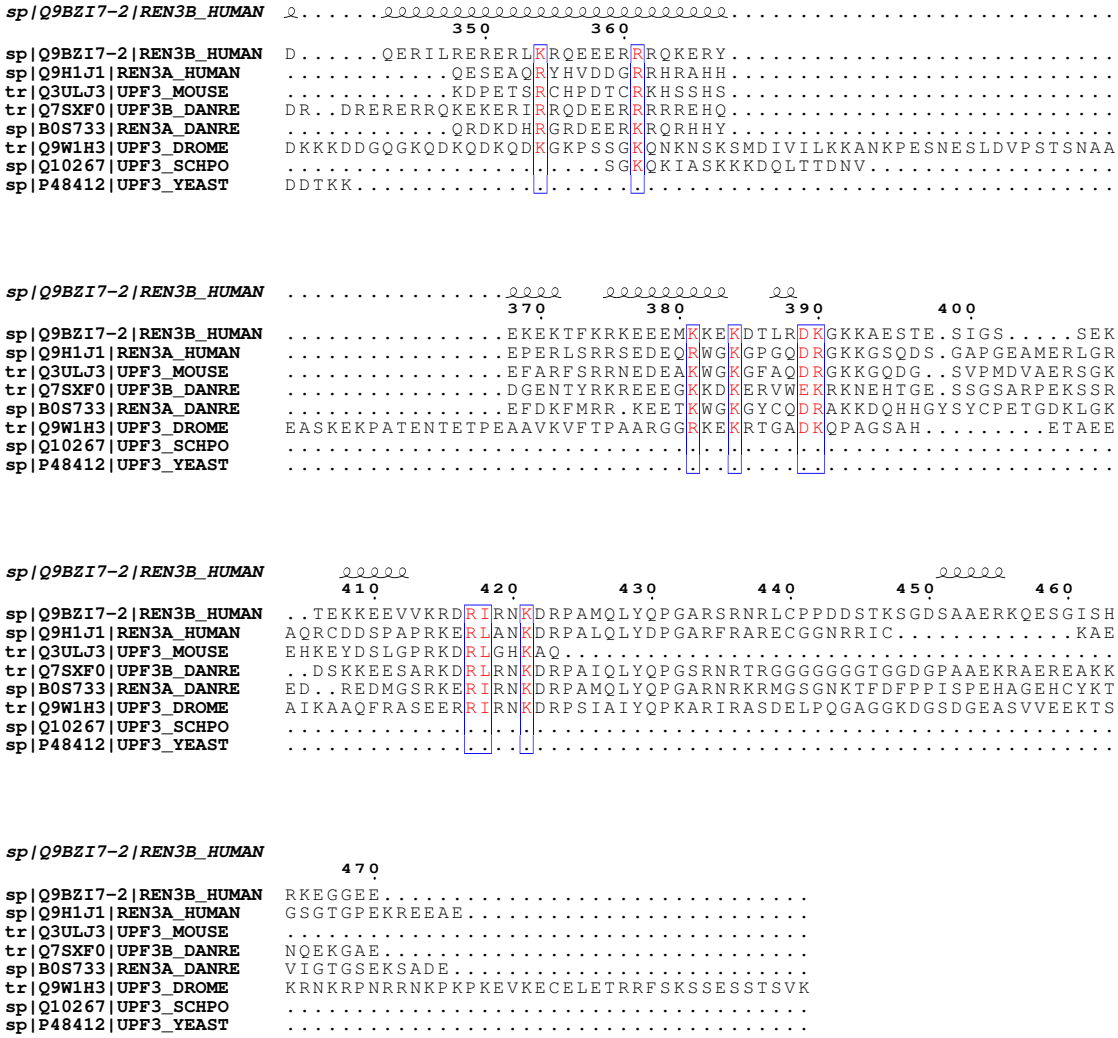
sp|Q9BZI7-2|REN3B_HUMAN
350
360
sp|Q9BZI7-2|REN3B_HUMAN D......QERILRERERLKRQEEERRRQKERY.....
sp|Q9H1J1|REN3A_HUMAN .....QESEAQRYHVDDGRRHRAHH.....
tr|Q3ULJ3|UPF3_MOUSE .....KDPETSRCHPDTCRKHSSHS.....
tr|Q7SXF0|UPF3B_DANRE DR..DRERERRQKEKERIRRQDEERRRRREHQ.....
sp|B0S733|REN3A_DANRE .....QRDKDHRGRDEERKRQRHHY.....
tr|Q9W1H3|UPF3_DROME DKKKDDGQGKQDKQDKQDKGKPSSGKQNKNSKSMDIVILKKANKPESNESLDVPSTSNAA
sp|Q10267|UPF3_SCHPO .....SGKQKIASKKKDQLTTDNV.....
sp|P48412|UPF3_YEAST DDTKK.....
sp|Q9BZI7-2|REN3B_HUMAN
370
380
390
400
sp|Q9BZI7-2|REN3B_HUMAN .....EKEKTFKRKEEEMKKEKDTLRDKGKKAESTE.SIGS.....SEK
sp|Q9H1J1|REN3A_HUMAN .....EPERLSRRSEDEQRWGKGPGQDRGKKGSQDS.GAPGEAMERLGR
tr|Q3ULJ3|UPF3_MOUSE .....EFARFSRRNEDEAKWGKGFAQDRGKKGQDG..SVPMDVAERSGK
tr|Q7SXF0|UPF3B_DANRE .....DGENTYRKREEEGKKDKERVWEKRKNEHTGE.SSGSARPEKSSR
sp|B0S733|REN3A_DANRE .....EFDKFMRR.KEETKWGKGYCQDRAKKDQHHGYSYCPETGDKLGK
tr|Q9W1H3|UPF3_DROME EASKEKPATENTETPEAAVKVFTPAARGGRKEKRTGADKQPAGSAH.....ETAEE
sp|Q10267|UPF3_SCHPO .....
sp|P48412|UPF3_YEAST .....
sp|Q9BZI7-2|REN3B_HUMAN
410
420
430
440
450
460
sp|Q9BZI7-2|REN3B_HUMAN ..TEKKEEVVKRDRIRNKDRPAMQLYQPGARSRNRLCPPDDSTKSGDSAAERKQESGISH
sp|Q9H1J1|REN3A_HUMAN AQRCDDSPAPRKERLANKDRPALQLYDPGARFRARECGGNRRIC.....KAE
tr|Q3ULJ3|UPF3_MOUSE EHKEYDSLGPRKDRLGHKAQ.....
tr|Q7SXF0|UPF3B_DANRE ..DSKKEESARKDRLRNKDRPAIQLYQPGSRNRTRGGGGGGGTGGDGPAAEKRAEREAKK
sp|B0S733|REN3A_DANRE ED..REDMGSRKERIRNKDRPAMQLYQPGARNRKRMGSGNKTFDFPPISPEHAGEHCYKT
tr|Q9W1H3|UPF3_DROME AIKAAQFRASEERRIRNKDRPSIAIYQPKARIRASDELPQGAGGKDGSDGEASVVEEKTS
sp|Q10267|UPF3_SCHPO .....
sp|P48412|UPF3_YEAST .....
sp|Q9BZI7-2|REN3B_HUMAN
470
sp|Q9BZI7-2|REN3B_HUMAN RKEGGEE.....
sp|Q9H1J1|REN3A_HUMAN GSGTGPEKREEAE.....
tr|Q3ULJ3|UPF3_MOUSE .....
tr|Q7SXF0|UPF3B_DANRE NQEKGAE.....
sp|B0S733|REN3A_DANRE VIGTGSEKSADE.....
tr|Q9W1H3|UPF3_DROME KRNKRPNRRNKPKPKEVKECELETRRFSKSSESSTSVK
sp|Q10267|UPF3_SCHPO .....
sp|P48412|UPF3_YEAST .....

B.3 Alignment and prediction of UPF3A and UPF3B

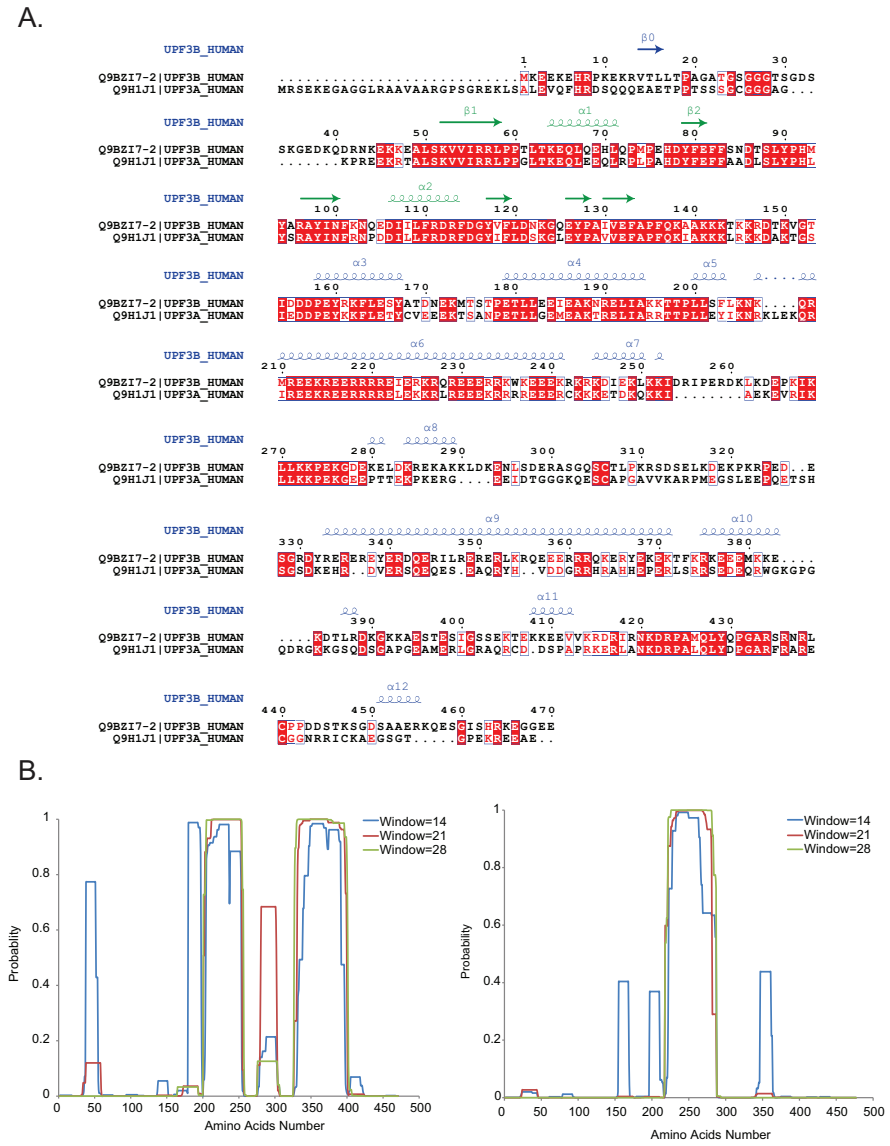

A. Sequence alignment of human UPF3A and UPF3B (Uniprot Q9H1J1 and Q9Z17-2 respectively). Residues that are 100% conserved are in red boxes. Similarities above 70% are in red. The secondary structure of UPF3B from the PDB 1UW4 (Kadlec et al. 2004) is in light blue and the prediction is in blue: α, alpha helix. Helices larger than 2 amino acids were annotated (α3-12). Figure was generated using NPS@ (Combet et al. 2000), CLUSTALO (Sievers et al. 2011) and ESPrit (Gouet et al. 2003). (B) Coiled coil predictions for UPF3B (left panel) and UPF3A (right panel) using COILED COIL prediction server on NPS@. The 3 different lengths of amino acids windows used to predict the coiled coil regions are represented in blue, red and green lines.

Résumés

Environ un tiers des maladies humaines, héréditaires ou acquises, sont dues à la génération d'un codon stop prématuré (PTC). Le système de contrôle appelé dégradation des ARNm non-sens (NMD) permet de détecter puis de dégrader des ARNm contenant un PTC. Les facteurs principaux de la NMD : UPF1, UPF2 et UPF3 reconnaissent les PTCs en interagissant avec le complexe de terminaison de traduction contenant les ribosomes, les facteurs de terminaison eRF1, eRF3 et la protéine poly(A) binding (Pab1p en levure). Nous avons pu résoudre la structure d'un tel complexe en levure comprenant un ribosome en cours de traduction en présence d'un ARNt dans le site P et de facteurs de terminaisons dans le site A. Aucune densité n'a pu être observée pour Pab1p indiquant la flexibilité de l'interaction avec ce complexe. Nous avons aussi évalué l'impact des facteurs de la NMD sur la terminaison dans un système de traduction *in vitro* humain. UPF3B retarde la reconnaissance du codon stop et favorise la dissociation des sous-unités ribosomales. UPF2 abolit l'effet de UPF3B tandis que l'addition de UPF1 n'a pas d'influence dans la terminaison. Par *in vivo* et *in vitro* pulldowns, nous avons montré que UPF3B interagit avec eRF3a et UPF1 et pourrait constituer le lien manquant entre la terminaison et la NMD. Nos résultats illustrent la complexité des mécanismes de la terminaison et de la NMD.

Mots clés: dégradation des ARNm non-sens, terminaison de la traduction, UPF3B

Premature termination codons (PTCs) account for approximately one third of inherited and acquired diseases. A surveillance pathway called nonsense-mediated mRNA decay (NMD) detects and degrades PTC-containing transcripts. NMD core factors UPF1, UPF2 and UPF3 mediate the recognition of PTCs by associating with the terminating translation machinery composed of the ribosome, the release factors eRF1 and eRF3 and the poly(A) binding protein (Pab1p in yeast). Using electron cryomicroscopy, we solved such a complex in yeast and observed the translating ribosome, containing a P-site tRNA and an A-site density for the release factors but not for Pab1p indicating that Pab1p is flexibly bound. We also probed the function of NMD factors in mammalian termination using a reconstituted human *in vitro* translation system. Surprisingly, we found that UPF3B delayed stop codon recognition and promoted ribosomal dissociation. The addition of UPF2 could abolish UPF3B's effect on translation termination. UPF1 had no influence in the termination process alone or in combination with UPF2. Using *in vitro* and *in vivo* pulldowns we found that UPF3B interacts with eRF3a and UPF1, indicating that UPF3B could be the missing link between termination and NMD. Our results point to a complex interplay between the NMD factors and the termination apparatus.

Keywords: nonsense-mediated mRNA decay, translation termination, UPF3B